

UNIVERSIDAD DE LA LAGUNA
Departamento de Astrofísica



*Cosmology and Galaxy Cluster Physics
with the Second Planck Galaxy Cluster
Catalogue*

A dissertation submitted by
Alejandro Aguado Barahona
in partial fulfillment of the requirements for the degree of
Doctor of Philosophy in Astrophysics
at the Universidad de La Laguna



INSTITUTO DE ASTROFÍSICA DE CANARIAS
San Cristóbal de La Laguna, Tenerife
March 2021

Este documento incorpora firma electrónica, y es copia auténtica de un documento electrónico archivado por la ULL según la Ley 39/2015.
Su autenticidad puede ser contrastada en la siguiente dirección <https://sede.ull.es/validacion/>

Identificador del documento: 3248012 Código de verificación: RmbjVJW6

Firmado por: ALEJANDRO AGUADO BARAHONA
UNIVERSIDAD DE LA LAGUNA

Fecha: 01/03/2021 09:35:30

María de las Maravillas Aguiar Aguilár
UNIVERSIDAD DE LA LAGUNA

22/03/2021 13:39:32

Thesis directors: José Alberto Rubiño Martín and Rafael Barrena Delgado
Thesis tutor: José Alberto Rubiño Martín
© Alejandro Aguado Barahona 2021

Este documento incorpora firma electrónica, y es copia auténtica de un documento electrónico archivado por la ULL según la Ley 39/2015.
Su autenticidad puede ser contrastada en la siguiente dirección <https://sede.ull.es/validacion/>

Identificador del documento: 3248012 Código de verificación: RmbjVJW6

Firmado por: ALEJANDRO AGUADO BARAHONA
UNIVERSIDAD DE LA LAGUNA

Fecha: 01/03/2021 09:35:30

María de las Maravillas Aguiar Aguilár
UNIVERSIDAD DE LA LAGUNA

22/03/2021 13:39:32

iii

*Dedicada a mi gran familia,
en especial a mis padres*

Este documento incorpora firma electrónica, y es copia auténtica de un documento electrónico archivado por la ULL según la Ley 39/2015.
Su autenticidad puede ser contrastada en la siguiente dirección <https://sede.ull.es/validacion/>

Identificador del documento: 3248012 Código de verificación: RmbjVJW6

Firmado por: ALEJANDRO AGUADO BARAHONA
UNIVERSIDAD DE LA LAGUNA

Fecha: 01/03/2021 09:35:30

María de las Maravillas Aguiar Aguilár
UNIVERSIDAD DE LA LAGUNA

22/03/2021 13:39:32



Este documento incorpora firma electrónica, y es copia auténtica de un documento electrónico archivado por la ULL según la Ley 39/2015.
Su autenticidad puede ser contrastada en la siguiente dirección <https://sede.ull.es/validacion/>

Identificador del documento: 3248012 Código de verificación: RmbjVJW6

Firmado por: ALEJANDRO AGUADO BARAHONA
UNIVERSIDAD DE LA LAGUNA

Fecha: 01/03/2021 09:35:30

María de las Maravillas Aguiar Aguilár
UNIVERSIDAD DE LA LAGUNA

22/03/2021 13:39:32

Summary

The second catalogue of *Planck* Sunyaev-Zeldovich (SZ) sources, hereafter PSZ2, is the largest sample of galaxy clusters selected through their SZ signature in the full sky. At the time of publication, 21% of these objects had no known counterpart at other wavelengths. Using telescopes at the Canary Island observatories, we conducted the long-term observational program 128-MULTIPLE-16/15B (hereafter LP15), a large and complete optical follow-up campaign of all the unidentified PSZ2 sources in the northern sky, with declinations above -15° and no correspondence in the first *Planck* catalogue PSZ1. The main aim of LP15 is to validate all those SZ cluster candidates, and to contribute to the characterisation of the actual purity and completeness of full *Planck* SZ sample. In this thesis, I describe the full program and present the results of the two years of observations.

The LP15 program was awarded 44 observing nights, spread over two years in three telescopes at the Roque de los Muchachos Observatory. The full LP15 sample comprises 190 previously unidentified PSZ2 sources. For each target, we performed deep optical imaging and spectroscopy. Our validation procedure combined this optical information with SZ emission as traced by the publicly available *Planck* Compton y -maps. The final classification of the new galaxy clusters as optical counterparts of the SZ signal is established according to several quantitative criteria based on the redshift, velocity dispersion and richness of the clusters.

This thesis presents the detailed study of 184 objects out of the LP15 sample, corresponding to all the observations carried out during the full program. We confirmed the optical counterpart for 81 new PSZ2 sources, 49 of them being validated using also velocity dispersion based on our spectroscopic information. This is the largest data-set of newly confirmed PSZ2 sources without any previous optical information. All the confirmed counterparts are rich structures (i.e. they show high velocity dispersion), and are well aligned with the nominal *Planck* coordinates (i.e., $\sim 70\%$ of them are located at less than $3'$ distance). In total, 103 SZ sources are classified as unconfirmed, being 89 of them due to the absence of an optical over-density, and 14 of them due to a weak association with the observed SZ signal. After the LP15 observational program the purity of the PSZ2 catalogue has increased from 76.7% originally to 86.2%, confirming the theoretical predictions of $\sim 88\%$ from the *Planck* Collaboration. Moreover, we study the possible reasons for false detection, and we report a clear correlation between the number of unconfirmed sources and galactic thermal dust emission.

In addition to the LP15 sample, I here study 42 additional PSZ2 objects that were originally validated as real clusters because they matched a WISE or PSZ1 counterpart, but they had no measured spectroscopic redshift.

Furthermore, I present all the spectroscopic observations of the full program. I complement these LP15 spectroscopic results with Sloan Digital Sky Survey (SDSS) archival data and other observations from a previous program (ITP13-08), and present a catalogue of 388 clusters and groups of galaxies including estimates of their velocity dispersion and dynamical mass. The majority of them (356) are the optical counterpart

Este documento incorpora firma electrónica, y es copia auténtica de un documento electrónico archivado por la ULL según la Ley 39/2015.
Su autenticidad puede ser contrastada en la siguiente dirección <https://sede.ull.es/validacion/>

Identificador del documento: 3248012 Código de verificación: RmbjVJW6

Firmado por: ALEJANDRO AGUADO BARAHONA
UNIVERSIDAD DE LA LAGUNA

Fecha: 01/03/2021 09:35:30

María de las Maravillas Aguiar Aguilár
UNIVERSIDAD DE LA LAGUNA

22/03/2021 13:39:32

of a PSZ2 source.

A subset of 297 of those clusters is used to construct the $M_{SZ} - M_{dyn}$ scaling relation, based on the estimated SZ mass from *Planck* measurements and our dynamical mass estimates. I discuss and correct for different statistical and physical biases in the estimation of the masses, such as the Eddington bias when estimating M_{SZ} and the aperture and the number of galaxies used to calculate M_{dyn} . The SZ-to-dynamical mass ratio for those 297 PSZ2 clusters is $(1 - b) = 0.80 \pm 0.04$ (stat) ± 0.05 (sys), with only marginal evidence for a possible mass dependence of this factor. This value is consistent with previous results in the literature, but presents a significantly smaller uncertainty due to the use of the largest sample size for this type of studies. This result confirms the apparent tension in the $\Omega_m - \sigma_8$ plane between the cluster counts and the primordial CMB results.

Este documento incorpora firma electrónica, y es copia auténtica de un documento electrónico archivado por la ULL según la Ley 39/2015.
Su autenticidad puede ser contrastada en la siguiente dirección <https://sede.ull.es/validacion/>

Identificador del documento: 3248012 Código de verificación: RmbjVJW6

Firmado por: ALEJANDRO AGUADO BARAHONA
UNIVERSIDAD DE LA LAGUNA

Fecha: 01/03/2021 09:35:30

María de las Maravillas Aguiar Aguilár
UNIVERSIDAD DE LA LAGUNA

22/03/2021 13:39:32

Resumen

El segundo catálogo *Planck* de fuentes Sunyaev-Zeldovich (SZ), PSZ2 en lo sucesivo, representa la mayor muestra de cúmulos de galaxias seleccionados por su señal SZ cubriendo todo el cielo. En el momento de su publicación, el 21% de estos objetos no tenía una contrapartida conocida en otras longitudes de onda. Usando telescopios de los Observatorios de las Islas Canarias, hemos ejecutado el programa observacional a largo plazo 128-MULTIPLE-16/15B (LP15 en lo sucesivo), una campaña de seguimiento completa de las fuentes no identificadas del catálogo PSZ2 en el hemisferio norte, con declinaciones superiores a -15° y sin correspondencia en el primer catálogo *Planck* PSZ1. El objetivo principal del programa LP15 es validar los candidatos SZ y contribuir a la caracterización de la pureza y completitud de la muestra PSZ2 de *Planck*. En este trabajo de tesis, se describe el programa observacional y se presentan los resultados de los dos años de observaciones.

Para el LP15, fueron concedidas 44 noches de observación, distribuidas en tres telescopios del observatorio Roque de los Muchachos en la isla de La Palma. La muestra LP15 completa consta de 190 fuentes SZ previamente no identificadas. Para cada objetivo, realizamos imagen óptica profunda y espectroscopía multi-objeto. Nuestro procedimiento de validación combina la información óptica con la señal SZ disponible públicamente en los mapas de Comptonización de *Planck*. La clasificación final de los nuevos cúmulos de galaxias encontrados asociados a la señal SZ se realiza en base a una serie de criterios cuantitativos como son el desplazamiento al rojo, la velocidad de dispersión y la riqueza de los cúmulos.

En este trabajo de tesis se presenta el estudio detallado de 184 objetos de la muestra LP15 correspondiente a las observaciones realizadas durante el programa completo. Una vez finalizado el programa, hemos confirmado 81 nuevas contrapartidas ópticas de fuentes SZ del catálogo PSZ2, siendo 49 de ellas validadas usando la velocidad de dispersión como criterio. Esta es la mayor muestra de fuentes SZ confirmadas hasta la fecha del catálogo PSZ2 sin ninguna información óptica previa. Todos los cúmulos confirmados son estructuras ricas (o lo que es lo mismo, presentan una elevada velocidad de dispersión) y están correctamente alineadas con la señal SZ nominal ($\sim 70\%$ yacen a menos de $3'$ de distancia). En total, 103 fuentes SZ son clasificadas como no detectadas, siendo 89 de ellas por la ausencia de una sobredensidad óptica de galaxias y 14 de ellas por una asociación débil con la señal SZ. Tras el programa LP15, la pureza del PSZ2 ha aumentado desde el 76.7% hasta el 86.2%, confirmando las predicciones teóricas del 88% realizadas por la Colaboración *Planck*. Además, hemos estudiado las posibles causas de las detecciones falsas y hemos reportado una correlación clara entre el número de fuentes no validadas y la emisión térmica del polvo galáctico.

Por otra parte, se han estudiado 42 objetos del PSZ2 fuera de la muestra LP15 que ya habían sido validados usando WISE o eran una contrapartida del PSZ1 pero que no tenían asociado desplazamiento al rojo alguno en el catálogo.

En esta tesis también presento los resultados espectrocópicos del programa completo. Complemento estos resultados con datos espectrocópicos obtenidos de los archivos

Este documento incorpora firma electrónica, y es copia auténtica de un documento electrónico archivado por la ULL según la Ley 39/2015.
Su autenticidad puede ser contrastada en la siguiente dirección <https://sede.ull.es/validacion/>

Identificador del documento: 3248012 Código de verificación: RmbjVJW6

Firmado por: ALEJANDRO AGUADO BARAHONA
UNIVERSIDAD DE LA LAGUNA

Fecha: 01/03/2021 09:35:30

María de las Maravillas Aguiar Aguilár
UNIVERSIDAD DE LA LAGUNA

22/03/2021 13:39:32

públicos del Sloan Digital Sky Survey (SDSS) y de observaciones previas del programa ITP13-08. Se presenta un catálogo de 388 cúmulos y grupos de galaxias incluyendo estimaciones de sus velocidades de dispersión y masas dinámicas. La gran mayoría de ellos (356) son contrapartidas ópticas de fuentes del PSZ2.

Una submuestra de 297 cúmulos se usa para construir la relación de escala $M_{SZ} - M_{dyn}$ basada en las estimaciones de la masa SZ de *Planck* y de nuestras masa dinámicas. Se discute y se corrige por varios sesgos físicos y estadísticos como el Eddington bias al estimar las M_{SZ} , o la apertura y el número de galaxias usado para calcular la M_{dyn} . El cociente entre la masa SZ y la dinámica para la muestra de 297 cúmulos es $(1 - b) = 0.80 \pm 0.04$ (est) ± 0.05 (sis), con una evidencia marginal de una posible dependencia con la masa. Este valor es consistente con la mayoría de resultados de la literatura pero presenta un error significativamente más pequeño debido al uso de una muestra tan amplia en tamaño para este tipo de estudios. Este resultado confirma la aparente tensión en el plano $\Omega_m - \sigma_8$ entre los resultados de conteo de cumulos de galaxias y los de CMB primordial.

Este documento incorpora firma electrónica, y es copia auténtica de un documento electrónico archivado por la ULL según la Ley 39/2015.
Su autenticidad puede ser contrastada en la siguiente dirección <https://sede.ull.es/validacion/>

Identificador del documento: 3248012 Código de verificación: RmbjVJW6

Firmado por: ALEJANDRO AGUADO BARAHONA
UNIVERSIDAD DE LA LAGUNA

Fecha: 01/03/2021 09:35:30

María de las Maravillas Aguiar Aguilár
UNIVERSIDAD DE LA LAGUNA

22/03/2021 13:39:32

Contents

1	Introduction: Galaxy Clusters through history of Cosmology	1
1.1	The early history of Galaxy Clusters	1
1.2	Detection of Galaxy Clusters	3
1.2.1	Optical and near-infrared	4
1.2.1.1	Optical richness	4
1.2.1.2	Galaxy velocities	4
1.2.1.3	Gravitational lensing	6
1.2.2	X-ray	6
1.2.3	Radio	7
1.2.3.1	The Sunyaev Zeldovich effect	7
1.3	The Planck mission	9
1.3.1	The PSZ2 catalogue	10
1.3.2	Validation programs	13
1.4	Mass proxies and scaling relations	15
1.4.1	The mass bias	17
1.5	Cosmology with Galaxy Clusters	19
1.5.1	Baryon fraction	19
1.5.2	Combined X-ray and SZ distances	21
1.5.3	SZ power spectrum	22
1.5.4	Cluster counts	22
1.6	Objectives of this work	24
2	The <i>Planck</i> PSZ2 optical follow-up: observational strategy	25
2.1	The LP15 program: sample definition and strategy	25
2.2	The LP15 program: imaging	30
2.2.1	Observations	30
2.2.2	Data reduction and photometry	31
2.2.3	Photometric redshift estimation	31
2.3	The LP15 program: spectroscopy	32
2.3.1	Observations	32
2.3.2	Data reduction	34
2.3.3	Spectroscopic redshift determination	36

Este documento incorpora firma electrónica, y es copia auténtica de un documento electrónico archivado por la ULL según la Ley 39/2015.
 Su autenticidad puede ser contrastada en la siguiente dirección <https://sede.ull.es/validacion/>

Identificador del documento: 3248012 Código de verificación: RmbjVJW6

Firmado por: ALEJANDRO AGUADO BARAHONA
 UNIVERSIDAD DE LA LAGUNA

Fecha: 01/03/2021 09:35:30

María de las Maravillas Aguiar Aguilár
 UNIVERSIDAD DE LA LAGUNA

22/03/2021 13:39:32

3	The <i>Planck</i> PSZ2 optical follow-up: results	38
3.1	Cluster identification and validation criteria	38
3.1.1	Photometric analysis	38
3.1.2	Spectroscopic analysis	41
3.1.3	Summary of our validation criteria	42
3.2	LP15 sample: 1st year of observations	43
3.2.1	Results	43
3.2.2	Notes on individual objects	47
3.2.3	Unconfirmed cluster candidates	51
3.3	LP15 sample: 2nd year of observations	54
3.3.1	Results	54
3.3.2	Notes on individual objects	58
3.4	Observations of other PSZ2 candidates beyond the LP15 sample	60
3.4.1	Results	62
3.4.2	Notes on individual objects	64
3.5	PSZ2 statistics in the northern sky	66
4	Velocity dispersion and dynamical masses for 388 Galaxy Clusters and groups.	
	Calibrating the $M_{SZ} - M_{dyn}$ scaling relation for the PSZ2 sample	72
4.1	The reference sample	72
4.1.1	LP15 data set	73
4.1.2	ITP13 data set	75
4.1.3	SDSS data	75
4.1.4	Other PSZ2 clusters	76
4.1.5	Beyond the PSZ2 sample	76
4.2	Velocity dispersion estimates	76
4.3	Mass estimates	88
4.3.1	Dynamical mass estimates	88
4.3.2	SZ mass estimates	88
4.4	$M_{SZ} - M_{dyn}$ scaling relation	89
4.4.1	Testing the regression methods	90
4.4.1.1	Regression methods	91
4.4.1.2	Simulations	92
4.4.1.3	Results	95
4.4.2	The mass bias	97
4.4.2.1	Eddington bias	98
4.4.2.2	Redshift dependence	100
4.5	Comparison with literature	101
4.6	Discussion	106
5	Conclusions	108
	Bibliography	111

Este documento incorpora firma electrónica, y es copia auténtica de un documento electrónico archivado por la ULL según la Ley 39/2015.
 Su autenticidad puede ser contrastada en la siguiente dirección <https://sede.ull.es/validacion/>

Identificador del documento: 3248012 Código de verificación: RmbjVJW6

Firmado por: ALEJANDRO AGUADO BARAHONA
 UNIVERSIDAD DE LA LAGUNA

Fecha: 01/03/2021 09:35:30

María de las Maravillas Aguiar Aguilár
 UNIVERSIDAD DE LA LAGUNA

22/03/2021 13:39:32

1

Introduction: Galaxy Clusters through history of Cosmology

This thesis is framed in the field of Galaxy Clusters (hereafter GCs) and their use for cosmological purposes. The precursor of the use of GCs as cosmological tools was Fritz Zwicky back in the early 30's with his discovery of dark matter in the Coma Cluster (Zwicky 1933). During the last decade, the use of modern telescopes and antennas on the ground and in space has yielded to the epoch of Precision Cosmology in which this thesis is embedded. The work performed here is focused on the analysis of the Second *Planck* Galaxy Cluster Catalogue (PSZ2) of Sunyaev-Zeldovic (SZ) sources (Planck Collaboration XXVII 2016) and on its use for future cosmological studies. In this Chapter, I review the history of GCs and how we detect them. I describe the *Planck* mission (The Planck Collaboration 2006) and its data products related to galaxy clusters, which is the benchmark of this work. Then, I present the mass determination problem as well as how to perform cosmological studies using GCs. Finally, I will introduce the main scientific motivations and goals of this thesis.

1.1 The early history of Galaxy Clusters

The discovery of GCs was not an straight forward process. It took more than one and a half centuries from the first reference until Humason et al. (1956) declared that there was an 'increasing evidence' of the clustering phenomenon dismissing Hubble's theory of a uniform galaxy distribution across the whole Universe. But let's start from the beginning.

The history of GCs is closely related to the history of galaxies or what they were called in past times nebulae. The very first reference of a GC is probably that of the Messier

Este documento incorpora firma electrónica, y es copia auténtica de un documento electrónico archivado por la ULL según la Ley 39/2015.
Su autenticidad puede ser contrastada en la siguiente dirección <https://sede.ull.es/validacion/>

Identificador del documento: 3248012 Código de verificación: RmbjVJW6

Firmado por: ALEJANDRO AGUADO BARAHONA
UNIVERSIDAD DE LA LAGUNA

Fecha: 01/03/2021 09:35:30

María de las Maravillas Aguiar Aguilár
UNIVERSIDAD DE LA LAGUNA

22/03/2021 13:39:32

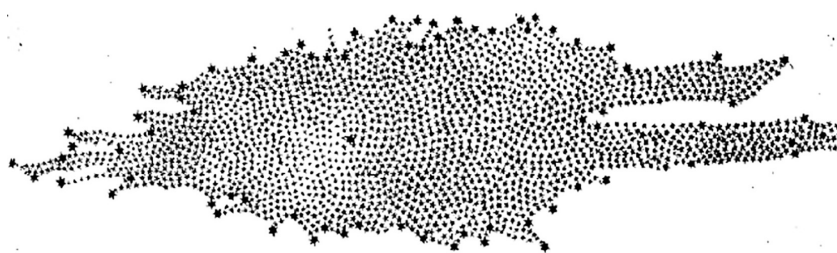


Figure 1.1: First drawing of the shape of the Milky Way. Credit: Caroline Herschel.

catalogue (Messier 1781). Charles Messier was a comet hunter and this profession made him to come across often with diffuse objects that could misidentify as comets. For this reason, he listed 103 nebulae in his catalogue called *Catalogue des nébuleuses et des amas d'étoiles que l'on découvre parmi les étoiles fixes, sur l'horizon de Paris*. In this catalogue, there are very different types of objects: globular clusters (28), open cluster (26), asterism (1), double star (1), galaxies (34) and different types of nebulae (13). Messier noticed the accumulation of galaxies around the Virgo constellation, what we now name as the the Virgo cluster and supercluster. Thirteen of the galaxies in the Messier catalogue are included in The Extended Virgo Cluster Catalogue (Kim et al. 2014). He was never interested in the study of this type of objects, he used his catalogue only for the reason explained above. Although, this catalogue was the precursor for the modern extra-galactic catalogues that exists today.

We can not forget to mention the enormous contribution of William and Caroline Lucretia Herschel to the field of extra-galactic astronomy. Caroline, William's sister, is not as known as her brother but she made many discoveries side by side with William and I am sure they would not have achieved if they had not have each other. Herschel was first known for a very important discovery, the planet Uranus in 1781. However, he was more interested in the field of what we call now the Large Scale Structure of the Universe. In his article *On the Construction of the Heavens* (Herschel 1785) he not only suggested that we live in a nebulae but also specifically wrote about the concentration of nebulae around Coma: *'...the appearance of that remarkable collection of many hundreds of nebulae which are to be seeing what I have called the nebulous stratus of Coma Berenices...'* During his whole life, William catalogued more than 2500 nebulae and his work was continued by his son John Herschel who published, in 1864, the *General Catalogue of Nebulae and Clusters of Stars* containing more than 6000 entries. As Messier before him, John wrote about the concentration of nebulae around the Virgo constellation, what we now know is the Virgo supercluster.

In 1888, Dreyer published his *New General Catalogue* (Dreyer 1888) which was a continuation of Herschel family's work and contained approximately 13000 objects by the end of the first decade of the XX century. During this first decade, Max Wolf published a detailed description of Perseus and Coma clusters based on his photographic observations

Este documento incorpora firma electrónica, y es copia auténtica de un documento electrónico archivado por la ULL según la Ley 39/2015.
Su autenticidad puede ser contrastada en la siguiente dirección <https://sede.ull.es/validacion/>

Identificador del documento: 3248012 Código de verificación: RmbjVJW6

Firmado por: ALEJANDRO AGUADO BARAHONA
UNIVERSIDAD DE LA LAGUNA

Fecha: 01/03/2021 09:35:30

María de las Maravillas Aguiar Aguilár
UNIVERSIDAD DE LA LAGUNA

22/03/2021 13:39:32

(Wolf 1901, 1903a,b, 1906).

The nature of these nebulae was not clear at that time. There were astronomers that supported that these nebulae were external objects from our own galaxy, while others thought that they were inside the Milky Way. This topic was addressed in *The Great Debate* in 1920 where Shapley and Curtis discussed with no clear winner. Some years later, Hubble discovered cepheids in M31 ending the debate and consolidating the external nature of these objects. This discovery led Hubble to his most famous work on the velocity-distance relation for extra-galactic nebulae (Hubble 1929).

There were many authors that stated a non uniform distribution of the nebulae: J. Hershel in the XIX century continuing with Easton (1904) and Reynolds (1923). Despite this predominant current, Hubble published in his book *Realm of the Nebulae* (Hubble 1936) that the distribution of nebulae were moderately uniform although he included the Milky Way inside a galaxy group which he called *The Local Group*. It was Zwicky, two years later, who noted that our own galaxy might be a part of the Virgo Cluster Zwicky (1938).

Humason et al. (1956) published the results for twenty years of spectroscopic observations. In this work, more than 800 redshifts of galaxies were reported, 75 in Virgo, 23 in Coma, etc. The authors noted an ‘increasing evidence’ of the clustering phenomenon dismissing Hubble’s theory of a uniform galaxy distribution.

During the last years of the 1950s, plenty of astronomers were working on cataloguing GCs (Herzog, Wild, Zwicky...). However, the most important work was Abell’s paper *The distribution of rich clusters of galaxies* (Abell 1957), a catalogue which the community still consults today, more than 60 years later.

From this point and on, GC has been studied in several forms. During the 1970’s, X-ray observations started to be the main instrument of research among this topic. Thanks to these observations we now know plenty of properties of GCs. However, during the last decades, a new form of GCs detection in radio waves has overtake X-ray studies. The *Sunyaev Zeldovich (SZ) effect*, in which this thesis is embedded, detectable in the *Cosmic Microwave Background (CMB)* has become a valuable technique to use GCs as a cosmological tool. Furthermore, the study of GCs and their properties has taken a quantitative leap with the appearance of extensive spectroscopic surveys such as 2dF Galaxy Redshift Survey (2dFGRS; De Propriis et al. 2002), Sloan Digital Sky Survey (SDSS; York et al. 2000) and The Hectospec Survey of Sunyaev-Zeldovich-selected Clusters (HeCS-SZ; Rines et al. 2016). In addition, projects like the ESO Nearby Abell Cluster Survey (ENACS; Mazure et al. 1995) and the WIdE-field Nearby Galaxy-cluster Survey (WINGS; Fasano et al. 2006; Varela et al. 2009) focused on a significant number of nearby clusters have been carried out.

1.2 Detection of Galaxy Clusters

Galaxy Clusters are multi-component systems composed not only of dark matter but also of baryonic matter in several phases (see Fig. 1.2). The variety of these phases make GCs detectable in multiple wavelengths. However, as noticed in Sect. 1.1, they

Este documento incorpora firma electrónica, y es copia auténtica de un documento electrónico archivado por la ULL según la Ley 39/2015.
Su autenticidad puede ser contrastada en la siguiente dirección <https://sede.ull.es/validacion/>

Identificador del documento: 3248012 Código de verificación: RmbjVJW6

Firmado por: ALEJANDRO AGUADO BARAHONA
UNIVERSIDAD DE LA LAGUNA

Fecha: 01/03/2021 09:35:30

María de las Maravillas Aguiar Aguilár
UNIVERSIDAD DE LA LAGUNA

22/03/2021 13:39:32

4 Chapter 1. Introduction: Galaxy Clusters through history of Cosmology

were first discovered by the emission of optical light of the stars within galaxies. Stars and galaxies are a small fraction of the total cluster mass. Other baryonic components inside a GC are cold, molecular gas, warm and hot gas and nonthermal plasma. The complexity of their composition is what makes them unique objects. This complexity is a clear advantage so we can observe the different phases in different wavelengths and the combination of this observations makes us induce several properties that we would have not been able to understand by single observations.

1.2.1 Optical and near-infrared

Since the discovery of GCs, optical and near-infrared approaches have been the only way of studying their properties until the appearance of X-ray observations in the early 1970's. Mainly stars within galaxies are the only visible component in these wavelengths. The three most commonly used techniques to infer properties of the GCs are the optical richness, the galaxy velocities and the gravitational lensing.

1.2.1.1 Optical richness

The optical richness of a cluster can be defined in many ways, but it is mainly the count of galaxies inside a given region. This magnitude is very interesting as it can be related to the cluster mass. The first to apply this technique was George Abell who made his catalogues based on richness estimates. He obtained the distance of each cluster candidate from the apparent brightness of its tenth brightest member galaxy. Then, he counted every galaxy brighter than two magnitudes fainter than the third brightest member lying within a fixed projected radius. This projected radius was approximately 2 Mpc and it was the same for each candidate. He only considered candidates with more than 50 galaxies in his counts.

Abell's basic technique has been improved over the years. Including colour information has been very useful for large photometric surveys in which clusters must be found (Gladders & Yee 2000). The colours of the galaxies are necessary because the contrast of clusters against the background galaxy counts decreases with cluster distance. In the last decade red sequence based methods that do not do a binary classification but assign a probability for each galaxy candidate have become popular and very useful (Rykoff et al. 2014a; Rozo et al. 2015).

1.2.1.2 Galaxy velocities

Other method to extract information from the galaxies is to retrieve their radial velocities v_r . The velocity distribution (σ_{1D}) of a relaxed GC is expected to be gaussian in the velocity space. The deviation of the distribution from the gaussianity means either a non-relaxed cluster (i.e. with substructures, or in the formation process), or a superposition of smaller objects. The accuracy on its determination depends critically on the number of galaxies with measured velocities and on the method to identify members and interlopers (galaxies not gravitationally bounded to the cluster). There are several methods to

Este documento incorpora firma electrónica, y es copia auténtica de un documento electrónico archivado por la ULL según la Ley 39/2015.
Su autenticidad puede ser contrastada en la siguiente dirección <https://sede.ull.es/validacion/>

Identificador del documento: 3248012 Código de verificación: RmbjVJW6

Firmado por: ALEJANDRO AGUADO BARAHONA
UNIVERSIDAD DE LA LAGUNA

Fecha: 01/03/2021 09:35:30

María de las Maravillas Aguiar Aguilár
UNIVERSIDAD DE LA LAGUNA

22/03/2021 13:39:32

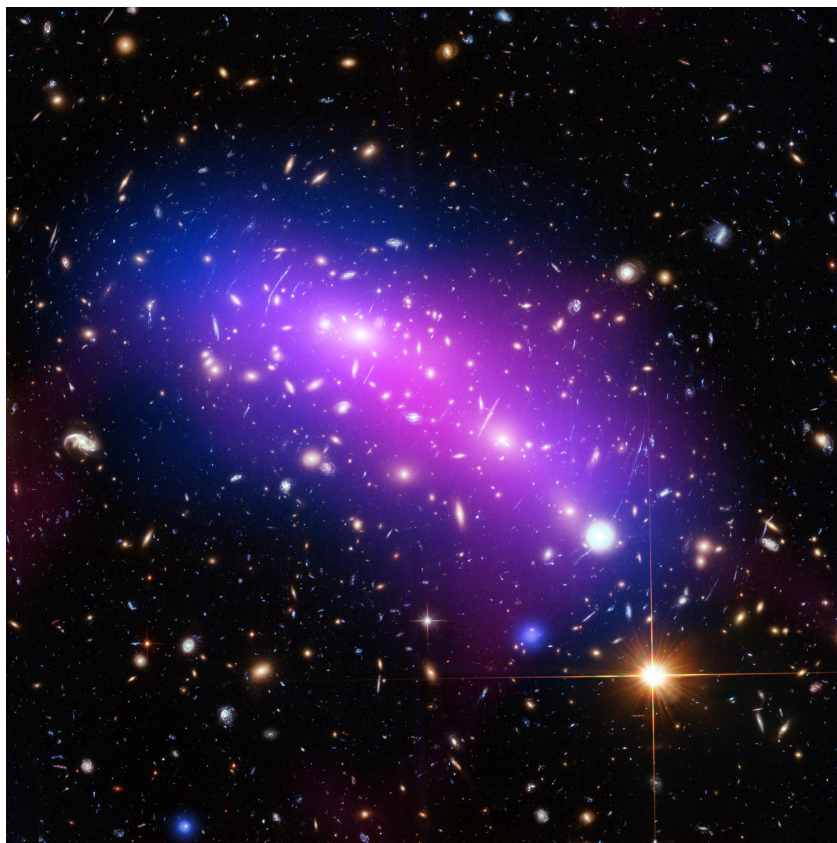


Figure 1.2: A composite, multi-wavelength image of MACS J0416.1-2403. It contains data from three different telescopes: NASA's Chandra X-ray Observatory (diffuse emission in blue), Hubble Space Telescope (red, green, and blue), and the NSF's Jansky Very Large Array (diffuse emission in pink). Chandra and Hubble data trace the hot gas and the galaxies respectively. On the contrary, the radio data trace shock waves and turbulence. Image credit: X-ray: NASA/CXC/SAO/G. Ogrea et al. (2015); Optical: NASA/STScI; Radio: NSF/NRAO/VLA.

Este documento incorpora firma electrónica, y es copia auténtica de un documento electrónico archivado por la ULL según la Ley 39/2015.
Su autenticidad puede ser contrastada en la siguiente dirección <https://sede.ull.es/validacion/>

Identificador del documento: 3248012 Código de verificación: RmbjVJW6

Firmado por: ALEJANDRO AGUADO BARAHONA
UNIVERSIDAD DE LA LAGUNA

Fecha: 01/03/2021 09:35:30

María de las Maravillas Aguiar Aguilár
UNIVERSIDAD DE LA LAGUNA

22/03/2021 13:39:32

6 Chapter 1. Introduction: Galaxy Clusters through history of Cosmology

estimate σ_{1D} . The classical standard deviation, the gapper (Wainer & Thissen 1976) and the biweight (Beers et al. 1990) are the most common ones.

The first one to measure a cluster's velocity dispersion was Fritz Zwicky (Zwicky 1933, 1937). In his works, he showed that the Coma Cluster presented a velocity dispersion of $\sigma_{1D} \sim 700 \text{ km s}^{-1}$. He also estimated the cluster's overall radius finding that the cluster mass must be much greater than the observed mass in stars. This was the first strong evidence for the existence of dark matter in the Universe.

1.2.1.3 Gravitational lensing

It was non other than Zwicky in his paper about the Coma Cluster (Zwicky 1937) who proposed that the cluster mass can be measured by the gravitational lensing of the background galaxies. This proposal could not be carried out until a few decades ago. But nowadays is one of the preferred techniques to compute the mass of GCs. The first proofs of a GC acting as a gravitational lens traces back to the late eighties. Soucail et al. (1987) and Lynds & Petrosian (1989) found gravitational arcs (strong lensing) in A370 and CL2244-02 clusters. Tyson et al. (1990) used the distortion introduces by background galaxies distortions (weak lensing) around the high-velocity dispersion clusters A1689 and CL 1409+52 to extract information about the cluster masses and their spatial distributions.

1.2.2 X-ray

Clusters emit in X-ray because the baryonic gas inside the intra cluster medium (ICM), resultant of the inefficient process of galaxy formation, is heated into the deep gravitational potential well, reaching temperatures in which X-ray photons are released. The physical process involved is *thermal bremsstrahlung* or *free-free emission*, produced by accelerated charged particles (Sarazin 1988).

Until the 1970s, the only way to study GCs was in optical wavelengths. Since then, multiple satellites have been launched to observe the sky in the X-ray range. From *Uhuru*, which performed the first X-Ray catalogue from the space (Giacconi et al. 1972) to *SRG/eROSITA* (Predehl et al. 2010), successfully launched on 2019 and already producing science information. It is worth mentioning here, the most fruitful X-ray mission when speaking about GCs, the *ROSAT* All-Sky Survey (Voges et al. 1999). All the cluster products were collected and unified in the Meta-catalogue of X-ray detected clusters of galaxies (Piffaretti et al. 2011, MCXC). The *ROSAT* mission came to an end in 1999 and it was replaced by *Chandra* (Weisskopf et al. 2002) and *XMM-Newton* (Jansen et al. 2001). Both space telescopes are complementary to each other, while *Chandra* has a high spatial resolution ($\sim 0.5''$), *XMM-Newton* has higher sensitivity and large *field of view* (FoV).

Este documento incorpora firma electrónica, y es copia auténtica de un documento electrónico archivado por la ULL según la Ley 39/2015.
Su autenticidad puede ser contrastada en la siguiente dirección <https://sede.ull.es/validacion/>

Identificador del documento: 3248012 Código de verificación: RmbjVJW6

Firmado por: ALEJANDRO AGUADO BARAHONA
UNIVERSIDAD DE LA LAGUNA

Fecha: 01/03/2021 09:35:30

María de las Maravillas Aguiar Aguilár
UNIVERSIDAD DE LA LAGUNA

22/03/2021 13:39:32

1.2 Detection of Galaxy Clusters

7

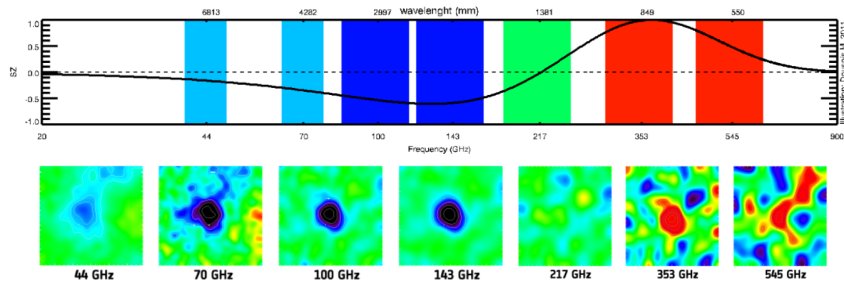


Figure 1.3: Top panel. Typical spectral distortion produced by the SZ effect relative to the main CMB spectrum. Vertical colored regions represent the frequency channels in which the *Planck* mission operated. Figure credit: Douspis (2011). Low panels. Galaxy Cluster A2319 as seen by *Planck* in the individual frequency channels. Credit: ESA/LFI & HFI Consortia.

1.2.3 Radio

We can measure the distortion of the CMB photons when they pass through the interior of GCs. I will describe this phenomenon in more detail as this work is based on it.

1.2.3.1 The Sunyaev Zeldovich effect

The *Sunyaev Zeldovich (SZ) effect* (Sunyaev & Zeldovich 1970, 1972) is a small spectral distortion of the CMB photons due to inverse Compton scattering by high energy electrons in the hot gas of the ICM. As a result of this interaction, the CMB photons gain energy and the overall CMB spectrum is shifted towards higher frequencies, producing a characteristic spectral dependence that can be used to detect them (see Fig. 1.3). The energy is boosted by a quantity of the order of $k_B T_e / m_e c^2$, with k_B being the Boltzmann constant, T_e the electron temperature and m_e the electron mass (Birkinshaw 1999).

The SZ effect produces a drop of intensity of the CMB black-body spectrum at low frequencies and an increase of the intensity at high frequencies, the zero point is around $\nu_0 \simeq 218$ GHz. The temperature variation is around $T \lesssim 1$ mK for average sized GCs, and its amplitude can be expressed as

$$\frac{\Delta T_{SZ}}{T_0} = y f(x), \quad (1.1)$$

where y is the *Compton y-parameter*:

$$y = \int dl n_e \frac{k_B T_e}{m_e c^2} \sigma_T, \quad (1.2)$$

which represents the integrated electron pressure ($n_e T_e$) along the line of sight. The quantity σ_T is the Thomson cross section. This parameter accounts for the energy

Este documento incorpora firma electrónica, y es copia auténtica de un documento electrónico archivado por la ULL según la Ley 39/2015.
 Su autenticidad puede ser contrastada en la siguiente dirección <https://sede.ull.es/validacion/>

Identificador del documento: 3248012 Código de verificación: RmbjVJW6

Firmado por: ALEJANDRO AGUADO BARAHONA
 UNIVERSIDAD DE LA LAGUNA

Fecha: 01/03/2021 09:35:30

María de las Maravillas Aguiar Aguilár
 UNIVERSIDAD DE LA LAGUNA

22/03/2021 13:39:32

8 Chapter 1. Introduction: Galaxy Clusters through history of Cosmology

transfer from the electron plasma to the CMB. The quantity we are interested in is the total SZ flux, which is proportional to the mass of the gas component divided by the angular distance squared:

$$Y = \int y \, d\Omega \propto \frac{M_{gas}}{d_A^2(z)}. \quad (1.3)$$

The second factor of the right hand side in eq.1.1 represents the frequency modulation of the energy transfer. It can be expressed as a function of the dimensionless photon frequency, $x = h\nu/k_B T_{CMB}$:

$$f(x) = \left(x \frac{e^x + 1}{e^x - 1} - 4 \right) (1 + \delta_{SZ}(x, T_e)), \quad (1.4)$$

where $\delta_{SZ}(x, T_e)$ is a relativistic correction term. Equation 1.1 can be expressed in terms of the intensity rather than the temperature as:

$$\frac{\Delta I}{I_0} = y g(x), \quad (1.5)$$

with $I_0 = 2(k_B T)^3 / (hc)^2$ and the frequency dependency

$$g(x) = \frac{x^4 e^x}{(e^x - 1)^2} f(x). \quad (1.6)$$

There is a remarkable feature of both equations 1.1 and 1.5: they do not depend on the redshift because both ν and T_{CMB} evolve in the same way. This fact allow methods based on this effect to detect high redshift clusters in an ‘easy’ way since it does not suffer from redshift dimming, in contrast to X-ray emission.

So far, I have described the so called *thermal SZ effect*. There is an additional spectral distortion due to a Doppler term if the galaxy cluster is moving with respect to the CMB rest frame, the *kinetic SZ effect*. This component can be observed if the cluster has a peculiar velocity along the line of sight (Sunyaev & Zeldovich 1970, 1972), but it is indistinguishable from the CMB anisotropies using spectral information only. As the result of this effect is an absolute shift of the temperature, it can be either positive or negative depending on the relative velocity of the cluster (Birkinshaw 1999).

Although the *SZ effect* was theorised in the early 70’s, it was not until the last years of the decade when it was observed for the first time. I quote here the work with the OVRO 40 m telescope (Birkinshaw et al. 1978b,a). Nowadays, large SZ catalogues have been constructed. Ground-based observatories such as the South Pole Telescope (SPT) and the Atacama Cosmology Telescope (ACT) are still working on their products but they have already published plenty of catalogues (Staniszewski et al. 2009; Marriage et al. 2011; Hasselfield et al. 2013a; Bleem et al. 2015a, 2020; Hilton et al. 2018, 2020; Huang et al. 2020). From space, the *Planck* mission takes all the merits. It is the benchmark of this thesis and I will extensively talk about it in the next section.

Este documento incorpora firma electrónica, y es copia auténtica de un documento electrónico archivado por la ULL según la Ley 39/2015.
 Su autenticidad puede ser contrastada en la siguiente dirección <https://sede.ull.es/validacion/>

Identificador del documento: 3248012 Código de verificación: RmbjVJW6

Firmado por: ALEJANDRO AGUADO BARAHONA
 UNIVERSIDAD DE LA LAGUNA

Fecha: 01/03/2021 09:35:30

María de las Maravillas Aguiar Aguilár
 UNIVERSIDAD DE LA LAGUNA

22/03/2021 13:39:32

1.3 The Planck mission

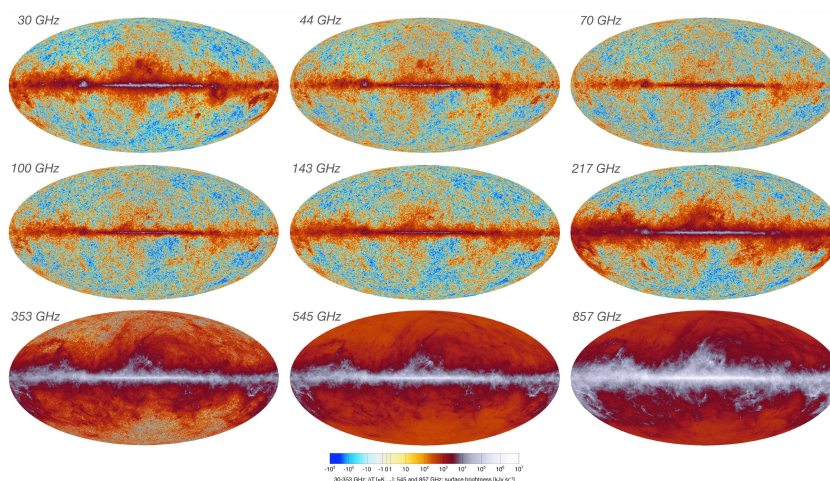


Figure 1.4: Fluctuations of sky emission in each of the nine Planck frequency bands (from 30 to 857 GHz) in intensity. Credit: Planck Collaboration I (2020)

1.3 The Planck mission

The *Planck* mission (The Planck Collaboration 2006) was the merge of two different proposals with similar objectives: the Cosmic Background Radiation Anisotropy Satellite (COBRAS) and the Satellite for Measurement of Background Anisotropies (SAMBA). It was originally named COBRAS/SAMBA and it was selected in 1995 as the third Medium-Sized Mission (M3) of ESA's Horizon 2000 Scientific Program. This mission was the natural continuation of the Cosmic Background Explorer (COBE; Boggess et al. 1992) and the Wilkinson Microwave Anisotropy Probe (WMAP; Bennett et al. 2003). *Planck* had unprecedented sensitivity and angular resolution in comparison with those missions. Its main goal was not only to map the full sky with an angular resolution of $\sim 5'$ but also to extract as much information as possible from the millimetre sky, including the secondary anisotropies such as the SZ effect (see section 1.2.3), the Sachs-Wolfe effect (Sachs & Wolfe 1967) and the polarisation of the CMB. In addition, it performed observations of infrared and radio emitters such as dusty galaxies and active galactic nuclei (AGN) (Planck Collaboration XV 2011). It studied the interstellar medium and made the Milky Way's first map at 3 mm (Planck Collaboration int. XIV 2014). This mission also observed the solar system to study the temperature and the microwave light curve of planets (Planck Collaboration int. LII 2017), asteroids, comets and the zodiacal light (Planck Collaboration XIV 2014)

The *Planck* satellite was launched on 14 May 2009 and stopped operations on 23 October 2013. It worked perfectly for almost 30 months, about twice the time originally

Este documento incorpora firma electrónica, y es copia auténtica de un documento electrónico archivado por la ULL según la Ley 39/2015.
 Su autenticidad puede ser contrastada en la siguiente dirección <https://sede.ull.es/validacion/>

Identificador del documento: 3248012 Código de verificación: RmbjVJW6

Firmado por: ALEJANDRO AGUADO BARAHONA
 UNIVERSIDAD DE LA LAGUNA

Fecha: 01/03/2021 09:35:30

María de las Maravillas Aguiar Aguilár
 UNIVERSIDAD DE LA LAGUNA

22/03/2021 13:39:32

10 Chapter 1. Introduction: Galaxy Clusters through history of Cosmology

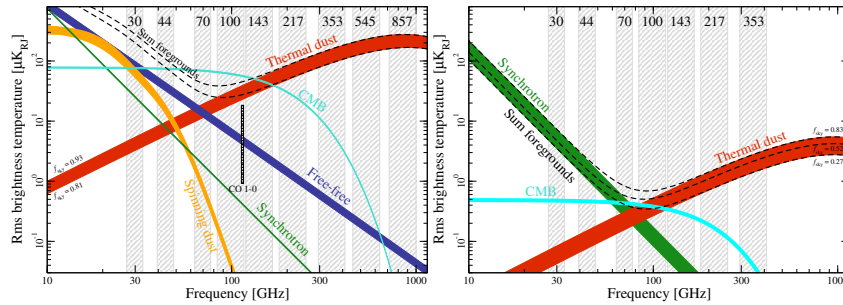


Figure 1.5: Frequency dependence of the main components of the sub-millimetre sky in temperature (left) and polarisation (right). The (vertical) grey bands show the Planck channels, with the coloured bands indicating the major signal and foreground components. Credit: Planck Collaboration I (2020)

required, and was able to perform five full-sky surveys with both instruments: the Low Frequency Instrument (LFI; Mandolesi et al. 2000) and the High Frequency Instrument (HFI; Lamarre et al. 2003).

The LFI was designed to observe the sky in three channels 30, 44 and 70 GHz, while the HFI increases the range to six channels at 100, 143, 217, 353, 545 and 857 GHz. The channel at 217 GHz is of special importance for the detection of the SZ effect which has its null at that value. The optimal windows in which the CMB component is dominant are the bands of 70 and 100 GHz. At higher frequencies, there are different physical processes that dominate the signal. These processes are mainly the thermal dust emission, the bremsstrahlung and synchrotron emission, the spinning dust grains and the CO line-emission (see Fig. 1.5). Despite of these foreground signals, the wide range of frequencies covered, allow us to accurately separate the foreground components from the CMB (Planck Collaboration XII 2014; Planck Collaboration IX 2016; Planck Collaboration X 2016; Planck Collaboration XXV 2016; Planck Collaboration IV 2020). Figure 1.6 shows the foreground amplitude maps derived from the *Planck* 2018 data set in intensity.

1.3.1 The PSZ2 catalogue

The PSZ2 catalogue (Planck Collaboration XXVII 2016) is the second *Planck* catalogue of SZ sources derived from the full 29 months of mission data. It is the third and last all-sky catalogue produced from *Planck* SZ data. The early Sunyaev-Zeldovich (ESZ; Planck Collaboration VIII 2011) catalogue presented 189 clusters detected from 10 months of survey data. The PSZ1 (Planck Collaboration XXIX 2014), the full-sky catalogue assembled from the nominal mission data, presented 1227 cluster candidates detected from 15.5 months of data. The PSZ2 presents 1653 candidates detected from the full HFI mission survey of 29 months. 1203 of them were confirmed in ancillary data and 1094 had redshift estimates at the time of its publication. The PSZ2 increased

Este documento incorpora firma electrónica, y es copia auténtica de un documento electrónico archivado por la ULL según la Ley 39/2015.
 Su autenticidad puede ser contrastada en la siguiente dirección <https://sede.ull.es/validacion/>

Identificador del documento: 3248012 Código de verificación: RmbjVJW6

Firmado por: ALEJANDRO AGUADO BARAHONA
 UNIVERSIDAD DE LA LAGUNA

Fecha: 01/03/2021 09:35:30

María de las Maravillas Aguiar Aguiar
 UNIVERSIDAD DE LA LAGUNA

22/03/2021 13:39:32

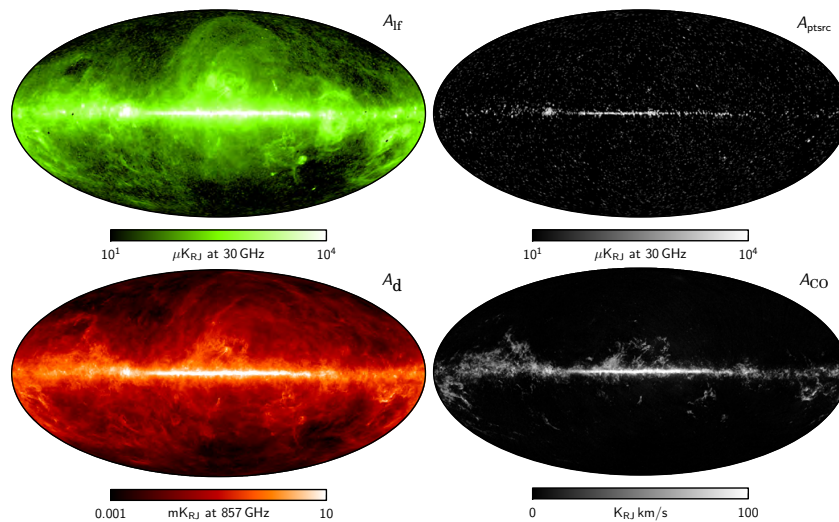


Figure 1.6: Foreground amplitude maps, derived from the Planck 2018 data set in intensity. Top-left panel: combined low-frequency foreground map at 40' FWHM resolution, evaluated at 30 GHz, and accounts for synchrotron, free-free, and anomalous microwave emission. Top-right panel: derived radio point source map, as observed in the 30 GHz frequency channel. Bottom-left panel: thermal dust emission at 10' FWHM resolution, evaluated at 857 GHz. Bottom-right panel: CO line-emission map, evaluated for the 100 GHz channel. Credit: Planck Collaboration IV (2020)

Este documento incorpora firma electrónica, y es copia auténtica de un documento electrónico archivado por la ULL según la Ley 39/2015.
 Su autenticidad puede ser contrastada en la siguiente dirección <https://sede.ull.es/validacion/>

Identificador del documento: 3248012 Código de verificación: RmbjVJW6

Firmado por: ALEJANDRO AGUADO BARAHONA
 UNIVERSIDAD DE LA LAGUNA

Fecha: 01/03/2021 09:35:30

María de las Maravillas Aguiar Aguilár
 UNIVERSIDAD DE LA LAGUNA

22/03/2021 13:39:32

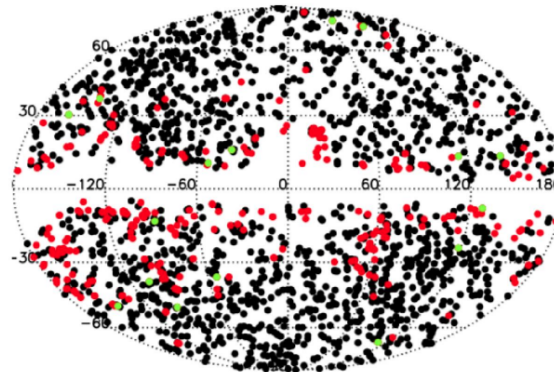


Figure 1.7: Distribution of raw SZ detections, with deleted infra-red flagged candidates in red and retained infra-red flagged detections in green. Black points denote detections without an IR flag. Credit: Planck Collaboration XXVII (2016).

the number of lower mass clusters available for study as well as many new high-redshift clusters, with respect to the previous catalogues. The distribution of raw SZ detections is shown in Fig. 1.7.

In order to construct the catalogues, the SZ detection and parameter estimations algorithms are a refined extension of the algorithms used for the PSZ1. Two of them (MMF1 and MMF3) are based on the same technique (matched multi-filter) while the third one (PwS for PowellSnakes) relies on Bayesian inference.

The matched multi-filter technique was first proposed for SZ maps by Haehnelt & Tegmark (1996) and later developed by Herranz et al. (2002) and Melin et al. (2006). This method has been also adopted by the SPT and ACT collaborations (Staniszewski et al. 2009; Marriage et al. 2011). The technique implemented specifically for *Planck* data consists in firstly divide each all-sky map into 640/504 tangential maps (14.66/10 degrees on a side) for MMF1/MMF3, respectively. Then, the tangential maps are filtered varying the cluster size from $\theta_S = 0.8$ to 32 arcmin. The peaks with a *signal-to-noise* (S/N) threshold of 4 are selected. The resultant candidates are combined into a single all-sky catalogue by merging candidates separated by less than 10 arcmin. In the MMF3, a second step is performed by creating sets of smaller rectangular frequency maps centred on the cluster candidates identified in the first step and the same procedure is repeated in these centred tangential maps. The background determination is better estimated and it yields to a more precise estimation of the sizes and fluxes of the candidates. This second step only applies for the MMF3 as the overlap of the tangential maps in the first step is small compared to MMF1 and PwS.

The PwS method is based on a fast, fully Bayesian approach to discrete object detection. It is designed to identify and characterise compact objects embedded in a

Este documento incorpora firma electrónica, y es copia auténtica de un documento electrónico archivado por la ULL según la Ley 39/2015.
 Su autenticidad puede ser contrastada en la siguiente dirección <https://sede.ull.es/validacion/>

Identificador del documento: 3248012 Código de verificación: RmbjVJW6

Firmado por: ALEJANDRO AGUADO BARAHONA
 UNIVERSIDAD DE LA LAGUNA

Fecha: 01/03/2021 09:35:30

María de las Maravillas Aguiar Aguilár
 UNIVERSIDAD DE LA LAGUNA

22/03/2021 13:39:32

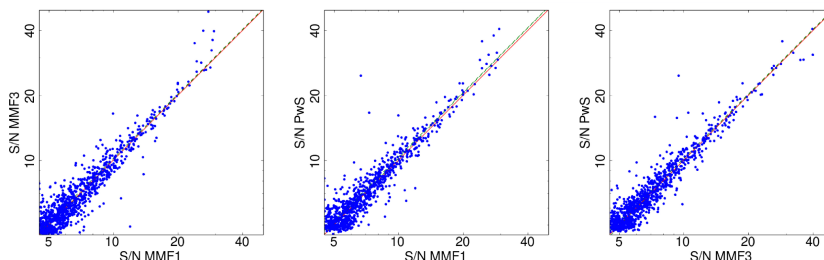


Figure 1.8: Comparison of the S/N estimates from the three detection codes. The dashed green curves show the best-fit relation for a correlation of 0.8 and the red line is the line of equality. Credit: Planck Collaboration XXVII (2016).

diffuse background, as described in Carvalho et al. (2009, 2012). It runs using about 2800 square patches of 14.66 degree on a side. It guarantees a very large overlap and, on average, each cluster is detected about 4.7 times. Then each catalogue for each patch is merged and criterion of acceptance/rejection is applied.

A comparison on the S/N estimates from the three detection codes is shown in Fig. 1.8

The product of each method is an image with the two-dimensional probability distribution in θ_S and Y for each detection, the coordinates of the centre of the candidate and the S/N ratio of detection. The individual catalogues also contain *Planck* measurements of the SZ mass observable, M_{SZ} as calculated using the Y-M scaling relation found in Planck Collaboration XX (2014) and an assumed redshift to break the Y- θ_S degeneracy (see Fig. 1.9). These are provided for each detection as functions of assumed redshift, in the range $0.01 \leq z \leq 1$. The mass topic is addressed on Section 1.4.

The final catalogue is built combining the three individual catalogues for each detection method into an union catalogue. The catalogue contains all objects detected by at least one of these three methods with a measured significance $S/N > 4.5$. To clean the PSZ2 catalogue from spurious detections associated with galactic diffuse emission, some additional restrictions were added into the pipeline, together with the removal of those detections confirmed to be spurious by the PSZ1 follow-ups.

1.3.2 Validation programs

In order to confirm the SZ candidates from the PSZ2, a first validation process was performed in Planck Collaboration XXVII (2016). *Planck* made a internal quality assessment to avoid redundant detection of candidates and a search for and rejection of solar system objects, artifacts, galactic sources, etc. Then, a cross match with the PSZ1 was performed, continuing the search for possible counterparts in the Meta-Catalogue of the compiled properties of X-ray detected Clusters of galaxies (MCXC) catalogue (Piffaretti et al. 2011) which is based on the *ROSAT* All Sky Survey (RASS; Voges

Este documento incorpora firma electrónica, y es copia auténtica de un documento electrónico archivado por la ULL según la Ley 39/2015.
 Su autenticidad puede ser contrastada en la siguiente dirección <https://sede.ull.es/validacion/>

Identificador del documento: 3248012 Código de verificación: RmbjVJW6

Firmado por: ALEJANDRO AGUADO BARAHONA
 UNIVERSIDAD DE LA LAGUNA

Fecha: 01/03/2021 09:35:30

María de las Maravillas Aguiar Aguiar
 UNIVERSIDAD DE LA LAGUNA

22/03/2021 13:39:32

14 Chapter 1. Introduction: Galaxy Clusters through history of Cosmology

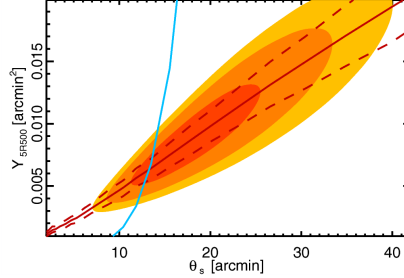


Figure 1.9: Posterior probability contours in the Y - θ_S plane for a cluster detected by *Planck*. The contours show the 68, 95 and 99% confidence levels. The red continuous line shows the ridge line of the contours, while the dashed lines are the $\pm 1\sigma$ probability value at each θ_S . The cyan line is the expected relation from X-ray at a given redshift. Credit: Planck Collaboration XXVII (2016).

Table 1.1: Summary for PSZ2 compared to PSZ1.

Sample	PSZ1 2013	PSZ1 2015	PSZ2	Common	New PSZ2
Union	1227	1227	1653	937	716
Intersection	546	546	827	502	325
Confirmed	861	947	1203	820	383
Candidates	366	292	546	99	447
Low reliability	142	131	143	39	104
Total X-ray	501	501	603	477	126
MCXC	455	455	551	427	124
SZ clusters	82	82	110	79	31

Note. Common samples are defined as those PSZ2 detections with the given property that has a counterpart with that property in the PSZ1 2015. The intersection comprises those detections common to all three detector codes. Low reliability candidates possess a poor neural-network quality assessment flag. In the PSZ1, low reliability candidates possess the lowest external quality assessment flag. “SZ clusters” here means clusters with SZ detections in ACT or SPT. “PSZ1 2013” refers to the 2013 release of the catalogue (Planck Collaboration XXIX 2014), and “PSZ1 2015” to an addendum updating the counterpart information of the catalogue (Planck Collaboration XXXII 2015). Credits: Planck Collaboration XXVII (2016).

Este documento incorpora firma electrónica, y es copia auténtica de un documento electrónico archivado por la ULL según la Ley 39/2015.
 Su autenticidad puede ser contrastada en la siguiente dirección <https://sede.ull.es/validacion/>

Identificador del documento: 3248012 Código de verificación: RmbjVJW6

Firmado por: ALEJANDRO AGUADO BARAHONA
 UNIVERSIDAD DE LA LAGUNA

Fecha: 01/03/2021 09:35:30

María de las Maravillas Aguiar Aguilár
 UNIVERSIDAD DE LA LAGUNA

22/03/2021 13:39:32

et al. 1999, 2000) and on the serendipitous *ROSAT* and Einstein cluster catalogues, in the Sloan Digital Sky Survey (SDSS; York et al. 2000), in the redMaPPer catalogue (Rykoff et al. 2014b), in NED¹, in the AllWISE mid-infrared source catalogues (Cutri et al. 2013) as well as in SZ catalogues such as the catalogues obtain by the SPT (Bleem et al. 2015b), by the ACT (Hasselfield et al. 2013b) and by direct follow-up with the Arc-minute Micro-kelvin Interferometer (AMI; Perrott et al. 2015).

In addition to the validation performed before the release of the catalogue, optical follow-up programs were planned in order to finish the process of validation. In particular, for the Northern Hemisphere, a systematic follow-up of PSZ2 sources was performed from the Canary Islands observatories and this is the program in which this thesis is embedded. It lasted for 4 complete terms (2015B, 2016A/B and 2017A). The observations were carried out at the Roque de los Muchachos Observatory (ORM) located at La Palma island (Spain). The three telescopes used in this work are (a) the 2.5 m Isaac Newton Telescope (INT) operated by the Isaac Newton Group of Telescopes, (b) the 3.6 m Italian Telescopio Nazionale Galileo (TNG) operated by the Galileo Galilei Foundation of the Istituto Nazionale di Astrofisica (INAF), and (c) the 10.4 m Gran Telescopio Canarias (GTC) operated by the Instituto de Astrofisica de Canarias (IAC).

1.4 Mass proxies and scaling relations

Observations of the ICM in X-ray, the SZ *effect*, the richness, the gravitational lensing and the galaxy velocities can trace the gravitational potential of a galaxy cluster. So one expects correlations, which can be described as scaling relations between the mass and the X-ray luminosity (L_X), the SZ flux (Y_{SZ}), the galaxy counts, the lensing parameters or the velocity dispersion of GCs (see Voit 2005; Allen et al. 2011, and references therein).

Following the theory of spherical collapse (Padmanabhan 1993; Liddle & Lyth 2000), the vitalised part of a GC approximately corresponds to a density contrast of $\Delta \sim 500$. The equation that governs the vitalised region is:

$$\frac{M_\Delta}{\frac{4\pi}{3} R_\Delta^3} = \Delta \cdot \rho_c(z), \quad (1.7)$$

where $\rho_c(z)$ is the critical density of the Universe at a certain epoch (z).

This equation is analogous to that of the dark matter halos within the corresponding radius R_Δ . It means that there is no characteristic scale in the gravitational collapse so the gas evolution is only driven by gravitation. From this consideration, it follows that the gas mass fraction (f_{gas}) is constant:

$$\frac{M_{gas,\Delta}}{M_\Delta} = f_{gas} = constant. \quad (1.8)$$

¹The NASA/IPAC Extragalactic Database (NED) is operated by the Jet Propulsion Laboratory, California Institute of Technology, under contract with the National Aeronautics and Space Administration

Este documento incorpora firma electrónica, y es copia auténtica de un documento electrónico archivado por la ULL según la Ley 39/2015.
 Su autenticidad puede ser contrastada en la siguiente dirección <https://sede.ull.es/validacion/>

Identificador del documento: 3248012 Código de verificación: RmbjVJW6

Firmado por: ALEJANDRO AGUADO BARAHONA
 UNIVERSIDAD DE LA LAGUNA

Fecha: 01/03/2021 09:35:30

María de las Maravillas Aguiar Aguilár
 UNIVERSIDAD DE LA LAGUNA

22/03/2021 13:39:32

16 Chapter 1. Introduction: Galaxy Clusters through history of Cosmology

Additionally, considering the gas in hydrostatic equilibrium (HE), the virial theorem states:

$$T_X = \beta \frac{G \mu m_p M_\Delta}{R_\Delta}, \quad (1.9)$$

where μ is the mean molecular weight in atomic mass units for an ionised plasma, m_p is the proton mass, T_X is the gas mean temperature, and β is the normalisation factor which depends on the cluster internal structure. As this structure is universal, β does not depend on redshift nor mass, i.e. it is a constant.

Therefore, a galaxy cluster can be unequivocally defined by its mass and redshift only. Using the basic equations 1.8 and 1.9 a scaling relation for each physical property, Q , can be derived. This relation links Q to the redshift and mass of the cluster:

$$Q \propto A(z) M_\Delta^\alpha \quad (1.10)$$

where $A(z)$ is the evolution factor that accounts for the evolution of the mean dark matter (and thus gas) density. Here are some examples of how theoretically the mass scales with different physical properties.

- The gas mass: $M_{\text{gas},\Delta} \propto M_\Delta$
- The temperature: $T_X \propto E^{2/3}(z) M_\Delta^{2/3}$
- The integrated SZ signal: $Y_{\text{SZ}} \propto E^{2/3}(z) M_\Delta^{5/3}$
- The integrated X-ray signal: $Y_X \propto E^{2/3}(z) M_\Delta^{5/3} \propto M_{\text{gas},\Delta} T_X$
- The X-ray luminosity: $L_X \propto E^{7/3}(z) M_\Delta^{4/3}$
- The velocity dispersion: $\sigma_v \propto M^{1/3}$

The estimation of the mass is accomplished through the so-called mass proxies, i.e. global physical properties, directly related to the mass, as the examples above. However, there are limitations to these estimates due to the normalisation of the relations that depends on the formation history. For this reason, the scaling laws must be calibrated using numerical simulations. Moreover, non gravitational physics such as cooling or AGN feedback play a significant role in the normalisation. Big efforts have been undertaken during the last decade to understand the dependence on these non gravitational factors (Munari et al. 2013; Pike et al. 2014; Planelles et al. 2014; Le Brun et al. 2014; Truong et al. 2018). Lately, there has been agreement by the community that the AGN feedback is the key ingredient to obtain realistic simulations and proper scaling relations.

Este documento incorpora firma electrónica, y es copia auténtica de un documento electrónico archivado por la ULL según la Ley 39/2015.
 Su autenticidad puede ser contrastada en la siguiente dirección <https://sede.ull.es/validacion/>

Identificador del documento: 3248012 Código de verificación: RmbjVJW6

Firmado por: ALEJANDRO AGUADO BARAHONA
 UNIVERSIDAD DE LA LAGUNA

Fecha: 01/03/2021 09:35:30

María de las Maravillas Aguiar Aguilár
 UNIVERSIDAD DE LA LAGUNA

22/03/2021 13:39:32

1.4.1 The mass bias

The problem in the mass estimation arises from the fact that the base assumption is that the gas/galaxies is in hydrostatic/dynamical equilibrium inside the dark matter potential. This assumption leads to an underestimation of the mass due to neglect bulk motions and turbulence in the ICM (Pratt et al. 2019). This effect, the so-called hydrostatic mass bias, is not very important for relaxed clusters ($\lesssim 10\%$) but for dynamically disturbed systems it can be critical (up to $\sim 30\%$). The mass bias parameter $(1 - b)$ is introduced as $M_X = (1 - b)_X M_{\text{true}}$ for $X = \text{X-ray, SZ, dynamical, lensing mass, respectively}$.

During the last decade, there has been plenty of observational works estimating the mass bias with different methodologies. A deeply revision has been made by Ferragamo (2019), here, I will briefly present the main results of each work.

The *Planck* Collaboration presented the calibration of their SZ masses using X-Ray observations of nearby clusters. Their estimation of the mass bias is very close to the HE mass bias as they used 20 nearby relaxed clusters. They assumed for the mass bias the median value obtained for the mass at the pivot point $M_{500} = 6 \times 10^{14}$ (Planck Collaboration XX 2014)

$$(1 - b) = 0.8_{-0.1}^{+0.2}. \quad (1.11)$$

The next four works presented here used the velocity dispersion as the mass proxy to estimate the dynamical mass and compared them to the SZ mass from different surveys and samples.

Ruel et al. (2014) estimated the mass bias from 43 SZ selected clusters from the SPT catalogues. Their sample are massive objects $2.7 \leq M_{500}^{\text{SPT}} \leq 18.0$ ($\times 10^{14} M_{\odot}$), clusters at $z \geq 0.3$. They found

$$\exp \left[\left\langle \ln \left(\frac{M_{200}^{\text{SPT}}}{M_{200}^{\text{dyn}}} \right) \right\rangle \right] = (1 - B) = 0.72 \pm 0.57. \quad (1.12)$$

In Sifón et al. (2016), the authors used a sub-sample of 21 GCs from the ACT cluster sample with $S/N > 5.1$, at redshifts $0.2 \leq z \leq 1.06$, in a mass range $1.0 < M_{200}^{\text{dyn}} < 13.0$ ($\times 10^{14} M_{\odot}$). They found

$$\frac{\langle M_{\text{SZ}} \rangle}{\langle M_{\text{dyn}} \rangle} = \frac{(1 - b_{\text{SZ}})}{\beta_{\text{dyn}}} = 1.10 \pm 0.13, \quad (1.13)$$

with $\beta_{\text{dyn}} = \langle M_{\text{dyn}} \rangle / \langle M_{\text{true}} \rangle$.

Amodeo et al. (2018) used 17 low- z clusters ($z < 0.5$) from the PZS2 catalogue in the mass range $3.0 < M_{200}^{\text{dyn}} < 14.0$ ($\times 10^{14} M_{\odot}$) founding a mass bias of

$$(1 - b) = 0.64 \pm 0.11. \quad (1.14)$$

To finish with the works that used the velocity dispersion as the mass proxy for the dynamical masses, Ferragamo et al. (2021, submitted) used 207 GCs from the PSZ1

Este documento incorpora firma electrónica, y es copia auténtica de un documento electrónico archivado por la ULL según la Ley 39/2015.
 Su autenticidad puede ser contrastada en la siguiente dirección <https://sede.ull.es/validacion/>

Identificador del documento: 3248012 Código de verificación: RmbjVJW6

Firmado por: ALEJANDRO AGUADO BARAHONA
 UNIVERSIDAD DE LA LAGUNA

Fecha: 01/03/2021 09:35:30

María de las Maravillas Aguiar Aguilár
 UNIVERSIDAD DE LA LAGUNA

22/03/2021 13:39:32

18 Chapter 1. Introduction: Galaxy Clusters through history of Cosmology

catalogue in the mass range $0.8 < M_{500}^{\text{dyn}} < 20 (\times 10^{14} M_{\odot})$ in the redshift interval $0.029 < z < 0.844$. They found

$$(1 - B) = \frac{(1 - b_{\text{SZ}})}{(1 - b_{\text{dyn}})} = 0.83 \pm 0.07 \pm 0.02. \quad (1.15)$$

Now, I will present 8 works that estimated the mass bias using weak lensing (WL) masses. The advantage of this kind of methodologies is that this mass can be considered the true mass but the problem is that it is very model dependent.

von der Linden et al. (2014) used 38 GCs from the Weighing the Giants (WtG) project in common with the PSZ1 and found the following value for the bias:

$$\left\langle \frac{M_{500}^{\text{SZ}}}{M_{500}^{\text{WtG}}} \right\rangle = (1 - b) = 0.698 \pm 0.062. \quad (1.16)$$

They also found a dependence of the mass bias with the mass:

$$\frac{M_{500}^{\text{SZ}}}{10^{15} M_{\odot}} = (0.699^{+0.059}_{-0.060}) \left(\frac{M_{500}^{\text{WtG}}}{10^{15} M_{\odot}} \right)^{0.68^{+0.15}_{-0.11}}. \quad (1.17)$$

Hoekstra et al. (2015) used 37 WL masses from the Canadian Cluster Comparison Project (CCCP) and from the PSZ1 to obtain

$$(1 - b) = 0.76 \pm 0.05. \quad (1.18)$$

They also fitted the relation allowing a dependence on the mass obtaining

$$\frac{M_{500}^{\text{SZ}}}{10^{15} h_{70}^{-1} M_{\odot}} = (0.76 \pm 0.04) \times \left(\frac{M_{500}^{\text{CCCP}}}{10^{15} h_{70}^{-1} M_{\odot}} \right)^{0.64 \pm 0.17}. \quad (1.19)$$

In Smith et al. (2016), the authors analysed a sample of 44 GCs common to the Local Cluster Substructure Survey (LoCuSS) and the PSZ2 catalogue. They found

$$(1 - b) = 0.95 \pm 0.04. \quad (1.20)$$

Battaglia et al. (2016) determined the mass bias from two samples consisting of 9 and 10 GCs from the Canada France Hawaii Telescope Stripe- Survey (CS82) in common with the ACT equatorial sample. They found

$$(1 - b)_{S/N > 5} = 0.87 \pm 0.50, (1 - b)_{S/N < 5} = 0.82 \pm 0.75. \quad (1.21)$$

Sereno et al. (2017) used 32 clusters from the PSZ2LenS sample extracted from the Canada France Hawaii Telescope Lensing Survey (CF-HTLenS; Heymans et al. 2012). They obtained

$$\exp \left(\frac{\ln \langle M_{\text{SZ}} \rangle}{\ln \langle M_{\text{WL}} \rangle} \right) = (1 - b) = 0.76 \pm 0.08. \quad (1.22)$$

Este documento incorpora firma electrónica, y es copia auténtica de un documento electrónico archivado por la ULL según la Ley 39/2015.
 Su autenticidad puede ser contrastada en la siguiente dirección <https://sede.ull.es/validacion/>

Identificador del documento: 3248012 Código de verificación: RmbjVJW6

Firmado por: ALEJANDRO AGUADO BARAHONA
 UNIVERSIDAD DE LA LAGUNA

Fecha: 01/03/2021 09:35:30

María de las Maravillas Aguiar Aguilár
 UNIVERSIDAD DE LA LAGUNA

22/03/2021 13:39:32

Penna-Lima et al. (2017) took 21 WL masses from the Cluster Lensing And Supernova survey with Hubble (CLASH; Postman et al. 2012). Thirteen of them were included in the PSZ1 catalogue while the remaining 8 had low significance in that catalogue and were extracted directly from the *Planck* SZ maps. A Bayesian analysis lead to a mass bias of

$$(1 - b) = 0.73 \pm 0.10, \quad (1.23)$$

To finish with, two more works are presented from the Hyper Suprime-Cam Subaru Strategic Program (HSC-SSP; Aihara et al. 2018). In the first one, 5 GCs in common with the PSZ2 are used by (Medezinski et al. 2018) finding a mass bias of

$$\frac{\langle M_{SZ} \rangle}{\langle M_{WL} \rangle} = (1 - b) = 0.80 \pm 0.14. \quad (1.24)$$

In a second work, (Miyatake et al. 2019) used 8 GCs in common with the ACTPol sample (Hilton et al. 2018) finding

$$\frac{\langle M_{SZ} \rangle}{\langle M_{WL} \rangle} = (1 - b) = 0.74^{+0.13}_{-0.12}. \quad (1.25)$$

Figure 1.10 and Table 1.2 summarise the results presented above.

The estimation of the mass bias is a critical topic when performing cosmological analysis. A small difference in its value can produce huge changes in the determination of cosmological parameters, in particular the matter content (Ω_M) and density fluctuation power spectrum amplitude (σ_8). This topic is still controversial. As shown above, there is not a consensus for the value of the mass bias. The *Planck* CMB analysis (Planck Collaboration VI 2020) derived a mass bias of

$$(1 - b) = 0.62 \pm 0.03, \quad (1.26)$$

which is in a great tension with every value presented here. At the moment there is no explanation plausible away from modified gravity theories that alleviate this tension between CMB and SZ analysis, but still extreme departure from general relativity is needed.

1.5 Cosmology with Galaxy Clusters

In this section, I will review the methods to perform cosmological analyses using clusters: baryon fractions f_{gas} , XSZ distances, SZ power spectrum and cluster counts $N(M, z)$. The results of this thesis will contribute to a cluster counts analysis that will be accomplished in the future.

1.5.1 Baryon fraction

The mass fraction of hot gas, f_{gas} , is a standard quantity related to cosmology by $f_{gas}(z) \propto d(z)^{3/2}$. This proportion comes from the fact that there is a mismatch in the

Este documento incorpora firma electrónica, y es copia auténtica de un documento electrónico archivado por la ULL según la Ley 39/2015.
 Su autenticidad puede ser contrastada en la siguiente dirección <https://sede.ull.es/validacion/>

Identificador del documento: 3248012 Código de verificación: RmbjVJW6

Firmado por: ALEJANDRO AGUADO BARAHONA
 UNIVERSIDAD DE LA LAGUNA

Fecha: 01/03/2021 09:35:30

María de las Maravillas Aguiar Aguilár
 UNIVERSIDAD DE LA LAGUNA

22/03/2021 13:39:32

20 Chapter 1. Introduction: Galaxy Clusters through history of Cosmology

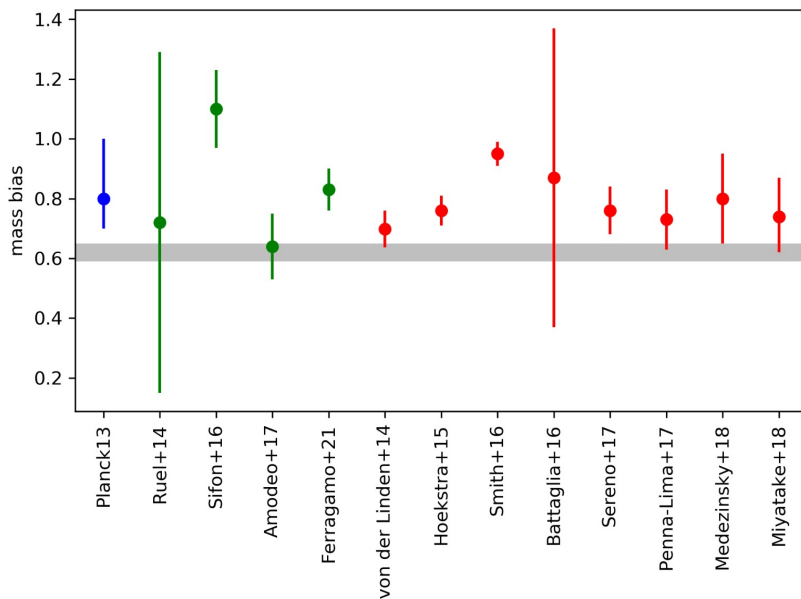


Figure 1.10: Value of the mass bias from previous studies. In blue, the result from Planck Collaboration XX (2014), using a scaling relation from X-ray observations; in green, the mass bias from $M_{SZ} - M_{dyn}$ scaling relations, in red, those from weak lensing studies, respectively. The grey shaded region represents the mass bias values that reconcile the tension between CMB and SZ number counts from Planck Collaboration VI (2020). Credits: Ferragamo (2019)

Este documento incorpora firma electrónica, y es copia auténtica de un documento electrónico archivado por la ULL según la Ley 39/2015.
 Su autenticidad puede ser contrastada en la siguiente dirección <https://sede.ull.es/validacion/>

Identificador del documento: 3248012 Código de verificación: RmbjVJW6

Firmado por: ALEJANDRO AGUADO BARAHONA
 UNIVERSIDAD DE LA LAGUNA

Fecha: 01/03/2021 09:35:30

María de las Maravillas Aguiar Aguiar
 UNIVERSIDAD DE LA LAGUNA

22/03/2021 13:39:32

Table 1.2: Summary of mass bias value from the literature. Credits: Ferragamo (2019)

SURVEY	REFERENCE SAMPLE	N. CLUSTERS	(1-b)	reference
X-RAY				
	<i>Planck</i> PSZ1	189	$0.8^{+0.1}_{-0.2}$	Planck Collaboration XXIX (2014)
VELOCITY DISPERSION				
	SPT	44	0.72 ± 0.57	Ruel et al. (2014)
	ACT	21	1.10 ± 0.13	Sifón et al. (2016)
	<i>Planck</i> PSZ2	17	0.64 ± 0.11	Amodeo et al. (2018)
	<i>Planck</i> PSZ1	207	$0.83 \pm 0.07 \pm 0.02$	Ferragamo et al. (2021, submitted)
WEAK LENSING				
WtG	<i>Planck</i> PSZ1	38	0.688 ± 0.072	von der Linden et al. (2014)
CCCP	<i>Planck</i> PSZ1	37	0.76 ± 0.05	Hoekstra et al. (2015)
LoCuSS	<i>Planck</i> PSZ2	44	0.95 ± 0.04	Smith et al. (2016)
CSS2	ACT	19	0.87 ± 0.50	Battaglia et al. (2016)
PSZ2LenS	<i>Planck</i> PSZ2	32	0.76 ± 0.08	Sereno et al. (2017)
CLASH	<i>Planck</i> PSZ1	21	0.73 ± 0.10	Penna-Lima et al. (2017)
HSC-SSP	<i>Planck</i> PSZ2	5	0.80 ± 0.15	Medezinski et al. (2018)
HSC-SSP	ACTPol	8	$0.74^{+0.13}_{-0.12}$	Miyatake et al. (2019)

dependence on metric distance between the gas mass ($\propto d^{5/2}$) and the total mass ($\propto d$) (Sasaki 1996; Pen 1997). The predicted value of $f_{gas}(z)$ of a halo at a given z can be expressed in terms of Ω_b and Ω_m as

$$f_{gas}(z) = \Upsilon(z) \left(\frac{\Omega_b}{\Omega_m} \right), \quad (1.27)$$

where $\Upsilon(z)$ is the term that accounts for baryon effects such as star formation. Different analysis showed that incorporating weak priors on h , $\Omega_b h^2$ and $\Upsilon(z)$ combined with the normalisation of the $f_{gas}(z)$ curve provides a constraint in Ω_m (LaRoque et al. 2006; Allen et al. 2008; Ettori et al. 2009).

1.5.2 Combined X-ray and SZ distances

A different way to determine distances to clusters is to combined X-ray and SZ measurements. Using the SZ signal y_{SZ} , which governs the CMB spectral shift, and a predicted signal y_X based on X-ray measurements of the ICM density and temperature, the angular diameter distance can be expressed as

$$d_A \propto \left(\frac{y_{SZ}}{y_X} \right)^2. \quad (1.28)$$

The dependence on the cosmology comes from the fact that $y_X(z) \propto d(z)^{1/2}$. Bonamente et al. (2006) used X-ray data from Chandra and SZ effect data from the Owens Valley Radio Observatory and the Berkeley-Illinois-Maryland Association interferometric arrays and obtained $H_0 = 76.9^{+3.9}_{-3.4} {}^{+10.0}_{-8.0} \text{ km s}^{-1} \text{ Mpc}^{-1}$ (statistical followed by systematic uncertainty at 68% confidence) for an $\Omega_M = 0.3$, $\Omega_\lambda = 0.7$. Kozmanyán et al. (2019) applied their own method to a sample of 61 galaxy clusters with redshifts up to $z < 0.5$ observed with Planck and XMM-Newton and found $H_0 = 67 \pm 3 \text{ km s}^{-1} \text{ Mpc}^{-1}$.

Este documento incorpora firma electrónica, y es copia auténtica de un documento electrónico archivado por la ULL según la Ley 39/2015.
 Su autenticidad puede ser contrastada en la siguiente dirección <https://sede.ull.es/validacion/>

Identificador del documento: 3248012 Código de verificación: RmbjVJW6

Firmado por: ALEJANDRO AGUADO BARAHONA
 UNIVERSIDAD DE LA LAGUNA

Fecha: 01/03/2021 09:35:30

María de las Maravillas Aguiar Aguilár
 UNIVERSIDAD DE LA LAGUNA

22/03/2021 13:39:32

1.5.3 SZ power spectrum

The thermal SZ signature (tSZ) of unresolved clusters can be studied statistically, as it is encoded inside the angular power spectrum at certain frequency. Heavy clusters contribute to its amplitude at large angular scales while the abundance of less massive clusters regulates the amplitude at small angular scales ($l \gtrsim 1000$). The halo population causes a fluctuation spectrum if the distortion shape from a single halo is described by an angular Fourier transform $\tilde{y}(M, z, l)$

$$C_l \propto \int dz \frac{dV}{dz} \int d \ln M \frac{dn}{d \ln M} \tilde{y}^2(M, z, l). \quad (1.29)$$

The Planck Collaboration, the SPT and the ACT have contributed to this topic in a very significant way. In particular, Planck Collaboration was the first to obtain the tSZ power spectrum up to multipole $l \approx 10^3$ (Planck Collaboration XXII 2016). They found a significant shift in the value $\sigma_8(\Omega_m/0.28)^{3/8}$ depending on the mass bias. In the case of a mass bias of 0.2 they have $\sigma_8(\Omega_m/0.28)^{3/8} = 0.80_{-0.03}^{+0.01}$, while for a mass bias of 0.4 they have $\sigma_8(\Omega_m/0.28)^{3/8} = 0.90_{-0.03}^{+0.01}$. Using the one-point PDF of the y -map, a methodology proposed by Rubiño-Martín & Sunyaev (2003), the ACT collaboration found $\sigma_8 = 0.793 \pm 0.018 \pm 0.017 \pm 0.006$ (Hill et al. 2014).

1.5.4 Cluster counts

Cluster counts, $N(M, z)$, is usually studied as the abundance of GCs as a function of redshift and mass (Carlstrom et al. 2002; Allen et al. 2011). In Planck Collaboration XX (2014) the analysis was integrated in mass, $N(z)$. And for the first time, Planck Collaboration XXIV (2016) introduced $N(q, z)$, that includes the information on the *signal-to-noise* ratio (q) as well (see Fig. 1.11):

$$\frac{dN}{dzdq} = \int d\Omega \int dM \frac{dN}{dzdM d\Omega} P[q|\tilde{q}_m(z, M, l, b)], \quad (1.30)$$

where

$$\frac{dN}{dzdM d\Omega} = \frac{dN}{dV dM} \frac{dV}{dzd\Omega}, \quad (1.31)$$

i.e., the dark matter halo mass function times the volume element, basically the cluster density distribution as a function of mass and redshift. Since the halo mass function depends on the mean matter density and the amplitude of matter clustering, one can use these observables to constraint Ω_m and σ_8 .

The quantity $P[q|\tilde{q}_m(z, M, l, b)]$ is the distribution of q (*signal-to-noise* ratio) given the mean value $\tilde{q}_m(z, M, l, b)$ which depends on the redshift, the mass and the sky coordinates, i.e. a way to represent the survey selection function not depending on the SZ observable (Y_{SZ}, θ_{SZ}) but on the mass and redshift.

The mass function and the survey selection function are two of the three key ingredients in which cluster counts is based. The third one is the mass bias ($1 - b$) derived from the scaling relation which converts observable quantities into mass. This mass bias was deeply discussed in Sect. 1.4.

Este documento incorpora firma electrónica, y es copia auténtica de un documento electrónico archivado por la ULL según la Ley 39/2015.
 Su autenticidad puede ser contrastada en la siguiente dirección <https://sede.ull.es/validacion/>

Identificador del documento: 3248012 Código de verificación: RmbjVJW6

Firmado por: ALEJANDRO AGUADO BARAHONA
 UNIVERSIDAD DE LA LAGUNA

Fecha: 01/03/2021 09:35:30

María de las Maravillas Aguiar Aguilár
 UNIVERSIDAD DE LA LAGUNA

22/03/2021 13:39:32

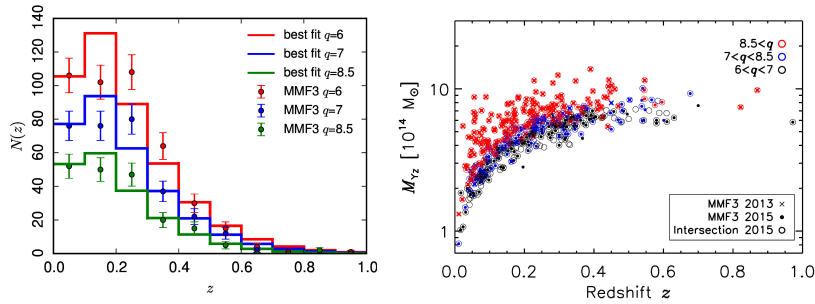


Figure 1.11: Left panel. Comparison of observed counts (points with error bars) with predictions of the best-fit models (solid lines) from the one-dimensional likelihood for three different thresholds applied to the 2015 MMF3 cosmology sample. Right panel. Mass-redshift distribution of the Planck cosmological samples colour-coded by their *signal-to-noise*, q . The baseline MMF3 2015 cosmological sample is shown as the small filled circles. Objects which were in the MMF3 2013 cosmological sample are marked by crosses, while those in the 2015 intersection sample are shown as open circles. The final samples are defined by $q > 6$. The mass M_{Yz} is the Planck mass proxy. Credits: Planck Collaboration XXIV (2016).

Planck Collaboration XXIV (2016) showed how the calibration of the mass bias is essential for the use of cluster counts as cosmological probes. Table 1.3 presents a comparison of the cosmological parameters estimation using different data sets, that correspond to different values of the mass bias and the baryonic acoustic oscillations (BAO), Big Bang nucleosynthesis (BBN) and H_0 priors.

The next two works use the weak gravitational lensing mass determinations from the Weighing the Giants program. Mantz et al. (2015) analysed a sample of X-ray-selected clusters from the ROSAT All-Sky survey, finding $\sigma_8(\Omega_m/0.3)^{0.17} = 0.81 \pm 0.03$. de Haan et al. (2016) analysed a sample of 377 clusters from the 2500 Square-degree SPT-SZ Survey, finding $\sigma_8(\Omega_m/0.27)^{0.3} = 0.797 \pm 0.031$.

Schellenberger & Reiprich (2017) use a sample of 64 X-ray selected GCs and the mass bias extracted from the simulations of Biffi et al. (2016) to obtain $\Omega_m = 0.303 \pm 0.009$, $\sigma_8 = 0.790^{+0.030}_{-0.028}$ and $S_8 = \sigma_8(\Omega_m/0.3)^{1/2} = 0.792 \pm 0.054$.

A recent study combining *Planck* CMB-Lensing and cluster counts (Zubeldia & Challinor 2019) took into account the new estimation of the optical depth τ from the *Planck* analysis found $\sigma_8(\Omega_m/0.33)^{0.25} = 0.765 \pm 0.035$ which is in good agreement with the *Planck* base- Λ CDM cosmology.

Este documento incorpora firma electrónica, y es copia auténtica de un documento electrónico archivado por la ULL según la Ley 39/2015.
 Su autenticidad puede ser contrastada en la siguiente dirección <https://sede.ull.es/validacion/>

Identificador del documento: 3248012 Código de verificación: RmbjVJW6

Firmado por: ALEJANDRO AGUADO BARAHONA
 UNIVERSIDAD DE LA LAGUNA

Fecha: 01/03/2021 09:35:30

María de las Maravillas Aguiar Aguilár
 UNIVERSIDAD DE LA LAGUNA

22/03/2021 13:39:32

Table 1.3: Summary of *Planck* 2015 cluster cosmology constraints.

Data set	$\sigma_8 \left(\frac{\Omega_m}{0.31}\right)^{0.3}$	Ω_m	σ_8
WtG + BAO + BBN	0.806 ± 0.032	0.34 ± 0.03	0.78 ± 0.03
CCCP + BAO + BBN [Baseline]	0.774 ± 0.034	0.33 ± 0.03	0.76 ± 0.03
CMBlens + BAO + BBN	0.723 ± 0.038	0.32 ± 0.03	0.71 ± 0.03
CCCP + H_0 + BBN	0.772 ± 0.034	0.31 ± 0.04	0.78 ± 0.04

Note. For detailed information about the different data sets, see Planck Collaboration XXIV (2016).

1.6 Objectives of this work

This thesis is focused on the observational study of galaxy clusters. Through this thesis, I will build a reference sample based on the PSZ2 catalogue which will be exploited in the future for cosmological purposes. The main scientific goals of this work are the following:

1. To perform the optical follow-up (128-MULTIPLE-16/15B) validating new galaxy cluster candidates detected by *Planck* satellite in the PSZ2 catalogue. The data processing and analysis of the images and spectra taken with optical telescopes (INT, TNG, GTC). To develop codes to identify the red sequence of the cluster candidates and to extract the cluster photometric redshifts.
2. To characterise the confirmed clusters estimating their precise redshift, velocity dispersion and mass, as well as possible interacting substructures.
3. To characterise the $M_{SZ} - M_{dyn}$ scaling relation, studying the existence of possible biases. To do so, the analysis will include the sample of clusters characterised in the 128-MULTIPLE-16/15B observational program, which are those detected in the *Planck* SZ maps with lower *signal-to-noise*, and other clusters already validated from the PSZ2 catalogue with higher *signal-to-noise*, for which there is multitude of radial velocities in public archives, mainly in the SDSS archive. Finally, to obtain the mass bias parameter $(1 - b)$, which will be the base for future cosmological analysis.

Este documento incorpora firma electrónica, y es copia auténtica de un documento electrónico archivado por la ULL según la Ley 39/2015.
 Su autenticidad puede ser contrastada en la siguiente dirección <https://sede.ull.es/validacion/>

Identificador del documento: 3248012 Código de verificación: RmbjVJW6

Firmado por: ALEJANDRO AGUADO BARAHONA
 UNIVERSIDAD DE LA LAGUNA

Fecha: 01/03/2021 09:35:30

María de las Maravillas Aguiar Aguilár
 UNIVERSIDAD DE LA LAGUNA

22/03/2021 13:39:32

2

The *Planck* PSZ2 optical follow-up: observational strategy

This Chapter is the compilation of a series of papers where optical characterisation of SZ sources were performed using the Canary Islands Observatories: Streblyanska et al. (2019, hereafter Paper I) and Aguado-Barahona et al. (2019, hereafter Paper II). They are based on the long-time program 128-MULTIPLE-16/15B (hereafter LP15) to study the PSZ2 sources. The main motivation of these follow-up campaigns is to identify and confirm optical cluster counterparts of those PSZ2 targets in the Northern Hemisphere with no known counterparts at the time of publication of the PSZ2 catalogue. We perform photometric and spectroscopic observations in order to study the optical richness and estimate the velocity dispersion of the GCs. The observational strategy is presented in this Chapter while the results of the program are detailed in Chapter 3. We also estimate the dynamical mass and compare it to the SZ mass in order to calibrate the scaling relation $M_{SZ} - M_{dyn}$ (Chapter 4).

2.1 The LP15 program: sample definition and strategy

The main idea of our observational effort was to perform a systematic follow-up of the complete set of PSZ2 cluster candidates in the northern sky, with no confirmed counterparts at the moment of the catalogue publication. We found that for declination $Dec. > -15^\circ$ this corresponded to 190 targets, out of the 350 sources with no counterparts in the full sky. We define the LP15 sample as these 190 sources. This sample was observed during 4 semesters, 2015B–2017A, in the frame of the long-term program (128-MULTIPLE-16/15B, P.I. José Alberto Rubiño). All the observations were carried out at the Roque de los Muchachos Observatory (ORM) on the island of La Palma (Spain) using the following telescopes: the 2.5 m Isaac Newton Telescope (INT), the 3.5 m Italian Telescopio Nazionale Galileo (TNG), and the 10.4 m Gran Telescopio Canarias (GTC). Photographs of these telescopes and the instruments used for this program are shown in figures 2.1 and 2.2. For these three telescopes, we requested in total 44 nights, approxi-

Este documento incorpora firma electrónica, y es copia auténtica de un documento electrónico archivado por la ULL según la Ley 39/2015.
Su autenticidad puede ser contrastada en la siguiente dirección <https://sede.ull.es/validacion/>

Identificador del documento: 3248012 Código de verificación: RmbjVJW6

Firmado por: ALEJANDRO AGUADO BARAHONA
UNIVERSIDAD DE LA LAGUNA

Fecha: 01/03/2021 09:35:30

María de las Maravillas Aguiar Aguilár
UNIVERSIDAD DE LA LAGUNA

22/03/2021 13:39:32

Table 2.1: Summary information for the 2-years long-term program LP15.

Telescope	Aperture [m]	Instrument	N_{nights}	$N_{\text{ima}}(\text{y1/y2})$	$N_{\text{spec}}(\text{y1/y2})$
INT	2.5	WFC	21	210 (102/108)	–
TNG	3.5	DOLORES	13	–	33 (16/17)
GTC	10.4	OSIRIS	80h (~ 10 nights)	–	55 (24/31)

Column 4 shows the total number of awarded nights per telescope. The last two columns present the total number of observed SZ clusters (imaging and spectroscopy), with the separated information for the first and second year of the program.

mately 50% of them were dedicated to obtain photometric data (INT) and other 50% of nights to spectroscopic observations (TNG and GTC). We summarised the main information about LP15 in Table 2.1. Our sample of 190 sources corresponded to $\sim 54\%$ of all unidentified PSZ2 objects, making our program the largest optical validation campaign of unconfirmed PSZ2 clusters to date.

Figure 2.3 presents the distribution of cluster counts as a function of S/N for the full sample of sources observed during LP15 campaign, in comparison with the total set of 1003 PSZ2 sources located at $\text{Dec.} > -15^\circ$, defined as the PSZ2-North sample (see Sect. 3.5). As it was expected, most of our sources have $S/N < 6$, as being the most difficult to validate using some serendipitous shallow surveys available before our program.

We adopt an observational strategy very similar to ITP13-08 Program (PSZ1 sources Planck Collaboration int. XXXVI 2016; Barrena et al. 2018, 2020). Before including PSZ2 sources for photometric observations, we did the initial pre-screenings of proposed targets searching for possible counterparts in the SDSS. In Streblyanska et al. (2018) we presented the results of such pre-screening using the Sloan Digital Sky Survey (SDSS)¹ DR12 photometric and spectroscopic data. If a cluster counterpart is confirmed in the SDSS data, new imaging observations were not required in our LP15 program and the cluster was directly considered for spectroscopy with the aim of obtaining its mean redshift, velocity dispersion, and dynamical mass. Galaxy cluster members with SDSS spectroscopic information were also considered for the mean cluster redshift calculation. After such pre-screening, we include all unidentified PSZ2 sources as targets for the deep images using g' , r' , and i' broad band filters.

If cluster counterparts were identified using either our images or SDSS data, we performed spectroscopic observations using multi-object spectroscopy (MOS). We use the GTC telescope to observe the most distant cluster candidates (at $z_{\text{phot}} > 0.354$), while TNG were used for the nearest ones (at $z_{\text{phot}} < 0.35$). As the last step, taking into account all the photometric and spectroscopic information, the cluster validation was performed using the selection criteria outlined in Section 3.1.

¹<http://skyserver.sdss.org>

Este documento incorpora firma electrónica, y es copia auténtica de un documento electrónico archivado por la ULL según la Ley 39/2015.
 Su autenticidad puede ser contrastada en la siguiente dirección <https://sede.ull.es/validacion/>

Identificador del documento: 3248012 Código de verificación: RmbjVJW6

Firmado por: ALEJANDRO AGUADO BARAHONA
 UNIVERSIDAD DE LA LAGUNA

Fecha: 01/03/2021 09:35:30

María de las Maravillas Aguiar Aguiar
 UNIVERSIDAD DE LA LAGUNA

22/03/2021 13:39:32



Figure 2.1: Top panel: Isaac Newton Telescope (INT). Credit: IAC. Bottom panel: Telescopio Nazionale Galileo (TNG) on the left and Gran Telescopio Canarias (GTC) on the right under a spectacular sunset. Credit: Giovanni Tessicini/TNG.

Este documento incorpora firma electrónica, y es copia auténtica de un documento electrónico archivado por la ULL según la Ley 39/2015.
Su autenticidad puede ser contrastada en la siguiente dirección <https://sede.ull.es/validacion/>

Identificador del documento: 3248012 Código de verificación: RmbjVJW6

Firmado por: ALEJANDRO AGUADO BARAHONA
UNIVERSIDAD DE LA LAGUNA

Fecha: 01/03/2021 09:35:30

María de las Maravillas Aguiar Aguilár
UNIVERSIDAD DE LA LAGUNA

22/03/2021 13:39:32

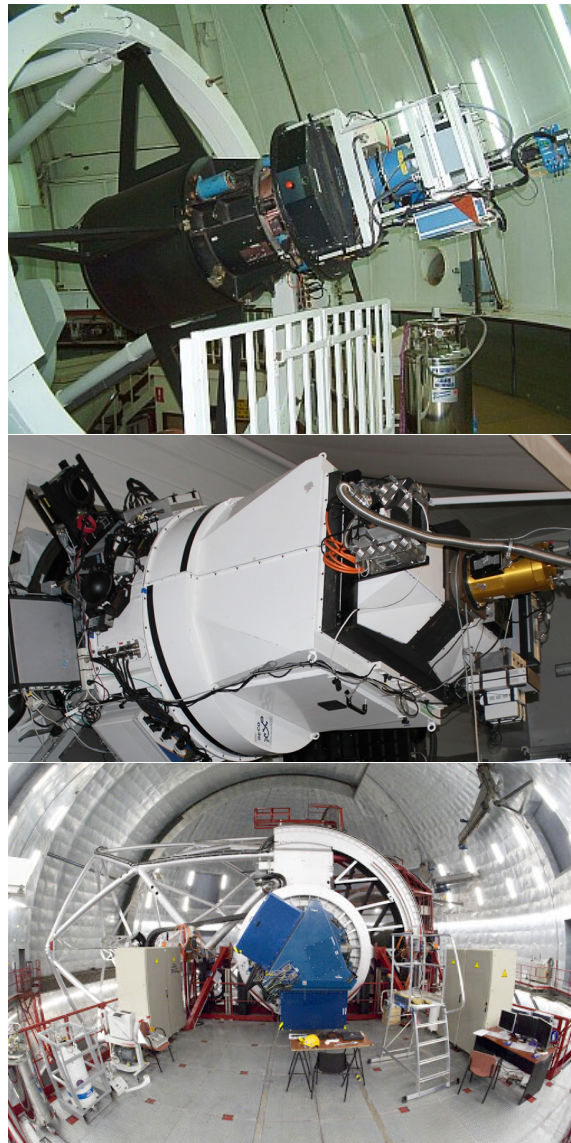


Figure 2.2: Top panel: the Wide Field Camera (WFC) at INT. Credit: Isaac Newton Group of Telescopes (ING). Middle panel: DOLORES spectrograph at TNG. Credit: La Palma 24. Bottom panel: OSIRIS spectrograph at GTC. Credit: Miguel Briganti (SMM/IAC).

Este documento incorpora firma electrónica, y es copia auténtica de un documento electrónico archivado por la ULL según la Ley 39/2015.
Su autenticidad puede ser contrastada en la siguiente dirección <https://sede.ull.es/validacion/>

Identificador del documento: 3248012 Código de verificación: RmbjVJW6

Firmado por: ALEJANDRO AGUADO BARAHONA
UNIVERSIDAD DE LA LAGUNA

Fecha: 01/03/2021 09:35:30

María de las Maravillas Aguiar Aguilár
UNIVERSIDAD DE LA LAGUNA

22/03/2021 13:39:32

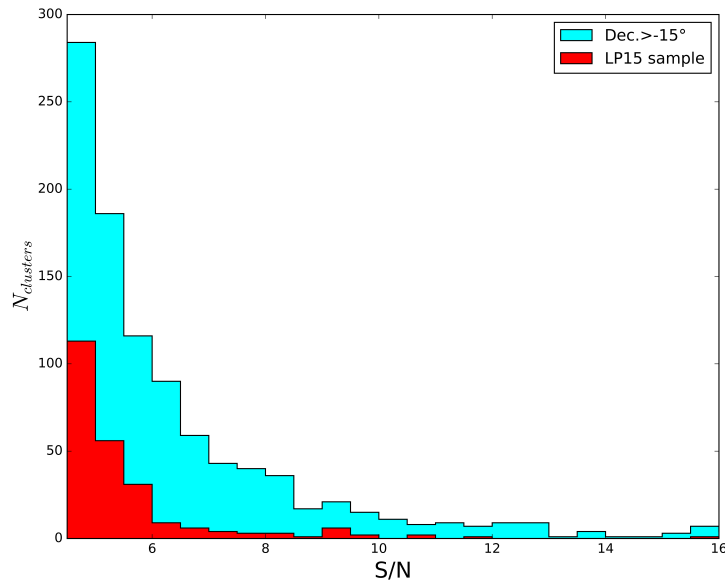


Figure 2.3: Distribution of PSZ2 objects as a function of the S/N of the SZ detection, and sample definition for this program. For displaying purposes, we only show the S/N range up to 16, as this is the maximum S/N value in our sub-sample. The complete sample of sources at $\text{Dec.} > -15^\circ$ (represented in light blue) has additional 26 clusters uniformly distributed in the range $16 < S/N < 50$. The sources observed during LP15 are shown in red. The bin size is 0.5.

Este documento incorpora firma electrónica, y es copia auténtica de un documento electrónico archivado por la ULL según la Ley 39/2015.
 Su autenticidad puede ser contrastada en la siguiente dirección <https://sede.ull.es/validacion/>

Identificador del documento: 3248012 Código de verificación: RmbjVJW6

Firmado por: ALEJANDRO AGUADO BARAHONA
 UNIVERSIDAD DE LA LAGUNA

Fecha: 01/03/2021 09:35:30

María de las Maravillas Aguiar Aguilár
 UNIVERSIDAD DE LA LAGUNA

22/03/2021 13:39:32

Table 2.2: Completeness and limit magnitudes for WFC/INT.

Filters	Completeness magnitudes	Limit magnitudes
g'	22.4	24.0
r'	21.8	23.2
i'	21.4	22.6

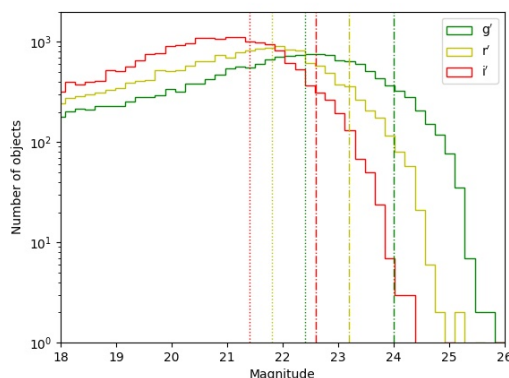


Figure 2.4: Magnitude histograms for 10 random fields observed during the LP15 program with the WFC/INT. The green, yellow and red solid, dotted and dash-dotted lines represent g' , r' and i' counts, completeness and limit magnitudes respectively.

2.2 The LP15 program: imaging

2.2.1 Observations

Imaging observations were obtained using the Wide Field Camera (WFC) installed in the 2.5 m Isaac Newton Telescope (INT). The WFC camera at the INT is a four CCDs mosaic with a field of view (FoV) of $34' \times 34'$ and a pixel scale of $0.''33$. To acquire the images, we have performed a small dithering technique of three points with offsets of $10''$, in order to clear the resultant image from bad pixels, vignetting and fringing effects and be able to minimise the impact of cosmic rays. The exposure times vary between 900 s and 1500 s per band depending on the magnitudes of the galaxies observed. Table 2.2 shows the completeness and limit magnitudes for the WFC/INT. We define these values at the point when the counts fall to 90% and 30% of the count peak, respectively (see Fig. 2.4). The seeing conditions also vary from $0.''8$ to $1.''8$.

Este documento incorpora firma electrónica, y es copia auténtica de un documento electrónico archivado por la ULL según la Ley 39/2015.
 Su autenticidad puede ser contrastada en la siguiente dirección <https://sede.ull.es/validacion/>

Identificador del documento: 3248012 Código de verificación: RmbjVJW6

Firmado por: ALEJANDRO AGUADO BARAHONA
 UNIVERSIDAD DE LA LAGUNA

Fecha: 01/03/2021 09:35:30

María de las Maravillas Aguiar Aguilár
 UNIVERSIDAD DE LA LAGUNA

22/03/2021 13:39:32

2.2.2 Data reduction and photometry

The photometric data were reduced using standard IRAF² routines. The USNO B1.0 catalogue (Monet et al. 2003) was used as reference and the astrometry were obtained using the `images.imcoords` task. The typical *rms* obtained across the full FoV was $\sim 0.''2$. The photometric calibration refers to SDSS photometry and SDSS standard fields. Images obtained during non-photometric nights were calibrated in posteriors runs. In order to detect the sources in the images, we have used `SExtractor` (Bertin & Arnouts 1996) in single-image mode. We detected sources in *g'*-, *r'*- and *i'*-bands with $S/N \sim 3$ in at least 10 adjacent pixels that implies a 1.5σ detection thresholds in the filtered maps. Using the `MAGAUTO` mode, elliptical aperture photometry was performed setting the `Kron factor` and the `minimum radius` to the default values (2.5 and 3.5 respectively). Finally, the resultant catalogues were merged to create a master catalogue containing the information of every band.

We also used images in *g'*-, *r'*- and *i'*-bands to create the deep RGB images which have been used for the visual inspection in our validation work (see Chapter 3).

2.2.3 Photometric redshift estimation

Our method to identify the member galaxies in the galaxy cluster candidates and to derive the photometric redshifts is based on the cluster-red sequence (CRS) method by Gladders & Yee (2000). Colour cuts in (*g' - r'*) or (*r' - i'*) are combined with the spatial distribution of the full catalogue to search for possible candidates. We have modified this method with the empirical relations of Lopes (2007) for the photometric redshifts of galaxy clusters (see Sect. 4.2 in that paper), to obtain photometric redshift estimates for galaxy overdensities and to select the probable cluster members for spectroscopic follow-up observations. To the first order, the photometric redshifts can be estimated with

$$z_{\text{phot}} \approx 0.361 (g' - r') - 0.278, \text{ if } (r' - i') \lesssim 0.75, \quad (2.1)$$

$$z_{\text{phot}} \approx 0.364 (r' - i') + 0.182, \text{ if } (r' - i') \gtrsim 0.75. \quad (2.2)$$

After applying our method to all candidates, the results are evaluated and consolidated with a careful inspection of the individual and RGB images, as well as the colour-magnitude diagrams (CMD). Figure 2.5 shows an example of RGB image and figure 2.6 presents the CMD of the same cluster. We found that the visual inspection is particularly important for detecting low-redshift systems ($z < 0.1$), poor systems, fossil groups or high redshift systems ($z > 0.6$), which usually are not easily detected by automatic algorithms searching for over-densities in colour space.

²IRAF (<http://iraf.noao.edu/>) is distributed by the National Optical Astronomy Observatories, which are operated by the Association of Universities for Research in Astronomy, Inc., under cooperative agreement with the National Science Foundation.

Este documento incorpora firma electrónica, y es copia auténtica de un documento electrónico archivado por la ULL según la Ley 39/2015.
 Su autenticidad puede ser contrastada en la siguiente dirección <https://sede.ull.es/validacion/>

Identificador del documento: 3248012 Código de verificación: RmbjVJW6

Firmado por: ALEJANDRO AGUADO BARAHONA
 UNIVERSIDAD DE LA LAGUNA

Fecha: 01/03/2021 09:35:30

María de las Maravillas Aguiar Aguilár
 UNIVERSIDAD DE LA LAGUNA

22/03/2021 13:39:32



Figure 2.5: WFC/INT RGB image of the optical counterpart of PSZ2 G152.40+75.00. The image is centred at the BCG position. This cluster is located at $z_{\text{spec}} = 0.455$ and the estimated photometric redshift from the RS is $z_{\text{phot}} = 0.42 \pm 0.03$. The colour-magnitude diagram for this cluster is shown in figure 2.6.

2.3 The LP15 program: spectroscopy

2.3.1 Observations

Spectroscopic observations were obtained using the multi-object spectrographs Device Optimised for the LOW RESolution (DOLORES) installed at the TNG and Optical System for Imaging and low-Intermediate-Resolution Integrated Spectroscopy (OSIRIS) mounted in the GTC.

DOLORES is a low resolution spectrograph and camera mounted in the Nasmyth B focus of the TNG. In MOS mode, it can carry up to 5 masks per night, allowing us to include between 40 and 50 slits per mask. It has a CCD of 2048×2048 pixels with a pixel size of $13.5 \mu\text{m}$ and a plate scale of $0.''252/\text{pixel}$. We obtained the spectra using the LR-B grism which provides a resolution of $R = 600$, a dispersion of $2.75 \text{ \AA}/\text{pixel}$ and a wavelength coverage in the range 3800–8500 \AA . We obtained Hg-Ne and He arcs in order to make the wavelength calibration of the spectra achieving a *rms* error below $0.1 \text{ \AA}/\text{pixel}$ over the whole wavelength range. We exposed typically 3×1800 s per mask but depending on the magnitude of the galaxies observed, this time could change.

OSIRIS is a low and intermediate resolution spectrograph and camera located in the Nasmyth-B focus of the GTC. Its MOS mode allows up to 70 slits per mask with a typical length of $4\text{--}5''$. The instrument is composed of a double CCD of 2048×4096 pixels with a pixel size of $15 \mu\text{m}$ and a plate scale of $0.''13 \text{ pixel}^{-1}$. In this program we have used the R300B grism which operates in the range 4000–9000 \AA and gives a dispersion of $5.2 \text{ \AA} \text{ pixel}^{-1}$ using the 2×2 binning set-up ($R \sim 500$). We obtained Hg-Ar and Ne arcs in order to make the wavelength calibration of the spectra achieving a *rms* error

Este documento incorpora firma electrónica, y es copia auténtica de un documento electrónico archivado por la ULL según la Ley 39/2015.
 Su autenticidad puede ser contrastada en la siguiente dirección <https://sede.ull.es/validacion/>

Identificador del documento: 3248012 Código de verificación: RmbjVJW6

Firmado por: ALEJANDRO AGUADO BARAHONA
 UNIVERSIDAD DE LA LAGUNA

Fecha: 01/03/2021 09:35:30

María de las Maravillas Aguiar Aguiar
 UNIVERSIDAD DE LA LAGUNA

22/03/2021 13:39:32

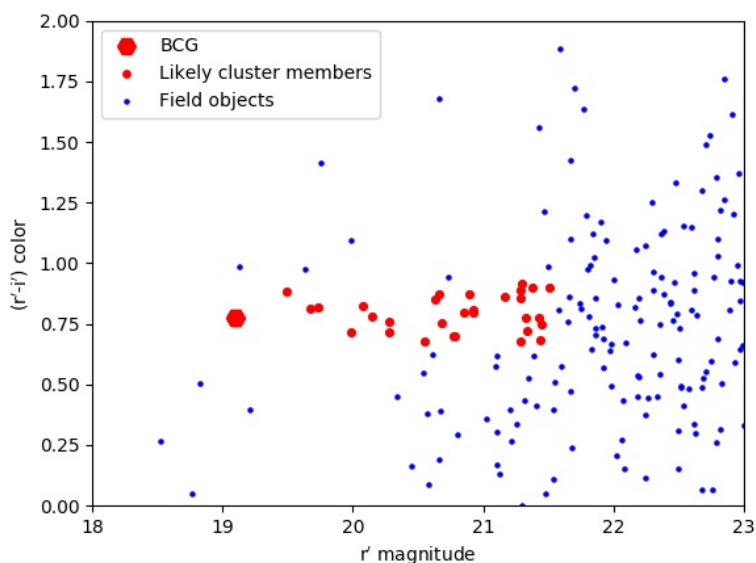


Figure 2.6: Colour-magnitude diagram ($r'-i'$, r') for PSZ2 G152.40+75.00. The red hexagon represents the BCG and together with the red circles (likely cluster members) form the red sequence of the cluster. Blue dots represent field objects. The RGB image of this cluster is shown in figure 2.5.

Este documento incorpora firma electrónica, y es copia auténtica de un documento electrónico archivado por la ULL según la Ley 39/2015.
 Su autenticidad puede ser contrastada en la siguiente dirección <https://sede.ull.es/validacion/>

Identificador del documento: 3248012 Código de verificación: RmbjVJW6

Firmado por: ALEJANDRO AGUADO BARAHONA
 UNIVERSIDAD DE LA LAGUNA

Fecha: 01/03/2021 09:35:30

María de las Maravillas Aguiar Aguilár
 UNIVERSIDAD DE LA LAGUNA

22/03/2021 13:39:32

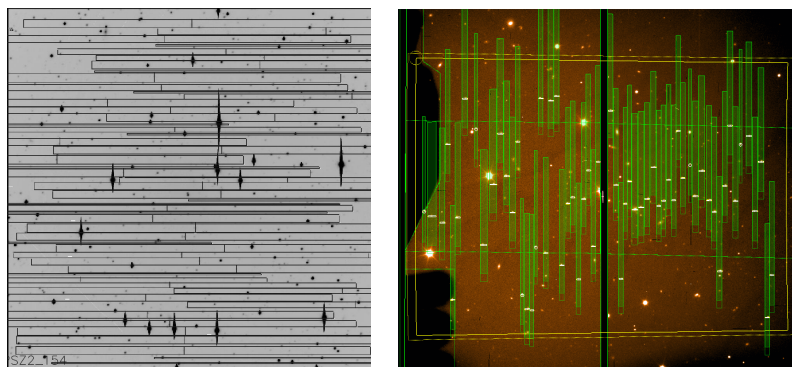


Figure 2.7: Left panel: DOLORES/TNG MOS mask of PSZ2 G042.54+18.02. Black rectangles represent the position of the expected spectra. Right panel: OSIRIS/GTC MOS mask of PSZ2 G120.76+44.14. Green regions represent the position of the expected spectra. The MOS FoV lies within the yellow lines.

below $0.2 \text{ \AA pixel}^{-1}$ over the whole wavelength range. We exposed typically $3 \times 1000 \text{ s}$ per mask obtaining typical $S/N \sim 5$ for galaxies with magnitudes $r' = 21.6$.

The design of the masks has been a very time consuming process. I was personally responsible for the design of the great majority of the masks used for this program. The softwares used were the TNG Interactive Mask Design Interface (IMDI), developed by Enrico Held (INAF-Padova Observatorio) and the MaskDesigner tool (MD), design by Txinto Vaz Cedillo (IAC). The masks were designed by using previous images obtained for each field in the corresponding instrument. We used RGB images (composed by g' -, r' - and i' -bands taken in the INT) as reference and we included slits with galaxies considered cluster likely members, with coherent colours and laying in the red-sequence of the clusters (see Sec. 2.2.3). By using this criteria, actual cluster members were selected with a success rate of typically 50–60 % in the inner regions of the cluster while in the outer regions ($> 0.3 \text{ Mpc}$ from the bright cluster galaxy, BCG) the success rate was around 20%. For this thesis, approximately 90 masks were designed.

2.3.2 Data reduction

The reduction process of the spectra followed the subsequent steps: combination of images, subtraction of sky component from each slit, extraction of spectra, cosmic ray rejection and finally wavelength calibration. Every step was carried out using standard IRAF tasks. We decided not to apply bias and flat-field corrections, because, after meticulous tests we only obtain data with poor S/N of the spectra. We used Hg-Ne and He-Ne arcs for DOLORES spectra and Hg-Ar and Ne arcs for OSIRIS spectra to perform the wavelength calibration. Approximately 5000 spectra have been reduced in this thesis.

Este documento incorpora firma electrónica, y es copia auténtica de un documento electrónico archivado por la ULL según la Ley 39/2015.
 Su autenticidad puede ser contrastada en la siguiente dirección <https://sede.ull.es/validacion/>

Identificador del documento: 3248012 Código de verificación: RmbjVJW6

Firmado por: ALEJANDRO AGUADO BARAHONA
 UNIVERSIDAD DE LA LAGUNA

Fecha: 01/03/2021 09:35:30

María de las Maravillas Aguiar Aguilár
 UNIVERSIDAD DE LA LAGUNA

22/03/2021 13:39:32

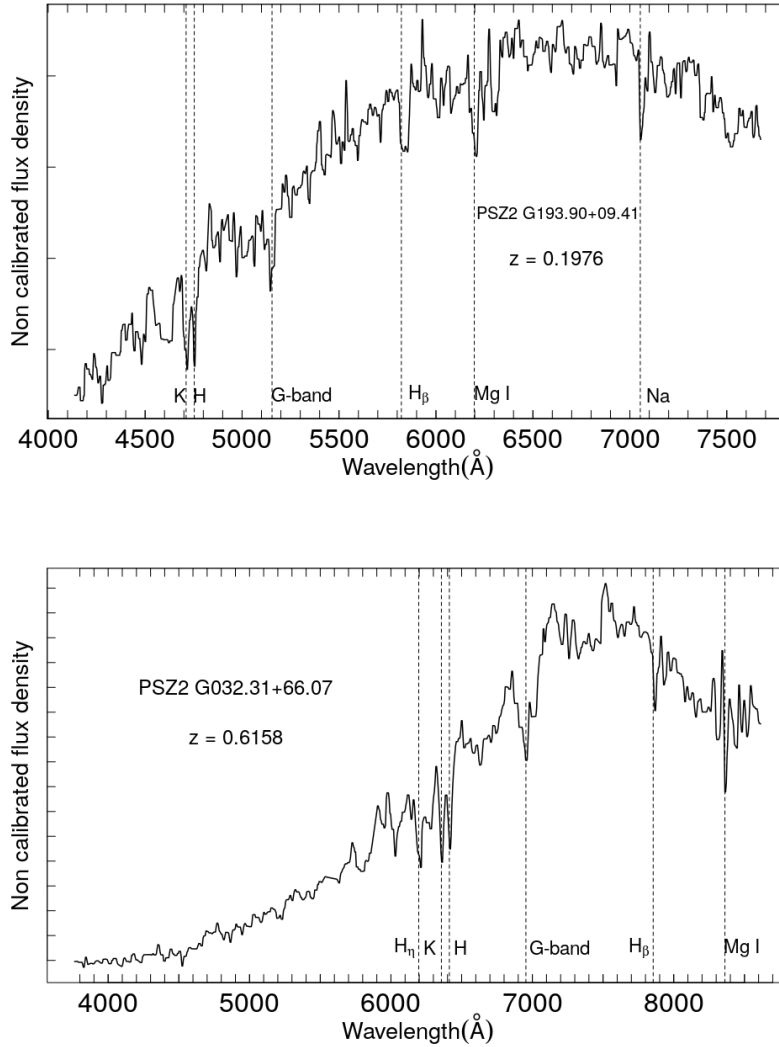


Figure 2.8: Example of the spectra obtained with DOLORES/TNG (top panel) and OSIRIS/GTC (low panel) for two luminous galaxy members in the PSZ2 G193.90+09.41 and PSZ2 G032.31+66.07 clusters, at $z_{\text{spec}} = 0.1976$ and $z_{\text{spec}} = 0.6158$, respectively. Dashed lines correspond to the wavelength of the absorption features identified in each spectrum at the redshift of the clusters. Flux density is plotted in arbitrary units.

Este documento incorpora firma electrónica, y es copia auténtica de un documento electrónico archivado por la ULL según la Ley 39/2015.
 Su autenticidad puede ser contrastada en la siguiente dirección <https://sede.ull.es/validacion/>

Identificador del documento: 3248012 Código de verificación: RmbjVJW6

Firmado por: ALEJANDRO AGUADO BARAHONA
 UNIVERSIDAD DE LA LAGUNA

Fecha: 01/03/2021 09:35:30

María de las Maravillas Aguiar Aguiar
 UNIVERSIDAD DE LA LAGUNA

22/03/2021 13:39:32

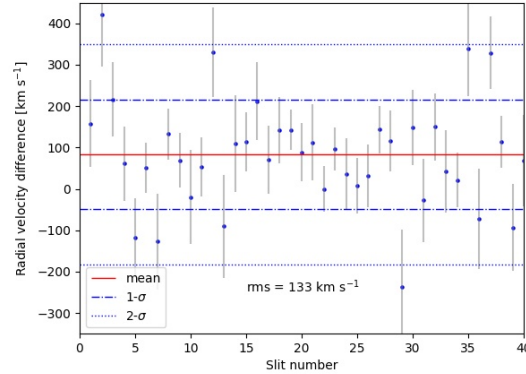


Figure 2.9: Comparison of the two independent redshift estimates for a set of 40 galaxies from PSZ2 G009.04+31.09. Red line represents the mean difference (83 km s^{-1}). Dash-dotted and dotted blue lines represent 1- and 2- σ deviations. The $rms = 133 \text{ km s}^{-1}$.

2.3.3 Spectroscopic redshift determination

In order to obtain the radial velocities of the galaxies, we used the task RVSAO³ implemented in IRAF. This routine is based on the cross-correlation technique developed by Tonry & Davis (1979). The method consists in performing a cross-correlation between the spectrum of our galaxies and six templates (Kennicutt 1992) of different galaxy type: E, S0, Sa, Sb, Sc and Irr. We adopt the radial velocity for each galaxy that corresponds to the higher value of the parameter R that measures the S/N ratio of the cross-correlation peak. In general, this method worked properly but in some cases the procedure obtained a non-realistic spectroscopic redshift (z_{spec}), mainly due to the low S/N of the spectra. For this reason, we inspected by eye every result and checked that it was done accurately. In the majority of the spectra, absorption lines were present (mainly H and K, CaI doublet, H_{β} , G-Band and MgI triplet) when they fall on the wavelength range depending on each galaxy redshift. In a few cases, we could distinguish emission lines such as OII and OIII doublet which were used to determined the redshift.

The cross-correlation technique together with the quality and the spectral resolution of the spectra yields to a mean error in the radial velocity estimation of $\Delta v \sim 75 \text{ km s}^{-1}$. However, taking into account two independent redshift estimates for a set of 40 galaxies we were able to determine the systematic errors. Making a comparison of the two velocity estimates we obtained a rms of $\Delta v \sim 130 \text{ km s}^{-1}$ (see Fig. 2.9).

³RVSAO was developed at the Smithsonian Astrophysical Observatory Telescope Data Center.

Este documento incorpora firma electrónica, y es copia auténtica de un documento electrónico archivado por la ULL según la Ley 39/2015.
 Su autenticidad puede ser contrastada en la siguiente dirección <https://sede.ull.es/validacion/>

Identificador del documento: 3248012 Código de verificación: RmbjVJW6

Firmado por: ALEJANDRO AGUADO BARAHONA
 UNIVERSIDAD DE LA LAGUNA

Fecha: 01/03/2021 09:35:30

María de las Maravillas Aguiar Aguilár
 UNIVERSIDAD DE LA LAGUNA

22/03/2021 13:39:32

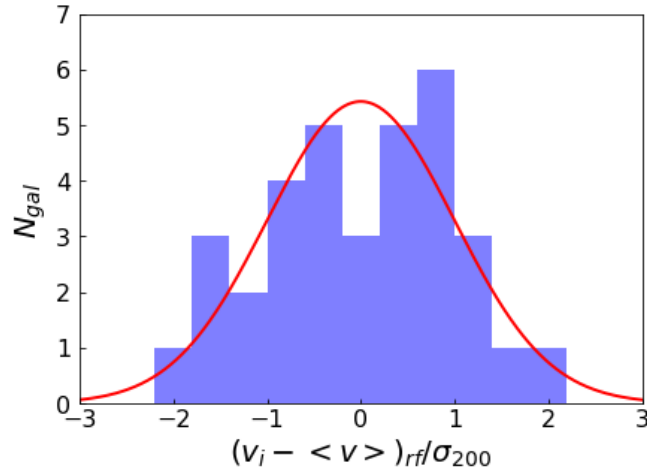


Figure 2.10: Example of the distribution of galaxies in PSZ2 G009.04+31.09 as a function of the rest frame difference in radial velocity to the mean radial velocity of the cluster. In blue are represented the cluster members used to estimate the velocity dispersion. The red line represents the normal distribution expected for the estimated velocity dispersion of $\sigma_{200} = 1068 \text{ km s}^{-1}$.

The benefits of using multi-object rather than long-slit spectroscopy is the fact that not only we can determine the redshift of the clusters by obtaining the radial velocities for a large number of objects, but also we can infer their velocity dispersion, the proxy used to estimate the dynamical mass. On average, we retrieved between 10 and 25 cluster members per mask. In a first approximation, a galaxy is considered to be a member of the cluster if its radial velocity lays within 2500 km s^{-1} in the rest frame from the cluster mean radial velocity. Then, we follow an iterative method considering galaxies as members if their radial velocity is less than 2.5 times the velocity dispersion away from the cluster mean velocity (see Fig. 2.10). In this way we guarantee that the majority of the galaxies selected are members minimising the presence of interlopers. This technique is further explained in Chapter 4.

Este documento incorpora firma electrónica, y es copia auténtica de un documento electrónico archivado por la ULL según la Ley 39/2015.
 Su autenticidad puede ser contrastada en la siguiente dirección <https://sede.ull.es/validacion/>

Identificador del documento: 3248012 Código de verificación: RmbjVJW6

Firmado por: ALEJANDRO AGUADO BARAHONA
 UNIVERSIDAD DE LA LAGUNA

Fecha: 01/03/2021 09:35:30

María de las Maravillas Aguiar Aguilár
 UNIVERSIDAD DE LA LAGUNA

22/03/2021 13:39:32

3

The *Planck* PSZ2 optical follow-up: results

This Chapter, together with Chapter 4, represents the nuclear part of this thesis. As the previous Chapter, it is based on two papers already published, Streblyanska et al. (2019) and Aguado-Barahona et al. (2019). Here, I present the results of the two years of observations of the program LP15. In Section 3.1, I define the process of cluster identification and validation. In Sections 3.2 and 3.3 the results of this process is shown, separated by years, in correspondence with the published papers. Furthermore, in Section 3.4 I discuss observations beyond the LP15 sample. The last section is reserved for the statistical analysis of the PSZ2 in the northern sky.

3.1 Cluster identification and validation criteria

Here, I describe the method we used to validate a cluster candidate as the optical counterpart of a PSZ2 target. This procedure is an extension of the method applied in Planck Collaboration int. XXXVI (2016); Barrena et al. (2018, 2020) for the PSZ1 catalogue. Compared to other methods in the literature, we have improved the validation criteria by including visual inspection and comparison between the RGB images, and also the Compton y -maps (Planck Collaboration XXII 2016), making photometric redshift estimates and analysing the red sequence (hereafter RS; Gladders & Yee 2000) using colour-magnitude diagrams. We also performed a richness study considering galaxy counts in clusters. For approximately 30% of our sample we performed spectroscopic confirmation by estimating the velocity dispersion of the candidates.

3.1.1 Photometric analysis

Our validation steps provide quantitative criteria for a robust association between PSZ2 source and the observed optical cluster. The visual inspection of deep RGB images around the official *Planck* position allows direct identification of clusters and rich groups

Este documento incorpora firma electrónica, y es copia auténtica de un documento electrónico archivado por la ULL según la Ley 39/2015.
Su autenticidad puede ser contrastada en la siguiente dirección <https://sede.ull.es/validacion/>

Identificador del documento: 3248012 Código de verificación: RmbjVJW6

Firmado por: ALEJANDRO AGUADO BARAHONA
UNIVERSIDAD DE LA LAGUNA

Fecha: 01/03/2021 09:35:30

María de las Maravillas Aguiar Aguilár
UNIVERSIDAD DE LA LAGUNA

22/03/2021 13:39:32

in the redshift range $0.1 < z < 0.8$ as a concentration of galaxies of the same colour. In addition, we always inspect the flux density contours observed in the Compton y -map (Planck Collaboration XXII 2016), and compare them with the positions of the possible optical association. These maps, constructed from linear combinations of the individual *Planck* frequency charts, preserve the SZ signal and cancel the influence of the CMB and galactic emission. For most of the clusters we observe the direct dependence between the peak of SZ signal, shifted sometimes from the *Planck* PSZ2 nominal source position, and the optical counterpart (Streblyanska et al. 2018). Also, if the location of detected over-density is above the expected uncertainty in the *Planck* detection ($\sim 5'$, see Fig. 3 in Planck Collaboration int. XXXVI 2016) then the structures observed in the y -map allows us to confirm or reject the association.

Once the clusters were identified, we inspected colour-magnitude diagrams looking for the cluster RS, using the $(g' - r', r')$ and $(r' - i', i')$. We fit the RS considering all galaxies with colours within the range ± 0.05 with respect to the colour of the BCG. We derive the photometric redshift of the galaxy over-densities following equations 2.1 and 2.2. After estimating the z_{phot} , we evaluated the richness of detected systems to validate the observed galaxy clusters as actual SZ counterparts.

The PSZ2 survey selection function (see Fig. 26 of Planck Collaboration XXVII 2016) shows that the expected *Planck* SZ detections are massive systems, with a mean mass over the whole redshift range of $4.82 \times 10^{14} M_{\odot}$. Therefore, we would expect our sample to be composed of massive rich clusters, and thus, no poor systems should in principle be validated if they are found along the line of sight of the *Planck* detection. In order to adopt an objective criterion for discarding low mass systems, we defined a richness parameter (R). There are multiple approaches in the literature to calculate the richness of the observed systems. In this thesis, I present a refined procedure with respect to the methodology of previous works (Barrena et al. 2012), taking into account the local background variance and making it more robust in comparison with other validation works in the literature. In short, R is computed as the number of likely members (galaxies in the RS ± 0.15 magnitude locus) in $g' - r'$ and $r' - i'$ for clusters at $z < 0.35$ and $z \geq 0.35$, respectively, showing r' -magnitudes in the range $[m_{r'}^* - 1, m_{r'}^* + 1.5]$, where $m_{r'}^*$ is the characteristic relative magnitude and depends on the redshift (see Barrena et al. 2012). We count galaxies within a projected region of 1 Mpc radius from the optical centre of the cluster at its redshift. This initial value of the richness (R_0) is then corrected for the field galaxy counts (R_f), which is computed in the same way but outside the 1 Mpc radius region for each cluster. We must stress that this final value ($R_{\text{cor}} \equiv R_0 - R_f$) should be considered as a lower limit to the richness of the system, as we are formally counting in the R_f estimation some clusters members that might lay outside the 1 Mpc region.

We based our confirmation criterion in the value σ_R , which is computed as $R_{\text{cor}}/\sqrt{R_f}$, and describes the richness significance above the local background level, using Poisson statistics. Given that in our calculations the richness is not a fixed value and depends on the local environment, we can, in principle, validate equally well clusters observed either in crowded star fields or in empty areas.

Este documento incorpora firma electrónica, y es copia auténtica de un documento electrónico archivado por la ULL según la Ley 39/2015.
 Su autenticidad puede ser contrastada en la siguiente dirección <https://sede.ull.es/validacion/>

Identificador del documento: 3248012 Código de verificación: RmbjVJW6

Firmado por: ALEJANDRO AGUADO BARAHONA
 UNIVERSIDAD DE LA LAGUNA

Fecha: 01/03/2021 09:35:30

María de las Maravillas Aguiar Aguilár
 UNIVERSIDAD DE LA LAGUNA

22/03/2021 13:39:32

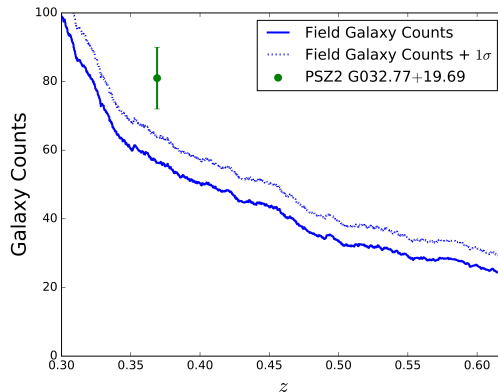


Figure 3.1: Illustration of our methodology to compute the cluster richness using PSZ2 G032.77+19.69 cluster detected at $z = 0.369$. The panel presents galaxy counts as a function of redshift for this observed field. The blue line represents the galaxy counts outside 1Mpc region from the optical centre of the cluster and the dashed blue line represents $1\text{-}\sigma$ above the latter. The green point shows the galaxy counts (or R_0 , i.e., our initial value of the richness) for this particular cluster and its $1\text{-}\sigma$ error bars. The corrected value of the richness R_{cor} is then calculated by subtracting from R_0 the background galaxy counts detected at the redshift of the cluster. The complete description of the calculations and discussion of these clusters are presented in Sec. 3.1.1.

Despite the flexibility and robustness of this approach to calculate the richness, we observed in two situations the caveats of this method. First, the method is not working properly when the FoV is relatively small compared to the cluster size. Also, it could produce wrong results if we observe an over-density of sources in the background. The algorithm then calculates artificially a high background R_f and, consequently, shows an underestimated value of R_{cor} due to the over-subtraction of this local background from the data. If this is the case, after the careful inspection of the images, we decided to keep the original (uncorrected) R value (see notes in Table 3.2).

Figure 3.1 illustrates our method used to determine the richness using one of the confirmed clusters from our sample. The initial values of richness for the the cluster was $R_0 = 81$. PSZ2 G032.77+19.69 is located in a crowded star area, so the richness of the field at the redshift of the cluster is also high ($R_f = 56.4$) yielding $R_{\text{cor}} = 24.6$ and $\sigma_R = 3.28$.

Este documento incorpora firma electrónica, y es copia auténtica de un documento electrónico archivado por la ULL según la Ley 39/2015.
 Su autenticidad puede ser contrastada en la siguiente dirección <https://sede.ull.es/validacion/>

Identificador del documento: 3248012 Código de verificación: RmbjVJW6

Firmado por: ALEJANDRO AGUADO BARAHONA
 UNIVERSIDAD DE LA LAGUNA

Fecha: 01/03/2021 09:35:30

María de las Maravillas Aguiar Aguiar
 UNIVERSIDAD DE LA LAGUNA

22/03/2021 13:39:32

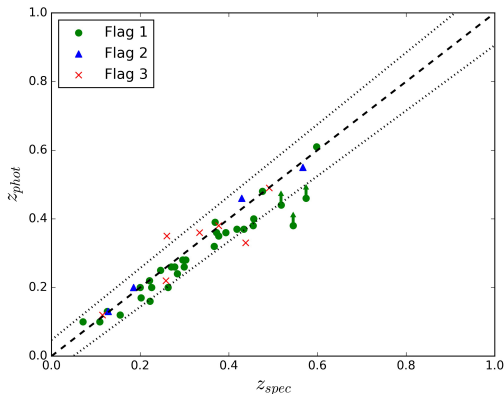


Figure 3.2: Comparison between derived photometric and spectroscopic redshifts for a sample of sources validated with **Flag**= 1–3. The dashed line shows the 1:1 relation. The dotted lines represent the photometric error $\delta_z/(1+z) \sim 0.047$. We underestimate the photometric redshift for clusters at $z > 0.5$ due to lack of z -band photometry in our follow-up. Therefore we assume these values as lower limits.

3.1.2 Spectroscopic analysis

In addition to the photometric data, we obtained spectroscopic information for almost all the clusters. This includes our own observations and publicly available data from the SDSS survey.

We find a good agreement between the photometric and spectroscopic redshifts for all our PSZ2 sources, except for high- z clusters (see Fig. 3.2). We recall that our photometric redshift is based in the $r' - i'$ colour of likely cluster members (Planck Collaboration int. XXXVI 2016), which is not an appropriate estimator for systems at $z > 0.7$. Obtaining secure redshift for sources at $0.5 < z_{\text{phot}} < 0.7$ is also limited by the lack of z -band photometry and obtained values must be considered as a lower limit. Our study yields a photometric redshift error of $\delta_z/(1+z) \sim 0.047$ when considering clusters with $z < 0.7$ (~ 0.04 for $z < 0.5$).

On average, we typically obtain about 20–40 spectroscopic members per cluster, and, consequently, a velocity dispersion σ_v can be estimated. We used this value of σ_v to investigate whether these clusters are poor or massive systems. There is a direct dependence between the redshift and mass of the *Planck* clusters, reported first in Planck Collaboration XXXII (2015) and studied in detail for high- z ($z > 0.5$) clusters in van der Burg et al. (2016). We expect that clusters at $z < 0.2$ with $M_{500} > 10^{14} M_{\odot} h_{70}^{-1}$ will present $\sigma_v > 500 \text{ km s}^{-1}$, whereas clusters at $z > 0.2$ with $M_{500} > 2 \times 10^{14} M_{\odot} h_{70}^{-1}$ should show $\sigma_v > 650 \text{ km s}^{-1}$ (Munari et al. 2013). We assume these values in the

Este documento incorpora firma electrónica, y es copia auténtica de un documento electrónico archivado por la ULL según la Ley 39/2015.
 Su autenticidad puede ser contrastada en la siguiente dirección <https://sede.ull.es/validacion/>

Identificador del documento: 3248012 Código de verificación: RmbjVJW6

Firmado por: ALEJANDRO AGUADO BARAHONA
 UNIVERSIDAD DE LA LAGUNA

Fecha: 01/03/2021 09:35:30

María de las Maravillas Aguiar Aguilera
 UNIVERSIDAD DE LA LAGUNA

22/03/2021 13:39:32

Table 3.1: Validation criteria adopted to confirm or reject candidates associated with the SZ emission.

Flag	Spectroscopy	σ_v (km s ⁻¹)	σ_R
1	YES	> 500 km s ⁻¹ ($z < 0.2$)	> 1.5
		> 650 km s ⁻¹ ($z > 0.2$)	> 1.5
2	NO	–	> 1.5
3	YES	< 500 km s ⁻¹ ($z < 0.2$)	> 1.5
		< 650 km s ⁻¹ ($z > 0.2$)	> 1.5
	NO	–	< 1.5
ND	–	–	–

velocity dispersion to distinguish between actual and detectable systems by *Planck* and chance identifications not linked to the SZ effect.

3.1.3 Summary of our validation criteria

Table 3.1 summarises the set of criteria we adopted in order to confirm or reject a cluster candidate as the optical counterpart of the SZ signal. They provide a classification of the candidates according to four possible values of a **Flag**. Values of **Flag** = 1 or 2 correspond to validated clusters, **Flag** = 3 corresponds to clusters located along the line of sight of the *Planck* signal but that may not be associated with the SZ emission, and ND refers to a nondetection.

When we had enough spectroscopic information to provide an estimate of σ_v , we validated the candidate with **Flag** 1 if that value was found to be above the corresponding threshold. However, when σ_v was below the threshold, we assumed that the system has a low mass and is probably not linked to the SZ emission. These candidates are classified as **Flag** 3. When no spectroscopic information is available, or when we were unable to estimate the velocity dispersion due to an insufficient number of galaxy members (fewer than five members), we validated the candidates using the richness estimate. Systems with $\sigma_R > 1.5$ were validated photometrically, but still await a definitive spectroscopic confirmation. These systems are classified with **Flag** 2. Clusters with **Flag** 3 represent very poor systems ($\sigma_R < 1.5$) without spectroscopic information. The ND flag was used for SZ candidates without a galaxy over-density in the optical images. We also considered the criterion that a *Planck* cluster must be placed within a 5' radius from the nominal pointing because it represents 2.5 times the mean position error with respect to the SZ peak emission. Nevertheless, this criterion can be modulated due to the wide range of uncertainties in the position error in the PSZ2 catalogue and the different shapes of the *y*-maps. The cases that do not match the validation criteria but are positively confirmed are discussed in Sections 3.2.2 and 3.3.2.

Este documento incorpora firma electrónica, y es copia auténtica de un documento electrónico archivado por la ULL según la Ley 39/2015.
 Su autenticidad puede ser contrastada en la siguiente dirección <https://sede.ull.es/validacion/>

Identificador del documento: 3248012 Código de verificación: RmbjVJW6

Firmado por: ALEJANDRO AGUADO BARAHONA
 UNIVERSIDAD DE LA LAGUNA

Fecha: 01/03/2021 09:35:30

María de las Maravillas Aguiar Aguilár
 UNIVERSIDAD DE LA LAGUNA

22/03/2021 13:39:32

3.2 LP15 sample: 1st year of observations

The results presented in this section have been published in Streblyanska et al. (2019).

3.2.1 Results

Table 3.2 summarises the results for the 106 PSZ2 sources explored in the first year of our optical follow-up. The first three columns provide information from the PSZ2 catalogue and correspond to the index number, official name of the SZ source and the signal-to-noise ratio respectively. The J2000 coordinates (column 4 and 5) correspond to the BCG position or geometrical centre of the identified counterpart. Column 6 provides distance (in arcmin) between PSZ coordinates and optical centre. Column 7 shows the photometric redshift of the cluster. Columns 8, 9, and 10 list (if available) the mean spectroscopic redshift, spectroscopic redshift of the BCG (in the case of absence of the apparent BCG we write “-1”), and the number of galaxies with spectroscopic measurements. Columns 11 and 12 provide optical richness of the cluster and its significance, where possible, see Section 3.1.1 for details. Column 13 provides our cluster classification, following the flagging scheme described in Section 3.1.3 and presented in Table 3.1. The complete version of this table is published in (Streblyanska et al. 2019), including some comments on individual clusters, such as alternative names and correlations with other surveys.

Some of our clusters were pre-selected from Streblyanska et al. (2018) (mainly for MOS observations) and, thus, they have SDSS photometric information available. In summary, we update the information for 14 clusters, being 13 of them members of the LP15 sample. The remaining one is PSZ2 G310.81+83.91, which was also identified in the PSZ1 catalogue, and thus it is not included in the LP15 sample.

At the moment of the publication, several articles reported confirmation of some clusters from our sample. For example, Boada et al. (2019) presented photometric redshifts for eight clusters. For all matched sources, except for three clusters, we have secure spectroscopic redshift measurements which are in perfect agreement with the reported photometric information. For PSZ2 G106.11+24.11, PSZ2 G107.83-45.45 and PSZ2 125.55+32.72 we have only photometric confirmation. Therefore, and for completeness, we presented in Table 3.2 our alternative photometric measurements.

Following the confirmation criteria given above, we find that 50 PSZ2 sources present clear over-densities around the nominal *Planck* position. However, after the inspection of obtained σ_v , we classified eight clusters as weak associations with the corresponding SZ source (i.e., **Flag** = 3). Thus, in total, we were able to confirm 41 new PSZ2 sources, 31 of them classified with **Flag** = 1 (spectroscopic confirmation) and 10 with **Flag** = 2 (photometric confirmation). In three cases, we found multiple optical counterparts along line of sight.

The detailed description of cluster counterparts with the spectroscopic confirmation and its corresponding physical properties, such as velocity dispersions and dynamical masses, will be discussed in detail in Chapter 4.

Este documento incorpora firma electrónica, y es copia auténtica de un documento electrónico archivado por la ULL según la Ley 39/2015.
 Su autenticidad puede ser contrastada en la siguiente dirección <https://sede.ull.es/validacion/>

Identificador del documento: 3248012 Código de verificación: RmbjVJW6

Firmado por: ALEJANDRO AGUADO BARAHONA
 UNIVERSIDAD DE LA LAGUNA

Fecha: 01/03/2021 09:35:30

María de las Maravillas Aguiar Aguilár
 UNIVERSIDAD DE LA LAGUNA

22/03/2021 13:39:32

Table 3.2: List of 107 PSZ2 sources analysed during the first year of the program. We show information for 106 LP15 cluster candidates plus one cluster from Streblyanska et al. (2018) with updated redshift information.

ID	Planck name	S/N	R. A.	Decl.	distance (")	z_{phot}	z_{spec}	$z_{\text{spec}}(BGG)$	N_{spec}	R_{corr}	σ_R	flag
34 ^d	PSZ2 G009.04+31.09	5.04	16:18:26.70	-04:11:11.06	1.52	0.25 ^g	0.246	-1	34	31 ^e	-	1
78	PSZ2 G023.87-13.88	4.90	19:25:40.06	-14:11:25.04	1.52	0.12	0.0	0.0	0	30.0	2.64	2
86	PSZ2 G027.49+15.73	5.22	-	-	-	-	-	-	0	0.0	0.0	ND
90	PSZ2 G027.77+10.88	6.41	-	-	-	-	-	-	0	0.0	0.0	ND
91	PSZ2 G027.77+10.88	6.41	-	-	-	-	-	-	0	0.0	0.0	ND
106	PSZ2 G029.87-17.81	4.91	-	-	-	-	-	-	0	0.0	0.0	ND
116	PSZ2 G032.77+19.69	4.78	17:40:23.30	+08:41:12.12	2.10	0.39	0.369	0.368	61	24.6	3.28	1
126 ^e	PSZ2 G036.36+16.01	4.58	17:59:45.60	+10:08:29.15	4.21	0.13	0.128	-1	3	1.39	-	2
127	PSZ2 G036.69-15.67	5.69	-	-	-	-	-	-	0	0.0	0.0	ND
130	PSZ2 G036.80-14.95	4.72	-	-	-	-	-	-	0	0.0	0.0	ND
133	PSZ2 G036.86+18.70	4.75	-	-	-	-	-	-	0	15.3	0.1	ND
143	PSZ2 G039.86+18.70	4.55	20:15:55.00	-05:55:59.25	4.40	0.46	0.574	-1	0	0.0	0.0	ND
146-A ^c	PSZ2 G040.11+42.58	5.08	21:36:59.42	-18:08:02.70	2.63	0.17	0.202	0.201	54	45.7	7.8	1
155	PSZ2 G042.54+18.02	4.78	21:37:17.15	-18:01:10.77	5.47	0.57	0.62	0.62	15	4.9	1.71	1
158	PSZ2 G043.44+41.27	5.55	18:02:59.10	+16:21:15.37	6.56	0.22	0.258	-1	8	40.2	3.28	3
161 ^d	PSZ2 G044.21+52.13	4.64	21:36:43.74	-10:19:01.69	1.23	0.37	0.454	-1	33	52.9	11.5	1
169	PSZ2 G045.20+15.63	4.65	15:42:50.44	+27:49:52.90	2.35	0.38	0.377	-1	6	2.9	0.75	3
171	PSZ2 G045.47+17.80	4.66	18:16:04.76	+17:47:00.12	1.30	0.13	0.126	0.128	22	16.2	1.67	1
176 ^d	PSZ2 G045.96-26.94	5.1	18:08:14.70	+18:51:54.00	1.74	0.36	0.372	0.372	34	8.7	2.47	1
181	PSZ2 G046.39+11.71	4.62	20:50:01.00	-01:35:23.85	1.84	0.22	0.0	0.0	0	9.5	1.51	2
187	PSZ2 G048.07+07.76	4.77	-	-	-	-	-	-	0	0.0	0.0	ND
208	PSZ2 G048.30+8.87	4.90	-	-	-	-	-	-	0	0.0	0.0	ND
209	PSZ2 G052.08+46.13	4.75	-	-	-	-	-	-	0	0.0	0.0	ND
217	PSZ2 G053.80+36.49	5.16	-	-	-	-	-	-	0	0.0	0.0	ND
233	PSZ2 G057.09+11.19	4.96	18:54:14.08	+26:27:26.46	2.61	0.35	0.377	-1	20	14.3	1.49	1
248	PSZ2 G059.52+16.23	4.77	18:37:15.08	+30:40:53.17	1.71	0.24	0.284	-1	17	100.8	31.64	1
250	PSZ2 G059.76+14.59	4.88	18:44:42.47	+30:17:31.54	2.87	0.28	0.303	-1	9	-1	-1	1
266	PSZ2 G064.98+16.71	4.57	18:44:30.25	+35:42:19.52	1.26	0.16	0.222	-1	5	23.3	3.3	1
269	PSZ2 G065.35-08.01	5.82	-	-	-	-	-	-	0	0.0	0.0	ND
279 ^d	PSZ2 G066.99-58.51	5.01	23:07:11.30	-07:31:43.15	3.58	0.36	0.334	0.334	16	2.1	0.61	3
283	PSZ2 G066.76-08.42	4.81	21:13:28.80	+18:03:27.28	0.33	0.32	0.367	0.366	0	0.0	0.0	ND
284	PSZ2 G067.09+14.13	4.93	21:36:33.70	+14:03:47.30	2.37	0.36	0.393	0.393	44	9.2	1.92	1
287	PSZ2 G067.72+24.13	5.14	21:46:02.11	+14:01:26.25	2.2	0.36	0.393	0.393	44	9.2	1.92	1
295-A ^{c,d}	PSZ2 G069.47-29.06	5.14	21:45:51.19	+14:03:23.00	4.66	0.21	0.19	-1	30	8.7	1.58	1
295-B ^{c,d}	PSZ2 G072.96-12.26	4.58	18:46:41.11	+45:47:04.30	1.27	0.2	0.0	0.0	0	18.9	-1	2
319	PSZ2 G075.08+19.83	5.73	18:46:41.11	+45:47:04.30	1.27	0.2	0.0	0.0	0	18.9	-1	2
326	PSZ2 G076.51+21.73	4.68	18:38:35.82	+47:33:35.78	4.12	0.37	0.418	0.42	47	50.4	8.98	1
328	PSZ2 G076.81-32.57	4.68	-	-	-	-	-	-	0	0.0	0.0	ND

Este documento incorpora firma electrónica, y es copia auténtica de un documento electrónico archivado por la ULL según la Ley 39/2015.
 Su autenticidad puede ser contrastada en la siguiente dirección <https://sede.ull.es/validacion/>

Identificador del documento: 3248012 Código de verificación: RmbjVJW6

Firmado por: ALEJANDRO AGUADO BARAHONA
 UNIVERSIDAD DE LA LAGUNA

Fecha: 01/03/2021 09:35:30

María de las Maravillas Aguiar Aguiar
 UNIVERSIDAD DE LA LAGUNA

22/03/2021 13:39:32

3.2 LP15 sample: 1st year of observations

Table 3.2: Continue.

ID	Planck name	S/N	R. A.	Decl.	distance	z_{phot}	z_{spec}	$z_{\text{spec}}(BCG)$	N_{spec}	R_{corr}	σ_r	flag
330 ^d	PSZ2 G077.67+30.59	5.03	174:65:0.85	+50:31:12.28	3.18	0.22	0.221	0.219	10	6.6	1.43	1
337	PSZ2 G079.36+38.06	4.94	165:59:09.10	+52:06:09.80	2.92	0.26	0.299	-1	53	31.8	11.45	1
351	PSZ2 G081.60+18.47	5.57	19:07:17.98	+51:05:14.46	2.78	0.44	0.518	0.519	21	11.4	2.57	1
353	PSZ2 G082.06+27.23	5.32	-	-	-	-	-	-	0	0.0	0.0	ND
364	PSZ2 G084.15-08.63	4.82	-	-	-	-	-	-	0	0.0	0.0	ND
371 ^d	PSZ2 G084.69-58.60	4.73	23:36:37.50	-01:27:52.30	7.17	0.2	0.185	-1	2	21.6	5.04	2
380	PSZ2 G086.07-41.99	4.78	-	-	-	-	-	-	0	0.0	0.0	ND
382	PSZ2 G086.35-13.94	5.42	21:49:41.40	+35:43:13.89	0.84	0.26	0.278	0.277	11	33.0	5.93	1
400	PSZ2 G089.06-11.79	5.71	21:52:58.09	+39:04:30.53	1.14	0.38	0.455	0.455	32	12.3	1.79	1
407	PSZ2 G090.42-08.42	4.76	22:53:42.06	+38:05:42.42	4.88	0.31	0.321	0.324	13	10.4	1.67	1
412	PSZ2 G091.56+08.50	4.71	20:36:18.61	+54:59:04.90	0.89	0.26	0.27	0.27	13	86.7	20.82	1
415	PSZ2 G092.11-33.73	5.81	-	-	-	-	-	-	0	0.0	0.0	ND
420	PSZ2 G092.64+20.78	5.12	19:16:45.42	+61:40:41.47	0.15	0.38	0.545	0.549	39	-1	-1	1
426	PSZ2 G093.71-30.90	5.0	-	-	-	-	-	-	0	0.0	0.0	ND
429	PSZ2 G093.94+13.75	4.88	-	-	-	-	-	-	0	0.0	0.0	ND
444	PSZ2 G095.75-11.16	5.32	-	-	-	-	-	-	0	0.0	0.0	ND
445	PSZ2 G096.10+12.46	5.08	-	-	-	-	-	-	0	0.0	0.0	ND
447	PSZ2 G096.45-20.89	5.8	22:48:09.42	+35:33:49.49	0.48	0.2	0.226	-1	34	33.3	4.31	1
451	PSZ2 G097.15-08.43	4.53	22:42:55.75	+39:15:19.56	2.12	0.4	0.456	0.456	32	37.8	6.65	1
463	PSZ2 G098.39+57.68	5.07	-	-	-	-	-	-	0	0.0	0.0	ND
465	PSZ2 G098.62+51.76	4.53	-	-	-	-	-	-	0	0.0	0.0	ND
480	PSZ2 G100.07+17.06	5.01	-	-	-	-	-	-	0	0.0	0.0	ND
483 ^d	PSZ2 G100.22+33.81	5.68	17:13:41.57	+69:21:45.24	0.65	0.61	0.598	-1	18	3.3	1.27	1
484	PSZ2 G100.38+16.73	5.08	-	-	-	-	-	-	0	0.0	0.0	ND
485	PSZ2 G100.45+16.79	11.78	-	-	-	-	-	-	0	0.0	0.0	ND
497	PSZ2 G104.15-38.85	6.41	-	-	-	-	-	-	0	0.0	0.0	ND
501	PSZ2 G104.58-15.41	4.62	-	-	-	-	-	-	0	0.0	0.0	ND
505	PSZ2 G105.00+39.08	4.97	15:25:52.42	+70:30:57.64	1.70	0.2	0.2	0.201	30	31.7	6.18	1
512	PSZ2 G105.45-08.43	4.7	17:43:42.46	+37:05:42.46	0.31	0.2	0.2	0.2	0	0.0	0.0	ND
514	PSZ2 G106.21+26.32	4.9	18:48:31.20	+75:03:29.99	0.09	0.08	0.0	0.0	0	-1	-1	2
522	PSZ2 G107.41-09.57	10.68	00:07:35.62	+16:07:01.87	0.83	0.55	0.567	0.567	2	6.8	2.7	2
525	PSZ2 G107.83-45.45	7.09	-	-	-	-	-	-	0	0.0	0.0	ND
538	PSZ2 G110.69-46.25	5.04	-	-	-	-	-	-	0	0.0	0.0	ND
542	PSZ2 G112.07-39.86	5.72	-	-	-	-	-	-	0	0.0	0.0	ND
568	PSZ2 G116.05+20.00	5.16	23:28:53.00	+73:22:13.00	5.92	0.35	0.26	-1	18	-1	-1	3
574	PSZ2 G117.11+11.48	5.45	13:24:21.08	+69:17:24.72	7.46	0.34	0	0	0	0.0	0.0	ND
585	PSZ2 G118.38-52.47	5.45	-	-	-	-	-	-	0	0.0	0.0	ND
591	PSZ2 G120.36+26.03	5.20	13:42:31.07	+72:50:54.41	2.54	0.36	0.363	0.295	41	17.0	5.68	1
593-A ^c	PSZ2 G120.76+44.14	5.58	13:42:31.07	+72:50:54.41	2.54	0.36	0.363	-1	12	-1	-1	1
597	PSZ2 G121.87-45.97	4.85	-	-	-	-	-	-	0	0.0	0.0	ND
609	PSZ2 G124.11+25.02	5.52	-	-	-	-	-	-	0	0.0	0.0	ND
612	PSZ2 G125.11+28.14	4.98	11:25:46.87	+83:55:04.58	2.43	0.27	0.0	0.0	0	0.0	0.0	ND
617	PSZ2 G125.35+32.72	6.48	01:13:25.70	+57:56:01.00	1.32	0.2	0.263	-1	19	36.7	9.37	1
636	PSZ2 G128.19-24.71	4.74	-	-	-	-	-	-	0	0.0	0.0	ND

Este documento incorpora firma electrónica, y es copia auténtica de un documento electrónico archivado por la ULL según la Ley 39/2015.
 Su autenticidad puede ser contrastada en la siguiente dirección <https://sede.ull.es/validacion/>

Identificador del documento: 3248012 Código de verificación: RmbjVJW6

Firmado por: ALEJANDRO AGUADO BARAHONA
 UNIVERSIDAD DE LA LAGUNA

Fecha: 01/03/2021 09:35:30

María de las Maravillas Aguiar Aguiar
 UNIVERSIDAD DE LA LAGUNA

22/03/2021 13:39:32

Table 3.2: Continue.

ID	Planck name	S/N	R. A.	Decl.	distance	z _{phot}	z _{spec}	z _{spec} (FCG)	N _{spec}	R _{cor}	σ _R	flag
655	PSZ2 G134.26-44.28	5.08	-	-	-	-	-	-	0	0.0	0.0	ND
666	PSZ2 G135.94-68.22	6.86	-	-	-	-	-	-	0	0.0	0.0	ND
668	PSZ2 G136.31+54.67	6.91	-	-	-	-	-	-	0	0.0	0.0	ND
673 ^e	PSZ2 G137.24+53.93	7.87	11:40:59.55	+61:07:07.04	4.61	0.48	0.476	0.477	19	2.3	2.74	1
684	PSZ2 G139.72-17.13	5.11	02:19:44.22	+42:50:13.26	2.06	0.12	0.155	0.156	18	9.1	1.2	1
706	PSZ2 G144.84-35.16	4.83	-	-	-	-	-	-	0	0.0	0.0	ND
713	PSZ2 G145.42-48.72	4.71	-	-	-	-	-	-	0	0.0	0.0	ND
723	PSZ2 G148.60-48.61	4.71	01:52:41.75	+11:13:01.36	3.01	0.49	0.491	0.491	20	0.0	0.0	ND
744	PSZ2 G153.56+36.82	15.89	-	-	-	-	-	-	0	0.0	0.0	ND
763	PSZ2 G158.45-42.92	4.8	-	-	-	-	-	-	0	0.0	0.0	ND
771	PSZ2 G161.73-28.58	4.8	03:18:09.80	+23:01:53.40	2.13	0.33	0.438	0.442	12	9.0	2.6	3
776	PSZ2 G163.22-26.48	6.34	-	-	-	-	-	-	0	0.0	0.0	ND
785	PSZ2 G164.85-16.55	5.01	-	-	-	-	-	-	0	0.0	0.0	ND
795	PSZ2 G166.27-25.02	8.08	-	-	-	-	-	-	0	0.0	0.0	ND
796	PSZ2 G166.27-24.11	9.97	-	-	-	-	-	-	0	0.0	0.0	ND
813	PSZ2 G171.79-42.08	4.87	-	-	-	-	-	-	0	0.0	0.0	ND
827	PSZ2 G176.07-26.95	5.84	-	-	-	-	-	-	0	0.0	0.0	ND
845	PSZ2 G181.88-30.77	9.29	-	-	-	-	-	-	0	0.0	0.0	ND
1244 ^d	PSZ2 G269.02+46.30	4.67	11:19:07.43	-10:22:57.81	1.22	0.12 ^b	0.115	0.114	9	-1	-1	3
1465 ^{f,j}	PSZ2 G310.81+83.91	8.28	12:55:18.02	+21:02:31.22	5.0	0.46	0.429	-1	2	5.7	1.7	2
1621	PSZ2 G347.96+80.46	4.73	-	-	-	-	-	-	0	0.0	0.0	ND
1626	PSZ2 G349.18+38.66	5.15	15:11:40.98	-11:11:27.36	6.01	0.1	0.109	0.108	26	-1	-1	1

^a Richness calculated using SDSS DR12 data (no LP15 photometric data available)

^b Photometric redshift obtained from SDSS DR12 data (Streblyanska et al. (2018))

^c SZ targets identified with the ID followed by an A or B label indicate the presence of multiple counterparts

^d Confirmed in Streblyanska et al. (2018). New LP15 photometric/spectroscopic data are available

^e Classified as "potentially associated" in Streblyanska et al. (2018)

^f An extra source from Streblyanska et al. (2018) with new spectroscopic information. Not included in LP15 sample

^g Richness calculated without local background subtraction due to the small FoV or poor observing conditions

Este documento incorpora firma electrónica, y es copia auténtica de un documento electrónico archivado por la ULL según la Ley 39/2015.
 Su autenticidad puede ser contrastada en la siguiente dirección <https://sede.ull.es/validacion/>

Identificador del documento: 3248012 Código de verificación: RmbjVJW6

Firmado por: ALEJANDRO AGUADO BARAHONA
 UNIVERSIDAD DE LA LAGUNA

Fecha: 01/03/2021 09:35:30

María de las Maravillas Aguiar Aguiar
 UNIVERSIDAD DE LA LAGUNA

22/03/2021 13:39:32

For 50 detected clusters (with **Flag** 1–3) we studied the dependence between the position of optical centre and the nominal *Planck* SZ coordinates. The position error predicted for SZ detections in the *Planck* SZ maps was about $2'$ for targets in the PSZ1 sample and it was calculated that the cluster associated with the SZ effect should be closer than $\sim 5'$ (e.g., the beam size of the SZ detection) from the SZ PSZ1 source coordinates. However, it was shown during the follow-up campaigns (e.g., *Planck* Collaboration int. XXXVI 2016; Barrena et al. 2018; Streblyanska et al. 2018; Barrena et al. 2020) that even if this is true for most of the sources, some small percentage of true counterparts are located at distances of $\sim 6 - 8'$. In most of the cases, it corresponds to nearby systems at $z < 0.25$ with large apparent radius or fields affected by the optical structures, such as galactic cirri, which influence the *Planck* maps and, consequently, the final position of the detected SZ source. Figure 3.3 (top panel) shows the final offset distribution of cluster optical centre relative to their *Planck* SZ position. As it was expected, 68% of the 50 confirmed cluster sample are enclosed within $2'.6$, while for 95% of the sources this corresponds to $6'$. We also studied dependence between this observed offset and redshift of the cluster (Fig. 3.3, bottom panel). As was expected, most of the clusters are located not only inside the $5'$ region, but also inside the physical 1 Mpc region at the cluster redshift. In six cases (one of which corresponds to multiple optical counterpart detection) we observe the true counterparts at distances $> 5'$. The largest distance from the *Planck* pointing, confirmed by contours from the y -map, was $7.4'$ (see discussion below).

3.2.2 Notes on individual objects

In the following, we describe, as examples, a few clusters showing some particular features.

PSZ2 G023.87-13.88 is the only fossil¹ cluster in our sample. It contains about 25 photometric members at $z_{\text{phot}} = 0.12$.

PSZ2 G079.36+38.06. This cluster is one of the richest systems in our data-set. We detected more than 300 photometric members, distributed across the image and grouped in a few clumps (Fig. 3.4). We were able to obtain spectroscopy for 53 sources and confirm $z_{\text{spec}} = 0.299$ with a $\sigma_v = 904 \text{ km s}^{-1}$.

PSZ2 G084.69-58.60 and PSZ2 G118.79+47.50. Even though these clusters are beyond the limit of the official $5'$ distance accepted for SZ sources ($7'.1$ and $7'.4$, for PSZ2 G084.69-58.60 and PSZ2 G118.79+47.50, respectively) the MILCA contours confirm that these clusters are actual counterparts to the SZ signal (Fig. 3.5). In total, we have six cases where the clusters are located beyond $5'$ limit ($5'.4-7'.4$) and in all cases the contours from y -maps support the validation. For some sources we even observed the shift between the peak of the SZ signal (y -map) and the nominal *Planck* position, similar to figure 8 in Streblyanska et al. (2018).

PSZ2 G120.76+44.14 is an example of SZ sources with multiple optical counterparts.

¹defined as galaxy systems with a magnitude difference of at least two magnitudes in the r -band between the BCG and the second-brightest galaxy within half the virial radius R_{200}

Este documento incorpora firma electrónica, y es copia auténtica de un documento electrónico archivado por la ULL según la Ley 39/2015.
 Su autenticidad puede ser contrastada en la siguiente dirección <https://sede.ull.es/validacion/>

Identificador del documento: 3248012 Código de verificación: RmbjVJW6

Firmado por: ALEJANDRO AGUADO BARAHONA
 UNIVERSIDAD DE LA LAGUNA

Fecha: 01/03/2021 09:35:30

María de las Maravillas Aguiar Aguilár
 UNIVERSIDAD DE LA LAGUNA

22/03/2021 13:39:32

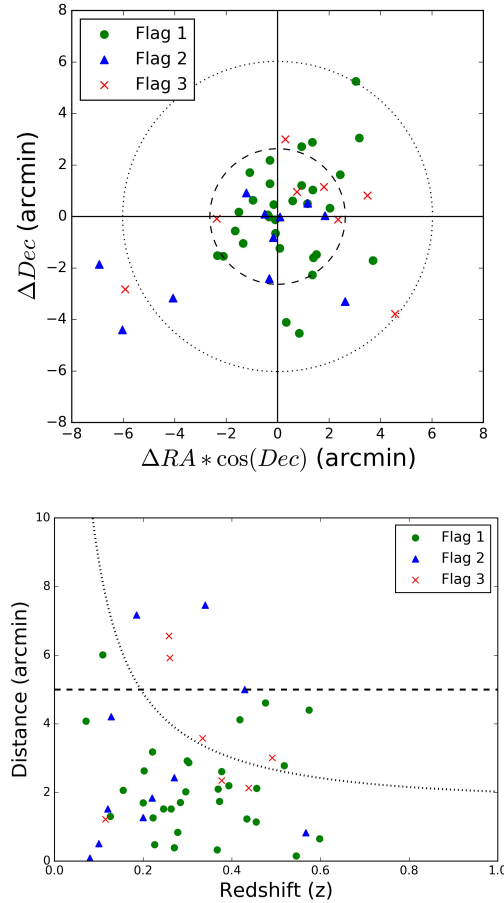


Figure 3.3: Top: Distribution of the optical centre offsets relative to their *Planck* SZ positions for the validated clusters (Flag= 1–3) presented in Table 3.2. The inner dashed line corresponds to 2' radius region, which encloses the 68% of the PSZ2 confirmed clusters. External dotted line encloses the 95% of clusters and corresponds to 6'. Cases with multiple optical counterparts have been excluded from this analysis. Bottom: Cluster optical centre offsets relative to their *Planck* SZ position as a function of cluster redshift for a sample of 50 sources. The dashed horizontal line is 5', which represents the maximum offset expected for a *Planck* SZ detection (i.e. FWHM *Planck* multi-frequency combined beam). The dotted line corresponds to the physical 1 Mpc radius region at the corresponding redshift.

Este documento incorpora firma electrónica, y es copia auténtica de un documento electrónico archivado por la ULL según la Ley 39/2015.
 Su autenticidad puede ser contrastada en la siguiente dirección <https://sede.ull.es/validacion/>

Identificador del documento: 3248012 Código de verificación: RmbjVJW6

Firmado por: ALEJANDRO AGUADO BARAHONA
 UNIVERSIDAD DE LA LAGUNA

Fecha: 01/03/2021 09:35:30

María de las Maravillas Aguiar Aguiar
 UNIVERSIDAD DE LA LAGUNA

22/03/2021 13:39:32

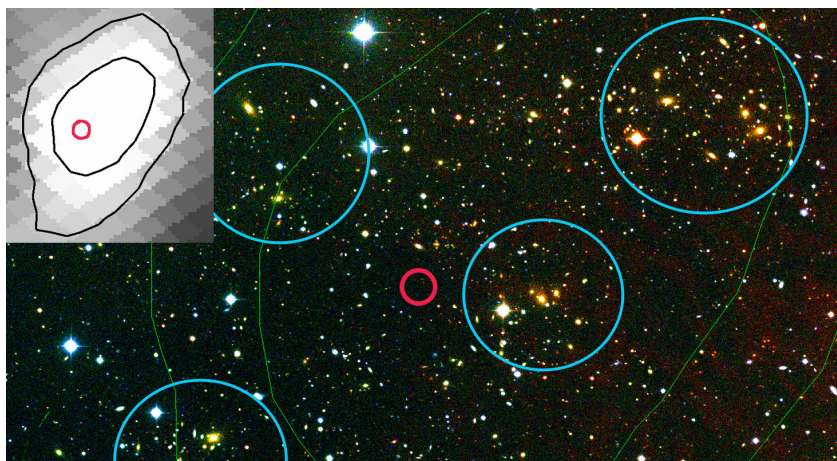


Figure 3.4: The zoomed RGB image of the PSZ2 G079.36+38.06. This cluster is one of the richest in our data-set, with more than 300 photometric members, 53 of them confirmed through the spectroscopy at $z_{\text{spec}} = 0.299$. The observed galaxies are grouped in several clumps (marked as blue circles) and distributed across the FoV ($\sim 11' \times 19'$) of the optical image. The top-left panel shows the MILCA y -map with black contours corresponding to the 3 and 6×10^{-6} levels of the y -map in this area (in the RGB image the same contours are represented as green lines). The red circles in both images correspond to the nominal *Planck* position.

Este documento incorpora firma electrónica, y es copia auténtica de un documento electrónico archivado por la ULL según la Ley 39/2015.
Su autenticidad puede ser contrastada en la siguiente dirección <https://sede.ull.es/validacion/>

Identificador del documento: 3248012 Código de verificación: RmbjVJW6

Firmado por: ALEJANDRO AGUADO BARAHONA
UNIVERSIDAD DE LA LAGUNA

Fecha: 01/03/2021 09:35:30

María de las Maravillas Aguiar Aguilera
UNIVERSIDAD DE LA LAGUNA

22/03/2021 13:39:32

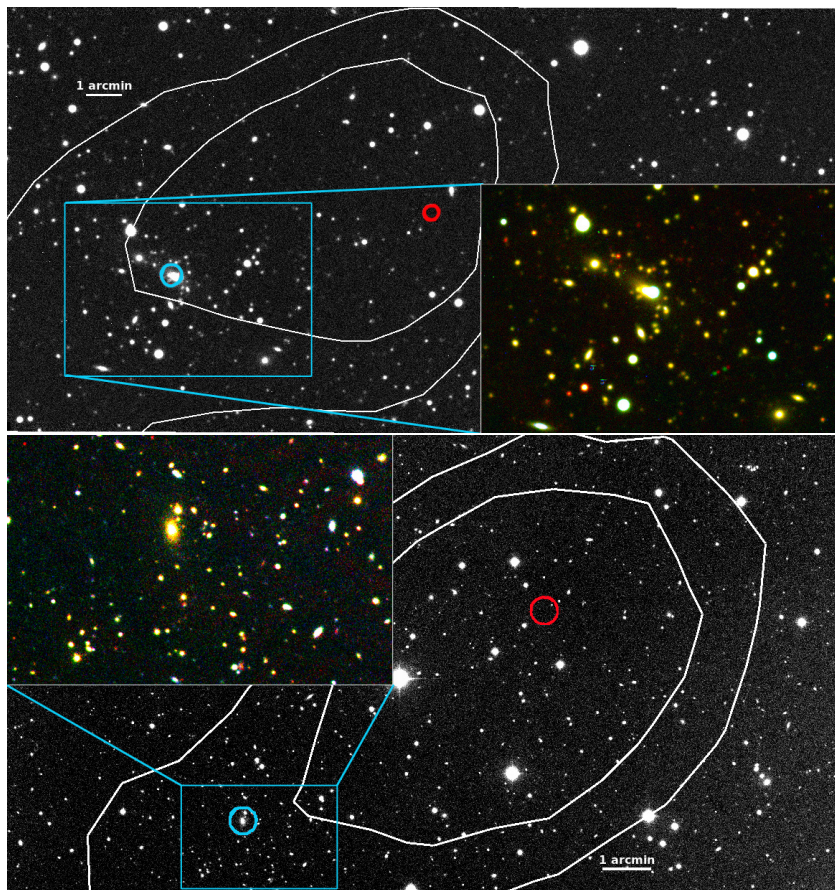


Figure 3.5: Two examples of the clusters where the distance between the optical counterparts and the nominal PSZ2 position are beyond the official 5' limit. Top: PSZ2 G084.69-58.60 with BCG at 7.1' at $z_{\text{spec}} = 0.185$. Bottom: PSZ2 G118.79+47.50 with BCG at 7.4' at $z_{\text{phot}} = 0.34$. For both clusters we show WFC/INT r -band images with white contours corresponding to the 3 and 6×10^{-6} levels of the Compton y -map in this area. The red circle indicates the nominal *Planck* PSZ2 position. The blue circle marks the BCG and the zoomed RGB image shows the central area of these rich clusters. The elongated shape of y -map contours towards the clusters supports these associations.

Este documento incorpora firma electrónica, y es copia auténtica de un documento electrónico archivado por la ULL según la Ley 39/2015.
 Su autenticidad puede ser contrastada en la siguiente dirección <https://sede.ull.es/validacion/>

Identificador del documento: 3248012 Código de verificación: RmbjVJW6

Firmado por: ALEJANDRO AGUADO BARAHONA
 UNIVERSIDAD DE LA LAGUNA

Fecha: 01/03/2021 09:35:30

María de las Maravillas Aguiar Aguiar
 UNIVERSIDAD DE LA LAGUNA

22/03/2021 13:39:32

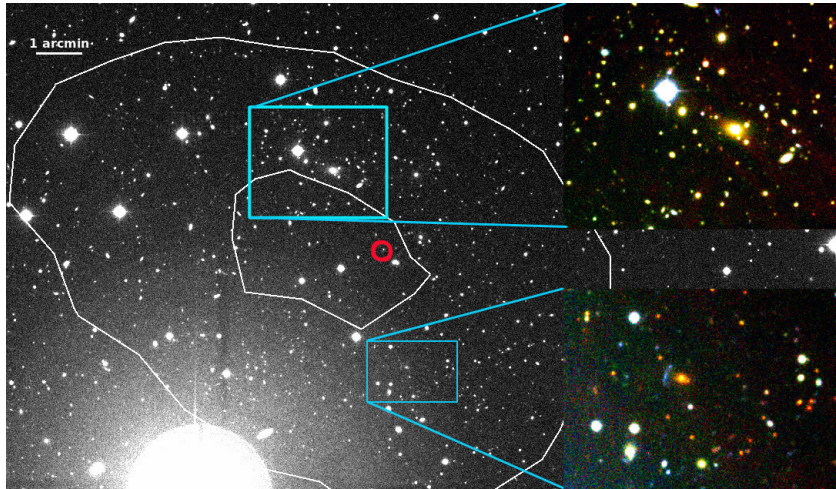


Figure 3.6: WFC/INT r-band image of the PSZ2 G120.76+44.14 which shows the presence of 2 optical counterparts at different redshifts located at almost the same distance from the official *Planck* PSZ2 position ($\sim 2'$). The white contours correspond to the 3 and 6×10^{-6} levels of the Compton y -map in this area, and enclosed both observed sources. The small red circle indicates the position of *Planck* PSZ2 source. The small RGB images show the zoomed regions around the two clusters, one at $z_{\text{spec}} = 0.296$ (top panel), and a second cluster at $z_{\text{spec}} = 0.393$ (bottom panel). We also detected a gravitational arc around the BCG of the second cluster.

Both clusters are rich systems and located at a similar distance from the nominal *Planck* position ($\sim 2'$) and confirmed by y -map contours. One of these two clusters is a system at $z_{\text{spec}} = 0.296$, while the second has $z_{\text{spec}} = 0.363$ and presents a clear gravitational arc around the BCG (Fig. 3.6). Both clusters probably contribute to the SZ emission. In total, we find three cases like this, where multiple counterparts are associated with a single SZ source. We denote these sources with a special symbol in the Table 3.2.

3.2.3 Unconfirmed cluster candidates

Out of the 106 sources studied during the first year of the program, 57 remain unconfirmed. Most of those SZ targets are located close to the galactic plane and are associated with areas with strong dust contamination, thus, probably, producing false SZ detections in the *Planck* maps (see e.g. Fig. 3.7). Similar cases were already reported and intensively discussed in our previous follow-up works for PSZ1 targets (Section 4.3 in Barrena et al. 2020) and pre-selected PSZ2 sources (Section 4.3 in Streblyanska et al. 2018). In the presented field, as in the majority of other cases, we detect important

Este documento incorpora firma electrónica, y es copia auténtica de un documento electrónico archivado por la ULL según la Ley 39/2015.
 Su autenticidad puede ser contrastada en la siguiente dirección <https://sede.ull.es/validacion/>

Identificador del documento: 3248012 Código de verificación: RmbjVJW6

Firmado por: ALEJANDRO AGUADO BARAHONA
 UNIVERSIDAD DE LA LAGUNA

Fecha: 01/03/2021 09:35:30

María de las Maravillas Aguiar Aguiar
 UNIVERSIDAD DE LA LAGUNA

22/03/2021 13:39:32

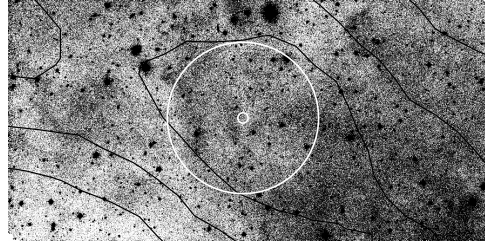


Figure 3.7: WFC/INT g-band image of the PSZ2 G100.07+17.06. The black contours correspond to the 3, 6, 9×10^{-6} levels of the Compton y -map in this area. The small and big white circles indicate the nominal *Planck* position and the $5'$ region, respectively. No cluster counterpart is identified in this case. Most probably, the presence of important galactic gas and dust structures influenced on the SZ emission in this area, creating spurious enhancements of the SZ signal and, consequently, a false SZ detection. We also observe that the elongation and direction of a dust Galactic filament strongly correlates with observed SZ flux profile, supporting our hypothesis.

galactic cirrus around the PSZ2 G100.07+17.06 in the optical images. Moreover, the distribution of the signal in the y -map is not compact, and shows an elongated profile along the observed Galactic dust structures. We emphasise here, the importance of using optical and infrared observations to confirm the absence of a cluster counterpart in those regions of strong dust contamination and for sources detected with relative low S/N . For example, Khatri (2016) proposed a theoretical approach for the validation of the PSZ2 clusters based on the combination of CO and y -maps only. They classified all sources in groups based on their χ^2_{CO-y} determining whether a source is a cluster or a molecular cloud. However, only 61% of 1094 previously confirmed PSZ2 sources with secure z information were classified as clusters (*CLG* + *pCLG*) using this method. The rest of the confirmed clusters were classified either as indeterminable (*IND*) or as molecular clouds (*MOC* + *pMOC*). Studying their classification for our sub-sample of 106 sources, we found that 55% of our confirmed clusters were classified as molecular clouds, and 14% of our unconfirmed sources classified as clusters. However, we note that all our high S/N sources without an optical counterpart are classified as *MOC* by this approach.

We note that for some sources, we cannot explain the absence of optical counterparts in terms of dust contamination. A relatively high number of non-detections in “clean” fields were found already in the PSZ1 sample, and it is re-confirmed in the PSZ2 set. Inspecting in detail all our unconfirmed sources, we found that most of them have neural network quality flag *Q_NEURAL* (Aghanim et al. 2015) close to 0. This flag was introduced already for the PSZ1 data-set, and the value of 0.4 was used to separate the high quality detections from the low-reliability ones. The original PSZ2 catalogue included 171 detections considered likely to be spurious by the neural network classifi-

Este documento incorpora firma electrónica, y es copia auténtica de un documento electrónico archivado por la ULL según la Ley 39/2015.
 Su autenticidad puede ser contrastada en la siguiente dirección <https://sede.ull.es/validacion/>

Identificador del documento: 3248012 Código de verificación: RmbjVJW6

Firmado por: ALEJANDRO AGUADO BARAHONA
 UNIVERSIDAD DE LA LAGUNA

Fecha: 01/03/2021 09:35:30

María de las Maravillas Aguiar Aguilár
 UNIVERSIDAD DE LA LAGUNA

22/03/2021 13:39:32

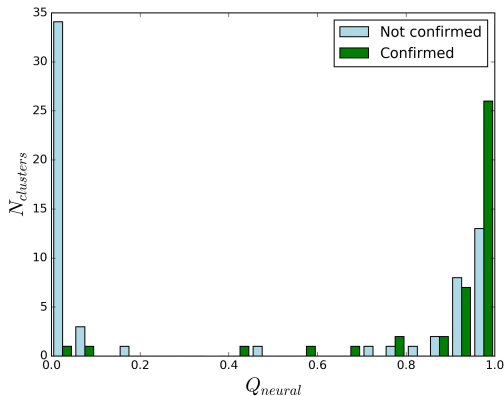


Figure 3.8: Number of cluster-candidates versus the neural network quality flag value for the sub-sample of 106 sources studied in this paper. By construction, Q_{NEURAL} values smaller than 0.4 denote low-reliability detections. This figure confirms that this parameter indeed effectively separates real and spurious SZ identifications. However, we note that some of the unconfirmed sources with high Q_{NEURAL} values are located in areas of strong dust contamination, probably producing the false SZ detections.

cation, and from them only 19 were confirmed clusters with redshift information. Our sub-sample of 106 sources contains 37 objects with $Q_{\text{NEURAL}} < 0.4$, and all of them, except PSZ2 G137.24+53.93 and PSZ2 G310.81+83.91, were classified as unconfirmed. This result demonstrates again that this flag effectively separates between real and spurious detections, and thus it should be considered as valuable information in the validation process. In figure 3.8 we plot a distribution of confirmed and unconfirmed sources versus Q_{NEURAL} values. Some of the non validated clusters with high values of Q_{NEURAL} are located at the areas with strong dust contamination being, most probably, result of spurious enhancements of the SZ signal.

Finally, we mention that some of these unconfirmed sources with the low value of Q_{NEURAL} flag at the same time present a high S/N of the SZ detection (values greater than 10), like PSZ2 G100.45+16.79, PSZ2 G153.56+36.82 and PSZ2 G107.41-09.57. This again demonstrates the importance to perform multi-wavelength follow-ups which include optical data, which allow us to correctly validate SZ sources and establish the actual completeness of *Planck* detection.

We will address a topic on the purity of complete *Planck* SZ sample and provide a detailed study on galactic dust contamination in the Section 3.5.

Este documento incorpora firma electrónica, y es copia auténtica de un documento electrónico archivado por la ULL según la Ley 39/2015.
 Su autenticidad puede ser contrastada en la siguiente dirección <https://sede.ull.es/validacion/>

Identificador del documento: 3248012 Código de verificación: RmbjVJW6

Firmado por: ALEJANDRO AGUADO BARAHONA
 UNIVERSIDAD DE LA LAGUNA

Fecha: 01/03/2021 09:35:30

María de las Maravillas Aguiar Aguilár
 UNIVERSIDAD DE LA LAGUNA

22/03/2021 13:39:32

Table 3.3: Summary information of the long-term LP15 program.

Year	Observed	val	spec	Flag 1	Flag 2	Flag 3	ND
1	106	41	34	31	10	8	57
2	78	40	22	18	22	6	32
TOTAL:	184	81	56	49	32	14	89

For each year of the program, we show the total number of observed candidates (column 2), the total number of validated clusters (column 3), and the number of those with spectroscopic measurements (column 4). For completeness, columns 5–8 also include the classification of the candidates according to our validation criteria described in Table 3.1. Note that validated clusters (column 3) are those with flags 1 or 2. The full LP15 sample contained 190 candidates. Thus, there are still 6 additional objects to be studied.

3.3 LP15 sample: 2nd year of observations

The results presented in this section have been published in Aguado-Barahona et al. (2019).

3.3.1 Results

Table 3.3 summarises the basic information of program LP15 after the two years of observations, concerning the characterisation of the LP15 sample. The results for year one of the program were already discussed in the previous section.

Here, table 3.4 presents the results for 78 PSZ2 galaxy cluster candidates studied in this optical follow-up during the second and last year. The table is organised as follows. Columns 1, 2 and 3 are the official ID number, the *Planck* Name and the SZ signal-to-noise ratio, respectively, as they appear in the PSZ2 catalogue. Columns 4 and 5 are the J2000 coordinates of the BCG when present, otherwise geometrical centre of the cluster is provided. Column 6 is the distance between *Planck* and the optical centre reported in this work. Columns 7 and 8 present the spectroscopic information when available: the mean spectroscopic redshift of the cluster and/or the BCG, and the number of spectroscopic members retrieved. Columns 9, 10 and 11 provide the photometric information: the photometric redshift, the estimation of the richness and the value σ_R as explained in Sect. 3.1.1. Column 12 lists the cluster classification following the **Flag** system described in Sect. 3.1.3. The complete version of this table is published in (Aguado-Barahona et al. 2019), including some comments on individual clusters, such as alternative names and correlations with other surveys.

Following the confirmation criteria explained in Sect. 3.1.3, we find that 37 of our candidates have a single optical counterpart, and one additional is classified as double detection. We classify a source as double detection when we find two or more overdensities around the SZ emission peak that might contribute to this emission. The ones

Este documento incorpora firma electrónica, y es copia auténtica de un documento electrónico archivado por la ULL según la Ley 39/2015.
 Su autenticidad puede ser contrastada en la siguiente dirección <https://sede.ull.es/validacion/>

Identificador del documento: 3248012 Código de verificación: RmbjVJW6

Firmado por: ALEJANDRO AGUADO BARAHONA
 UNIVERSIDAD DE LA LAGUNA

Fecha: 01/03/2021 09:35:30

María de las Maravillas Aguiar Aguilár
 UNIVERSIDAD DE LA LAGUNA

22/03/2021 13:39:32

validated with a single optical counterpart are classified as follows: 17 as **Flag 1** and 22 as **Flag 2**. In addition, we find 32 non-detections, flagged as ND and six systems not associated with the corresponding SZ source (**Flag 3**). This means a total of 38 PSZ2 sources remaining unconfirmed.

We have partially focused our work using SDSS DR12 data to confirm PSZ2 clusters classified by Streblyanska et al. (2018) as ‘potentially associated’ with the SZ emission. We have obtained the redshift and the velocity dispersion for six of the photometrically confirmed clusters and we have re-confirmed six clusters using our own deep INT imaging data classifying them as **Flag 1** and **2**, respectively. From the ‘potentially associated’ sub-sample of Streblyanska et al. (2018) we have confirmed five as **Flag 1**. Here, we invalidate the PSZ2 G328.96+71.97, confirmed by Streblyanska et al. (2018). New SDSS DR14 data reveals that the counterpart proposed by the authors is part of a larger system whose BCG is 34.6′ away from the *Planck* SZ pointing. This system will be discussed in detail in Section 3.3.2.

Finally, we note that there are six objects in the LP15 sample that have not been observed during the program. One of them, PSZ2 G186.50–13.45, was already validated in Streblyanska et al. (2018), with a photometric redshift of $z_{\text{phot}} = 0.25$. According to our validation criteria, this case would correspond to a **Flag= 2**.

Este documento incorpora firma electrónica, y es copia auténtica de un documento electrónico archivado por la ULL según la Ley 39/2015.
 Su autenticidad puede ser contrastada en la siguiente dirección <https://sede.ull.es/validacion/>

Identificador del documento: 3248012 Código de verificación: RmbjVJW6

Firmado por: ALEJANDRO AGUADO BARAHONA
 UNIVERSIDAD DE LA LAGUNA

Fecha: 01/03/2021 09:35:30

María de las Maravillas Aguiar Aguilár
 UNIVERSIDAD DE LA LAGUNA

22/03/2021 13:39:32

Table 3.4: List of 78 PSZ2 cluster candidates analysed in the second year of the program.

ID ¹	Planck Name	SZ SNR	Position (J2000)			Dist.([∘])	< $\dot{s}_{\text{spec}} >$; $\dot{s}_{\text{spec,BCC}}$	N_{spec}	\dot{s}_{phot}	R_{cor}	σ_R	Flag
			R. A.	Decl.	l							
115 ^{a,b}	PSZ2 G032.31+66.07	5.14	14 37 23.35	+24 24 21.70	3.10	0.610 ;	38	0.62±0.05	13.6±3.7	5.4	1	
194	PSZ2 G048.47+34.86	5.74	—	—	—	—	—	—	—	—	ND	
242	PSZ2 G058.31+41.96	4.54	14 26 03.78	+51 14 18.50	3.85	0.462 ; 0.4568	25	0.50±0.05	11.6±3.4	4.3	1	
421-A ^c	PSZ2 G092.69+59.92	4.90	14 26 13.10	+51 11 53.17	4.42	0.844 ;	5	—	—	—	3	
421-B ^c	PSZ2 G093.41+16.26	4.59	22 24 07.25	+37 58 30.46	3.10	—	27	0.24±0.03	40.6±6.4	7.9	2	
432 ^{a,b}	PSZ2 G094.31+11.31	4.72	22 12 56.10	+42 35 46.34	1.08	0.204 ;	—	0.30±0.04	16.8±4.1	7.8	2	
500	PSZ2 G104.52+39.39	4.60	15 58 38.88	+70 27 24.20	5.62	—	—	—	—	—	ND	
545	PSZ2 G112.64+59.53	5.37	—	—	—	—	—	—	—	—	ND	
546	PSZ2 G112.64+59.53	4.78	16 19 49.39	+79 06 24.49	4.78	0.521 ; 0.5194	15	0.51±0.03	—	—	ND	
592	PSZ2 G122.81+24.74	4.69	—	—	—	—	—	—	—	—	ND	
600	PSZ2 G122.81+24.74	4.69	—	—	—	—	—	—	—	—	ND	
613	PSZ2 G125.25+33.33	5.38	11 41 11.26	+83 27 38.91	1.80	—	—	0.20±0.03	21.0±4.6	4.1	2	
620 ^b	PSZ2 G125.41+27.95	4.76	01 06 55.65	+44 04 25.72	1.81	0.189 ;	46	0.19±0.01	—	—	1	
624 ^b	PSZ2 G126.36+19.11	5.01	01 09 19.57	+43 37 40.41	0.60	0.203 ; 0.2007	22	0.22±0.01	—	—	1	
627	PSZ2 G126.62+53.42	4.55	—	—	—	—	—	—	—	—	ND	
628 ^b	PSZ2 G126.72+21.03	4.68	01 10 27.91	+41 40 57.27	0.84	0.196 ;	9	0.22±0.03	—	—	1	
640	PSZ2 G129.99+22.42	4.55	—	—	—	—	—	—	—	—	ND	
644-A ^b	PSZ2 G130.64+37.16	4.80	10 47 45.54	+77 59 56.67	2.82	0.473 ; 0.4722	14	0.44±0.03	16.7±4.1	5.0	1	
644-B ^b	PSZ2 G131.15+14.72	5.37	10 46 29.31	+78 07 44.06	6.07	—	—	0.24±0.02	49.3±7.0	11.9	2	
647	PSZ2 G131.19+14.48	4.80	01 38 42.22	+47 22 35.27	1.71	—	—	0.22±0.03	50.2±7.1	11.3	2	
648	PSZ2 G131.27+25.82	4.50	—	—	—	—	—	—	—	—	ND	
667 ^c	PSZ2 G136.02+47.15	4.64	01 28 23.61	+14 41 13.60	7.09	0.466 ; 0.4648	8	0.50±0.03	13.1±3.6	4.2	3	
676	PSZ2 G136.02+47.15	4.64	—	—	—	—	—	—	—	—	ND	
712 ^a	PSZ2 G140.55+55.55	4.67	01 42 46.53	+04 59 48.72	4.71	0.429 ;	1	0.42±0.04	10.8±3.3	3.0	2	
713	PSZ2 G140.55+55.55	4.67	09 40 17.10	+66 24 02.56	7.18	0.342 ; 0.3379	4	0.34±0.04	7.0±2.6	3.5	2	
717	PSZ2 G146.88+17.13	6.13	—	—	—	—	—	—	—	—	ND	
720	PSZ2 G147.17+42.67	4.92	09 50 01.152	+64 55 29.52	1.34	— ; 0.4401	1	0.46±0.04	7.4±2.7	3.1	2	
727	PSZ2 G149.73+24.49	4.52	—	—	—	—	—	—	—	—	ND	
732 ^{a,b}	PSZ2 G150.64+14.21	4.68	03 17 04.20	+40 41 33.22	3.08	—	—	0.22±0.02	26.1±5.1	8.2	2	
739 ^{a,c}	PSZ2 G152.40+75.00	4.70	12 13 19.17	+39 46 26.84	5.06	0.455 ;	9	0.42±0.03	31.3±5.6	9.0	1	
740	PSZ2 G152.47+42.11	4.81	09 29 52.64	+61 39 40.00	0.24	0.900 ;	6	—	—	—	3	
746	PSZ2 G153.08+36.96	5.07	—	—	—	—	—	—	—	—	ND	
747	PSZ2 G153.08+36.96	4.72	—	—	—	—	—	—	—	—	ND	
754	PSZ2 G156.24+22.32	4.79	06 45 02.14	+59 27 13.30	0.75	—	—	0.30±0.05	—	—	2	
769	PSZ2 G160.94+44.85	4.98	—	—	—	—	—	—	—	—	ND	
780	PSZ2 G163.89+11.55	4.78	—	—	—	—	—	—	—	—	ND	
788	PSZ2 G165.39+09.22	5.60	05 48 09.37	+46 04 41.41	4.39	—	—	0.70±0.10	15.1±3.9	5.4	2	
789	PSZ2 G165.41+25.93	4.51	07 23 27.93	+52 07 32.70	4.83	—	—	0.67±0.04	4.3±2.1	1.8	2	
797	PSZ2 G166.56+17.69	4.76	04 04 53.39	+28 18 31.85	3.44	—	—	0.70±0.07	3.3±1.8	1.4	ND	
799	PSZ2 G167.43+53.67	4.65	—	—	—	—	—	—	—	—	ND	
812 ^{a,c}	PSZ2 G171.48+16.17	4.75	06 38 00.94	+43 50 57.20	0.75	0.385 ; 0.3881	25	0.40±0.05	15.9±4.0	2.7	1	
813	PSZ2 G171.48+16.17	4.63	07 17 48.66	+43 50 57.20	3.03	0.383 ; 0.0652	2	0.06±0.02	—	—	2	
831 ^a	PSZ2 G177.03+32.64	4.93	08 13 08.56	+43 13 53.07	3.50	0.511 ;	9	—	—	—	1	
835	PSZ2 G179.33+22.42	5.02	—	—	—	—	—	—	—	—	ND	
836 ^{a,b}	PSZ2 G179.45+43.92	4.54	03 19 18.34	+02 05 35.60	2.58	0.397 ; 0.4005	23	0.34±0.03	19.1±4.4	5.8	1	

Este documento incorpora firma electrónica, y es copia auténtica de un documento electrónico archivado por la ULL según la Ley 39/2015.
 Su autenticidad puede ser contrastada en la siguiente dirección <https://sede.ull.es/validacion/>

Identificador del documento: 3248012 Código de verificación: RmbjVJW6

Firmado por: ALEJANDRO AGUADO BARAHONA
 UNIVERSIDAD DE LA LAGUNA

Fecha: 01/03/2021 09:35:30

María de las Maravillas Aguiar Aguiar
 UNIVERSIDAD DE LA LAGUNA

22/03/2021 13:39:32

Table 3.4: Continue.

ID ¹	Planck Name	SZ SNR	Position (J2000)		Dist.(^o)	< z _{spec} >	z _{spec} :BCG	N _{spec}	z _{phot}	R _{cor}	σ _R	Flag
			R. A.	Decl.								
849	PSZ2 G183.32-31.51	4.56	04 05 20.11	+07 51 26.07	2.31	—	—	—	0.55±0.10	1.8±1.3	—	3
852	PSZ2 G183.32+16.36	4.97	07 01 30.22	+32 54 51.20	6.61	0.091 ; 0.0914	18	18	0.15±0.03	30.3±5.5	4.4	1
878	PSZ2 G185.72-39.23	5.18	06 37 14.55	+28 35 02.80	1.47	0.390 ; 0.3897	39	39	0.40±0.03	—	—	1
860	PSZ2 G191.57-58.88	5.12	—	—	—	—	—	—	—	—	—	ND
878	PSZ2 G193.90+09.41	5.06	—	—	—	—	—	—	—	—	—	ND
887	PSZ2 G201.20-42.83	4.70	06 51 11.80	+21 08 10.16	0.73	0.194 ; 0.1936	29	29	0.16±0.03	23.5±4.8	3.0	1
912	PSZ2 G202.61-26.26	4.87	04 59 50.17	-03 16 47.52	5.52	—	—	—	0.23±0.03	8.5±2.9	4.6	3
917 ^{a,c}	PSZ2 G202.66+66.98	4.63	11 07 30.90	+28 51 01.20	4.68	0.482 ; 0.4814	20	20	0.48±0.04	11.9±3.4	5.3	1
920 ^{a,c,d}	PSZ2 G203.32+08.91	5.15	07 05 56.53	+12 30 33.66	4.25	—	—	—	0.27±0.03	9.4±3.0	4.6	2
921 ^a	PSZ2 G203.71+50.82	4.65	09 55 15.56	+26 19 37.70	2.03	0.082 ; —	22	22	—	—	—	1
952	PSZ2 G210.71+63.08	7.37	—	—	—	—	—	—	—	—	—	ND
953	PSZ2 G210.78-36.25	6.32	07 52 40.27	-01 03 21.55	3.10	—	—	—	0.55±0.05	30.7±5.5	7.6	2
954	PSZ2 G210.85-36.77	4.43	07 52 40.27	-01 03 21.55	3.10	—	—	—	0.30±0.05	28.9±5.4	10.2	2
1018	PSZ2 G227.30+09.02	4.62	07 58 81	-07 29 23.70	2.96	—	—	—	0.24±0.03	—	—	2
1023	PSZ2 G227.30+09.02	4.62	07 50 15.74	-08 24 32.56	1.85	—	—	—	0.35±0.03	—	—	2
1049 ^{a,b}	PSZ2 G231.41+77.48	4.54	12 00 26.54	+22 34 19.55	6.32	0.346 ; 0.3469	2	2	0.28±0.04	35.3±5.9	10.3	2
1062	PSZ2 G233.46+25.46	4.79	08 12 39.17	-10 52 02.90	2.35	—	—	—	—	—	—	ND
1074 ^{a,b}	PSZ2 G237.68+57.83	5.36	10 53 17.80	+10 52 37.13	4.88	—	—	—	0.70±0.05	—	—	2
1095	PSZ2 G241.98+16.56	4.51	08 58 04.54	-14 43 01.87	3.95	—	—	—	0.27±0.04	33.1±5.7	8.3	2
1151	PSZ2 G252.45+73.44	5.57	—	—	—	—	—	—	—	—	—	ND
1162	PSZ2 G253.95+39.12	4.66	—	—	—	—	—	—	—	—	—	ND
1216	PSZ2 G254.52+02.32	4.88	—	—	—	—	—	—	—	—	—	ND
1219	PSZ2 G263.96+40.04	4.58	—	—	—	—	—	—	—	—	—	ND
1262 ^{a,b}	PSZ2 G271.33+56.41	5.19	11 05 10.71	-19 50 15.61	4.73	—	—	—	0.50±0.03	—	—	2
1302	PSZ2 G271.33+56.41	5.19	13 02 14.77	-07 58 48.29	3.02	0.527 ; 0.5395	27	27	0.30±0.05	12.7±3.6	3.3	2
1510 ^{a,c}	PSZ2 G320.94+83.69	7.32	13 00 05.74	+21 01 28.29	7.00	0.461 ; 0.4612	5	5	0.45±0.04	—	—	3
1513	PSZ2 G321.94+75.57	4.66	—	—	—	—	—	—	—	—	—	ND
1532	PSZ2 G325.19+49.12	4.62	13 49 55.18	-11 15 24.44	3.61	—	—	—	0.20±0.03	28.1±5.3	6.5	2
1548 ^{a,b}	PSZ2 G328.96+71.97	5.85	13 23 02.10	+11 01 32.12	18.03	0.090 ; 0.0937	94	94	0.09±0.01	—	—	3

¹ SZ targets identified with the ID followed by an A or B label indicate the presence of multiple counterparts.
^a Photometric and/or spectroscopic redshift obtained from SDSS DR14 data.
^b Already confirmed in Streblyanska et al. (2018)
^c Classified as "potentially associated" in Streblyanska et al. (2018)
^d Richness study from PAN-STARRS

Este documento incorpora firma electrónica, y es copia auténtica de un documento electrónico archivado por la ULL según la Ley 39/2015.
 Su autenticidad puede ser contrastada en la siguiente dirección <https://sede.ull.es/validacion/>

Identificador del documento: 3248012 Código de verificación: RmbjVJW6

Firmado por: ALEJANDRO AGUADO BARAHONA
 UNIVERSIDAD DE LA LAGUNA

Fecha: 01/03/2021 09:35:30

María de las Maravillas Aguiar
 UNIVERSIDAD DE LA LAGUNA

22/03/2021 13:39:32

3.3.2 Notes on individual objects

PSZ2 G058.31+41.96. This candidate is flagged as a nondetection because a bright star is located near the *Planck* pointing. The star prevents photometric measurements of this region, and we are therefore unable to visually identify an over-density of galaxies. Despite this problem, we cannot identify visually any over-density of galaxies in the region.

PSZ2 G104.52+39.39. The distance from the optical centre and the *Planck* nominal pointing is 5.62. Nevertheless, we validate this cluster with **Flag** = 2 because the MILCA *y*-map contours are elongated along the line that links the optical and *Planck* centres. In addition, the position error in the *Planck* catalogue is too high (5.40) compared to the nominal error (2.43).

PSZ2 G130.64+37.16. This candidate has two optical counterparts that have been validated in Streblyanska et al. (2018); one was also validated by Burenin (2017). This is a difficult case as we show in figure 3.9. For a detailed description see caption of Fig. 3.9.

PSZ2 G146.13+40.97. The optical centre of the proposed counterpart (its BCG) is 7.18 away from the *Planck* SZ pointing, which is affected by a position error of 5.89. The *y*-map contours present a very irregular shape, possibly as a result of galactic dust contamination in this region. We estimate a richness of $\sigma_R = 3.5$ for this system and find four cluster members at $z_{\text{spec}} = 0.342$ in the SDSS DR14 spectroscopic sample. We therefore classify this counterpart with **Flag** = 2. The ultimate confirmation will be obtained using MOS observations.

PSZ2 G152.47+42.11. We find a possible cluster counterpart at $z_{\text{spec}} = 0.900$. The deepness of our images makes it impossible to estimate the richness at this redshift. However, we have observed this system spectroscopically and found six cluster members. From these six galaxies, we obtain a very low-velocity dispersion ($< 400 \text{ km s}^{-1}$), revealing a low-mass galaxy system. In this case, we therefore classify this optical counterpart with **Flag** = 3.

PSZ2 G156.24+22.32. This region encloses two very bright stars, which makes it very difficult to obtain accurate photometry or richness. However, by eye inspection, we identified a cluster with a galaxy population with coherent colours. A detailed study of the photometry of some individual likely members and the BCG revealed $z_{\text{phot}} = 0.30$. In addition, the *y*-map contours present a very regular profile centred on this system. For all these reasons, we classify this system with **Flag** = 2.

PSZ2 G177.03+32.64. Burenin (2017) reported a counterpart for this candidate at $z \sim 0.28$. We analysed this overdensity and found seven galaxies with spectroscopic redshifts in the SDSS archive. Four of these galaxies are more than 4 Mpc away from the *Planck* centre, and the velocity dispersion accounting for the seven galaxies is lower than 300 km s^{-1} . For this reason, we show here only one counterpart at $z_{\text{spec}} = 0.511$ whose velocity dispersion, calculated using nine members, is approximately 1000 km s^{-1} .

PSZ2 G183.92+16.36. The distance between the BCG of this cluster and the *Planck* pointing is 6.61, which is only 0.67 Mpc at the redshift of the cluster, $z_{\text{spec}} = 0.091$. We performed multi-object spectroscopy and retrieved 18 cluster members, showing $\sigma_v \sim 650 \text{ km s}^{-1}$. In addition, this cluster is known as Abell 567. It is well consolidated

Este documento incorpora firma electrónica, y es copia auténtica de un documento electrónico archivado por la ULL según la Ley 39/2015.
 Su autenticidad puede ser contrastada en la siguiente dirección <https://sede.ull.es/validacion/>

Identificador del documento: 3248012 Código de verificación: RmbjVJW6

Firmado por: ALEJANDRO AGUADO BARAHONA
 UNIVERSIDAD DE LA LAGUNA

Fecha: 01/03/2021 09:35:30

María de las Maravillas Aguiar Aguilár
 UNIVERSIDAD DE LA LAGUNA

22/03/2021 13:39:32

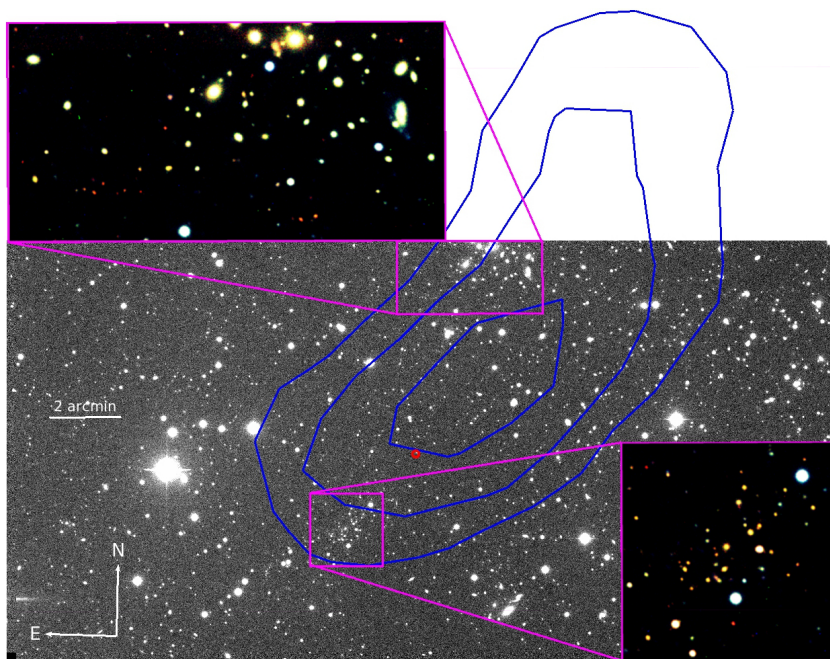


Figure 3.9: Compton y -map superimposed on the INT r' band of PSZ2 G130.64+37.16. Blue contours correspond to the 4, 4.6, and 5.2×10^{-6} levels of the Compton y -map in this area. The nominal SZ pointing (red) is clearly closer to cluster 644-A (zoomed-in in the lower right region), which has 14 spectroscopic members and shows a velocity dispersion close to 1000 km s^{-1} ; cluster 644-B (zoomed-in in the upper left region) is $6'.07$ away from the SZ centre, but the MILCA y -map shows that the contours are elongated along this counterpart location, which is twice as rich as that of 644-A. The position error in the *Planck* catalogue here is $5'.38$, which is more than twice the mean position error.

Este documento incorpora firma electrónica, y es copia auténtica de un documento electrónico archivado por la ULL según la Ley 39/2015.
 Su autenticidad puede ser contrastada en la siguiente dirección <https://sede.ull.es/validacion/>

Identificador del documento: 3248012 Código de verificación: RmbjVJW6

Firmado por: ALEJANDRO AGUADO BARAHONA
 UNIVERSIDAD DE LA LAGUNA

Fecha: 01/03/2021 09:35:30

María de las Maravillas Aguiar Aguiar
 UNIVERSIDAD DE LA LAGUNA

22/03/2021 13:39:32

by other observations in the past (Abell et al. 1989). We therefore confirm Abell 567 as the counterpart of this SZ source and classify it with **Flag** = 1.

PSZ2 G202.61−26.26 and PSZ2 G203.32+08.91 Both candidates were analysed using PANSTARRS photometric data (Chambers et al. 2016). Both systems are rich, but the optical centre of the first lies more than 5′ away from the *Planck* nominal pointing, therefore it was classified with **Flag** = 3.

PSZ2 G227.30+09.00 This is an SZ source placed at very low galactic latitude, so that many stars crowd this field. For this reason, we were unable to compute the richness: the galaxies of the background are partially masked by the foreground stars. However, this system presents X-ray emission and has been catalogued as 1RXS J075020.3-082605 in the ROSAT survey. We therefore classify this source with **Flag** = 2.

PSZ2 G237.68+57.83 This cluster has previously been validated by Streblyanska et al. (2018) using SDSS data. Here, we confirm this association using the INT images. Although we are unable to perform a richness estimation at this redshift, the photometry of some individual likely cluster members agrees with a $z_{\text{phot}} = 0.70 \pm 0.05$. We also find two additional over-densities at (RA=10:53:35.55, Dec=+10:43:45.71) and (RA=10:53:59.602, Dec=+10:46:38.23). However, they are at a distance greater than 10′ from the SZ coordinates and therefore probably do not contribute to the SZ signal. Therefore we validated PSZ2 G237.68+57.83 as a single counterpart at $z_{\text{phot}} = 0.70$.

PSZ2 G271.53+36.41 This candidate was confirmed photometrically in Streblyanska et al. (2018) as a double detection. However, only one cluster is visible in the INT images. This cluster is at $z_{\text{phot}} = 0.50 \pm 0.03$. No more systems are associated with this SZ source.

PSZ2 G328.96+71.97 was validated by Streblyanska et al. (2018) using SDSS DR12 data. Here, we used new spectroscopic information provided by SDSS DR14 in order to update the information. We find 94 cluster members at $\langle z_{\text{spec}} \rangle = 0.090$. However, the BCG of this structure is at 34′ from the *Planck* pointing. Figure 3.10 shows the scenario around this region. The profile of the SZ emission is very spread out and irregular, with several peaks. The 94 cluster members have $\sigma_v \sim 800 \text{ km s}^{-1}$ and a virial radius of 1.6 Mpc, but the cluster seems to be placed completely off the SZ peak. The distance between the *Planck* pointing and the optical cluster centre is twice as large than the virial radius of the cluster. For all these reasons, we conclude that no optical counterpart is found for this SZ source, and the actual counterpart (if it exists) is still unknown.

3.4 Observations of other PSZ2 candidates beyond the LP15 sample

In the PSZ2 catalogue, 73 clusters are validated using the AllWISE mid-infrared source catalogue, see Planck Collaboration XXVII (2016). This catalogue is based on the observations from the Wide-field Infrared Survey Explorer mission (WISE; Wright et al. 2010). In Sect. 7.4 in Planck Collaboration XXVII (2016), the authors searched for galaxy over-densities in the redshift range $0.3 < z < 1.5$ using the (W1-W2) colour. These objects had **validation** = 16 in the original PSZ2 catalogue, and were therefore

Este documento incorpora firma electrónica, y es copia auténtica de un documento electrónico archivado por la ULL según la Ley 39/2015.
 Su autenticidad puede ser contrastada en la siguiente dirección <https://sede.ull.es/validacion/>

Identificador del documento: 3248012 Código de verificación: RmbjVJW6

Firmado por: ALEJANDRO AGUADO BARAHONA
 UNIVERSIDAD DE LA LAGUNA

Fecha: 01/03/2021 09:35:30

María de las Maravillas Aguiar Aguilár
 UNIVERSIDAD DE LA LAGUNA

22/03/2021 13:39:32

3.4 Observations of other PSZ2 candidates beyond the LP15 sample 61

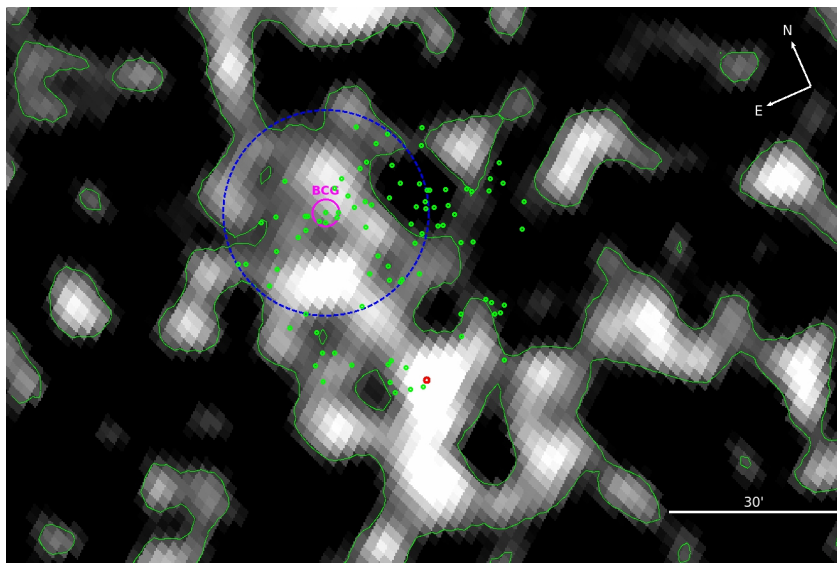


Figure 3.10: SZ emission as seen in the Compton y -maps for the source PSZ2 G328.96+71.97. The red dot represents the SZ coordinate as it appears in the PSZ2 catalogue. The BCG of the cluster is plotted in magenta, and the remaining galaxies members are shown in green. The blue circle encloses the virial radius of this cluster. The 94 cluster members are placed completely off the SZ peak, and the optical counterpart of this SZ source remains unknown.

Este documento incorpora firma electrónica, y es copia auténtica de un documento electrónico archivado por la ULL según la Ley 39/2015.
Su autenticidad puede ser contrastada en la siguiente dirección <https://sede.ull.es/validacion/>

Identificador del documento: 3248012 Código de verificación: RmbjVJW6

Firmado por: ALEJANDRO AGUADO BARAHONA
UNIVERSIDAD DE LA LAGUNA

Fecha: 01/03/2021 09:35:30

María de las Maravillas Aguiar Aguilár
UNIVERSIDAD DE LA LAGUNA

22/03/2021 13:39:32

Table 3.5: Update of already known optical counterparts from the PSZ1.

ID	Planck Name	SZ SNR	R. A.	Decl.	Dist.(')	z_{phot}	R_{cor}	σ_R	Flag
897	PSZ2 G196.65–45.51	4.91	03 42 54.40	–08 41 07.70	1.52	0.25±0.03	–	–	2
901	PSZ2 G198.73+13.34	6.03	–	–	–	–	–	–	ND
1130	PSZ2 G249.14+28.98	5.96	09 44 57.60	–13 48 11.22	1.16	0.15±0.03	18.6±4.3	5.3	2
1539	PSZ2 G326.73+54.80	5.92	13 45 14.70	–05 32 04.00	3.91	0.46±0.05	20.3±4.5	10.6	2

not included in the definition of the LP15 sample.

3.4.1 Results

Here, we present an update on 38 of these ALLWISE sources and provide their spectroscopic redshifts, which were obtained using dedicated observations carried out with the telescope time within the LP15 program. Table 3.6 presents this information, and it is organised in the same way as Table 3.4. The complete version of this table is published in (Aguado-Barahona et al. 2019), including some comments on individual clusters, such as alternative names and correlations with other surveys.

PSZ2 G086.28+74.76, PSZ2 G139.00+50.92, and PSZ2 G141.98+69.31 are, in principle, double detections. However, they can be considered single detections even though secondary clusters were detected because they are very low-mass systems and are therefore not capable of contributing significantly to the SZ signal.

As noted in earlier by the *Planck* Collaboration, the number of double cluster detections is somewhat higher than in other surveys in X-rays (Planck Collaboration int. I 2012) or in the optical (Planck Collaboration int. XXVI 2015).

We cross-checked our sample with two galaxy cluster catalogues, Wen, Han and Liu (WHL) (Wen et al. 2012) and Wen, Han and Yang (WHY) (Wen & Han 2018), which are based on optical and infrared data, respectively. The WHL catalogue was published using SDSS data, while WHY used 2MASS (Skrutskie et al. 2006), WISE (Wright et al. 2010), and SuperCOSMOS (Hambly et al. 2001) data. We can only find three matches with WHL. PSZ2 G076.55+60.29 and PSZ2 G141.98+69.31 are discussed in the next subsection together with PSZ2 G021.02–29.0, which is also part of the WHY catalogue. We find seven matches with the WHY catalogue. We agree at 1σ in redshift except for PSZ2 G056.38+23.36. In this case, we estimate a photometric redshift of $z_{\text{phot}} = 0.21 \pm 0.02$, while Wen & Han (2018) reported $z_{\text{phot}} = 0.31 \pm 0.04$. This is compatible within 2σ .

We also present in this section, an update on four sources that have been confirmed in the PSZ2 original catalogue, Planck Collaboration XXVII (2016), because they were matched with PSZ1 clusters but without a redshift estimate, PSZ1 G196.62–45.50, PSZ1 G198.67+13.34, PSZ1 G249.14+28.98 and PSZ1 G326.64+54.79. Here, we provide the photometric redshift for three of them and invalidate the previously confirmed PSZ2 G198.73+13.34, for which we were unable to find any galaxy over-density. In a future publication, we will discuss this type of source, which we believe to be a false validation. These four sources can be found in table 3.5.

Este documento incorpora firma electrónica, y es copia auténtica de un documento electrónico archivado por la ULL según la Ley 39/2015.
 Su autenticidad puede ser contrastada en la siguiente dirección <https://sede.ull.es/validacion/>

Identificador del documento: 3248012 Código de verificación: RmbjVJW6

Firmado por: ALEJANDRO AGUADO BARAHONA
 UNIVERSIDAD DE LA LAGUNA

Fecha: 01/03/2021 09:35:30

María de las Maravillas Aguiar Aguilera
 UNIVERSIDAD DE LA LAGUNA

22/03/2021 13:39:32

3.4 Observations of other PSZ2 candidates beyond the LP15 sample 63

Table 3.6: Updated information of other PSZ2 candidates beyond the LP15 sample.

ID ¹	Planck Name	SZ SNR	Position (J2000)			Dist.(²)	< z _{spec} > ; z _{spec} , BCG	N _{bgc}	z _{phot}	R _{cor}	σ _R	Flag
			R. A.	Decl.	Dec.							
65	PSZ2 G0290.91-36.84	5.17	20 51 57.42	-35 59 17.03	1.87	—	—	0.21±0.02	18.1±4.3	3.6	2	
68 ^{a,c}	PSZ2 G021.02-20.04	4.89	20 20 28.21	-22 25 14.78	1.83	0.300 ; 0.3017	25	0.32±0.04	—	—	1	
92	PSZ2 G027.77-49.72	4.60	21 53 03.42	-23 34 13.08	1.45	0.165 ; 0.1641	15	0.12±0.02	20.6±4.5	4.4	1	
93	PSZ2 G027.81-45.93	5.24	21 57 16.11	-22 32 19.80	2.23	—	—	0.45±0.05	15.8±4.0	5.2	2	
120	PSZ2 G033.83-46.57	5.53	21 45 12.35	-18 42 57.41	2.50	—	—	0.32±0.04	3.7±1.9	1.7	2	
206	PSZ2 G050.98-61.48	5.10	22 58 53.05	-15 35 30.87	1.76	—	—	0.18±0.03	14.2±3.8	6.5	2	
227	PSZ2 G056.38+23.36	4.85	18 01 16.53	+30 23 20.71	3.43	0.022 ; 0.0107	52	0.21±0.02	11.4±3.4	7.0	2	
277 ^{a,c}	PSZ2 G066.34+26.14	5.63	18 01 06.52	+39 52 06.73	1.64	—	—	0.63±0.06	—	—	1	
284	PSZ2 G069.55+22.48	4.88	18 20 08.12	+39 15 32.93	2.05	0.766 ; 0.7630	23	0.19±0.02	22.3±4.7	10.3	2	
284 ^{a,c}	PSZ2 G069.55+22.48	4.91	18 20 08.12	+39 15 32.93	2.06	—	—	0.70±0.06	—	—	1	
301 ^{a,c}	PSZ2 G072.32-56.05	4.71	23 41 36.32	+44 54 59.40	3.90	0.822 ; —	38	—	—	—	1	
301 ^{a,c}	PSZ2 G072.32-56.05	4.76	23 37 35.32	+44 54 59.40	3.30	—	—	0.30±0.03	7.8±2.8	7.3	2	
323	PSZ2 G075.85+15.53	4.64	19 10 50.62	+14 44 31.31	4.21	0.287 ; —	5	0.25±0.03	35.9±6.0	23.1	2	
327-A ^{a,d}	PSZ2 G076.55+60.29	5.42	14 52 00.51	+44 31 21.31	4.21	0.632 ; —	1	0.70±0.06	14.5±3.8	8.4	2	
333	PSZ2 G078.10-83.83	4.87	00 32 30.94	-22 42 10.95	2.00	—	—	0.28±0.03	18.4±4.3	8.7	2	
335	PSZ2 G082.37+22.35	5.93	18 44 31.37	+53 00 09.01	1.67	—	—	0.29±0.03	14.5±3.8	9.3	2	
359	PSZ2 G083.56+24.90	6.13	18 29 28.55	+54 43 08.80	1.60	—	—	0.32±0.04	7.0±2.6	2.7	2	
378	PSZ2 G085.95+25.23	5.55	18 30 23.81	+56 53 11.12	0.62	—	—	0.65±0.05	4.6±2.1	1.5	2	
381-A	PSZ2 G086.28+74.76	5.07	13 38 40.43	+38 52 32.57	8.93	0.246 ; —	20	—	—	—	3	
381-B ^{a,c}	PSZ2 G087.39-34.58	4.62	13 37 54.11	+38 53 30.94	1.28	0.701 ; —	21	0.80±0.06	—	—	1	
381-B ^{a,c}	PSZ2 G087.39-34.58	4.63	22 49 09.53	+19 44 30.50	1.39	0.772 ; —	31	0.70±0.07	—	—	1	
468	PSZ2 G087.50-28.63	4.74	22 49 09.53	+19 44 30.50	1.39	—	—	—	—	—	ND	
475	PSZ2 G098.75-28.63	5.34	17 10 33.34	+68 44 43.60	1.01	—	—	0.31±0.03	15.4±3.9	6.0	2	
548	PSZ2 G099.55+34.23	5.30	13 58 59.49	+67 25 50.29	0.75	—	—	0.32±0.03	7.9±2.8	4.5	2	
581	PSZ2 G113.27+48.39	5.16	13 23 55.03	+68 39 30.73	1.09	—	—	0.36±0.03	24.4±4.9	6.2	2	
582	PSZ2 G118.49+48.17	4.63	00 25 13.35	+49 30 35.84	0.50	—	—	0.28±0.03	20.9±4.6	3.7	2	
590	PSZ2 G120.30+44.47	5.31	13 16 38.50	+72 32 15.60	1.09	—	—	0.23±0.03	23.3±4.8	7.9	2	
623 ^b	PSZ2 G126.28+65.62	4.67	12 42 23.33	+51 26 20.98	1.67	0.819 ; 0.8201	16	—	—	—	1	
625 ^{a,c}	PSZ2 G126.57+51.61	6.35	12 29 47.56	+65 21 13.41	0.33	0.817 ; —	20	0.80±0.10	—	—	1	
654	PSZ2 G133.92-42.73	4.70	01 25 35.36	+19 22 53.51	1.65	0.381 ; —	3	0.65±0.07	2.3±1.5	1.1	ND	
681-A	PSZ2 G139.00+50.92	4.98	11 20 27.45	+63 14 46.15	2.04	0.784 ; —	11	—	—	—	1	
681-B	PSZ2 G141.98+69.31	4.71	12 12 38.98	+46 21 04.59	3.25	0.713 ; —	16	0.70±0.06	—	—	1	
690-A ^{a,d}	PSZ2 G141.98+69.31	4.71	12 12 38.98	+46 21 04.59	3.25	0.796 ; —	9	—	—	—	3	
701	PSZ2 G144.23-18.19	5.22	02 38 55.30	+40 11 11.57	0.41	—	—	0.31±0.03	13.4±3.7	2.2	2	
764	PSZ2 G159.40-40.67	6.05	02 42 22.99	+14 15 14.60	2.81	—	—	0.22±0.03	23.2±4.8	5.4	2	
768	PSZ2 G160.83-70.63	6.30	01 39 20.72	-11 22 19.49	1.20	—	—	0.24±0.03	26.2±5.1	7.7	2	
810 ^{a,c}	PSZ2 G171.08-80.38	4.90	01 21 53.44	-20 33 26.45	2.67	0.313 ; 0.3134	33	0.38±0.03	—	—	1	
902 ^b	PSZ2 G198.80-57.57	4.83	03 02 06.58	-15 33 41.69	0.53	0.530 ; 0.5292	16	—	—	—	1	
937 ^b	PSZ2 G208.57-44.31	4.53	04 02 36.08	-15 40 49.56	1.47	0.820 ; 0.8196	17	—	—	—	1	
1254 ^{a,c}	PSZ2 G270.78+36.83	4.99	11 04 21.06	-19 14 18.34	2.55	0.510 ; 0.5146	25	0.52±0.05	—	—	1	
1606	PSZ2 G333.46+52.65	4.89	14 24 23.15	-02 43 49.34	0.88	0.711 ; —	20	0.70±0.07	—	—	1	

¹ SZ targets identified with the ID followed by an A or B label indicate multiple counterparts.

^a Photometric and/or spectroscopic redshift obtained from SDSS DR14 data.

^b No imaging performed, private communication with the Sackey group

^c Previously confirmed in Streblyanska et al. (2018)

^d Classified as "potentially associated" in Streblyanska et al. (2018)

Este documento incorpora firma electrónica, y es copia auténtica de un documento electrónico archivado por la ULL según la Ley 39/2015.
 Su autenticidad puede ser contrastada en la siguiente dirección <https://sede.ull.es/validacion/>

Identificador del documento: 3248012 Código de verificación: RmbjVJW6

Firmado por: ALEJANDRO AGUADO BARAHONA
 UNIVERSIDAD DE LA LAGUNA

Fecha: 01/03/2021 09:35:30

María de las Maravillas Aguiar Aguiar
 UNIVERSIDAD DE LA LAGUNA

22/03/2021 13:39:32

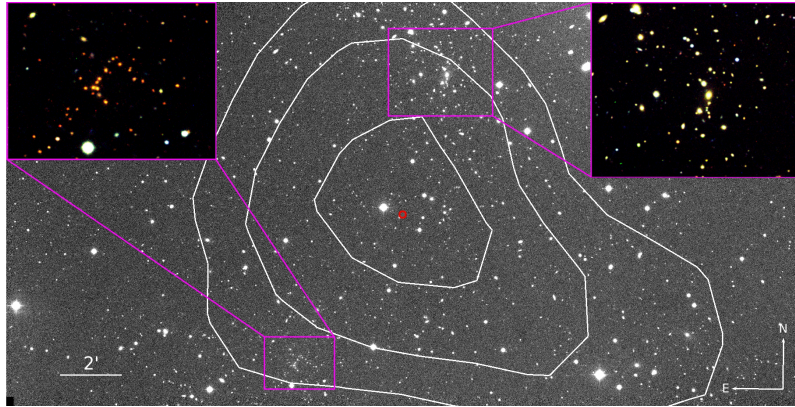


Figure 3.11: Compton y -map superimposed to the INT r' band of the PSZ2 G076.55+60.29. White contours correspond to the 3 , 4 , and 5×10^{-6} levels of the Compton y -map in this area. The *Planck* nominal pointing is represented in red. In the upper corners we show zoomed RGB images of 327-A (left) and 327-B (right). At $z_{\text{spec}} = 0.632$ and $z_{\text{spec}} = 0.287$, the two systems are associated with this SZ signal. This is a clear example of a multiple detection.

3.4.2 Notes on individual objects

We found that PSZ2 G076.55+60.29, which was classified as an individual counterpart by Streblyanska et al. (2018), is in fact a superposition of two clusters at $z_{\text{spec}} = 0.287$ and $z_{\text{spec}} = 0.632$, respectively. The first (327-A) has been proposed as a potentially associated cluster. Here, we have confirmed it with five spectroscopic members. The distance to the *Planck* nominal pointing of the second counterpart (327-B) is slightly greater than $5'$, but the MILCA y -map contours superimposed on an INT image (Fig. 3.11) shows that the SZ emission is clearly a superposition of both clusters. The two counterparts are two of the richest systems we studied and have σ_R of 23.1 (327-A) and 8.4 (327-B).

PSZ2 G086.28+74.76 We find two clusters around the SZ emission at $z_{\text{spec}} = 0.246$ and $z_{\text{spec}} = 0.701$ that we call 381-A and 381-B, respectively. They have a high-velocity dispersion. However, the centre of 381-A is 8.93 away from the *Planck* centre. We therefore concluded that this source has only one optical counterpart at $z_{\text{spec}} = 0.701$.

PSZ2 G126.57+51.61 is one of the most distant clusters in our sample, at $z_{\text{spec}} = 0.816$. Burenin et al. (2018) confirmed one galaxy at $z_{\text{spec}} = 0.815$. This cluster is at the detection limits of our deep optical images. Most of the members are detected almost at the noise level of the i' -band image. No RS for this cluster could be constructed. However, inspection of the RGB image revealed an over-density of red sources close to the *Planck* position supported by the contours extracted from the MILCA y -map (Fig. 3.12). Our spectroscopic data together with SDSS data confirm this cluster with

Este documento incorpora firma electrónica, y es copia auténtica de un documento electrónico archivado por la ULL según la Ley 39/2015.
 Su autenticidad puede ser contrastada en la siguiente dirección <https://sede.ull.es/validacion/>

Identificador del documento: 3248012 Código de verificación: RmbjVJW6

Firmado por: ALEJANDRO AGUADO BARAHONA
 UNIVERSIDAD DE LA LAGUNA

Fecha: 01/03/2021 09:35:30

María de las Maravillas Aguiar Aguilár
 UNIVERSIDAD DE LA LAGUNA

22/03/2021 13:39:32

3.4 Observations of other PSZ2 candidates beyond the LP15 sample 65

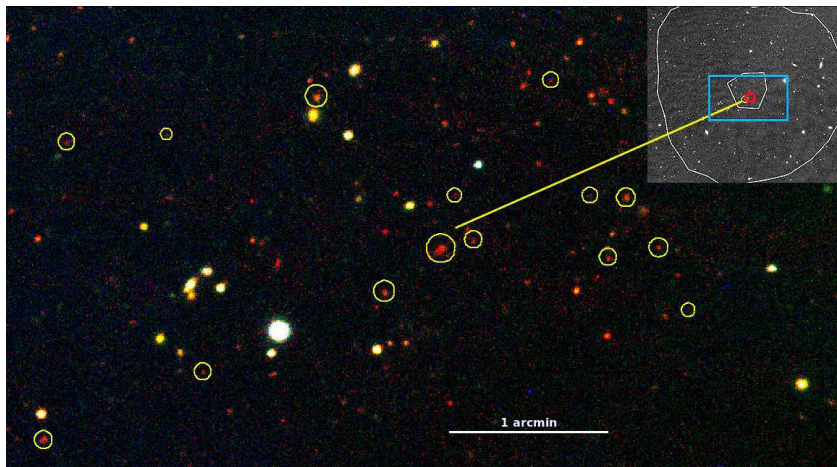


Figure 3.12: Zoomed RGB image of the central area of the high- z cluster ($z_{\text{spec}} = 0.816$) associated with PSZ2 G126.57+51.61. We mark spectroscopically confirmed cluster members with yellow circles. The small top panel shows the WFC/INT i' -band image, in which white contours correspond to the 3 and 6×10^{-6} levels of the Compton y -map in this area. The red circle indicates the nominal PSZ2 position. The blue square shows the size of the area that is presented in the main RGB image.

20 members and a $\sigma_v \sim 850 \text{ km s}^{-1}$.

PSZ2 G133.92-42.73 There is a potential counterpart, but it is discarded because of its low σ_R . In the RGB image (left panel, Fig. 3.13) it seems to be a high-redshift cluster, as seen in the WISE image (right panel, Fig. 3.13). The SDSS data include three galaxies with $z_{\text{spec}} \sim 0.581$. But they are not associated with any galaxy overdensity. Deeper imaging or spectroscopic observations are required in order to reject the possibility of a high- z ($z > 0.8$) cluster.

PSZ2 G139.00+50.92 has been confirmed by Streblyanska et al. (2018) at $z_{\text{phot}} = 0.6$. We performed spectroscopic observations for this cluster, which we call 681-A, and found a velocity dispersion below the confirmation limit ($\sigma_v < 650 \text{ km s}^{-1}$). We conclude that this is not the main counterpart to the SZ emission. However, another cluster (681-B) at $z_{\text{spec}} = 0.784$ has $\sigma_v > 800 \text{ km s}^{-1}$, therefore we conclude that this last counterpart is responsible for the SZ emission.

PSZ2 G141.98+69.31 This is a double detection. We find two over-densities in this field, but when we made spectroscopic observations and calculated the velocity dispersion, we realised that object 690-B had $\sigma_v < 400 \text{ km s}^{-1}$, which is very small for it to be associated with the SZ emission. Consequently, we only validate the object proposed in Streblyanska et al. (2018) with a spectroscopic redshift of $z_{\text{spec}} = 0.713$, here called

Este documento incorpora firma electrónica, y es copia auténtica de un documento electrónico archivado por la ULL según la Ley 39/2015.
 Su autenticidad puede ser contrastada en la siguiente dirección <https://sede.ull.es/validacion/>

Identificador del documento: 3248012 Código de verificación: RmbjVJW6

Firmado por: ALEJANDRO AGUADO BARAHONA
 UNIVERSIDAD DE LA LAGUNA

Fecha: 01/03/2021 09:35:30

María de las Maravillas Aguiar Aguilár
 UNIVERSIDAD DE LA LAGUNA

22/03/2021 13:39:32

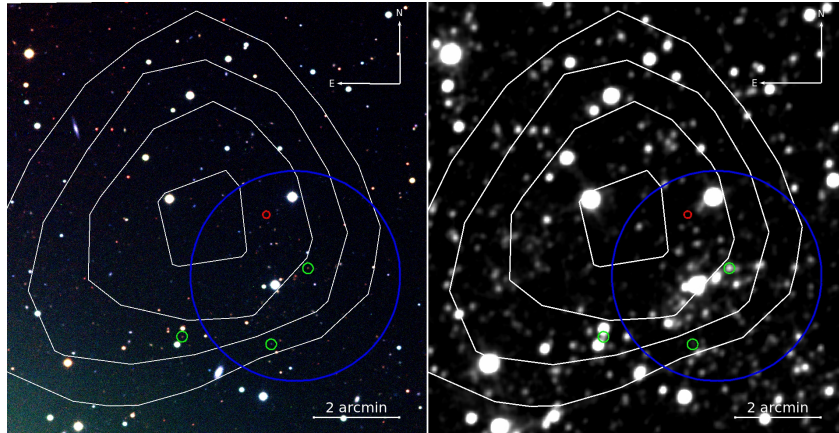


Figure 3.13: Left: RGB image of the source PSZ2 G133.92–42.73. Right: WISE *W1* band of the same region. In both images Compton *y*-maps are represented in white (5 , 5.8 , 6.6 , and 7.4×10^{-6} levels). The blue region corresponds to 1 Mpc (2.45) at the mean redshift of the three galaxies that are represented in green. The *Planck* nominal pointing is marked in red.

690-A.

PSZ2 G270.78+36.83 This candidate has been validated by Streblyanska et al. (2018) as a double detection. Here, we spectroscopically confirm one of these counterparts by detecting 25 cluster members at $z_{\text{spec}} = 0.516$, with $\sigma_v \sim 900 \text{ km s}^{-1}$. The second counterpart remains spectroscopically unconfirmed.

3.5 PSZ2 statistics in the northern sky

The PSZ2 catalogue lists 1003 sources with $Dec. > -15^\circ$. After the two years of LP15 observations, a total of 226 sources have been observed; 184 of them were part of the LP15 sample and thus were not validated at the time the PSZ2 catalogue was published. In addition, we updated the redshift for 42 other sources. In this section, we carry out the statistical analysis of this northern sky sub-sample of the PSZ2 for purity and effects on the PSZ detection. For clarity, we refer to this sub-sample as PSZ2-North, which represents the 60% of the complete PSZ2 sample.

We note that this PSZ2-North sample also includes some PSZ2 sources that are associated with PSZ1 objects that were observed during the ITP13 (Planck Collaboration int. XXXVI 2016; Barrena et al. 2018, 2020). Five sources ($< 0.5\%$) could not be observed in order to validate the full PSZ2-North, therefore we exclude them from the sample when we compute the statistics in this section.

Este documento incorpora firma electrónica, y es copia auténtica de un documento electrónico archivado por la ULL según la Ley 39/2015.
 Su autenticidad puede ser contrastada en la siguiente dirección <https://sede.ull.es/validacion/>

Identificador del documento: 3248012

Código de verificación: RmbjVJW6

Firmado por: ALEJANDRO AGUADO BARAHONA
 UNIVERSIDAD DE LA LAGUNA

Fecha: 01/03/2021 09:35:30

María de las Maravillas Aguiar Aguilár
 UNIVERSIDAD DE LA LAGUNA

22/03/2021 13:39:32

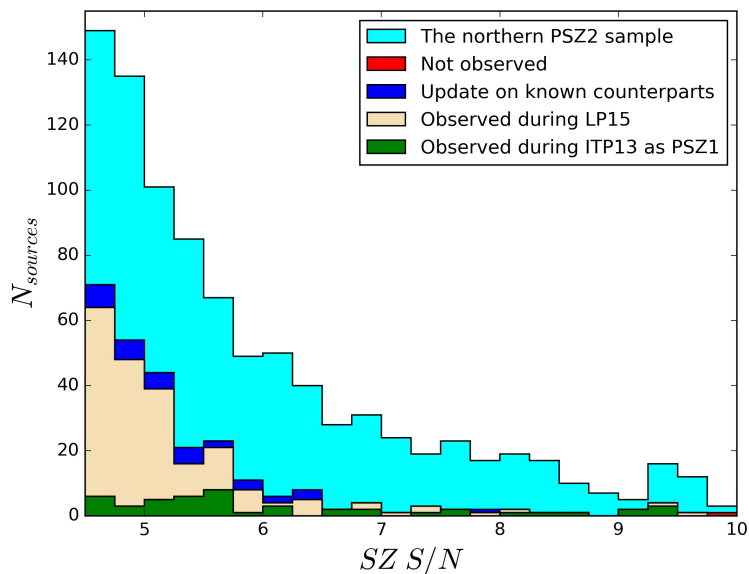


Figure 3.14: PSZ2 cluster counts as a function of the S/N of the SZ detection. The PSZ2-North sample is represented in light blue, the sources that are still not observed are represented in red ($< 0.5\%$), the updated sources described in Sect. 3.4 are shown in dark blue (3.4%), and the sources that were originally not confirmed and were observed during LP15 and ITP13 are shown in green (18.4% and 4.8% , respectively). The bin size is 0.25 .

Este documento incorpora firma electrónica, y es copia auténtica de un documento electrónico archivado por la ULL según la Ley 39/2015.
 Su autenticidad puede ser contrastada en la siguiente dirección <https://sede.ull.es/validacion/>

Identificador del documento: 3248012 Código de verificación: RmbjVJW6

Firmado por: ALEJANDRO AGUADO BARAHONA
 UNIVERSIDAD DE LA LAGUNA

Fecha: 01/03/2021 09:35:30

María de las Maravillas Aguiar Aguiar
 UNIVERSIDAD DE LA LAGUNA

22/03/2021 13:39:32

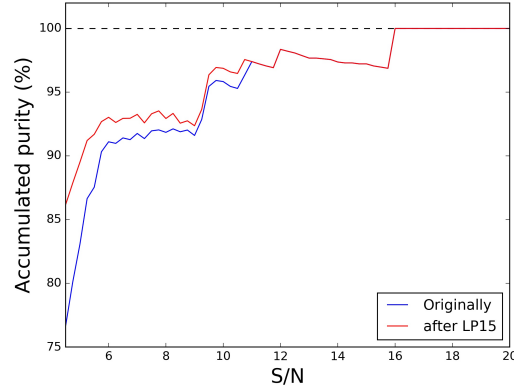


Figure 3.15: Accumulated purity of the PSZ2-North sample ($\text{Dec.} > -15^\circ$) studied as a function of the S/N , i.e., the percentage of the sources that are actual clusters and related to the SZ signal. In blue we represent the original purity of the catalogue, and in red the same purity, but after this work.

Figure 3.14 shows the number of clusters as a function of the S/N in the catalogue. The vast majority of the sources studied in this work has an $S/N < 6$, and this is within the range where this optical follow-up found the largest contribution. In particular, we observed 37% of the sources with $4.5 < S/N < 6$.

We define the purity as the ratio between confirmed clusters and the total number of SZ sources. It is important to take into account that we have explored the optical range in which the dust emission might be masking the possible counterpart. We quantify this effect below. Figure 3.15 shows the accumulated purity of the PSZ2-North sample as a function of S/N . While it originally showed a purity of 76.7%, the purity increased to 86.2% for $S/N > 4.5$ after all validation programs. The expected purity for the whole catalogue was $\sim 88\%$ (see figure 11 in Planck Collaboration XXVII 2016), so the result presented here confirms this prediction. The feature in figure 3.15 that shows a decrease in purity in the range $12 < S/N < 16$ is due to one nondetection that is listed in the PSZ2 as a high S/N source (PSZ2 G153.56+36.82). This has been studied in detail in Section 3.2.3.

Figure 3.16 shows the distribution of redshifts of the *Planck* -confirmed clusters. We note that 77% have a redshift between $0.05 < z < 0.4$, which is the ideal range for a cluster detection of the *Planck* mission. The median redshift of the PSZ2-North sample is 0.23, and the median redshift of the clusters that were confirmed during LP15 is 0.29. While we confirm about 10% of the clusters at $z < 0.4$, this rate is $\sim 20\%$ for $z > 0.4$. Moreover, Barrena et al. (2018) confirmed the most distant *Planck* SZ cluster in the

Este documento incorpora firma electrónica, y es copia auténtica de un documento electrónico archivado por la ULL según la Ley 39/2015.
 Su autenticidad puede ser contrastada en la siguiente dirección <https://sede.ull.es/validacion/>

Identificador del documento: 3248012 Código de verificación: RmbjVJW6

Firmado por: ALEJANDRO AGUADO BARAHONA
 UNIVERSIDAD DE LA LAGUNA

Fecha: 01/03/2021 09:35:30

María de las Maravillas Aguiar Aguilár
 UNIVERSIDAD DE LA LAGUNA

22/03/2021 13:39:32

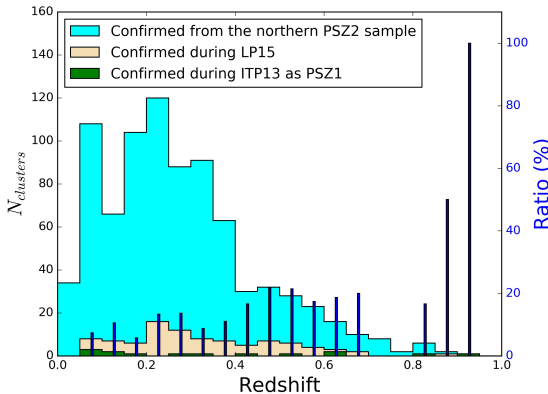


Figure 3.16: Cluster counts as a function of redshift. Colour codes are the same as in figure 3.14. Dark blue bars represent the ratio between clusters confirmed during our follow-ups and the total confirmed clusters. The size of the redshift bin is 0.05.

northern hemisphere: PSZ2 G123.35+25.39, at $z_{\text{phot}} = 0.95$.

Burenin (2017) presented an extension for the PSZ2 catalogue using SDSS and WISE. We find 28 matches in this catalogue and the LP15 sample. Our results agree well for most of the sources. For PSZ2 G069.47–29.06 and PSZ2 G130.64+37.16, the author only reported one counterpart, while we find two. PSZ2 G069.47–29.06 was discussed in section 3.2.2, where both candidates were confirmed with 44 and 30 spectroscopic members, as reported in Zaznobin et al. (2019). PSZ2 G130.64+37.16 was discussed in Sect. 3.3.2. In contrast, for PSZ2 G066.59–58.51, we find only one counterpart, while Burenin (2017) reported more than one.

We compared our results with those of Zohren et al. (2019). They used the WHT to validate high- z clusters of the *Planck* catalogues. They reported the redshift, richness, and mass for 23 candidates. Twenty of them were also observed during the LP15 program. We agree with their results except for three cases. They claimed, as did Burenin et al. (2018), that PSZ2 092.69+59.92 has two counterparts, at $z = 0.46$ and $z = 0.84$. Our spectroscopic observations reveal that the galaxy over-density at $z = 0.84$ is a low-mass system because it has $\sigma_v < 450 \text{ km s}^{-1}$. They found that the mass limit of PSZ2 G139.00+50.92 lay below their validation limit. As discussed in Sect. 3.4.2, we find two possible counterparts, one (681-B) with $\sigma_v > 800 \text{ km s}^{-1}$. PSZ2 G165.41+25.93 is also below their mass limit, whereas in our richness analysis, it has $\sigma_R = 1.8$, which is just above our validation limit of $\sigma_R = 1.5$.

We also compared our results with Zaznobin et al. (2019), who reported 38 spectroscopic redshifts for PSZ2 candidates. We find 20 matches between this catalogue and

Este documento incorpora firma electrónica, y es copia auténtica de un documento electrónico archivado por la ULL según la Ley 39/2015.
 Su autenticidad puede ser contrastada en la siguiente dirección <https://sede.ull.es/validacion/>

Identificador del documento: 3248012 Código de verificación: RmbjVJW6

Firmado por: ALEJANDRO AGUADO BARAHONA
 UNIVERSIDAD DE LA LAGUNA

Fecha: 01/03/2021 09:35:30

María de las Maravillas Aguiar Aguilár
 UNIVERSIDAD DE LA LAGUNA

22/03/2021 13:39:32

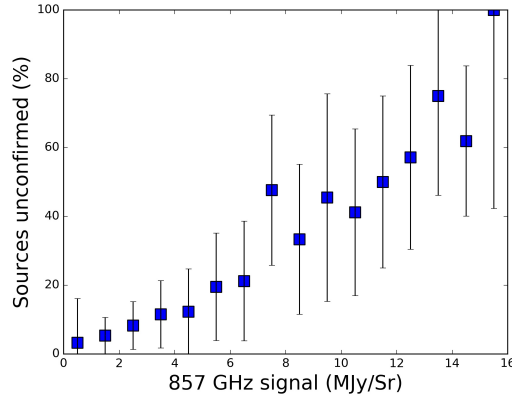


Figure 3.17: Ratio between unconfirmed and total number of sources for the PSZ2-North sample (Dec. > -15°) as a function of the 857 GHz signal in bins of 1 MJy sr^{-1} . Error bars correspond to a Poisson error in the distribution of the total number of sources.

the LP15 sample. We find discrepancies in only one case, PSZ2 G202.61–26.26. The authors reported three spectroscopic redshifts at $z_{\text{spec}} = 0.533$ while we find a galaxy over-density at $z_{\text{phot}} = 0.23$, but farther than $5'$ away from the *Planck* centre. This is therefore not linked to the SZ emission.

In order to study the galactic disturbance on the SZ *Planck* detection, we computed the number of nondetections as a function of the 857 GHz signal in the *Planck* map. This map could be used as a tracer of thermal dust emission (Planck Collaboration XI 2014). The signal was computed as the mean value within a region of 0.5° radius around the nominal pointing in the PSZ2 catalogue. Figure 3.17 represents the ratio between the unconfirmed and the total number of sources for the PSZ2-North sample as a function of the 857 GHz signal in bins of 1 MJy sr^{-1} . This figure shows a clear correlation between these two magnitudes. Below 7 MJy sr^{-1} , the ratio of unconfirmed sources is lower than 20%. However, in zones with high dust emission (mainly places in the galactic plane), the false SZ clusters can exceed 60–70%.

Figure 3.18 shows the number of cluster candidates versus the neural network quality flag value for the PSZ2-North sample (Q_{bad}). This value was defined in Aghanim et al. (2015). It is an indicator of how reliably an SZ source is confirmed as a real galaxy cluster. Candidates with values of $Q_{\text{bad}} > 0.6$ are considered low-reliability sources. In the PSZ2-North sample, we observe that the vast majority (> 93%) of the clusters with $Q_{\text{bad}} < 0.6$ are actual clusters, while fewer than 33% with $Q_{\text{bad}} > 0.6$ are confirmed.

Following the same idea as in section 3.2.3, we compared the full validation results with Khatri (2016), who published a validation method for the PSZ2 catalogue based on

Este documento incorpora firma electrónica, y es copia auténtica de un documento electrónico archivado por la ULL según la Ley 39/2015.
 Su autenticidad puede ser contrastada en la siguiente dirección <https://sede.ull.es/validacion/>

Identificador del documento: 3248012 Código de verificación: RmbjVJW6

Firmado por: ALEJANDRO AGUADO BARAHONA
 UNIVERSIDAD DE LA LAGUNA

Fecha: 01/03/2021 09:35:30

María de las Maravillas Aguiar Aguilár
 UNIVERSIDAD DE LA LAGUNA

22/03/2021 13:39:32

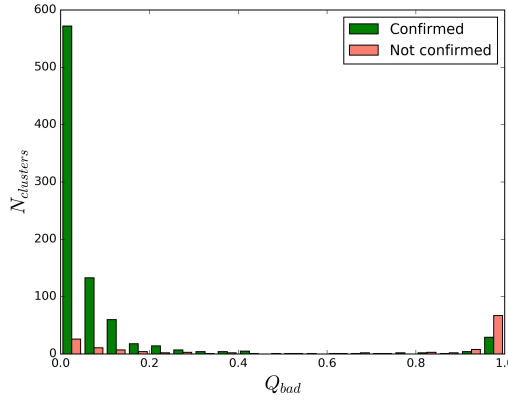


Figure 3.18: Number of cluster candidates vs. the neural network quality flag value for the PSZ2-North sample. Confirmed candidates are represented in green, and still unconfirmed clusters are shown in red. The bin size is 0.05.

combined CO and y -distortion maps. He classified the sources into five different groups depending on the value of his estimator: MOC , $pMOC$, CLG , $pCLG$, and IND . The signal of the sources classified as MOC and $pMOC$ was considered to come from molecular clouds, and CLG and $pCLG$ signals come from galaxy clusters. IND is indeterminable. We find that 95.2% of the IND and 94.6% of the $CLG + pCLG$ correspond to actual validated clusters. On the other hand, 64.7% of the $MOC + pMOC$ are also validated clusters. We expected that sources with this classification have a lower validation rate, but this is not the case. A possible explanation for these results is that the threshold used by Khatri (2016) to distinguish between molecular clouds and clusters was shifted toward high values of $\Delta(\Sigma\chi^2)_{CO-y}$. To illustrate this, for the 59 sources that the author classified as $pMOC$, 48 (81.3%) are actual clusters.

This Chapter represents the characterisation of the sample in which the next part of the thesis is based. In the next Chapter, I will use the confirmed GCs presented in tables 3.2 and 3.4 as well as other confirmed PSZ2 clusters to construct the $M_{SZ} - M_{dyn}$ scaling relation. Fitting this relation, I will be able to constrain the value for the mass bias parameter ($1 - b$) with the lower uncertainties ever using the largest SZ selected sample to date.

Este documento incorpora firma electrónica, y es copia auténtica de un documento electrónico archivado por la ULL según la Ley 39/2015.
 Su autenticidad puede ser contrastada en la siguiente dirección <https://sede.ull.es/validacion/>

Identificador del documento: 3248012 Código de verificación: RmbjVJW6

Firmado por: ALEJANDRO AGUADO BARAHONA
 UNIVERSIDAD DE LA LAGUNA

Fecha: 01/03/2021 09:35:30

María de las Maravillas Aguiar Aguiar
 UNIVERSIDAD DE LA LAGUNA

22/03/2021 13:39:32

4

Velocity dispersion and dynamical masses for 388 Galaxy Clusters and groups. Calibrating the $M_{\text{SZ}} - M_{\text{dyn}}$ scaling relation for the PSZ2 sample

This Chapter presents all the spectroscopic observations of the full LP15 program. We complement these LP15 spectroscopic results with Sloan Digital Sky Survey (SDSS) archival data and other observations. I present a catalogue of 388 clusters and groups of galaxies including estimates of their velocity dispersion. The majority of them (356) are the optical counterpart of a PSZ2 source. A subset of 297 of those clusters is used to construct the $M_{\text{SZ}} - M_{\text{dyn}}$ scaling relation, based on the estimated SZ mass from *Planck* measurements and our dynamical mass estimates. We discuss and correct for different statistical and physical biases in the estimation of the masses, such as the Eddington bias when estimating M_{SZ} and the aperture and the number of galaxies used to calculate M_{dyn} . Finally, I estimate the mass bias parameter $(1 - b)$ with the largest sample to date homogeneously selected and with spectroscopic measurements. All these results are included in a paper submitted for publication (Aguado-Barahona et al. 2021, submitted).

This Chapter is structured as follows. Section 4.1 describes our reference sample. Section 4.2 illustrates our methodology for the velocity dispersion estimates. In Section 4.3, I present our dynamical mass estimates, and compare them to the SZ masses. Section 4.4 shows the results for the characterisation of the scaling relation $M_{\text{SZ}} - M_{\text{dyn}}$ in the PSZ2 North, and the results for the mass bias factor $(1 - b)$.

4.1 The reference sample

The PSZ2-North sub-sample is defined in Chapter 3, as those 1003 objects within the PSZ2 catalogue with $Dec. > -15^\circ$. This Chapter presents the velocity dispersion and

Este documento incorpora firma electrónica, y es copia auténtica de un documento electrónico archivado por la ULL según la Ley 39/2015.
Su autenticidad puede ser contrastada en la siguiente dirección <https://sede.ull.es/validacion/>

Identificador del documento: 3248012 Código de verificación: RmbjVJW6

Firmado por: ALEJANDRO AGUADO BARAHONA
UNIVERSIDAD DE LA LAGUNA

Fecha: 01/03/2021 09:35:30

María de las Maravillas Aguiar Aguilár
UNIVERSIDAD DE LA LAGUNA

22/03/2021 13:39:32

Table 4.1: Summary of the data sets.

Data set	PSZ2-North	Others in PSZ2 (see Sect. 4.1.4)	Beyond PSZ2 (see Sect. 4.1.5)	Scaling relation	
				$1.5 \times r_{200}$	$1 \times r_{200}$
LP15	63	6	13	48	44
ITP13	43	0	4	38	33
SDSS	250	0	9	211	184
Total	356	6	26	297	261

dynamical mass for a set of 388 objects (see Table 4.1). The majority of them (356) are the optical counterpart of a SZ source in the PSZ2-North sample (note that double detections are counted as two different clusters). Six clusters are the optical counterpart of a PSZ2 source but outside the PSZ2-North sample. The remaining 26 objects were found during the process of analysis of the fields in which a SZ source is present, but were not associated with the SZ signal (see Sect. 4.1.5 for details). Each object in our sample comes from one particular data set. These data sets are described in the following sub-sections.

The possible presence of interlopers inside the cluster radial velocity catalogues might bias the velocity dispersion and mass estimates (Mamon et al. 2010). For this reason, we decided to analyse the clusters in two ways, trying to characterise the presence of this source of error. During the member selection process, explained in detail in Sect. 4.2, we use two different apertures, namely 1 and $1.5 \times r_{200}$, to select the cluster members. The comparison of the mass bias in both cases gives no significant difference between them, so we can safely assume that the number of interlopers within 1 and $1.5 \times r_{200}$ is sufficiently small (compared to our statistical error) to not account for them. Table 4.1 includes the details about these sub-samples.

Figure 4.1 shows the number of clusters belonging to the $1.5 \times r_{200}$ sub-sample in comparison with the total number of objects in the PSZ2-North sample, as a function of the signal-to-noise ratio (SNR) in the PSZ2 catalogue. Our sample covers the full range of SNR values, being approximately 30% of the total PSZ2-North sample. This fact allows us to consider this sample as statistically representative to infer global properties of the full PSZ2-North sample.

4.1.1 LP15 data set

The 128-MULTIPLE-16/15B follow-up program LP15 was designed to observe all PSZ2-North sources with no confirmed counterparts at the moment of the catalogue’s publication. This original LP15 sample contains 190 objects (see Chapter 2 and Aguado-Barahona et al. 2019). The program had two main goals: to validate the SZ sources by finding their optical counterparts, and to use them for the calibration of the $M_{SZ} - M_{dyn}$ scaling relation. The validation process was published in Streblyanska et al. (2019) and Aguado-Barahona et al. (2019), and it is detailed in Chapters 2 and 3. In total, 184

Este documento incorpora firma electrónica, y es copia auténtica de un documento electrónico archivado por la ULL según la Ley 39/2015.
 Su autenticidad puede ser contrastada en la siguiente dirección <https://sede.ull.es/validacion/>

Identificador del documento: 3248012 Código de verificación: RmbjVJW6

Firmado por: ALEJANDRO AGUADO BARAHONA
 UNIVERSIDAD DE LA LAGUNA

Fecha: 01/03/2021 09:35:30

María de las Maravillas Aguiar Aguilár
 UNIVERSIDAD DE LA LAGUNA

22/03/2021 13:39:32

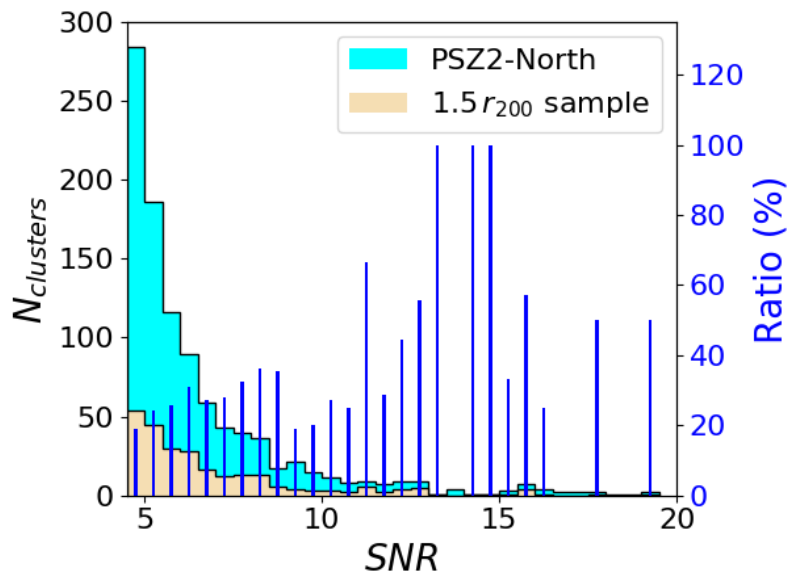


Figure 4.1: PSZ2 cluster counts as a function of the signal-to-noise ratio (SNR) of the SZ detection. The PSZ2-North sample is represented in light blue, and the $1.5 \times r_{200}$ sample is represented in wheat. Dark blue bars represent the ratio between the $1.5 \times r_{200}$ sample and the total number of clusters in the PSZ2-North sample. The bin size is 0.5.

Este documento incorpora firma electrónica, y es copia auténtica de un documento electrónico archivado por la ULL según la Ley 39/2015.
 Su autenticidad puede ser contrastada en la siguiente dirección <https://sede.ull.es/validacion/>

Identificador del documento: 3248012 Código de verificación: RmbjVJW6

Firmado por: ALEJANDRO AGUADO BARAHONA
 UNIVERSIDAD DE LA LAGUNA

Fecha: 01/03/2021 09:35:30

María de las Maravillas Aguiar Aguilár
 UNIVERSIDAD DE LA LAGUNA

22/03/2021 13:39:32

sources were observed, being 81 of them confirmed as optical counterparts of the PSZ2 detections.

As a summary, the LP15 program was performed during four consecutive terms (2015B, 2016A, 2016B and 2017A). Due to technical telescope issues we were not able to complete this program in time, so we were granted with other four observing nights during the term 2018A in the frame of the program CAT18A-12. All spectroscopic observations were obtained using the multi-object spectrographs Device Optimised for the LOw RESolution (DOLORES) at the Telescopio Nazionale Galileo (TNG) and Optical System for Imaging and low-Intermediate-Resolution Integrated Spectroscopy (OSIRIS) at the Gran Telescopio Canarias (GTC), both located at the Roque de los Muchachos Observatory (ORM) in La Palma (Spain). Details about the imaging and spectroscopic procedures can be found in Chapter 2.

In total, 94 sources were observed spectroscopically, 55 at the GTC and 39 at the TNG. We obtained good quality data to estimate the velocity dispersion for 82 clusters, which corresponds to a success rate of 87%. The mean (median) redshift of this data set is $z_{spec} = 0.41$ (0.39) and the mean (median) number of galaxy members for these clusters is $N = 26$ (22). All the spectroscopic results of these observations are presented for the first time in this thesis and in the associated publication (Aguado-Barahona et al. 2021, submitted).

4.1.2 ITP13 data set

In addition, we use part of the ITP13 sample described in Ferragamo et al. (2021, submitted). This sample consists of 61 PSZ1 clusters, from which 47 of them are also included in the PSZ2 catalogue. The observations of these objects were performed during four terms in the framework of the International Time Program ITP13B-08, a similar program to the LP15 but for the PSZ1 catalogue. We include these 47 objects in our analysis finding a mean (median) redshift of $z_{spec} = 0.37$ (0.31) and a mean (median) number of galaxies members of the clusters $N = 19$ (17). Out of those 47 objects, 43 of them are contained inside the PSZ2-North sample. We complement the individual cluster member catalogues from the two data sets described above using spectroscopic data from the Sloan Digital Sky Survey (SDSS, York et al. 2000) Data Release (DR) 14, when available.

4.1.3 SDSS data

SDSS archival data give us a unique opportunity to enlarge our original sample. We retrieve every spectroscopic redshift within $15'$ from the *Planck* nominal pointing for all the PSZ2 objects inside the SDSS footprint. For the cases with $z_{spec} < 0.1$, we expand this region to $30'$ radius to obtain as much cluster members as possible.

We identify 259 galaxy clusters following this procedure. In nine cases, the object found does not fulfil the criteria to be considered an optical counterpart of the corresponding SZ source. Those criteria are explained in detail in Chapter 3. The mean

Este documento incorpora firma electrónica, y es copia auténtica de un documento electrónico archivado por la ULL según la Ley 39/2015.
 Su autenticidad puede ser contrastada en la siguiente dirección <https://sede.ull.es/validacion/>

Identificador del documento: 3248012 Código de verificación: RmbjVJW6

Firmado por: ALEJANDRO AGUADO BARAHONA
 UNIVERSIDAD DE LA LAGUNA

Fecha: 01/03/2021 09:35:30

María de las Maravillas Aguiar Aguilár
 UNIVERSIDAD DE LA LAGUNA

22/03/2021 13:39:32

(median) redshift of this data set is $z_{spec} = 0.22$ (0.19), and the mean (median) number of galaxies members of the clusters is $N = 43$ (21).

4.1.4 Other PSZ2 clusters

Table 4.2 also includes six GCs that do not belong to the PSZ2-North sample, but they are inside PSZ2, see section 4.2 for a detailed description of the results presented in this table. These objects are PSZ2 G021.02–29.04, PSZ2 G027.77–49.72-A, PSZ2 G027.77–49.72-B, PSZ2 G171.08–80.38, PSZ2 G208.57–44.31 and PSZ2 G270.78+36.83. They were observed for a different project but inside the LP15 program, so for this reason they are described here. As they do not form part of the PSZ2-North sample, they will not be considered for the characterisation of the scaling relation. These objects are listed as “Others in PSZ2” (column 3) in Table 4.1.

4.1.5 Beyond the PSZ2 sample

During the LP15 program we have characterised 26 new clusters or groups that can not be formally associated with the PSZ2 detection because they do not fulfil the matching criteria for being considered the optical counterpart. These objects are presented in Table 4.3, including their velocity dispersion, dynamical mass, number of members and redshift. As they are not associated with any SZ source, they cannot be used for the characterisation of the scaling relation in section 4.4. They are listed as “Beyond PSZ2” in Table 4.1.

4.2 Velocity dispersion estimates

Here, I present the methodology and results for the estimation of the velocity dispersion for those 362 objects confirmed as the optical counterparts of SZ sources in the PSZ2 catalogue (columns two and three in Table 4.1). Table 4.2 shows the results for these GCs, and is organised as follows. Columns 1 and 2 are the official ID number and the *Planck* name in the PSZ2 catalogue. Columns 4 and 5 are the J2000 coordinates of the BCG when present; otherwise, the geometrical centre of the GC is provided. Columns 5 and 6 give the number of spectroscopic members retrieved. Columns 7, 8 and 9 provide the mean spectroscopic redshift of the cluster and, when available, the BCG’s. Columns 10 and 11 are our velocity dispersion estimates. Columns 12, 13 and 14 present the dynamical and SZ mass estimates. Column 15 indicates whether the object was used in Sect. 4.3. Column 16 lists the data set from where the cluster was extracted (see column 1 in Table 4.1).

I also show 26 clusters and groups found while studying the PSZ2 catalogue, that are not associated with any SZ source, due to either their large distance from the *Planck* pointing, or to their low mass. They are presented in Table 4.3, which is structured in a similar way as Table 4.2. The difference is that these clusters and groups are not associated with any SZ source, so instead of naming them with the *Planck* name, we simply quote the field around which they were found.

Este documento incorpora firma electrónica, y es copia auténtica de un documento electrónico archivado por la ULL según la Ley 39/2015.
 Su autenticidad puede ser contrastada en la siguiente dirección <https://sede.ull.es/validacion/>

Identificador del documento: 3248012 Código de verificación: RmbjVJW6

Firmado por: ALEJANDRO AGUADO BARAHONA
 UNIVERSIDAD DE LA LAGUNA

Fecha: 01/03/2021 09:35:30

María de las Maravillas Aguiar Aguilár
 UNIVERSIDAD DE LA LAGUNA

22/03/2021 13:39:32

I follow the procedure outlined in Ferragamo et al. (2020) to estimate the velocity dispersion. The authors demonstrate (using hydro-dynamical simulations) that the estimation of the velocity dispersion is biased in the low number of galaxies regime. They present a functional form, depending on the number of galaxies used, to correct for this effect (see eq. 11, Ferragamo et al. 2020). They also show that the aperture sub-sampling is a source of error, and provide a recipe to correct for this effect. Finally, the authors note that the appropriate value of the clipping in the line-of-sight velocity field to minimise the presence of interlopers is 2.7. I adopt this value in my analysis.

I obtain the velocity dispersion in two steps. I make a first estimate using an iterative σ -clipping method and then I apply the corrections to the estimator. For the iterative σ -clipping method, I use a clip of 2.7σ and a cut in aperture of 1 or $1.5 \times r_{200}$ which is included inside the clipping. Once I have obtained this first estimate, I apply the corrections due to the used estimator and the aperture. In this work, I choose the gapper estimator (Wainer & Thissen 1976), as it is the one with the least dependence on the number of galaxies (Ferragamo et al. 2020). Figure 4.2 shows an example of the final velocity histogram of the cluster members for a particular case in my sample. Figure 4.3 shows the stacked distribution of all the galaxies in the phase space, for all clusters.

As mentioned in Sect. 4.1 and above, I use two different apertures when selecting the cluster members. The main reason is to evaluate the possible bias introduced by the presence of interlopers inside the individual cluster catalogues. The interlopers are an important cause of uncertainty when estimating the velocity dispersion of a cluster as shown by many authors in the literature (see e.g. Mamon et al. 2010; Saro et al. 2013; Wojtak et al. 2018; Pratt et al. 2019). For each cluster, I present both the values for the case of an aperture of $1.5 \times r_{200}$ as well as for r_{200} . I note that when restricting the aperture limit to r_{200} , I find 36 GCs less, due to the drop in the number of members, as the minimum number of members that I consider to estimate the velocity dispersion is seven.

Among those 362 presented counterparts, five are what we call a “multiple detection”. This means that there are more than one cluster associated with the SZ signal. In addition, there are 16 objects that are clearly sub-structured, so their velocity dispersion estimates should not be trusted, as they probably overestimate the true underlying velocity. I do not use these objects when characterising the $M_{\text{SZ}} - M_{\text{dyn}}$ scaling relation.

Unfortunately, not all of the clusters we found are associated with the SZ emission. There might be low mass systems or objects too distant from the SZ peak to be considered the counterpart. These clusters are not used for the calibration of the scaling relation. We also mark these objects in Table 4.3.

Este documento incorpora firma electrónica, y es copia auténtica de un documento electrónico archivado por la ULL según la Ley 39/2015.
 Su autenticidad puede ser contrastada en la siguiente dirección <https://sede.ull.es/validacion/>

Identificador del documento: 3248012 Código de verificación: RmbjVJW6

Firmado por: ALEJANDRO AGUADO BARAHONA
 UNIVERSIDAD DE LA LAGUNA

Fecha: 01/03/2021 09:35:30

María de las Maravillas Aguiar Aguilár
 UNIVERSIDAD DE LA LAGUNA

22/03/2021 13:39:32

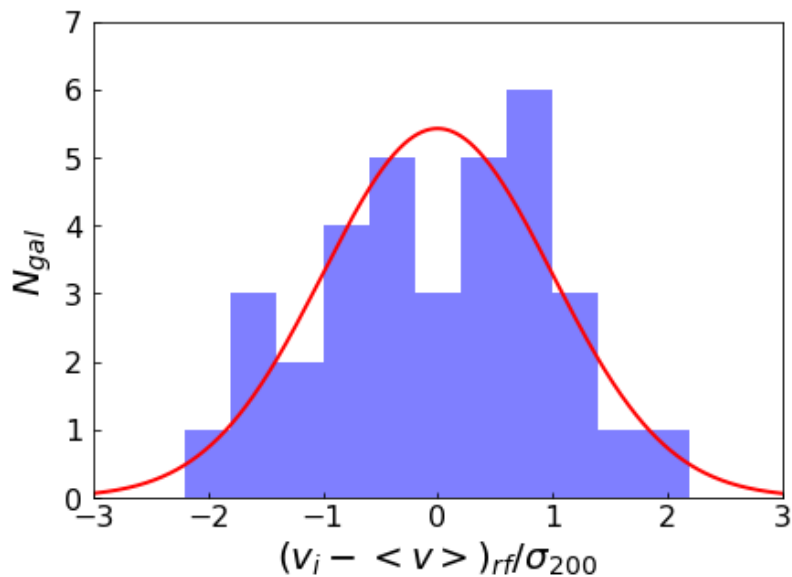


Figure 4.2: Example of the distribution of galaxies in PSZ2 G009.04+31.09 as a function of the rest frame difference in radial velocity to the mean radial velocity of the cluster. In blue are represented the cluster members used to estimate the velocity dispersion. The red line represents the normal distribution expected for the estimated velocity dispersion of $\sigma_{200} = 1068 \text{ km s}^{-1}$.

Este documento incorpora firma electrónica, y es copia auténtica de un documento electrónico archivado por la ULL según la Ley 39/2015.
 Su autenticidad puede ser contrastada en la siguiente dirección <https://sede.ull.es/validacion/>

Identificador del documento: 3248012 Código de verificación: RmbjVJW6

Firmado por: ALEJANDRO AGUADO BARAHONA
 UNIVERSIDAD DE LA LAGUNA

Fecha: 01/03/2021 09:35:30

María de las Maravillas Aguiar Aguilár
 UNIVERSIDAD DE LA LAGUNA

22/03/2021 13:39:32

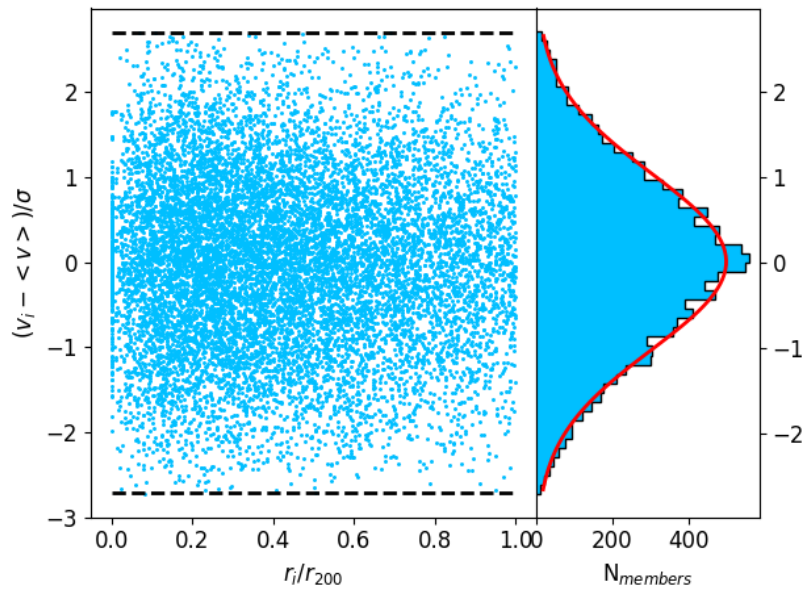


Figure 4.3: Projected phase space and velocities histogram distribution for all the 11867 galaxy members in my sample. Member velocities are normalised to the mean cluster velocity dispersion, whereas the distance to the centre of the cluster is normalised to the value of r_{200} in each cluster. Horizontal black dashed lines are the 2.7σ clip. The red line represents a Gaussian (normal) fit to the velocity histogram with $\sigma = 1$.

Este documento incorpora firma electrónica, y es copia auténtica de un documento electrónico archivado por la ULL según la Ley 39/2015.
 Su autenticidad puede ser contrastada en la siguiente dirección <https://sede.ull.es/validacion/>

Identificador del documento: 3248012 Código de verificación: RmbjVJW6

Firmado por: ALEJANDRO AGUADO BARAHONA
 UNIVERSIDAD DE LA LAGUNA

Fecha: 01/03/2021 09:35:30

María de las Maravillas Aguiar Aguilár
 UNIVERSIDAD DE LA LAGUNA

22/03/2021 13:39:32

Table 4.2.: 362 PSZ2 optical counterparts presented in this chapter.

ID ¹	NAME	N1.5	N1	z1.5	z1	z _{BGC}	$\sigma_{200,1.5}$ (km s ⁻¹)	$\sigma_{200,1}$ (km s ⁻¹)	$M_{500,1.5}^{dm}$ (10 ¹⁵ M _⊙)	$M_{500,1}^{dm}$ (10 ¹⁵ M _⊙)	M_{500}^{SZ} (10 ¹⁵ M _⊙)	Flag ²	Data set
1	PSZ2 G000.04+45.13	38	15	0.118	0.112	0.1169	652 ± 74	488 ± 83	0.20 ± 0.05	0.10 ± 0.05	0.38 ± 0.04	0	SDSS
2	PSZ2 G000.13+78.04	18	16	0.172	0.172	0.1730	1019 ± 158	1019 ± 166	0.68 ± 0.32	0.69 ± 0.35	0.51 ± 0.04	0	SDSS
7	PSZ2 G004.04+42.23	24	24	0.183	0.183	0.1856	1243 ± 249	1248 ± 250	1.22 ± 0.85	1.24 ± 0.85	0.30 ± 0.04	1	SDSS
14 ^a	PSZ2 G006.49+50.56	223	173	0.078	0.078	0.1518	1414 ± 187	1423 ± 188	1.63 ± 0.61	1.66 ± 0.62	0.31 ± 0.04	0	SDSS
21	PSZ2 G006.84+50.69	226	166	0.078	0.078	-	1058 ± 61	1109 ± 54	0.75 ± 0.05	0.85 ± 0.07	0.71 ± 0.02	1	SDSS
25	PSZ2 G009.04+31.09	34	34	0.246	0.246	-	1064 ± 64	1056 ± 52	0.76 ± 0.05	0.75 ± 0.06	0.17 ± 0.07	2	SDSS
34	PSZ2 G011.30+49.42	85	75	0.045	0.045	0.0442	631 ± 48	626 ± 46	0.19 ± 0.03	0.19 ± 0.03	0.48 ± 0.06	1	LP15
38	PSZ2 G011.30+49.42	85	75	0.045	0.045	0.0442	631 ± 48	626 ± 46	0.19 ± 0.03	0.19 ± 0.03	0.48 ± 0.06	1	SDSS
47 ^a	PSZ2 G014.33+60.23	12	11	0.214	0.212	0.2146	1490 ± 285	1548 ± 310	1.93 ± 1.25	2.17 ± 1.50	0.38 ± 0.05	0	SDSS
64	PSZ2 G020.08+37.47	13	10	0.339	0.339	0.3407	829 ± 156	744 ± 157	0.28 ± 0.21	0.28 ± 0.21	0.46 ± 0.06	1	SDSS
68	PSZ2 G021.02+39.04	25	25	0.301	0.301	0.3017	1304 ± 196	1304 ± 196	1.19 ± 0.43	1.19 ± 0.43	0.42 ± 0.06	1	LP15
69	PSZ2 G021.08+38.00	17	11	0.385	0.385	0.3815	744 ± 123	720 ± 144	0.26 ± 0.12	0.25 ± 0.17	0.56 ± 0.06	1	SDSS
72	PSZ2 G022.03+17.75	10	-	0.646	-	0.6488	859 ± 185	-	0.34 ± 0.25	-	0.82 ± 0.08	0	ITP13
92-A	PSZ2 G027.77-49.72	13	-	0.127	-	-	1089 ± 205	-	0.87 ± 0.52	-	-	0	LP15
92-B	PSZ2 G028.05+25.43	15	11	0.164	0.163	0.1641	728 ± 136	652 ± 136	0.28 ± 0.15	0.25 ± 0.17	-	0	LP15
96	PSZ2 G028.63-49.72	6	47	0.658	0.658	0.6641	823 ± 190	812 ± 182	0.32 ± 0.26	0.29 ± 0.24	0.85 ± 0.07	1	SDSS
101	PSZ2 G028.89+60.13	18	16	0.152	0.152	-	873 ± 140	852 ± 139	0.45 ± 0.21	0.43 ± 0.22	0.43 ± 0.03	1	SDSS
102	PSZ2 G029.06+44.55	246	246	0.037	0.037	0.0353	956 ± 44	958 ± 44	0.58 ± 0.04	0.58 ± 0.04	0.39 ± 0.02	0	SDSS
108	PSZ2 G030.70+09.44	17	17	0.052	0.052	0.0532	546 ± 108	546 ± 108	0.14 ± 0.07	0.14 ± 0.07	0.21 ± 0.03	1	ITP13
109	PSZ2 G031.93+78.71	141	141	0.073	0.073	0.1819	887 ± 167	769 ± 162	0.48 ± 0.29	0.34 ± 0.26	0.33 ± 0.04	1	SDSS
112 ^a	PSZ2 G032.31+66.07	36	26	0.609	0.609	-	1391 ± 74	1391 ± 74	1.57 ± 0.15	1.57 ± 0.15	0.26 ± 0.02	0	SDSS
116	PSZ2 G032.77+19.69	63	62	0.370	0.370	0.3676	943 ± 110	826 ± 104	0.40 ± 0.11	0.28 ± 0.10	0.58 ± 0.07	1	LP15
119	PSZ2 G033.14+77.58	110	96	0.063	0.063	0.0637	1204 ± 97	1206 ± 98	0.89 ± 0.16	0.90 ± 0.16	0.47 ± 0.05	1	SDSS
129	PSZ2 G034.38+51.57	110	96	0.043	0.043	0.0419	664 ± 42	553 ± 38	0.37 ± 0.09	0.36 ± 0.09	0.49 ± 0.02	1	SDSS
133	PSZ2 G037.31-21.54	31	27	0.574	0.574	-	812 ± 101	831 ± 103	0.27 ± 0.08	0.29 ± 0.10	0.55 ± 0.07	1	LP15
145 ^a	PSZ2 G037.48+71.52	9	-	0.477	-	0.4772	757 ± 173	-	0.28 ± 0.23	-	0.66 ± 0.06	2	SDSS
146-A	PSZ2 G040.03+74.95	92	92	0.072	0.072	0.0645	1846 ± 195	1846 ± 195	3.38 ± 0.45	3.38 ± 0.45	0.28 ± 0.02	0	SDSS
146-B	PSZ2 G040.11-42.58	55	55	0.202	0.202	0.2015	989 ± 87	998 ± 86	0.59 ± 0.12	0.29 ± 0.15	-	0	LP15
147	PSZ2 G040.28+37.36	15	15	0.620	0.620	0.6201	840 ± 147	819 ± 138	0.31 ± 0.17	0.29 ± 0.15	-	0	LP15
148	PSZ2 G040.58+77.12	87	60	0.075	0.075	0.1536	611 ± 120	650 ± 137	0.18 ± 0.12	0.22 ± 0.17	0.27 ± 0.04	1	SDSS
149	PSZ2 G041.47+50.58	12	12	0.152	0.152	-	689 ± 95	714 ± 99	0.25 ± 0.03	0.26 ± 0.05	0.25 ± 0.02	1	SDSS
151	PSZ2 G042.53+35.90	12	12	0.183	0.183	0.1813	1629 ± 316	1681 ± 317	2.50 ± 0.72	2.63 ± 0.76	0.30 ± 0.04	0	SDSS
156	PSZ2 G042.81+56.61	185	170	0.072	0.072	0.0690	1180 ± 57	1156 ± 56	1.01 ± 0.08	0.95 ± 0.08	0.41 ± 0.02	1	SDSS
158	PSZ2 G043.44-41.27	33	33	0.435	0.435	-	959 ± 109	959 ± 109	0.47 ± 0.14	0.47 ± 0.14	0.60 ± 0.07	1	LP15
160	PSZ2 G044.20+48.66	259	167	0.090	0.090	0.0908	1014 ± 62	988 ± 49	0.66 ± 0.04	0.62 ± 0.05	0.88 ± 0.02	1	SDSS
168	PSZ2 G045.13+97.78	7	-	0.221	-	0.2191	743 ± 195	-	0.33 ± 0.33	-	0.45 ± 0.04	2	SDSS
169	PSZ2 G045.20+15.63	22	22	0.126	0.126	0.1276	798 ± 131	798 ± 131	0.36 ± 0.14	0.36 ± 0.14	0.24 ± 0.03	1	LP15
170	PSZ2 G045.33-38.46	29	26	0.584	0.584	0.5880	1132 ± 145	1144 ± 145	0.67 ± 0.21	0.69 ± 0.24	0.71 ± 0.06	1	LP15
171	PSZ2 G045.47+17.80	84	84	0.372	0.372	0.3724	1048 ± 121	1048 ± 121	0.62 ± 0.18	0.62 ± 0.18	0.44 ± 0.06	1	LP15
175	PSZ2 G045.87+57.70	35	29	0.697	0.697	0.6994	1016 ± 120	1003 ± 120	0.49 ± 0.14	0.48 ± 0.15	0.62 ± 0.06	1	ITP13
175	PSZ2 G045.87+57.70	35	29	0.697	0.697	0.6994	1016 ± 120	1003 ± 120	0.49 ± 0.14	0.48 ± 0.15	0.62 ± 0.06	1	ITP13
178	PSZ2 G046.13+30.72	12	10	0.567	0.567	0.5673	686 ± 135	627 ± 132	0.19 ± 0.12	0.15 ± 0.12	0.55 ± 0.07	2	ITP13
183	PSZ2 G046.88+56.48	91	89	0.114	0.114	0.1135	1039 ± 69	1039 ± 69	0.70 ± 0.10	0.70 ± 0.10	0.53 ± 0.02	1	SDSS
190	PSZ2 G048.10+57.16	100	97	0.078	0.078	0.0788	732 ± 47	731 ± 47	0.62 ± 0.04	0.62 ± 0.04	0.36 ± 0.02	1	SDSS
192	PSZ2 G048.24-51.59	32	27	0.530	0.530	0.5322	1089 ± 126	877 ± 109	0.28 ± 0.19	0.35 ± 0.12	0.66 ± 0.06	1	ITP13
195	PSZ2 G048.75+53.18	25	23	0.097	0.097	0.0972	627 ± 82	630 ± 85	0.19 ± 0.07	0.19 ± 0.07	0.22 ± 0.03	1	SDSS
198	PSZ2 G049.15+65.05	12	-	0.231	-	0.2351	1456 ± 285	-	1.79 ± 1.16	-	0.43 ± 0.05	2	SDSS
199	PSZ2 G049.22+30.37	30	30	0.161	0.161	0.1601	960 ± 139	562 ± 118	0.32 ± 0.19	0.15 ± 0.11	0.58 ± 0.03	1	SDSS
200	PSZ2 G049.32+44.37	51	52	0.097	0.097	0.0960	769 ± 68	769 ± 68	0.92 ± 0.06	0.92 ± 0.07	0.36 ± 0.03	1	SDSS

Este documento incorpora firma electrónica, y es copia auténtica de un documento electrónico archivado por la ULL según la Ley 39/2015.
 Su autenticidad puede ser contrastada en la siguiente dirección <https://sede.ull.es/validacion/>

Identificador del documento: 3248012 Código de verificación: RmbjVJW6

Firmado por: ALEJANDRO AGUADO BARAHONA
 UNIVERSIDAD DE LA LAGUNA

Fecha: 01/03/2021 09:35:30

María de las Maravillas Aguiar Aguilár
 UNIVERSIDAD DE LA LAGUNA

22/03/2021 13:39:32

4.2 Velocity dispersion estimates

Table 4.2: Continued.

ID ¹	NAME	N _{1,5}	N ₁	z _{1,5}	z ₁	z _{BGC}	σ _{200,1.5} (km s ⁻¹)	σ _{200,1} (km s ⁻¹)	M _{500,1.5} (10 ¹⁵ M _☉)	M ₅₀₀ (10 ¹⁵ M _☉)	M ₅₀₀ (10 ¹⁵ M _☉)	Flag ²	Data set
204	PS22 G050.40+31.17	19	16	0.160	0.160	0.1589	991 ± 154	1012 ± 165	0.63 ± 0.28	0.68 ± 0.35	0.40 ± 0.03	1	SDSS
210	PS22 G052.35-31.98	11	-	0.275	0.326	0.2709	699 ± 144	1112 ± 222	0.24 ± 0.17	0.83 ± 0.57	0.40 ± 0.05	2	SDSS
212	PS22 G053.44-36.25	15	11	0.227	0.227	-	1146 ± 201	1112 ± 222	0.83 ± 0.46	0.83 ± 0.46	0.74 ± 0.05	1	SDSS
218	PS22 G054.09+33.42	14	14	0.227	0.227	-	1006 ± 159	784 ± 202	0.30 ± 0.21	0.88 ± 0.39	0.37 ± 0.04	1	SDSS
222	PS22 G054.99+33.41	11	7	0.227	0.228	-	784 ± 202	784 ± 202	0.30 ± 0.21	0.88 ± 0.39	0.37 ± 0.04	1	SDSS
223	PS22 G055.59+31.85	18	12	0.225	0.227	0.2233	1152 ± 185	1094 ± 209	0.32 ± 0.43	0.83 ± 0.54	0.78 ± 0.03	1	SDSS
224	PS22 G055.80+32.90	26	25	0.108	0.107	0.1086	826 ± 105	830 ± 107	0.39 ± 0.14	0.40 ± 0.14	0.23 ± 0.03	1	SDSS
228	PS22 G056.62+88.42	25.3	25.3	0.023	0.023	0.0239	955 ± 48	955 ± 48	0.59 ± 0.04	0.59 ± 0.04	0.31 ± 0.01	0	SDSS
229	PS22 G056.77+36.32	77	77	0.099	0.099	0.0993	1014 ± 77	1014 ± 77	0.67 ± 0.10	0.67 ± 0.10	0.45 ± 0.02	1	ITP13
230	PS22 G056.79-11.60	21	21	0.123	0.123	0.1217	944 ± 167	944 ± 167	0.57 ± 0.23	0.57 ± 0.23	0.39 ± 0.03	1	SDSS
233 ^a	PS22 G057.09+11.19	21	21	0.377	0.377	-	1356 ± 204	1356 ± 204	1.27 ± 0.53	1.27 ± 0.53	0.47 ± 0.06	0	LP15
235	PS22 G057.61+34.93	121	103	0.085	0.085	0.0792	947 ± 70	907 ± 61	0.55 ± 0.06	0.59 ± 0.07	0.38 ± 0.02	1	SDSS
236	PS22 G057.62+34.93	121	103	0.085	0.085	0.0792	947 ± 70	907 ± 61	0.55 ± 0.06	0.59 ± 0.07	0.38 ± 0.02	1	SDSS
237	PS22 G057.79+52.33	100	81	0.066	0.066	0.0653	718 ± 50	783 ± 56	0.30 ± 0.04	0.35 ± 0.05	0.23 ± 0.02	0	SDSS
238	PS22 G057.80+88.00	295	295	0.023	0.023	0.0215	1001 ± 83	1001 ± 83	0.67 ± 0.04	0.67 ± 0.04	0.63 ± 0.01	0	SDSS
245	PS22 G059.18+32.91	9	8	0.389	0.389	0.3928	902 ± 206	772 ± 185	0.47 ± 0.38	0.32 ± 0.29	0.47 ± 0.05	1	SDSS
248	PS22 G059.52+16.23	17	17	0.284	0.284	-	818 ± 137	818 ± 137	0.35 ± 0.17	0.35 ± 0.17	0.37 ± 0.05	1	LP15
250	PS22 G059.76+14.59	9	-	0.304	0.220	0.3086	619 ± 141	-	0.18 ± 0.15	-	0.41 ± 0.04	0	LP15
251	PS22 G059.81-39.09	10	9	0.218	0.220	0.2270	1351 ± 292	1238 ± 277	1.52 ± 1.14	1.23 ± 1.01	0.47 ± 0.05	0	SDSS
254 ^a	PS22 G060.13+11.44	23	23	0.225	0.225	0.2243	1854 ± 318	1854 ± 318	3.24 ± 1.24	3.24 ± 1.24	0.52 ± 0.05	0	ITP13
258	PS22 G061.73+88.11	276	276	0.023	0.023	0.0239	993 ± 73	993 ± 73	0.65 ± 0.04	0.65 ± 0.04	0.33 ± 0.04	0	SDSS
261	PS22 G062.94+43.69	163	163	0.030	0.030	0.0267	796 ± 52	796 ± 52	0.36 ± 0.03	0.36 ± 0.03	0.29 ± 0.01	1	SDSS
263	PS22 G063.80+11.42	13	13	0.428	0.428	0.4263	986 ± 186	986 ± 186	0.55 ± 0.33	0.55 ± 0.33	0.57 ± 0.05	1	ITP13
264	PS22 G063.91-16.75	16	15	0.392	0.391	0.3923	832 ± 140	837 ± 141	0.35 ± 0.18	0.35 ± 0.19	0.50 ± 0.06	1	ITP13
275	PS22 G066.19+12.86	12	12	0.246	0.246	0.2462	1238 ± 270	1238 ± 270	1.15 ± 0.74	1.15 ± 0.74	0.41 ± 0.04	1	LP15
277	PS22 G066.34+26.14	52	52	0.623	0.623	0.6167	1200 ± 109	1213 ± 107	0.75 ± 0.15	0.77 ± 0.16	0.55 ± 0.06	1	LP15
280 ^a	PS22 G066.68+68.44	16	14	0.163	0.162	0.1583	1302 ± 213	1198 ± 210	1.34 ± 0.69	1.09 ± 0.62	0.36 ± 0.03	0	SDSS
283	PS22 G067.17+67.46	23	16	0.167	0.168	0.1700	780 ± 111	879 ± 144	0.33 ± 0.13	0.46 ± 0.24	0.71 ± 0.03	1	SDSS
284	PS22 G067.17+67.46	23	16	0.167	0.168	0.1700	780 ± 111	879 ± 144	0.33 ± 0.13	0.46 ± 0.24	0.71 ± 0.03	1	SDSS
292	PS22 G068.31-81.81	20	20	0.314	0.314	0.3072	1178 ± 170	1149 ± 167	0.30 ± 0.20	0.35 ± 0.27	0.67 ± 0.06	1	SDSS
292	PS22 G068.31-81.81	42	35	0.059	0.059	0.059	646 ± 70	654 ± 71	0.20 ± 0.05	0.21 ± 0.06	0.18 ± 0.02	0	SDSS
294	PS22 G069.39+68.05	23	22	0.766	0.766	0.7630	1051 ± 150	1024 ± 141	0.49 ± 0.19	0.46 ± 0.18	1.10 ± 0.15	0	LP15
295 ^a	PS22 G069.47-29.06	29	29	0.190	0.190	-	598 ± 74	609 ± 73	0.16 ± 0.05	0.16 ± 0.05	-	0	LP15
295 ^b	PS22 G070.08-31.79	42	32	0.393	0.393	0.3929	690 ± 75	637 ± 72	0.20 ± 0.05	0.16 ± 0.05	-	0	LP15
298	PS22 G071.39+59.54	12	7	0.191	0.191	0.1931	1053 ± 198	1095 ± 219	0.76 ± 0.46	0.86 ± 0.60	0.47 ± 0.04	1	SDSS
301	PS22 G072.62+41.46	29	15	0.292	0.292	0.2914	946 ± 186	800 ± 207	0.54 ± 0.35	0.38 ± 0.39	0.59 ± 0.04	1	SDSS
307	PS22 G073.36+38.06	53	44	0.226	0.226	0.2246	1191 ± 133	1156 ± 135	0.97 ± 0.51	0.94 ± 0.51	1.10 ± 0.03	1	SDSS
325	PS22 G075.44+23.53	21	21	0.168	0.168	0.1682	885 ± 144	885 ± 144	0.36 ± 0.19	0.46 ± 0.19	0.26 ± 0.03	1	ITP13
326	PS22 G075.51+21.73	47	38	0.418	0.419	0.4203	919 ± 91	934 ± 97	0.42 ± 0.09	0.44 ± 0.12	0.36 ± 0.05	1	LP15
330	PS22 G077.67+30.59	10	10	0.222	0.222	0.2190	864 ± 183	864 ± 183	0.46 ± 0.34	0.46 ± 0.34	0.28 ± 0.04	1	LP15
332	PS22 G077.90-26.63	24	16	0.144	0.144	-	1205 ± 168	951 ± 155	1.07 ± 0.40	0.58 ± 0.30	0.50 ± 0.03	1	SDSS
337	PS22 G079.36+38.06	53	44	0.299	0.300	-	904 ± 85	951 ± 92	0.43 ± 0.09	0.50 ± 0.12	0.34 ± 0.04	1	LP15
338	PS22 G079.88+14.97	12	12	0.101	0.101	0.1020	532 ± 114	532 ± 114	0.13 ± 0.08	0.13 ± 0.08	0.22 ± 0.03	1	ITP13
339	PS22 G080.10+57.65	55	44	0.088	0.088	-	630 ± 62	678 ± 65	0.19 ± 0.04	0.23 ± 0.05	0.24 ± 0.02	1	SDSS
341	PS22 G080.41-33.24	14	9	0.110	0.110	-	649 ± 118	438 ± 98	0.22 ± 0.12	0.08 ± 0.07	0.38 ± 0.03	2	SDSS
343 ^a	PS22 G080.64+64.31	40	37	0.488	0.488	0.4862	955 ± 106	968 ± 102	0.45 ± 0.11	0.46 ± 0.12	-	0	LP15
346 ^a	PS22 G081.00-50.93	15	8	0.310	0.312	-	1657 ± 200	1357 ± 324	2.35 ± 1.27	1.52 ± 1.38	0.76 ± 0.04	0	SDSS
347	PS22 G081.02+50.57	26	20	0.509	0.510	0.5088	681 ± 92	578 ± 84	0.18 ± 0.06	0.12 ± 0.05	0.39 ± 0.04	2	LP15
348	PS22 G081.22-41.95	16	-	0.080	0.076	0.0776	556 ± 94	-	0.14 ± 0.07	-	0.21 ± 0.03	2	SDSS
349	PS22 G081.31-68.56	130	107	0.076	0.076	0.0776	797 ± 58	811 ± 50	0.35 ± 0.04	0.37 ± 0.04	0.27 ± 0.02	1	SDSS

Este documento incorpora firma electrónica, y es copia auténtica de un documento electrónico archivado por la ULL según la Ley 39/2015.
 Su autenticidad puede ser contrastada en la siguiente dirección <https://sede.ull.es/validacion/>

Identificador del documento: 3248012 Código de verificación: RmbjVJW6

Firmado por: ALEJANDRO AGUADO BARAHONA
 UNIVERSIDAD DE LA LAGUNA

Fecha: 01/03/2021 09:35:30

María de las Maravillas Aguilar
 UNIVERSIDAD DE LA LAGUNA

22/03/2021 13:39:32

Table 4.2: Continued.

ID ¹	NAME	N _{1,5}	N ₁	z _{1,5}	z ₁	z _{FCG}	σ _{200,1.5} (km s ⁻¹)	σ _{200,1} (km s ⁻¹)	M _{500,1.5} ^{dyn} (10 ¹⁵ M _⊙)	M _{500,1} ^{dyn} (10 ¹⁵ M _⊙)	M ₅₀₀ ^{dyn} (10 ¹⁵ M _⊙)	Flag ²	Data set
352	PSZ2 G081.72+70.15	12	10	0.250	0.250	0.2497	749 ± 147	638 ± 134	0.30 ± 0.19	0.20 ± 0.19	0.20 ± 0.15	0.37 ± 0.04	SDSS
357	PSZ2 G083.14+66.57	26	25	0.090	0.090	0.0893	655 ± 88	636 ± 82	0.21 ± 0.07	0.20 ± 0.07	0.20 ± 0.07	0.19 ± 0.02	SDSS
361	PSZ2 G083.29-31.03	27	21	0.412	0.411	0.4116	1119 ± 148	1051 ± 149	0.73 ± 0.25	0.63 ± 0.26	0.83 ± 0.04	0.83 ± 0.04	SDSS
363	PSZ2 G083.86+85.09	25	21	0.184	0.184	-	693 ± 95	676 ± 96	0.23 ± 0.08	0.22 ± 0.09	0.45 ± 0.03	0.45 ± 0.03	SDSS
366	PSZ2 G084.13-35.41	7	-	0.315	-	0.3020	1375 ± 361	-	1.62 ± 1.65	-	0.51 ± 0.05	0.51 ± 0.05	SDSS
370	PSZ2 G084.69+42.28	11	10	0.131	0.274	0.2763	1368 ± 209	1368 ± 209	1.38 ± 0.50	1.38 ± 0.50	0.50 ± 0.04	0.50 ± 0.04	ITP13
373	PSZ2 G084.82+20.66	8	8	0.373	0.373	0.3673	701 ± 144	717 ± 151	0.27 ± 0.19	0.29 ± 0.22	0.25 ± 0.02	0.25 ± 0.02	SDSS
374	PSZ2 G085.02+66.63	8	7	0.184	0.184	0.1838	907 ± 227	907 ± 227	0.49 ± 0.45	0.49 ± 0.45	0.41 ± 0.04	0.41 ± 0.04	ITP13
376	PSZ2 G085.72+10.66	12	12	0.084	0.084	0.0804	734 ± 140	734 ± 140	0.31 ± 0.20	0.31 ± 0.20	0.21 ± 0.02	0.21 ± 0.02	ITP13
377	PSZ2 G085.82+35.44	71	71	0.029	0.029	0.0273	552 ± 42	552 ± 42	0.13 ± 0.02	0.13 ± 0.02	0.10 ± 0.01	0.10 ± 0.01	SDSS
381	PSZ2 G086.28+74.76	22	21	0.701	0.701	-	1113 ± 162	1110 ± 157	0.60 ± 0.24	0.60 ± 0.25	0.34 ± 0.04	0.34 ± 0.04	LP15
382	PSZ2 G086.35-13.94	12	12	0.278	0.278	0.2766	1130 ± 228	1130 ± 228	0.88 ± 0.57	0.88 ± 0.57	0.42 ± 0.05	0.42 ± 0.05	LP15
385	PSZ2 G086.54-26.67	26	26	0.166	0.166	0.1682	819 ± 110	798 ± 101	0.37 ± 0.13	0.35 ± 0.12	0.32 ± 0.04	0.32 ± 0.04	SDSS
390	PSZ2 G086.95+53.18	12	12	0.766	0.766	0.7752	1162 ± 226	1162 ± 226	0.69 ± 0.44	0.69 ± 0.44	1.39 ± 0.13	1.39 ± 0.13	ITP13
391	PSZ2 G087.03-57.37	21	14	0.275	0.275	0.2772	1391 ± 207	1152 ± 202	1.46 ± 0.60	0.91 ± 0.52	0.73 ± 0.04	0.73 ± 0.04	SDSS
394	PSZ2 G087.39-34.58	32	27	0.773	0.773	0.7593	1137 ± 139	1187 ± 147	0.60 ± 0.18	0.67 ± 0.23	0.96 ± 0.10	0.96 ± 0.10	SDSS
398	PSZ2 G087.48+37.56	18	18	0.454	0.454	0.4538	1044 ± 120	965 ± 113	0.58 ± 0.17	0.47 ± 0.15	0.54 ± 0.06	0.54 ± 0.06	LP15
400	PSZ2 G089.06-11.70	32	30	0.455	0.455	0.4547	1070 ± 167	1030 ± 158	0.73 ± 0.32	0.66 ± 0.31	0.48 ± 0.04	0.48 ± 0.04	SDSS
403	PSZ2 G089.52+62.34	137	100	0.072	0.072	-	740 ± 53	769 ± 49	0.29 ± 0.03	0.32 ± 0.04	0.18 ± 0.02	0.18 ± 0.02	SDSS
404	PSZ2 G089.81-39.56	7	7	0.250	0.250	0.2488	1016 ± 266	990 ± 256	0.75 ± 0.76	0.70 ± 0.71	0.57 ± 0.05	0.57 ± 0.05	SDSS
407	PSZ2 G090.12-13.87	15	15	0.071	0.071	0.0738	639 ± 122	639 ± 122	0.21 ± 0.11	0.21 ± 0.11	0.18 ± 0.02	0.18 ± 0.02	LP15
413	PSZ2 G091.79-27.00	19	15	0.343	0.343	-	617 ± 96	641 ± 108	0.16 ± 0.07	0.18 ± 0.10	0.58 ± 0.04	0.58 ± 0.04	SDSS
414	PSZ2 G091.89+26.11	16	14	0.822	0.823	-	1111 ± 189	1153 ± 202	0.57 ± 0.29	0.63 ± 0.36	0.74 ± 0.04	0.74 ± 0.04	ITP13
417	PSZ2 G091.30-55.75	14	13	0.346	0.346	0.3467	1225 ± 222	1233 ± 225	1.03 ± 0.58	1.05 ± 0.64	0.45 ± 0.06	0.45 ± 0.06	SDSS
421	PSZ2 G092.02+59.92	24	23	0.462	0.462	0.4598	920 ± 129	882 ± 122	0.42 ± 0.16	0.38 ± 0.15	0.40 ± 0.03	0.40 ± 0.03	LP15
422 ^a	PSZ2 G092.71+73.46	19	15	0.232	0.234	0.2283	1388 ± 209	1425 ± 241	1.50 ± 0.67	1.64 ± 0.89	0.82 ± 0.03	0.82 ± 0.03	SDSS
425	PSZ2 G093.42-43.21	128	119	0.042	0.042	0.0416	655 ± 39	637 ± 37	0.21 ± 0.02	0.20 ± 0.02	0.17 ± 0.02	0.17 ± 0.02	SDSS
427	PSZ2 G093.92+34.92	202	181	0.080	0.080	0.0741	1150 ± 65	1168 ± 55	0.84 ± 0.07	0.98 ± 0.08	0.53 ± 0.01	0.53 ± 0.01	SDSS
432	PSZ2 G094.31-11.31	27	27	0.204	0.204	-	934 ± 136	934 ± 136	0.51 ± 0.17	0.51 ± 0.17	0.34 ± 0.05	0.34 ± 0.05	LP15
435	PSZ2 G094.56+51.03	45	34	0.541	0.542	0.5384	1389 ± 147	1286 ± 142	1.18 ± 0.27	0.97 ± 0.27	0.57 ± 0.04	0.57 ± 0.04	LP15
439	PSZ2 G095.29+67.41	63	46	0.063	0.063	-	522 ± 48	498 ± 47	0.11 ± 0.02	0.10 ± 0.02	0.13 ± 0.02	0.13 ± 0.02	SDSS
442	PSZ2 G095.49+11.11	19	19	0.445	0.445	0.4322	723 ± 84	758 ± 76	0.27 ± 0.07	0.27 ± 0.07	0.26 ± 0.02	0.26 ± 0.02	ITP13
443	PSZ2 G095.45+56.24	36	22	0.440	0.440	0.4399	723 ± 84	558 ± 76	0.27 ± 0.07	0.27 ± 0.07	0.13 ± 0.05	0.13 ± 0.05	SDSS
447	PSZ2 G096.43-20.89	36	36	0.226	0.226	-	1040 ± 127	1040 ± 127	0.67 ± 0.18	0.67 ± 0.18	0.40 ± 0.04	0.40 ± 0.04	LP15
451	PSZ2 G096.88+24.18	23	23	0.302	0.302	0.3035	896 ± 127	896 ± 127	0.44 ± 0.17	0.44 ± 0.17	0.47 ± 0.03	0.47 ± 0.03	ITP13
452	PSZ2 G096.99-53.64	36	31	0.056	0.056	-	665 ± 77	644 ± 74	0.22 ± 0.06	0.20 ± 0.06	0.17 ± 0.02	0.17 ± 0.02	SDSS
454	PSZ2 G097.37-17.11	32	27	0.456	0.456	0.4559	777 ± 95	736 ± 91	0.26 ± 0.08	0.23 ± 0.08	0.46 ± 0.06	0.46 ± 0.06	LP15
461	PSZ2 G098.30-41.15	17	13	0.434	0.434	-	825 ± 136	832 ± 152	0.33 ± 0.16	0.34 ± 0.21	0.63 ± 0.05	0.63 ± 0.05	SDSS
464-A	PSZ2 G098.44+56.59	27	20	0.131	0.131	-	553 ± 73	516 ± 75	0.13 ± 0.04	0.11 ± 0.05	-	-	SDSS
464-B	PSZ2 G098.44+56.59	27	20	0.131	0.131	-	1587 ± 322	1496 ± 324	1.86 ± 1.29	1.70 ± 1.30	0.28 ± 0.02	0.28 ± 0.02	SDSS
476	PSZ2 G099.48+45.60	11	9	0.492	0.491	0.1100	922 ± 116	885 ± 108	0.53 ± 0.17	0.47 ± 0.16	0.20 ± 0.03	0.20 ± 0.03	SDSS
478	PSZ2 G099.59+58.64	30	28	0.095	0.095	-	922 ± 116	885 ± 108	0.53 ± 0.17	0.47 ± 0.16	0.65 ± 0.05	0.65 ± 0.05	ITP13
483	PSZ2 G099.80+58.45	8	8	0.616	0.616	0.6140	643 ± 154	643 ± 154	0.17 ± 0.15	0.17 ± 0.15	0.41 ± 0.04	0.41 ± 0.04	LP15
490	PSZ2 G100.22+33.81	18	18	0.598	0.598	-	1062 ± 165	1076 ± 165	0.58 ± 0.27	0.60 ± 0.28	0.41 ± 0.04	0.41 ± 0.04	SDSS
492	PSZ2 G101.52-29.98	18	18	0.227	0.227	0.2269	904 ± 145	881 ± 145	0.48 ± 0.22	0.44 ± 0.21	0.45 ± 0.05	0.45 ± 0.05	SDSS
499	PSZ2 G101.68-49.21	16	10	0.073	0.072	-	639 ± 108	615 ± 130	0.21 ± 0.11	0.20 ± 0.11	0.22 ± 0.02	0.22 ± 0.02	SDSS
503	PSZ2 G104.30-48.99	38	35	0.201	0.201	0.2029	812 ± 92	821 ± 89	0.35 ± 0.09	0.36 ± 0.10	0.37 ± 0.04	0.37 ± 0.04	ITP13
503	PSZ2 G104.74+40.42	10	10	0.837	0.837	-	774 ± 172	774 ± 172	0.23 ± 0.17	0.23 ± 0.17	0.44 ± 0.05	0.44 ± 0.05	ITP13
505	PSZ2 G105.00+39.68	26	23	0.200	0.200	0.2009	453 ± 58	408 ± 55	0.07 ± 0.03	0.06 ± 0.02	0.23 ± 0.03	0.23 ± 0.03	LP15

Este documento incorpora firma electrónica, y es copia auténtica de un documento electrónico archivado por la ULL según la Ley 39/2015.
 Su autenticidad puede ser contrastada en la siguiente dirección <https://sede.ull.es/validacion/>

Identificador del documento: 3248012 Código de verificación: RmbjVJW6

Firmado por: ALEJANDRO AGUADO BARAHONA
 UNIVERSIDAD DE LA LAGUNA

Fecha: 01/03/2021 09:35:30

María de las Maravillas Aguiar
 UNIVERSIDAD DE LA LAGUNA

22/03/2021 13:39:32

4.2 Velocity dispersion estimates

Table 4.2: Continued.

ID ¹	NAME	N1.5	N1	z1.5	z1	zBCG	$\sigma_{200,1.5}$ (km s ⁻¹)	$\sigma_{200,1}$ (km s ⁻¹)	$M_{200,1.5}^{obs}$ (10 ¹⁵ M _☉)	$M_{200,1}^{obs}$ (10 ¹⁵ M _☉)	$M_{200,1.5}^{mod}$ (10 ¹⁵ M _☉)	$M_{200,1}^{mod}$ (10 ¹⁵ M _☉)	Flag ²	Data set
507	PSZ2 G105.40-50.43	30	28	0.167	0.167	-	709 ± 90	672 ± 82	0.25 ± 0.08	0.25 ± 0.07	0.25 ± 0.08	0.25 ± 0.07	1	SDSS
508	PSZ2 G105.55+77.21	109	74	0.072	0.072	-	843 ± 64	795 ± 59	0.41 ± 0.05	0.35 ± 0.05	0.41 ± 0.05	0.35 ± 0.05	1	SDSS
509	PSZ2 G105.70+54.73	9	9	0.319	0.319	-	1103 ± 265	1134 ± 253	0.97 ± 0.80	0.91 ± 0.74	0.97 ± 0.80	0.91 ± 0.74	1	SDSS
510	PSZ2 G107.00+65.82	24	22	0.278	0.277	0.1355	1132 ± 152	1080 ± 141	0.83 ± 0.31	0.73 ± 0.29	0.83 ± 0.31	0.73 ± 0.29	0	SDSS
521	PSZ2 G107.39-31.48	17	15	0.154	0.153	-	657 ± 108	598 ± 101	0.21 ± 0.10	0.17 ± 0.09	0.21 ± 0.10	0.17 ± 0.09	1	SDSS
524	PSZ2 G107.67-39.78	13	-	0.411	-	0.4117	551 ± 104	-	0.12 ± 0.07	-	0.12 ± 0.07	-	0	SDSS
527	PSZ2 G108.17-11.56	18	18	0.334	0.334	-	984 ± 154	984 ± 154	0.56 ± 0.26	0.56 ± 0.26	0.56 ± 0.26	0.56 ± 0.26	1	ITP13
528	PSZ2 G108.24+58.11	14	12	0.307	0.307	0.3080	562 ± 102	505 ± 96	0.13 ± 0.07	0.10 ± 0.06	0.13 ± 0.07	0.10 ± 0.06	0	SDSS
529	PSZ2 G108.27+48.66	29	24	0.671	0.671	0.6752	938 ± 120	949 ± 125	0.38 ± 0.12	0.40 ± 0.15	0.38 ± 0.12	0.40 ± 0.15	1	ITP13
531	PSZ2 G109.14-28.02	11	9	0.456	0.456	0.4527	1066 ± 219	1034 ± 231	0.68 ± 0.47	0.65 ± 0.53	0.68 ± 0.47	0.65 ± 0.53	1	SDSS
536 ^a	PSZ2 G109.99-70.28	11	9	0.305	0.305	0.3023	1357 ± 371	1357 ± 371	3.22 ± 2.24	1.48 ± 1.22	3.22 ± 2.24	1.48 ± 1.22	0	SDSS
543	PSZ2 G110.15-32.86	32	27	0.181	0.181	0.1797	1270 ± 156	1149 ± 143	1.08 ± 0.32	0.83 ± 0.28	1.08 ± 0.32	0.83 ± 0.28	1	SDSS
544	PSZ2 G112.48+56.09	146	110	0.071	0.071	-	896 ± 68	863 ± 52	0.48 ± 0.04	0.44 ± 0.05	0.48 ± 0.04	0.44 ± 0.05	1	SDSS
546	PSZ2 G112.69+33.37	15	14	0.521	0.521	0.5194	929 ± 163	937 ± 164	0.43 ± 0.23	0.44 ± 0.25	0.43 ± 0.23	0.44 ± 0.25	1	LP15
549	PSZ2 G113.29-29.69	41	37	0.103	0.103	-	966 ± 106	968 ± 102	0.59 ± 0.14	0.59 ± 0.16	0.59 ± 0.14	0.59 ± 0.16	1	SDSS
552	PSZ2 G114.14+58.96	47	33	0.116	0.116	0.1152	588 ± 61	609 ± 68	0.15 ± 0.03	0.17 ± 0.05	0.15 ± 0.03	0.17 ± 0.05	1	SDSS
553	PSZ2 G114.31+64.89	17	17	0.274	0.274	0.2824	1163 ± 192	1134 ± 179	0.92 ± 0.45	0.86 ± 0.42	0.92 ± 0.45	0.86 ± 0.42	1	SDSS
556	PSZ2 G114.79-33.71	37	33	0.095	0.095	-	872 ± 100	815 ± 91	0.45 ± 0.12	0.38 ± 0.11	0.45 ± 0.12	0.38 ± 0.11	1	SDSS
561	PSZ2 G114.99+70.36	31	28	0.225	0.225	0.2184	951 ± 118	961 ± 117	0.53 ± 0.16	0.55 ± 0.18	0.53 ± 0.16	0.55 ± 0.18	1	SDSS
562	PSZ2 G115.03+33.37	14	13	0.364	0.364	0.3636	1066 ± 137	1066 ± 137	0.66 ± 0.24	0.66 ± 0.24	0.66 ± 0.24	0.66 ± 0.24	1	SDSS
570	PSZ2 G116.32-36.33	14	14	0.364	0.364	0.3655	779 ± 141	760 ± 133	0.30 ± 0.17	0.28 ± 0.16	0.30 ± 0.17	0.28 ± 0.16	1	SDSS
571	PSZ2 G116.50-44.47	24	21	0.373	0.373	-	1010 ± 141	984 ± 139	0.57 ± 0.21	0.54 ± 0.22	0.57 ± 0.21	0.54 ± 0.22	1	SDSS
577	PSZ2 G118.03+31.10	15	15	0.195	0.195	0.1944	473 ± 82	473 ± 82	0.09 ± 0.05	0.09 ± 0.05	0.09 ± 0.05	0.09 ± 0.05	0	ITP13
578	PSZ2 G118.34+68.79	22	20	0.255	0.255	0.2521	817 ± 119	786 ± 114	0.35 ± 0.14	0.32 ± 0.14	0.35 ± 0.14	0.32 ± 0.14	1	SDSS
585	PSZ2 G118.92+52.38	12	11	0.218	0.217	0.2191	804 ± 158	780 ± 156	0.37 ± 0.24	0.34 ± 0.24	0.37 ± 0.24	0.34 ± 0.24	1	SDSS
593	PSZ2 G120.76+44.14	41	37	0.296	0.296	0.2946	791 ± 86	784 ± 83	0.30 ± 0.07	0.30 ± 0.08	0.30 ± 0.07	0.30 ± 0.08	1	SDSS
594	PSZ2 G121.03+57.02	15	13	0.346	0.345	-	1247 ± 218	1168 ± 213	1.07 ± 0.58	0.91 ± 0.55	1.07 ± 0.58	0.91 ± 0.55	1	SDSS
596	PSZ2 G121.49+49.54	20	18	0.233	0.232	-	717 ± 109	729 ± 112	0.22 ± 0.15	0.27 ± 0.19	0.22 ± 0.15	0.27 ± 0.19	0	SDSS
598	PSZ2 G121.77+54.75	20	18	0.233	0.232	-	717 ± 109	729 ± 112	0.22 ± 0.15	0.27 ± 0.19	0.22 ± 0.15	0.27 ± 0.19	0	SDSS
599	PSZ2 G122.30+54.52	19	17	0.309	0.309	0.3103	1088 ± 170	1115 ± 176	0.74 ± 0.33	0.80 ± 0.39	0.74 ± 0.33	0.80 ± 0.39	1	SDSS
601	PSZ2 G122.89-36.82	17	15	0.319	0.319	-	924 ± 152	958 ± 162	0.48 ± 0.23	0.53 ± 0.29	0.48 ± 0.23	0.53 ± 0.29	1	SDSS
602	PSZ2 G123.00-35.52	17	15	0.358	0.358	-	1050 ± 173	1044 ± 176	0.66 ± 0.32	0.66 ± 0.35	0.66 ± 0.32	0.66 ± 0.35	1	SDSS
604	PSZ2 G123.42+30.63	9	9	0.200	0.200	0.1979	644 ± 144	644 ± 144	0.21 ± 0.18	0.21 ± 0.18	0.21 ± 0.18	0.21 ± 0.18	1	ITP13
605	PSZ2 G123.55-10.36	30	30	0.106	0.106	0.1064	811 ± 102	811 ± 102	0.37 ± 0.12	0.37 ± 0.12	0.37 ± 0.12	0.37 ± 0.12	1	ITP13
606	PSZ2 G123.66+07.25	22	22	0.283	0.283	0.2834	1086 ± 158	1059 ± 146	0.74 ± 0.30	0.69 ± 0.28	0.74 ± 0.30	0.69 ± 0.28	1	SDSS
610	PSZ2 G124.20-36.48	26	24	0.192	0.193	-	889 ± 120	863 ± 112	0.45 ± 0.16	0.41 ± 0.15	0.45 ± 0.16	0.41 ± 0.15	1	SDSS
611	PSZ2 G124.20-36.48	26	24	0.192	0.193	0.2291	889 ± 120	863 ± 112	0.45 ± 0.16	0.41 ± 0.15	0.45 ± 0.16	0.41 ± 0.15	1	SDSS
618	PSZ2 G125.68-64.12	115	115	0.044	0.044	0.0445	900 ± 56	900 ± 56	0.50 ± 0.06	0.50 ± 0.06	0.50 ± 0.06	0.50 ± 0.06	1	SDSS
619	PSZ2 G125.71+53.86	26	24	0.298	0.298	0.3007	1025 ± 145	1015 ± 134	0.62 ± 0.22	0.61 ± 0.23	0.62 ± 0.22	0.61 ± 0.23	1	SDSS
620	PSZ2 G125.84-18.72	47	47	0.189	0.189	-	935 ± 105	935 ± 105	0.51 ± 0.11	0.51 ± 0.11	0.51 ± 0.11	0.51 ± 0.11	1	LP15
621	PSZ2 G126.07-49.55	13	9	0.503	0.504	0.5000	676 ± 127	620 ± 139	0.19 ± 0.11	0.16 ± 0.13	0.19 ± 0.11	0.16 ± 0.13	0	SDSS
622	PSZ2 G126.20-33.17	18	15	0.357	0.357	0.3577	711 ± 114	735 ± 124	0.23 ± 0.13	0.20 ± 0.14	0.23 ± 0.13	0.20 ± 0.14	1	SDSS
623	PSZ2 G126.28+05.62	13	13	0.820	0.820	0.8201	771 ± 145	751 ± 137	0.22 ± 0.13	0.20 ± 0.12	0.22 ± 0.13	0.20 ± 0.12	1	SDSS
624	PSZ2 G126.36-19.11	22	22	0.203	0.203	0.2036	795 ± 115	795 ± 115	0.34 ± 0.13	0.34 ± 0.13	0.34 ± 0.13	0.34 ± 0.13	1	LP15
625	PSZ2 G126.57+51.01	21	21	0.816	0.815	-	994 ± 148	609 ± 116	0.41 ± 0.17	0.42 ± 0.08	0.41 ± 0.17	0.42 ± 0.08	2	LP15
626	PSZ2 G126.72-72.82	84	53	0.055	0.055	0.0547	565 ± 47	543 ± 49	0.14 ± 0.02	0.13 ± 0.03	0.14 ± 0.02	0.13 ± 0.03	1	SDSS
629	PSZ2 G126.72-72.82	84	53	0.055	0.055	0.0547	565 ± 47	543 ± 49	0.14 ± 0.02	0.13 ± 0.03	0.14 ± 0.02	0.13 ± 0.03	1	ITP13
630	PSZ2 G127.01+26.21	13	12	0.577	0.576	0.5760	1063 ± 200	1070 ± 204	0.61 ± 0.37	0.62 ± 0.40	0.61 ± 0.37	0.62 ± 0.40	1	SDSS
632	PSZ2 G127.44-34.74	16	15	0.240	0.240	0.2453	797 ± 135	777 ± 131	0.34 ± 0.17	0.32 ± 0.14	0.34 ± 0.17	0.32 ± 0.14	1	SDSS
633	PSZ2 G127.50-30.52	18	14	0.334	0.334	-	835 ± 134	880 ± 154	0.36 ± 0.17	0.42 ± 0.24	0.36 ± 0.17	0.42 ± 0.24	1	SDSS
636 ^a	PSZ2 G128.15-24.71	22	22	0.264	0.264	-	1317 ± 200	1317 ± 200	1.26 ± 0.50	1.26 ± 0.50	1.26 ± 0.50	1.26 ± 0.50	0	LP15

Este documento incorpora firma electrónica, y es copia auténtica de un documento electrónico archivado por la ULL según la Ley 39/2015.
 Su autenticidad puede ser contrastada en la siguiente dirección <https://sede.ull.es/validacion/>

Identificador del documento: 3248012

Código de verificación: RmbjVJW6

Firmado por: ALEJANDRO AGUADO BARAHONA
 UNIVERSIDAD DE LA LAGUNA

Fecha: 01/03/2021 09:35:30

María de las Maravillas Aguiar Aguiar
 UNIVERSIDAD DE LA LAGUNA

22/03/2021 13:39:32

Table 4.2: Continued.

ID ¹	NAME	N1.5	N1	z1.5	z1	z_{BCG}	$\sigma_{200,1.5}$ (km s^{-1})	$\sigma_{200,1}$ (km s^{-1})	$M_{500,1.5}^{dyn}$ ($10^{15} M_{\odot}$)	$M_{500,1}^{dyn}$ ($10^{15} M_{\odot}$)	M_{500}^{SZ} ($10^{15} M_{\odot}$)	Flag ²	Data set
641	PSZ2 G130.13-17.02	20	20	0.211	0.211	0.2097	908 ± 139	908 ± 139	0.48 ± 0.21	0.48 ± 0.21	0.45 ± 0.05	1	ITP13
642	PSZ2 G130.21-02.60	24	18	0.273	0.273	0.2721	1425 ± 199	1330 ± 204	1.54 ± 0.61	1.31 ± 0.61	0.53 ± 0.05	1	SDSS
644	PSZ2 G130.64+37.16	15	15	0.472	0.472	0.4722	1166 ± 197	1168 ± 197	0.82 ± 0.44	0.82 ± 0.44	0.35 ± 0.07	1	LP15
652	PSZ2 G133.59+50.68	57	56	0.530	0.530	0.5242	1112 ± 107	1171 ± 100	0.65 ± 0.12	0.75 ± 0.14	0.45 ± 0.05	1	SDSS
653	PSZ2 G133.60+59.04	27	26	0.258	0.258	0.2588	1168 ± 155	1087 ± 131	0.91 ± 0.31	0.66 ± 0.23	0.59 ± 0.04	1	SDSS
657	PSZ2 G134.59+53.38	17	17	0.347	0.347	0.3452	1004 ± 165	978 ± 155	0.59 ± 0.29	0.55 ± 0.27	0.38 ± 0.05	1	SDSS
659	PSZ2 G134.70+48.91	63	43	0.116	0.115	0.1153	722 ± 67	676 ± 66	0.26 ± 0.05	0.22 ± 0.05	0.34 ± 0.02	1	SDSS
663	PSZ2 G135.19+57.88	61	46	0.103	0.103	0.1028	744 ± 70	704 ± 66	0.29 ± 0.05	0.25 ± 0.06	0.20 ± 0.02	1	SDSS
665	PSZ2 G135.19+57.88	61	46	0.103	0.103	0.1028	744 ± 70	704 ± 66	0.29 ± 0.05	0.25 ± 0.06	0.20 ± 0.02	1	SDSS
667	PSZ2 G135.92+50.46	142	139	0.065	0.065	0.065	679 ± 53	662 ± 48	0.23 ± 0.03	0.21 ± 0.03	0.17 ± 0.02	0	SDSS
672	PSZ2 G136.92+50.46	104	78	0.065	0.065	0.065	679 ± 53	662 ± 48	0.23 ± 0.03	0.21 ± 0.03	0.17 ± 0.02	0	SDSS
678	PSZ2 G138.32-30.82	40	36	0.279	0.279	-	1320 ± 147	1339 ± 143	1.23 ± 0.31	1.28 ± 0.35	0.56 ± 0.05	1	SDSS
681	PSZ2 G139.00+50.92	11	7	0.784	0.784	-	787 ± 162	836 ± 216	0.24 ± 0.17	0.31 ± 0.32	0.64 ± 0.08	1	LP15
682	PSZ2 G139.18+56.37	20	16	0.326	0.325	0.3220	1392 ± 212	1397 ± 228	1.42 ± 0.61	1.46 ± 0.75	0.69 ± 0.04	1	SDSS
683	PSZ2 G139.62+24.18	22	22	0.266	0.266	0.2660	938 ± 144	938 ± 144	0.51 ± 0.20	0.51 ± 0.20	0.76 ± 0.05	1	ITP13
684	PSZ2 G139.72-17.13	18	18	0.155	0.155	0.1561	645 ± 105	645 ± 105	0.20 ± 0.09	0.20 ± 0.09	0.32 ± 0.04	1	LP15
689	PSZ2 G141.77+14.19	19	20	0.818	0.819	0.8208	1158 ± 173	1257 ± 182	0.63 ± 0.28	0.78 ± 0.33	0.77 ± 0.09	1	ITP13
690	PSZ2 G141.98+69.31	16	15	0.713	0.713	0.713	1433 ± 240	1433 ± 240	1.16 ± 0.59	1.16 ± 0.59	0.57 ± 0.07	1	SDSS
697	PSZ2 G143.44+53.66	24	19	0.361	0.361	0.361	636 ± 126	610 ± 146	0.18 ± 0.11	0.17 ± 0.15	0.48 ± 0.05	0	SDSS
702	PSZ2 G144.33+62.85	39	31	0.131	0.131	-	647 ± 73	609 ± 70	0.20 ± 0.05	0.17 ± 0.05	0.23 ± 0.03	1	SDSS
709	PSZ2 G145.65+59.30	30	28	0.347	0.346	0.3474	1139 ± 144	1048 ± 128	0.80 ± 0.25	0.64 ± 0.21	0.40 ± 0.05	1	SDSS
721	PSZ2 G147.88+53.24	13	12	0.601	0.601	-	1435 ± 270	1455 ± 277	1.33 ± 0.81	1.40 ± 0.90	0.59 ± 0.05	1	SDSS
722	PSZ2 G148.36+75.23	16	16	0.305	0.305	0.3036	1053 ± 179	1026 ± 168	0.69 ± 0.35	0.64 ± 0.33	0.43 ± 0.05	1	SDSS
724	PSZ2 G149.22+54.18	44	35	0.136	0.136	0.1351	810 ± 87	763 ± 83	0.36 ± 0.08	0.31 ± 0.09	0.58 ± 0.02	1	SDSS
729	PSZ2 G150.24+48.72	23	19	0.200	0.199	0.1989	884 ± 126	830 ± 124	0.45 ± 0.17	0.38 ± 0.17	0.31 ± 0.04	1	SDSS
730	PSZ2 G150.24+48.72	23	19	0.200	0.199	0.1989	884 ± 126	830 ± 124	0.45 ± 0.17	0.38 ± 0.17	0.31 ± 0.04	1	SDSS
731	PSZ2 G150.56+58.52	21	19	0.369	0.369	0.3690	1066 ± 138	1045 ± 132	0.65 ± 0.27	0.63 ± 0.27	0.75 ± 0.05	1	SDSS
734	PSZ2 G151.19+48.27	16	15	0.288	0.288	0.2841	935 ± 159	908 ± 154	0.51 ± 0.26	0.47 ± 0.25	0.47 ± 0.04	1	SDSS
738	PSZ2 G152.33+81.28	11	10	0.331	0.331	-	777 ± 159	793 ± 167	0.32 ± 0.26	0.34 ± 0.25	0.49 ± 0.05	1	SDSS
739	PSZ2 G152.40+75.00	10	10	0.456	0.455	-	1138 ± 246	1083 ± 228	0.72 ± 0.54	0.72 ± 0.54	0.41 ± 0.06	0	LP15
742	PSZ2 G153.00-58.26	32	23	0.231	0.231	0.2297	1196 ± 147	944 ± 127	0.98 ± 0.29	0.53 ± 0.20	0.47 ± 0.05	1	SDSS
748	PSZ2 G154.13+40.19	11	10	0.277	0.277	-	1288 ± 264	1317 ± 278	1.27 ± 0.88	1.37 ± 1.03	0.49 ± 0.04	1	SDSS
752	PSZ2 G155.80+70.40	8	8	0.330	0.330	-	1152 ± 281	1123 ± 269	0.97 ± 0.88	0.90 ± 0.82	0.37 ± 0.05	1	SDSS
755	PSZ2 G156.26+59.64	12	8	0.617	0.617	0.3699	862 ± 169	933 ± 228	0.54 ± 0.22	0.48 ± 0.43	0.66 ± 0.06	1	SDSS
756	PSZ2 G156.26+59.64	12	8	0.617	0.617	0.3699	862 ± 169	933 ± 228	0.54 ± 0.22	0.48 ± 0.43	0.66 ± 0.06	1	SDSS
762	PSZ2 G158.35-47.40	9	9	0.310	0.310	0.3115	1024 ± 236	1024 ± 236	0.69 ± 0.57	0.69 ± 0.57	0.48 ± 0.06	1	ITP13
765	PSZ2 G159.80+42.57	22	19	0.278	0.277	0.2778	919 ± 134	902 ± 134	0.48 ± 0.19	0.46 ± 0.20	0.40 ± 0.05	1	SDSS
767	PSZ2 G160.83+81.66	52	49	0.891	0.890	0.8908	1078 ± 99	1084 ± 99	0.47 ± 0.10	0.48 ± 0.10	0.57 ± 0.07	1	LP15
771	PSZ2 G161.73-28.58	12	11	0.438	0.439	0.4416	459 ± 90	419 ± 84	0.07 ± 0.05	0.06 ± 0.04	0.61 ± 0.08	0	LP15
778 ^o	PSZ2 G163.69+53.52	150	82	0.153	0.155	-	2174 ± 151	1629 ± 114	4.98 ± 0.46	2.30 ± 0.33	0.46 ± 0.03	0	SDSS
779	PSZ2 G163.87+48.54	14	14	0.214	0.214	0.2152	874 ± 158	852 ± 149	0.45 ± 0.26	0.42 ± 0.24	0.32 ± 0.04	1	SDSS
784	PSZ2 G164.65+46.37	22	22	0.342	0.342	0.3420	808 ± 118	788 ± 109	0.32 ± 0.13	0.30 ± 0.12	0.56 ± 0.05	1	SDSS
786	PSZ2 G165.06+54.13	39	34	0.142	0.142	0.1422	1020 ± 108	1044 ± 115	0.71 ± 0.20	0.71 ± 0.20	0.49 ± 0.03	1	SDSS
787	PSZ2 G165.06+54.13	39	34	0.142	0.142	0.1422	1020 ± 108	1044 ± 115	0.71 ± 0.20	0.71 ± 0.20	0.49 ± 0.03	1	SDSS
793	PSZ2 G165.95+41.01	25	24	0.217	0.217	0.2040	750 ± 103	746 ± 98	0.28 ± 0.10	0.28 ± 0.10	0.39 ± 0.05	1	SDSS
794	PSZ2 G166.09+43.38	27	25	0.218	0.218	0.2168	1181 ± 156	1161 ± 150	0.96 ± 0.33	0.92 ± 0.33	0.69 ± 0.03	1	SDSS
804	PSZ2 G167.98-59.95	31	30	0.140	0.140	0.1393	762 ± 95	754 ± 89	0.31 ± 0.09	0.30 ± 0.09	0.41 ± 0.04	1	SDSS
805	PSZ2 G168.33+69.73	14	14	0.292	0.292	-	863 ± 137	866 ± 137	0.40 ± 0.18	0.41 ± 0.20	0.43 ± 0.04	1	SDSS
806	PSZ2 G169.62+33.84	14	14	0.346	0.346	0.3466	833 ± 151	832 ± 151	0.36 ± 0.21	0.36 ± 0.21	0.54 ± 0.06	1	SDSS
808	PSZ2 G170.26+73.90	17	12	0.164	0.165	0.1650	570 ± 94	569 ± 100	0.14 ± 0.07	0.15 ± 0.10	0.29 ± 0.04	1	SDSS
809	PSZ2 G170.98+39.45	9	8	0.554	0.555	0.5537	951 ± 217	969 ± 232	0.48 ± 0.40	0.52 ± 0.47	0.79 ± 0.07	1	SDSS
810	PSZ2 G171.08-60.38	33	33	0.343	0.343	0.3434	864 ± 101	864 ± 101	0.39 ± 0.11	0.39 ± 0.11	0.29 ± 0.06	1	LP15
812	PSZ2 G171.48+161.17	25	23	0.385	0.385	0.3881	641 ± 83	647 ± 87	0.17 ± 0.06	0.17 ± 0.07	0.40 ± 0.03	0	LP15

Este documento incorpora firma electrónica, y es copia auténtica de un documento electrónico archivado por la ULL según la Ley 39/2015.
 Su autenticidad puede ser contrastada en la siguiente dirección <https://sede.ull.es/validacion/>

Identificador del documento: 3248012 Código de verificación: RmbjVJW6

Firmado por: ALEJANDRO AGUADO BARAHONA
 UNIVERSIDAD DE LA LAGUNA

Fecha: 01/03/2021 09:35:30

María de las Maravillas Aguiar Aguilár
 UNIVERSIDAD DE LA LAGUNA

22/03/2021 13:39:32

4.2 Velocity dispersion estimates

Table 4.2: Continued.

ID ¹	NAME	N _{1,5}	N ₁	z _{1,5}	z ₁	z _{BCG}	σ _{200,1.5} (km s ⁻¹)	σ _{200,1} (km s ⁻¹)	M _{200,1.5} ^{min} (10 ¹⁵ M _⊙)	M _{200,1} ^{min} (10 ¹⁵ M _⊙)	M ₂₀₀ ^{min} (10 ¹⁵ M _⊙)	Flag ²	Data set
814	PS22 G171.98-40.66	15	15	0.272	0.272	-	1492 ± 300	1492 ± 300	1.81 ± 0.98	1.81 ± 0.98	1.08 ± 0.05	1	ITP13
815	PS22 G172.63+35.15	50	36	0.127	0.127	0.1290	733 ± 73	695 ± 74	0.27 ± 0.06	0.24 ± 0.07	0.37 ± 0.03	1	SDSS
816	PS22 G172.74+65.30	101	68	0.075	0.075	0.0781	680 ± 53	680 ± 53	0.19 ± 0.02	0.23 ± 0.04	0.23 ± 0.02	1	SDSS
817	PS22 G172.77+37.44	7	7	0.374	0.374	0.3726	1492 ± 300	1492 ± 300	1.81 ± 0.98	1.81 ± 0.98	1.08 ± 0.05	1	ITP13
818	PS22 G172.98-53.15	7	7	0.374	0.374	0.3726	1492 ± 300	1492 ± 300	1.81 ± 0.98	1.81 ± 0.98	1.08 ± 0.05	1	SDSS
819	PS22 G173.00-51.89	35	32	0.181	0.181	0.1803	770 ± 91	779 ± 87	0.31 ± 0.09	0.32 ± 0.09	0.32 ± 0.04	1	SDSS
821	PS22 G174.00-57.33	8	8	0.186	0.186	0.1852	878 ± 214	856 ± 205	0.51 ± 0.46	0.48 ± 0.43	0.36 ± 0.04	1	SDSS
824	PS22 G175.60+35.47	20	10	0.145	0.145	0.1450	680 ± 104	428 ± 90	0.23 ± 0.10	0.07 ± 0.05	0.27 ± 0.04	2	SDSS
826	PS22 G175.89+24.24	19	15	0.181	0.182	-	822 ± 128	807 ± 136	0.38 ± 0.17	0.37 ± 0.20	0.31 ± 0.05	1	SDSS
828	PS22 G176.25-52.57	22	20	0.237	0.237	0.2337	830 ± 121	846 ± 123	0.37 ± 0.15	0.39 ± 0.17	0.61 ± 0.05	1	SDSS
829	PS22 G176.27+37.54	15	13	0.636	0.636	-	1505 ± 264	1618 ± 295	1.46 ± 0.79	1.80 ± 1.09	0.51 ± 0.07	1	SDSS
831	PS22 G178.94+50.00	43	39	0.093	0.093	0.0914	172 ± 83	798 ± 82	0.32 ± 0.08	0.35 ± 0.09	0.20 ± 0.03	1	SDSS
833	PS22 G179.45-43.92	23	23	0.397	0.397	0.4005	1324 ± 186	1324 ± 186	1.17 ± 0.45	1.17 ± 0.45	0.47 ± 0.07	1	ITP13
836	PS22 G182.59+55.83	33	26	0.205	0.205	0.2056	1285 ± 155	1302 ± 149	1.20 ± 0.35	0.96 ± 0.33	0.58 ± 0.03	1	SDSS
850	PS22 G183.90+42.99	10	8	0.558	0.560	0.5635	1302 ± 281	1304 ± 312	1.10 ± 0.83	1.15 ± 0.95	0.63 ± 0.07	1	SDSS
852	PS22 G183.92+46.36	17	17	0.090	0.090	0.0914	505 ± 83	505 ± 83	0.11 ± 0.05	0.11 ± 0.05	0.27 ± 0.06	1	LP15
853	PS22 G184.24+43.69	9	7	0.394	0.394	0.3944	1101 ± 251	940 ± 243	0.80 ± 0.66	0.55 ± 0.56	0.46 ± 0.05	1	SDSS
859	PS22 G185.68+09.82	39	40	0.390	0.391	0.3897	1254 ± 129	1337 ± 135	0.99 ± 0.25	1.18 ± 0.29	0.58 ± 0.07	1	LP15
862	PS22 G186.37+37.26	9	-	0.285	-	0.2833	962 ± 220	-	0.60 ± 0.49	-	1.11 ± 0.04	2	SDSS
865	PS22 G186.83+37.32	20	13	0.221	0.270	0.3764	174 ± 118	1253 ± 229	0.28 ± 0.12	1.08 ± 0.65	0.49 ± 0.04	2	ITP13
867	PS22 G187.33+37.47	14	14	0.374	0.374	0.3726	1492 ± 300	1492 ± 300	1.81 ± 0.98	1.81 ± 0.98	1.08 ± 0.05	1	SDSS
873	PS22 G189.31+59.24	39	30	0.123	0.123	0.1192	753 ± 85	731 ± 86	0.30 ± 0.08	0.28 ± 0.09	0.31 ± 0.03	1	SDSS
881	PS22 G192.18+33.14	28	19	0.127	0.127	0.1272	708 ± 92	670 ± 100	0.26 ± 0.08	0.22 ± 0.10	0.35 ± 0.03	1	SDSS
883	PS22 G192.77+33.14	101	98	0.049	0.049	0.0503	815 ± 52	828 ± 53	0.38 ± 0.05	0.40 ± 0.05	0.15 ± 0.02	1	SDSS
884	PS22 G192.90+29.63	7	-	0.372	-	0.3699	790 ± 207	-	0.35 ± 0.36	-	0.43 ± 0.06	2	SDSS
887	PS22 G193.90+09.41	29	29	0.194	0.194	-	756 ± 99	756 ± 99	0.29 ± 0.09	0.29 ± 0.09	0.40 ± 0.05	1	LP15
890	PS22 G194.98+54.12	7	-	0.398	-	-	721 ± 189	-	0.27 ± 0.28	-	0.52 ± 0.06	1	SDSS
892	PS22 G195.24+29.34	14	10	0.286	0.286	0.2872	675 ± 123	450 ± 95	0.21 ± 0.12	0.08 ± 0.06	0.42 ± 0.05	2	SDSS
896	PS22 G197.13+33.46	17	15	0.459	0.297	0.4512	830 ± 206	1300 ± 220	0.37 ± 0.97	1.23 ± 0.67	0.59 ± 0.08	1	SDSS
898	PS22 G200.06+77.22	9	-	0.336	-	-	745 ± 170	-	0.29 ± 0.24	-	0.38 ± 0.05	0	SDSS
910	PS22 G200.82+27.42	8	-	0.455	-	-	1194 ± 291	-	0.98 ± 0.89	-	0.59 ± 0.06	2	SDSS
913	PS22 G201.50-27.31	47	47	0.540	0.540	-	1327 ± 141	1327 ± 141	1.04 ± 0.23	1.04 ± 0.23	0.81 ± 0.07	1	LP15
917	PS22 G202.66+66.98	20	18	0.481	0.481	0.4814	834 ± 128	834 ± 128	0.34 ± 0.15	0.32 ± 0.15	0.42 ± 0.06	1	LP15
918	PS22 G203.18+20.84	16	10	0.187	0.188	0.1865	706 ± 120	640 ± 135	0.25 ± 0.13	0.21 ± 0.16	0.32 ± 0.04	0	SDSS
922	PS22 G204.10+16.51	22	22	0.121	0.121	0.1222	817 ± 134	817 ± 134	0.38 ± 0.15	0.38 ± 0.15	0.36 ± 0.03	1	ITP13
924	PS22 G204.73+15.88	19	19	0.347	0.347	0.3471	1054 ± 161	1054 ± 161	0.66 ± 0.30	0.66 ± 0.30	0.58 ± 0.06	1	ITP13
932	PS22 G206.45+13.89	59	59	0.407	0.407	0.4123	1500 ± 136	1500 ± 136	1.58 ± 0.29	1.58 ± 0.29	0.70 ± 0.06	1	ITP13
932 ^a	PS22 G206.45+13.89	59	59	0.405	0.405	0.4123	1500 ± 136	1500 ± 136	1.58 ± 0.29	1.58 ± 0.29	0.70 ± 0.06	0	ITP13
936	PS22 G207.88+81.31	8	7	0.356	0.356	0.3507	649 ± 158	632 ± 163	0.20 ± 0.18	0.20 ± 0.20	0.75 ± 0.04	2	SDSS
937	PS22 G208.57-44.31	14	12	0.820	0.820	0.8196	702 ± 127	688 ± 131	0.17 ± 0.10	0.16 ± 0.10	0.66 ± 0.08	0	LP15
957	PS22 G212.44+63.19	9	-	0.530	-	-	684 ± 156	-	1.10 ± 0.77	-	0.47 ± 0.07	2	SDSS
963	PS22 G213.30+50.99	11	-	0.320	-	0.3196	1236 ± 254	-	1.10 ± 0.77	-	0.38 ± 0.05	2	SDSS
964	PS22 G213.39+80.59	16	12	0.559	0.559	0.5586	1013 ± 172	1083 ± 206	0.53 ± 0.27	0.65 ± 0.42	0.66 ± 0.06	1	SDSS
976 ^a	PS22 G216.62+47.00	15	10	0.391	0.391	0.3828	1533 ± 269	1429 ± 301	1.80 ± 0.97	1.58 ± 1.19	0.83 ± 0.05	0	SDSS
979	PS22 G217.09+40.15	50	29	0.139	0.140	0.1356	777 ± 79	551 ± 66	0.32 ± 0.07	0.13 ± 0.04	0.38 ± 0.03	1	SDSS
981	PS22 G218.50+71.31	40	30	0.137	0.137	0.2082	841 ± 93	816 ± 96	0.40 ± 0.10	0.37 ± 0.12	0.34 ± 0.03	1	ITP13
983	PS22 G218.50+71.31	40	30	0.137	0.137	-	867 ± 157	912 ± 162	0.41 ± 0.23	0.48 ± 0.33	0.44 ± 0.06	1	SDSS
985	PS22 G219.12+44.40	14	11	0.343	0.340	-	774 ± 146	797 ± 159	0.35 ± 0.21	0.39 ± 0.27	0.22 ± 0.03	1	SDSS
994	PS22 G222.52+20.58	13	11	0.087	0.087	-	976 ± 142	952 ± 142	0.59 ± 0.24	0.56 ± 0.25	0.53 ± 0.04	1	SDSS
1002	PS22 G224.00+69.33	22	19	0.193	0.193	0.1925	827 ± 103	827 ± 103	0.35 ± 0.12	-	0.49 ± 0.05	2	ITP13
1009	PS22 G224.82+13.62	28	-	0.274	-	0.2759	827 ± 103	-	0.35 ± 0.12	-	0.49 ± 0.05	2	ITP13

Este documento incorpora firma electrónica, y es copia auténtica de un documento electrónico archivado por la ULL según la Ley 39/2015.
 Su autenticidad puede ser contrastada en la siguiente dirección <https://sede.ull.es/validacion/>

Identificador del documento: 3248012 Código de verificación: RmbjVJW6

Firmado por: ALEJANDRO AGUADO BARAHONA
 UNIVERSIDAD DE LA LAGUNA

Fecha: 01/03/2021 09:35:30

María de las Maravillas Aguilar
 UNIVERSIDAD DE LA LAGUNA

22/03/2021 13:39:32

Table 4.2: Continued.

ID ¹	NAME	N _{1,5}	N ₁	z _{1,5}	z ₁	z _{BGG}	$\sigma_{200,1.5}$ (km s ⁻¹)	$\sigma_{200,1}$ (km s ⁻¹)	$M_{200,1.5}^{dyn}$ (10 ¹⁵ M _⊙)	$M_{200,1}^{dyn}$ (10 ¹⁵ M _⊙)	M_{200}^{dyn} (10 ¹⁵ M _⊙)	Flag ²	Data set
1020	PS22 G226.18+76.79	29	28	0.140	0.140	-	1032 ± 126	1036 ± 126	0.70 ± 0.22	0.71 ± 0.23	0.59 ± 0.02	1	SDSS
1030	PS22 G228.16+75.20	13	11	0.543	0.542	-	1463 ± 276	1509 ± 300	1.46 ± 0.80	1.60 ± 1.11	1.04 ± 0.05	1	SDSS
1031	PS22 G228.29+55.08	11	9	0.318	0.318	0.3152	763 ± 157	760 ± 170	0.30 ± 0.21	0.31 ± 0.25	0.41 ± 0.05	1	SDSS
1033	PS22 G228.50+34.96	9	-	0.208	-	0.2701	532 ± 124	532 ± 124	0.12 ± 0.10	0.12 ± 0.10	0.10 ± 0.04	0	SDSS
1035	PS22 G229.37+49.70	8	7	0.195	0.195	-	932 ± 149	932 ± 149	0.42 ± 0.24	0.42 ± 0.24	0.33 ± 0.04	0	SDSS
1038	PS22 G229.57+49.70	7	-	0.195	-	0.1975	932 ± 245	1351 ± 100	0.62 ± 0.63	1.44 ± 0.23	0.33 ± 0.04	2	SDSS
1040	PS22 G229.74+77.96	7	-	0.262	-	0.2640	1089 ± 286	-	0.90 ± 0.91	-	0.74 ± 0.04	2	SDSS
1045	PS22 G230.48+71.51	7	-	0.313	-	0.3134	715 ± 187	-	0.28 ± 0.28	-	0.50 ± 0.05	2	SDSS
1050	PS22 G231.56+60.03	7	-	0.301	-	0.2994	750 ± 197	-	0.26 ± 0.33	-	0.64 ± 0.05	2	SDSS
1056	PS22 G232.84+38.13	16	14	0.151	0.150	0.1530	706 ± 120	729 ± 128	0.26 ± 0.13	0.29 ± 0.16	0.31 ± 0.04	1	SDSS
1063	PS22 G233.68+36.14	9	9	0.357	0.356	-	1208 ± 276	1198 ± 267	1.05 ± 0.86	1.02 ± 0.84	0.47 ± 0.06	1	SDSS
1065	PS22 G234.09+10.45	29	138	0.294	0.292	0.2979	1274 ± 181	775 ± 62	1.12 ± 0.36	0.42 ± 0.05	0.42 ± 0.05	2	TF13
1066	PS22 G234.09+10.45	29	138	0.294	0.292	0.2979	1274 ± 181	775 ± 62	1.12 ± 0.36	0.42 ± 0.05	0.42 ± 0.05	2	TF13
1076 ^a	PS22 G238.69+63.26	6	21	0.165	0.167	0.0208	1724 ± 178	1083 ± 153	2.68 ± 0.58	0.49 ± 0.04	0.49 ± 0.04	0	SDSS
1093	PS22 G241.79+50.30	6	7	0.155	0.156	0.1553	575 ± 118	650 ± 153	0.16 ± 0.11	0.24 ± 0.24	0.26 ± 0.04	1	SDSS
1101	PS22 G243.02+42.87	65	65	0.045	0.045	-	751 ± 59	751 ± 59	0.31 ± 0.05	0.31 ± 0.05	0.16 ± 0.02	1	SDSS
1104	PS22 G243.64+67.74	95	63	0.081	0.081	0.0811	724 ± 58	711 ± 57	0.27 ± 0.03	0.26 ± 0.05	0.39 ± 0.02	1	SDSS
1174	PS22 G254.96+55.88	103	70	0.076	0.076	-	994 ± 77	758 ± 68	0.64 ± 0.08	0.31 ± 0.05	0.21 ± 0.02	2	SDSS
1175 ^a	PS22 G255.07+54.84	59	41	0.100	0.101	0.1031	1691 ± 146	1488 ± 149	2.65 ± 0.49	1.89 ± 0.46	0.21 ± 0.03	0	SDSS
1188	PS22 G257.51+57.54	79	63	0.049	0.049	0.0488	568 ± 48	529 ± 42	0.62 ± 0.43	0.52 ± 0.47	0.14 ± 0.02	1	SDSS
1192	PS22 G259.30+81.41	11	8	0.321	0.323	0.3228	989 ± 205	911 ± 218	0.62 ± 0.43	0.52 ± 0.47	0.43 ± 0.05	1	SDSS
1254	PS22 G273.78+36.83	21	24	0.516	0.516	0.5146	843 ± 109	855 ± 113	0.32 ± 0.12	0.33 ± 0.15	0.52 ± 0.06	1	SDSS
1274	PS22 G273.59+63.27	35	35	0.134	0.134	-	1360 ± 150	1360 ± 150	1.46 ± 0.41	1.46 ± 0.41	0.56 ± 0.03	0	SDSS
1319	PS22 G283.26+77.37	17	12	0.285	0.285	0.2835	1243 ± 205	1098 ± 209	1.09 ± 0.53	0.81 ± 0.52	0.50 ± 0.05	1	SDSS
1320	PS22 G283.91+73.87	119	77	0.086	0.086	-	793 ± 59	807 ± 59	0.34 ± 0.04	0.36 ± 0.06	0.30 ± 0.02	0	SDSS
1323	PS22 G284.59+70.84	99	81	0.090	0.090	0.0894	834 ± 66	815 ± 58	0.39 ± 0.05	0.37 ± 0.05	0.20 ± 0.03	1	SDSS
1329	PS22 G285.63+72.75	18	14	0.166	0.165	0.1705	956 ± 153	968 ± 170	0.58 ± 0.27	0.61 ± 0.35	0.56 ± 0.03	1	SDSS
1346	PS22 G287.46+81.12	131	103	0.072	0.072	0.0704	778 ± 56	810 ± 51	0.35 ± 0.03	0.37 ± 0.04	0.25 ± 0.02	1	SDSS
1418	PS22 G301.11+60.05	3	13	0.182	0.182	0.1849	1225 ± 192	990 ± 182	0.70 ± 0.43	0.66 ± 0.40	0.41 ± 0.04	1	SDSS
1458	PS22 G301.11+60.05	73	61	0.083	0.083	0.0823	708 ± 59	709 ± 58	0.25 ± 0.04	0.23 ± 0.05	0.19 ± 0.03	1	SDSS
1458	PS22 G301.11+60.05	73	61	0.083	0.083	0.0823	708 ± 59	709 ± 58	0.25 ± 0.04	0.23 ± 0.05	0.19 ± 0.03	1	SDSS
1493 ^a	PS22 G316.43+54.02	27	27	0.525	0.525	0.5325	1321 ± 164	1321 ± 164	1.06 ± 0.36	1.06 ± 0.36	0.55 ± 0.06	0	SDSS
1501	PS22 G318.25+73.24	7	-	0.528	-	-	1028 ± 270	-	0.64 ± 0.66	-	0.54 ± 0.07	0	SDSS
1504 ^a	PS22 G318.62+58.55	14	12	0.240	0.240	-	1625 ± 295	1580 ± 301	2.34 ± 1.34	2.22 ± 1.43	0.40 ± 0.05	1	SDSS
1518	PS22 G322.77+59.52	125	76	0.086	0.086	-	789 ± 58	755 ± 55	0.34 ± 0.04	0.30 ± 0.05	0.32 ± 0.02	1	SDSS
1522	PS22 G323.39+81.61	91	68	0.064	0.064	0.0635	768 ± 62	784 ± 61	0.32 ± 0.04	0.34 ± 0.06	0.17 ± 0.02	1	SDSS
1537	PS22 G331.12+62.31	96	72	0.077	0.077	0.0777	795 ± 63	820 ± 62	0.38 ± 0.04	0.38 ± 0.06	0.23 ± 0.02	1	SDSS
1584	PS22 G336.47+60.96	102	9	0.359	0.359	0.3579	707 ± 55	697 ± 51	0.44 ± 0.03	0.26 ± 0.24	0.25 ± 0.03	1	SDSS
1589	PS22 G336.47+60.96	102	9	0.359	0.359	0.3579	707 ± 55	697 ± 51	0.44 ± 0.03	0.26 ± 0.24	0.25 ± 0.03	1	SDSS
1606	PS22 G343.46+52.65	20	16	0.711	0.710	-	741 ± 113	723 ± 118	0.20 ± 0.09	0.19 ± 0.10	0.76 ± 0.09	1	LP15
1625	PS22 G349.12+67.62	2	-	0.237	-	0.2410	1224 ± 321	-	1.25 ± 1.27	-	0.36 ± 0.05	2	SDSS
1626	PS22 G349.18+38.66	24	24	0.109	0.109	0.1080	506 ± 68	506 ± 68	0.11 ± 0.04	0.11 ± 0.04	0.28 ± 0.04	0	LP15
1637	PS22 G355.50+54.72	91	90	0.027	0.027	0.0274	459 ± 31	455 ± 30	0.08 ± 0.01	0.08 ± 0.01	0.10 ± 0.02	0	SDSS
1639	PS22 G356.05+70.99	34	23	0.126	0.127	0.1268	574 ± 68	609 ± 81	0.14 ± 0.04	0.17 ± 0.06	0.27 ± 0.03	1	SDSS

¹ ID followed by an A or B label indicates the presence of multiple clusters associated with the same SZ source.
² This flag indicates whether an object is used in Sect.4.4: 0 = Not used; 1 = Used in both samples (1.5 and 1 × r₂₀₀); 2 = Used only in the sample 1.5 × r₂₀₀.
^a Substructured.

Este documento incorpora firma electrónica, y es copia auténtica de un documento electrónico archivado por la ULL según la Ley 39/2015.
 Su autenticidad puede ser contrastada en la siguiente dirección <https://sede.ull.es/validacion/>

Identificador del documento: 3248012 Código de verificación: RmbjvJW6

Firmado por: ALEJANDRO AGUADO BARAHONA
 UNIVERSIDAD DE LA LAGUNA

Fecha: 01/03/2021 09:35:30

María de las Maravillas Aguiar Aguiar
 UNIVERSIDAD DE LA LAGUNA

22/03/2021 13:39:32

Table 4.3: 26 clusters and groups beyond PSZ2.

Field	R.A.	Dec.	N _{1,5}	N ₁	z _{1,5}	z ₁	z _{BCC}	$\sigma_{200,1.5}$	$\sigma_{200,1}$	$M_{500,1.5}^{dgn}$	$M_{500,1}^{dgn}$	Data set
PSZ2 G032.12-14.96	19:43:11.20	-07:24:56.3	10	8	0.378	0.378	0.3775	522 ± 113	535 ± 128	0.11 ± 0.08	0.12 ± 0.11	ITP13
PSZ2 G037.48+71.52	14:14:54.57	+27:08:35.6	17	10	0.161	0.162	-	621 ± 102	489 ± 105	0.18 ± 0.09	0.11 ± 0.08	SDSS
PSZ2 G042.54+18.02	18:02:56.84	+16:21:52.6	0	8	0.258	0.164	-	414 ± 101	608 ± 145	0.06 ± 0.06	0.19 ± 0.17	LP15
PSZ2 G047.48+37.37	16:50:20.41	+26:58:21.4	10	8	0.230	0.230	0.2318	599 ± 129	494 ± 118	0.17 ± 0.13	0.11 ± 0.10	ITP13
PSZ2 G065.45+78.10	13:39:00.65	+32:58:12.0	7	-	0.486	-	1123 ± 295	-	0.84 ± 0.86	-	-	SDSS
PSZ2 G065.59-58.51	23:07:11.28	-07:31:43.6	17	17	0.334	0.334	0.3339	537 ± 88	523 ± 83	0.11 ± 0.05	0.10 ± 0.05	LP15
PSZ2 G071.82-56.55	23:09:35.43	-04:09:41.8	18	15	0.818	0.817	-	460 ± 74	485 ± 74	0.05 ± 0.02	0.05 ± 0.02	LP15
PSZ2 G081.60+18.47	19:07:18.13	+51:05:16.4	20	18	0.518	0.518	0.5196	622 ± 95	614 ± 94	0.14 ± 0.06	0.14 ± 0.06	LP15
PSZ2 G082.28+74.76	13:38:38.18	+38:52:19.7	20	10	0.246	0.246	-	777 ± 118	650 ± 137	0.31 ± 0.13	0.21 ± 0.16	LP15
PSZ2 G106.61+66.71	13:30:29.46	+49:45:37.8	16	13	0.382	0.382	0.3314	655 ± 106	580 ± 106	0.13 ± 0.07	0.14 ± 0.08	SDSS
PSZ2 G107.66+66.73	13:30:29.46	+49:45:37.8	16	13	0.382	0.382	0.3314	655 ± 106	580 ± 106	0.13 ± 0.07	0.14 ± 0.08	SDSS
PSZ2 G120.76+44.14	13:12:47.55	+72:50:49.2	20	-	0.572	0.361	-	532 ± 81	616 ± 130	0.10 ± 0.04	0.17 ± 0.13	LP15
PSZ2 G121.13+49.64	13:03:10.43	+67:25:33.0	14	11	0.105	0.105	-	500 ± 91	507 ± 101	0.11 ± 0.06	0.11 ± 0.08	SDSS
PSZ2 G136.02-47.15	01:28:23.61	+14:41:13.6	8	8	0.466	0.466	0.4648	519 ± 126	506 ± 121	0.10 ± 0.09	0.10 ± 0.09	LP15
PSZ2 G137.24+53.93	11:40:59.55	+61:07:07.2	22	17	0.475	0.476	0.4769	1281 ± 186	814 ± 129	1.02 ± 0.41	0.31 ± 0.15	LP15
PSZ2 G141.59+23.69	06:23:55.16	+72:50:15.7	14	11	0.306	0.306	0.3071	409 ± 74	418 ± 84	0.05 ± 0.03	0.06 ± 0.04	ITP13
PSZ2 G146.16-48.92	01:52:40.95	+11:14:31.2	14	9	0.491	0.491	0.4914	384 ± 70	416 ± 93	0.04 ± 0.02	0.05 ± 0.04	LP15
PSZ2 G171.48+16.17	06:37:45.46	+43:46:35.0	9	-	0.247	0.680	-	421 ± 94	-	0.07 ± 0.05	-	LP15
PSZ2 G183.99+16.36	01:57:34.28	+33:56:38.7	30	25	0.169	0.169	-	495 ± 107	463 ± 60	0.08 ± 0.02	0.08 ± 0.03	LP15
PSZ2 G213.27+78.38	11:58:46.26	+32:57:29.3	14	20	0.138	0.194	-	482 ± 89	595 ± 107	0.10 ± 0.06	0.11 ± 0.08	SDSS
PSZ2 G219.88+22.83	08:25:37.54	+04:29:18.3	40	26	0.102	0.103	-	766 ± 85	597 ± 76	0.32 ± 0.08	0.16 ± 0.06	SDSS
PSZ2 G220.11+22.91	08:26:01.69	+04:19:03.5	15	12	0.475	0.476	-	1096 ± 192	1042 ± 199	0.69 ± 0.37	0.62 ± 0.40	SDSS
PSZ2 G328.96+71.97	13:23:02.10	+11:01:32.1	75	35	0.091	0.091	0.0937	813 ± 71	855 ± 93	0.37 ± 0.06	0.43 ± 0.12	LP15
PSZ2 G341.69+50.67	14:25:12.30	-04:56:34.2	19	-	0.293	-	0.2913	449 ± 70	-	0.07 ± 0.03	-	ITP13

Este documento incorpora firma electrónica, y es copia auténtica de un documento electrónico archivado por la ULL según la Ley 39/2015.
 Su autenticidad puede ser contrastada en la siguiente dirección <https://sede.ull.es/validacion/>

Identificador del documento: 3248012 Código de verificación: RmbjVJW6

Firmado por: ALEJANDRO AGUADO BARAHONA
 UNIVERSIDAD DE LA LAGUNA

Fecha: 01/03/2021 09:35:30

María de las Maravillas Aguiar Aguiar
 UNIVERSIDAD DE LA LAGUNA

22/03/2021 13:39:32

4.3 Mass estimates

In the following sub-sections, I describe my methodology to obtain the dynamical and SZ masses. These masses are used in Sect. 4.4 to characterise their scaling relation and to obtain the bias parameter $(1 - b)$ which is of enormous importance for cosmological studies, as described in Chapter 1.

The mass estimates are presented in Columns 12, 13 and 14 of Table 4.2. Column 15 indicates whether an object is used in Sect. 4.4 to characterise the scaling relation. Columns 5, 6 in Table 4.1 show the total number of GCs in each data-set used for the estimation of the mass bias parameter.

4.3.1 Dynamical mass estimates

Estimating the dynamical mass (M_{dyn}) of a cluster is not a simple task. As shown in Old et al. (2014), the estimation of the mass using a low number of cluster members is problematic. For this reason, I use the method described in Ferragamo et al. (2020), where the authors study the behaviour of several velocity dispersion and dynamical mass estimators using hydro-dynamical simulations in the low number of galaxies regime. They demonstrate that the estimation of the velocity dispersion is biased in this regime, and propose a functional form that depends on the number of galaxies used to correct for this fact (Eqs. 15 and 16, Ferragamo et al. 2020).

The scaling relation used for the estimation of the dynamical mass is eq. 4.1 from Munari et al. (2013):

$$\frac{M_{200}^{\text{dyn}}}{10^{15}M_{\odot}} = \left(\frac{\sigma_{200}}{A}\right)^{\frac{1}{\alpha}}, \quad (4.1)$$

where $A = 1177.0 \text{ km s}^{-1}$ and $\alpha = 0.364$. Note that these parameters were obtained for a velocity dispersion calculated using the biweight estimator (Beers et al. 1990). Thus, for consistency, I convert our velocity dispersion estimates to that of the biweight, following the recipe in Ferragamo et al. (2020). After applying the corrections to M_{200}^{dyn} due to the number of cluster members, I convert this mass into M_{500}^{dyn} , so I can compare it to M_{500}^{SZ} . This last step is performed using the python package *NFW*¹ which implements the Navarro, Frenck and White (Navarro et al. 1997) density profile using the concentration parameter from Duffy et al. (2008):

$$c_{200} = 5.71 \cdot (1 + z)^{-0.47} \left(\frac{M_{200}}{2 \times 10^{12} h^{-1} M_{\odot}}\right)^{-0.084}. \quad (4.2)$$

4.3.2 SZ mass estimates

The *Planck* Collaboration provides, for every SZ source in the PSZ2 catalogue, an array of masses as a function of redshift, $M_{500,\text{nc}}^{\text{SZ}}(z)$. These values were obtained by breaking the size-flux degeneracy of the *Planck* measurements using a prior relating the SZ flux

¹<https://github.com/joergdietrich/NFW>

Este documento incorpora firma electrónica, y es copia auténtica de un documento electrónico archivado por la ULL según la Ley 39/2015.
 Su autenticidad puede ser contrastada en la siguiente dirección <https://sede.ull.es/validacion/>

Identificador del documento: 3248012 Código de verificación: RmbjVJW6

Firmado por: ALEJANDRO AGUADO BARAHONA
 UNIVERSIDAD DE LA LAGUNA

Fecha: 01/03/2021 09:35:30

María de las Maravillas Aguiar Aguilár
 UNIVERSIDAD DE LA LAGUNA

22/03/2021 13:39:32

(Y_{500}) and the cluster size (θ_{500}). In turn, this cluster size is connected to the total mass for a given redshift z . For each cluster in our sample, I interpolate these arrays into our measured redshift, and extract their SZ masses. Further details about the procedure to obtain $M_{500,\text{nc}}^{\text{SZ}}(z)$ can be found in Planck Collaboration XXVII (2016).

These SZ masses suffer from Eddington bias (see e.g. van der Burg et al. 2016), specially in the low signal-to-noise regime. Figure 5 in van der Burg et al. (2016) shows the magnitude of Eddington bias as a function of the signal-to-noise ratio in the PSZ2 catalogue for different redshifts. They estimate this Eddington bias by simulating a list of masses and redshifts following the Tinker et al. (2008) halo mass function and the redshift-dependent co-moving volume element for their assumed cosmology. I use that figure to create a hyper-surface and apply a 3D interpolation technique in order to correct my SZ masses for this effect and obtain the final M_{500}^{SZ} . I note that this treatment is an approximation, as the correction for each cluster is purely statistical (see e.g. Appendix A in Mantz et al. 2010, for an illustration of the effect of this type of statistical bias). For this reason, my individual corrected masses should be seen as an approximation. Nevertheless, the overall mass bias for the full sample should be correctly estimated.

4.4 $M_{\text{SZ}} - M_{\text{dyn}}$ scaling relation

In this section, I present and discuss the scaling relation between SZ and dynamical masses for a statistically representative sub-sample of the PSZ2 catalogue. Starting from the complete list of clusters presented in Sect. 4.1, I use two additional criteria to remove objects from the list. We exclude: (i) GCs that are clearly sub-structured, as the estimation of the dynamical mass is probably overestimated in this case, and (ii) those presenting multiple counterparts, as using *Planck* data alone and due to the beam size, it is not possible to disentangle the individual contribution of each cluster to the total SZ flux.

After applying these two exclusion criteria, the final sample adopted for the computation of the scaling relation contains 297 PSZ2 clusters, all of them with members selected within $1.5 \times r_{200}$. Column 5 in Table 4.1 shows the distribution of those objects in the three data sets considered in Sect. 4.1. Figure 4.7 presents the scaling relation obtained for those 297 objects. From here, the main goal is to find the so-called mass bias factor ($1 - b$), which accounts for any difference between the true mass and the SZ mass proxies ($Y_{500}^{\text{SZ}}, \theta_{500}^{\text{SZ}}$) used to establish the scaling relations. I define this bias as

$$M_{500}^{\text{SZ}} = (1 - b) M_{500}^{\text{true}}. \quad (4.3)$$

As explained in Sect. 4.2, we are not able to correct for all the physical effects potentially causing a bias when estimating the true velocity dispersion of the clusters. This leads to a bias between the true mass and the dynamical mass estimates. The main source of error are possibly the interlopers inside our sample. For this reason, I define the dynamical mass bias factor ($1 - b_{\text{dyn}}$) as

$$M_{500}^{\text{dyn}} = (1 - b_{\text{dyn}}) M_{500}^{\text{true}}. \quad (4.4)$$

Este documento incorpora firma electrónica, y es copia auténtica de un documento electrónico archivado por la ULL según la Ley 39/2015.
 Su autenticidad puede ser contrastada en la siguiente dirección <https://sede.ull.es/validacion/>

Identificador del documento: 3248012 Código de verificación: RmbjVJW6

Firmado por: ALEJANDRO AGUADO BARAHONA
 UNIVERSIDAD DE LA LAGUNA

Fecha: 01/03/2021 09:35:30

María de las Maravillas Aguiar Aguilera
 UNIVERSIDAD DE LA LAGUNA

22/03/2021 13:39:32

Combining the equations 4.3 and 4.4, I obtain

$$M_{500}^{SZ} = (1 - B) M_{500}^{\text{dyn}}, \quad (4.5)$$

where

$$(1 - B) \equiv \frac{(1 - b)}{(1 - b_{\text{dyn}})}. \quad (4.6)$$

I study this last bias $(1 - B)$ in our scaling relation. In principle, we would expect that this bias $(1 - B)$ represents a lower bound to $(1 - b)$, the reason being that the presence of interlopers generally produces an overestimation of the velocity dispersion, and thus of the dynamical mass (e.g. Ferragamo et al. 2020). However, and to estimate the real impact of interlopers in the sample, I repeat the same analysis with a smaller sub-sample of 261 clusters obtained by reducing the aperture when selecting the cluster members to r_{200} . As shown below, we find consistent results in this case, suggesting that the impact of interlopers for this particular sample is minimal (or at least smaller than our statistical error), as anticipated in Ferragamo et al. (2020). Column 6 in Table 4.1 shows the distribution of objects through the data sets of this smaller sub-sample.

4.4.1 Testing the regression methods

Here, I characterise with realistic simulations, matching the statistical properties of our sample, various regression methods. These simulations follow the very same procedure as the real data, using the same number of galaxies for each cluster to estimate the velocity dispersion and the dynamical mass uncertainties. These simulations are detailed in Sect. 4.4.1.2. I explore two possibilities. First, we consider the simplest case of fitting for a global bias. However, as there are hints that suggest a possible mass dependence of the mass bias, I also explore a fit to a power law in mass to account for this dependence, using as pivot scale $6 \times 10^{14} M_{\odot}$, to be able to consistently compare our results with other works in the literature (e.g. Planck Collaboration XXIV 2016). The parametric form of the fitting function in this second case is given by:

$$\frac{M_{500}^{SZ}}{6 \times 10^{14} M_{\odot}} = (1 - B) \left(\frac{M_{500}^{\text{dyn}}}{6 \times 10^{14} M_{\odot}} \right)^{\alpha}. \quad (4.7)$$

To be clear, when fitting this power law, the result of the mass bias is estimated at this given mass of $6 \times 10^{14} M_{\odot}$.

Due to the large uncertainties in the dynamical mass estimates for our sample, all the methods that I have tested do not behave well and give completely biased outputs. For this reason, we do the linear regression in the logarithmic space, fitting for the relation

$$\ln \left(\frac{M_{500}^{SZ}}{6 \times 10^{14} M_{\odot}} \right) = \alpha \ln \left(\frac{M_{500}^{\text{dyn}}}{6 \times 10^{14} M_{\odot}} \right) + \ln(1 - B), \quad (4.8)$$

where α and $\ln(1 - B)$ are the slope and the intercept, respectively. It is important to note that in our limit of large dynamical mass errors, these are also considerably greater

Este documento incorpora firma electrónica, y es copia auténtica de un documento electrónico archivado por la ULL según la Ley 39/2015.
 Su autenticidad puede ser contrastada en la siguiente dirección <https://sede.ull.es/validacion/>

Identificador del documento: 3248012 Código de verificación: RmbjVJW6

Firmado por: ALEJANDRO AGUADO BARAHONA
 UNIVERSIDAD DE LA LAGUNA

Fecha: 01/03/2021 09:35:30

María de las Maravillas Aguiar Aguilár
 UNIVERSIDAD DE LA LAGUNA

22/03/2021 13:39:32

than the expected intrinsic scatter of the relation $\sigma_{inM} = 0.096$ (Planck Collaboration XX 2014).

I test and validate five different regression methods that account for uncertainties in both axes, for the particular case of the sample discussed in this Chapter. This study is essential to verify the range of applicability of the methods, and to characterise the existence of statistical biases. Noise levels in the data and the intrinsic scatter of the underlying relation play an important role in the recovery of the best-fit estimates. To test these five methods, I perform simulations tailored to mimic the same statistical properties as in our parent sample. I show that for the noise levels of our reference sample, all the five methods present a bias in some of the recovered parameters. However, all of them are unbiased in the limit of high signal-to-noise (small uncertainties).

4.4.1.1 Regression methods

I study the dependence of the mass bias with mass by fitting the slope in equation 4.8. I consider the problem of carrying out a linear fit of two variables with errors in both axes and including intrinsic scatter. I use the following notation. The two variables are given by x_i and y_i . Each one of those has measured errors described by Gaussian statistics, with variance $\sigma_{x,i}$ and $\sigma_{y,i}$, respectively. The two variables are tracing underlying quantities ξ_i and η_i , in such a way that

$$x_i = \xi_i + \epsilon_{x,i}, \quad y_i = \eta_i + \epsilon_{y,i}. \quad (4.9)$$

By definition, $\langle \epsilon_{x,i} \rangle = \langle \epsilon_{y,i} \rangle = 0$, $\langle \epsilon_{x,i}^2 \rangle = \sigma_{x,i}^2$ and $\langle \epsilon_{y,i}^2 \rangle = \sigma_{y,i}^2$. The underlying model that I want to fit for is:

$$\eta_i = m\xi_i + n + \epsilon_i, \quad (4.10)$$

with parameters m (slope) and n (intercept). The intrinsic scatter, σ_{int} , is represented by $\langle \epsilon_i \rangle = 0$, and $\langle \epsilon_i^2 \rangle = \sigma_{int}^2$. Here, I consider the following regression methods:

- i) The Orthogonal Distance Regression (ODR) method, which uses a modified trust-region Levenberg-Marquardt-type algorithm (Boggs & Rogers 1990) to estimate the function parameters. It is implemented in the python *scipy.odr* package.
- ii) Nukers (Tremaine et al. 2002) method. It is based on the minimisation of the χ^2 function

$$\chi^2 = \sum_i \frac{(y_i - mx_i - n)^2}{\sigma_{y,i}^2 + m^2\sigma_{x,i}^2}. \quad (4.11)$$

- iii) Maximum Likelihood Estimator with Uniform prior (MLEU). In this case, the full posterior distribution, assuming Gaussian statistics and flat priors for the three parameters (m, n, σ_{int}) , is given by

$$\ln P \propto -\frac{1}{2} \left[\sum_i \frac{(y_i - mx_i - n)^2}{\sigma_{y,i}^2 + m^2\sigma_{x,i}^2 + \sigma_{int}^2} + \ln(\sigma_{y,i}^2 + m^2\sigma_{x,i}^2 + \sigma_{int}^2) \right]. \quad (4.12)$$

Este documento incorpora firma electrónica, y es copia auténtica de un documento electrónico archivado por la ULL según la Ley 39/2015.
 Su autenticidad puede ser contrastada en la siguiente dirección <https://sede.ull.es/validacion/>

Identificador del documento: 3248012 Código de verificación: RmbjVJW6

Firmado por: ALEJANDRO AGUADO BARAHONA
 UNIVERSIDAD DE LA LAGUNA

Fecha: 01/03/2021 09:35:30

María de las Maravillas Aguiar Aguilár
 UNIVERSIDAD DE LA LAGUNA

22/03/2021 13:39:32

- iv) Bivariate Correlated Errors and intrinsic Scatter (BCES, Akritas & Bershady 1996), which is a Bayesian method commonly used by the galaxy cluster community. I use here the python implementation from *astropy.stats*. In particular, the orthogonal distances method, which, in principle gives more accurate results.
- v) Complete Maximum Likelihood Estimation (CMLE) with correct priors (Kelly 2007). Here, I use the implementation of this method from <https://github.com/jmeyers314/linmix>.

BCES, MLEU and CMLE methods consider the intrinsic scatter (σ_{int}) explicitly in their calculations, and indeed both MLEU and CMLE provide an estimation of its value. The BCES implementation used here, do not provide this parameter. The ODR and Nukers methods do not take into account explicitly the intrinsic scatter. However, Tremaine et al. (2002) showed how to obtain an estimation of the σ_{int} for the Nukers method. Once the best-fit model has been obtained, we evaluate the reduced χ^2 in equation 4.11. If this value is smaller than one, then the intrinsic scatter is taken to be zero. Otherwise, the intrinsic scatter is calculated by replacing $\sigma_{y,i}^2$ by $\sigma_{y,i}^2 + \sigma_{\text{int}}^2$ in the denominator of equation 4.11 and balancing the right-hand side term until the reduced χ^2 is equal to one.

4.4.1.2 Simulations

The five methods described in the previous subsection are tested here in their complete forms, fitting simultaneously for the slope, intercept and the intrinsic scatter (if included in the method). In addition, the ODR, Nukers and MLEU are also tested in the particular case of fixing the slope to one, which in our case means that there is no mass dependence of the mass bias.

To test these methods, I carry out a set of realistic simulations, mimicking the sample size (297 objects) and noise conditions that I have in the cluster sample. The mass uncertainties are calculated using a fit to the variance proposed by Ferragamo et al. (2020), see Fig. 8 in that article. I run three sets of simulations. In the first two sets, I use the same GCs for every iteration while in the last one we generate a set of 297 synthetic clusters for each iteration. In more detail:

1. Set 1. I use the 297 real clusters from Table 4.2. I assume the estimated SZ masses M_{500}^{SZ} as the true masses M_{true} , and I fix the estimated redshift z and the number of cluster members N_{gal} to the real ones.
2. Set 2. Fitting the properties of the real parent sample from Table 4.2, I obtain a realistic distribution of dynamical masses, z and N_{gal} . I use these distributions to generate the true simulated mass M_{true} , z and N_{gal} of a set of 297 synthetic clusters.
3. Set 3. I build a set of 297 synthetic clusters in the same way as in 2, but for every iteration.

Este documento incorpora firma electrónica, y es copia auténtica de un documento electrónico archivado por la ULL según la Ley 39/2015.
Su autenticidad puede ser contrastada en la siguiente dirección <https://sede.ull.es/validacion/>

Identificador del documento: 3248012 Código de verificación: RmbjVJW6

Firmado por: ALEJANDRO AGUADO BARAHONA
UNIVERSIDAD DE LA LAGUNA

Fecha: 01/03/2021 09:35:30

María de las Maravillas Aguiar Aguilár
UNIVERSIDAD DE LA LAGUNA

22/03/2021 13:39:32

I use the procedure explained below to obtain the measured SZ and dynamical masses. Using the Munari et al. (2013) relation (Fig. 4.1, I obtain the true velocity dispersion σ_{200} . The next step is to simulate the measured velocity dispersion which is our observable. Here, for each cluster in every realisation I create a set of N_{gal} galaxies which are normally distributed around the σ_{200} and I estimate the measured velocity dispersion $\sigma_{measured}$ using these galaxies (only for 2 and 3, the N_{gal} for 1 is fixed). Now, I apply the same procedure as for the real data. I convert the $\sigma_{measured}$ into measured dynamical mass M_{dyn} using eq. 4.1. Then, I correct this mass using the corrections from Ferragamo et al. (2020) due to the low number of members. The measured uncertainties are directly calculated from eq. C.1 in Ferragamo et al. (2020). I do not include the intrinsic scatter of the relation 4.1 because it is expected to be smaller than 5% (Munari et al. 2013) and the uncertainties in the real data masses are not less than 10% and up to 80% with an average of 40%.

On the other hand, I simulate the SZ masses M_{SZ} by calculating the observable \hat{Y}_{SZ} using the inverse procedure than in *Planck* papers. To obtain \hat{Y}_{SZ} I introduce the true simulated masses into the equation:

$$E^{-\beta}(z) \left[\frac{D_A^2(z) \hat{Y}_{SZ}}{10^{-4} \text{Mpc}^2} \right] = Y_* \left[\frac{h}{0.7} \right]^{-2+\alpha} \left[\frac{(1-b)M_{true}}{6 \times 10^{14} M_{\odot}} \right]^{\alpha}, \quad (4.13)$$

where $D_A^2(z)$ is the angular-diameter distance to redshift z and $E^2(z) = \Omega_m(1+z)^3 + \Omega_{\Lambda}$. The coefficients Y_* , α and β are given in Table 1 in Planck Collaboration XXIV (2016). Once I have obtained \hat{Y}_{SZ} , I include the intrinsic scatter of this relation by adopting a log-normal distribution for the observed Y_{SZ} around its mean value \hat{Y}_{SZ} with $\sigma_{\log Y} = 0.075 \pm 0.01$ (see Planck Collaboration XX 2014). Finally I insert the observed Y_{SZ} into eq. 4.13 to obtain the measured M_{SZ} using the mass bias $(1-b) = 0.80$ and I apply a Gaussian random noise based on the real data measured uncertainties.

The theoretically predicted intrinsic scatter in the $M_{SZ} - M_{dyn}$ (eq. 4.8) is $\sigma_{\ln M} = 0.096$. It is calculated by propagating the intrinsic scatter $\sigma_{\log Y}$ from the $Y - M$ relation (eq. 4.13) into eq. 4.8. There are other sources of intrinsic scatter, such as the scatter in eq. 4.1, but in this simulations I only consider $\sigma_{\log Y}$ as it is the largest.

In this particular case, I assume no dynamical mass bias ($1 - b_{dyn}$) so what I am recovering is the SZ bias which is the same as the bias between the SZ and dynamical masses $(1 - B) = (1 - b)$.

Este documento incorpora firma electrónica, y es copia auténtica de un documento electrónico archivado por la ULL según la Ley 39/2015.
 Su autenticidad puede ser contrastada en la siguiente dirección <https://sede.ull.es/validacion/>

Identificador del documento: 3248012 Código de verificación: RmbjVJW6

Firmado por: ALEJANDRO AGUADO BARAHONA
 UNIVERSIDAD DE LA LAGUNA

Fecha: 01/03/2021 09:35:30

María de las Maravillas Aguiar Aguiar
 UNIVERSIDAD DE LA LAGUNA

22/03/2021 13:39:32

Table 4.4: Results for the recovered parameters. Input values are $(1 - b) = e^n$, $slope (m = 1)$, $\sigma_{\ln M} = 0.096$

Method	$(1 - b) = e^n$						$slope (m)$			$\sigma_{\ln M}$		
	Set 1	Set 2	Set 3	Set 1	Set 2	Set 3	Set 1	Set 2	Set 3	Set 1	Set 2	Set 3
ODR	0.848 ± 0.020	0.859 ± 0.021	0.861 ± 0.022	1.000	1.000	1.000	1.000	1.000	1.000	—	—	—
	0.856 ± 0.027	0.859 ± 0.036	0.861 ± 0.038	1.041	1.041	1.041	1.003	1.003	1.002	1.000	1.000	1.000
Nutlers	0.848 ± 0.020	0.859 ± 0.021	0.861 ± 0.022	1.000	1.000	1.000	1.000	1.000	1.000	0.283	0.276	0.272
	0.857 ± 0.056	0.859 ± 0.032	0.862 ± 0.036	1.042	1.042	1.042	1.005	1.005	1.003	0.308	0.307	0.276
MLE	0.868 ± 0.022	0.875 ± 0.023	0.876 ± 0.024	1.000	1.000	1.000	1.000	1.000	1.000	0.222	0.241	0.239
	0.772 ± 0.010	0.677 ± 0.015	0.672 ± 0.020	0.404	0.404	0.404	0.522	0.522	0.501	0.308	0.285	0.280
BCEs	0.852 ± 0.033	0.808 ± 0.064	0.800 ± 0.069	0.800	0.800	0.800	0.848	0.848	0.836	—	—	—
CMLE	0.846 ± 0.021	0.794 ± 0.027	0.786 ± 0.028	0.830	0.830	0.830	0.808	0.808	0.792	0.043	0.016	0.050

Este documento incorpora firma electrónica, y es copia auténtica de un documento electrónico archivado por la ULL según la Ley 39/2015.
 Su autenticidad puede ser contrastada en la siguiente dirección <https://sede.ull.es/validacion/>

Identificador del documento: 3248012 Código de verificación: RmbjVJW6

Firmado por: ALEJANDRO AGUADO BARAHONA
 UNIVERSIDAD DE LA LAGUNA

Fecha: 01/03/2021 09:35:30

María de las Maravillas Aguiar Aguiar
 UNIVERSIDAD DE LA LAGUNA

22/03/2021 13:39:32

4.4.1.3 Results

Table 4.4 shows the results of the regression tests performed over the simulations described in the previous subsection. The first column names the regression method. The second, third and fourth column presents the median value of the mass bias $(1 - b)$, the slope m and the natural logarithm of the intrinsic scatter when available, for the three different sets of simulations.

First, I discuss the results for the case of no mass dependence in the mass bias ($m = 1$). There is no particular method that recovers the $(1 - b) = 0.8$. All three tested methods are biased, regardless of the initial settings of the simulations. As shown in figure 4.4 the ODR and the Nukers are biased upwards by a 7% while the MLEU is biased by a 9% in the same direction. I consider this effect as a true bias as the standard deviations in the three methods are not greater than 3%, see figure 4.4 and table 4.4. The MLEU estimates the intrinsic scatter of the relation as $\sigma_{\ln M} = 0.24 \pm 0.04$ which is more than $3\text{-}\sigma$ away from the predicted one $\sigma_{\ln M} = 0.096$. The estimation that comes out from the Nukers method is $\sigma_{\ln M} = 0.27 \pm 0.05$, also more than $3\text{-}\sigma$ away. This might be the reason why the methods are biased, the overestimation of the intrinsic scatter may lead into a biased estimation of the intercept. The explanation for the latter is that the methods may not be able to disentangle the difference between the intrinsic scatter and the measurement errors as they are, on average, four times larger. Another possible explanation is that the error propagation might not be as precise as required. I use symmetric errors in the logarithm space and they are calculated as the uncertainty over the quantity in the real space. This is just an approximation that with our big uncertainties might produce this type of bias.

I also perform the same analysis varying the input value of the mass bias from 0.6 to 1.2 obtaining the same results as explained above. In every case, the $(1 - b)$ parameter and the slope are biased in the same percentage as when using $(1 - b) = 0.8$.

Now, I discuss the case of a possible dependence of the mass bias parameter with the mass, in other words, letting the slope of the regression free to vary. The following results are independent of the initial settings of the simulation as shown in table 4.4. The ODR and the Nukers methods, as in the case of fixed slope, are biased in the recovery of the parameter $(1 - b)$ exactly in the same percentage as the recovery of the slope is almost perfect. The only difference is that the standard deviation is greater. The MLEU, the BCES and the CMLE fail completely when trying to recover the slope. Although the BCES and the CMLE do recover the mass bias parameter, these methods must not be trusted as the slope they recover is between 15 and 20% lower than the input value. The MLEU fails catastrophically in both tasks. The bad behaviour of these methods might be caused by the wrong estimation of the intrinsic scatter because of the confusion with the huge measurement errors, similar to the case of fixed slope.

Figure 4.6 shows the distribution of the intrinsic scatter for the three methods that estimate it. I think this is one of the key questions and why the methods do not recover properly the input values of the parameters. As explained in the previous subsection, the theoretical intrinsic scatter can be calculated and there is no single method that estimate it correctly. I perform the same simulations setting the intrinsic scatter to zero

Este documento incorpora firma electrónica, y es copia auténtica de un documento electrónico archivado por la ULL según la Ley 39/2015.
 Su autenticidad puede ser contrastada en la siguiente dirección <https://sede.ull.es/validacion/>

Identificador del documento: 3248012 Código de verificación: RmbjVJW6

Firmado por: ALEJANDRO AGUADO BARAHONA
 UNIVERSIDAD DE LA LAGUNA

Fecha: 01/03/2021 09:35:30

María de las Maravillas Aguiar Aguilár
 UNIVERSIDAD DE LA LAGUNA

22/03/2021 13:39:32

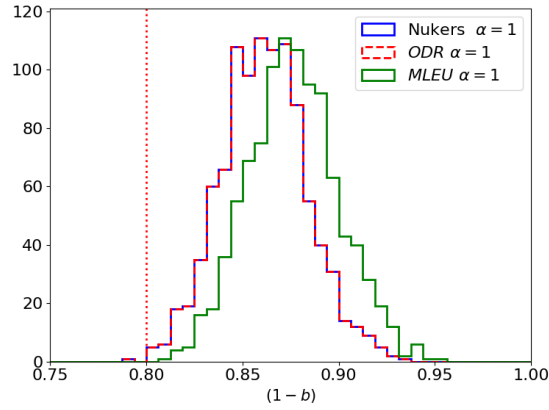


Figure 4.4: Distribution of the estimation of the mass bias parameter when fixing the slope to one for Nukers, ODR and MLEU methods (Set 3). Vertical dashed line represents the input value $(1 - b) = 0.8$.

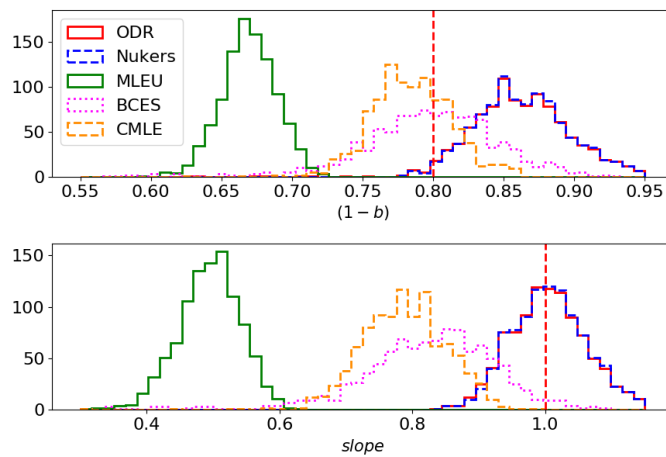


Figure 4.5: Distribution of the estimation of the mass bias parameter (top panel) and the slope (bottom panel) for the five tested regression methods (Set 3). Vertical dashed lines represent the input values of the simulation $(1 - b) = 0.8$ and $\alpha = 1$.

Este documento incorpora firma electrónica, y es copia auténtica de un documento electrónico archivado por la ULL según la Ley 39/2015.
 Su autenticidad puede ser contrastada en la siguiente dirección <https://sede.ull.es/validacion/>

Identificador del documento: 3248012 Código de verificación: RmbjVJW6

Firmado por: ALEJANDRO AGUADO BARAHONA
 UNIVERSIDAD DE LA LAGUNA

Fecha: 01/03/2021 09:35:30

María de las Maravillas Aguiar Aguilár
 UNIVERSIDAD DE LA LAGUNA

22/03/2021 13:39:32

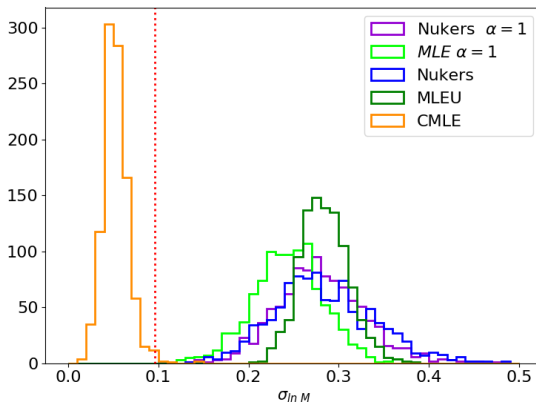


Figure 4.6: Distribution of the estimation of the intrinsic scatter for Nukers, MLEU and CMLE (Set 3). Vertical dashed line represents the theoretical value of the intrinsic scatter $\sigma_{in M} = 0.096$.

and I find very similar results to those discussed above. I also perform the simulations setting the measurement errors two orders of magnitude lower. In this case, all methods recover properly the input values even the intrinsic scatter within 1-, 2- σ depending on the method.

I conclude that there is no correct regression method to use in this configuration, in other words, each method is either biased or gives wrong results. The main source of trouble are the big measurements errors combined with the intrinsic scatter. I select the Nukers method as the reference method for two main reasons. It gives a robust estimation of the slope when I let it vary, and it has a small bias in the $(1 - b)$ parameter which I can correct or account for. Other methods might give better estimation of the $(1 - b)$ parameter, like the MLEU which is less biased than the Nukers but this method does not recovered correctly the slope (see Fig. 4.5). In combination of $(1 - b)$ and slope I recommend to use the Nukers method for our particular set of data.

When quoting the final values of the estimation of the mass bias, I correct the Nukers results accounting for the bias in the intercept (7%), and add a systematic uncertainty due to this bias.

4.4.2 The mass bias

Table 4.5 shows the results for the fitting of eq. 4.8 using the Nukers method described above, and for both samples. The statistical errors quoted in this table are computed with a bootstrapping technique.

The value of the slope is (in both samples) a bit more than 1- σ away from one, which

Este documento incorpora firma electrónica, y es copia auténtica de un documento electrónico archivado por la ULL según la Ley 39/2015.
 Su autenticidad puede ser contrastada en la siguiente dirección <https://sede.ull.es/validacion/>

Identificador del documento: 3248012 Código de verificación: RmbjVJW6

Firmado por: ALEJANDRO AGUADO BARAHONA
 UNIVERSIDAD DE LA LAGUNA

Fecha: 01/03/2021 09:35:30

María de las Maravillas Aguiar Aguilár
 UNIVERSIDAD DE LA LAGUNA

22/03/2021 13:39:32

Table 4.5: Results for the mass bias using both sub-samples 1 and $1.5 \times r_{200}$. I present the direct results of the Nukers method for both the case of fixed slope ($\alpha = 1$) and free-slope, and also the corresponding bias-corrected values. See text for details.

Method	$1.5 \times r_{200}$		$1 \times r_{200}$	
	$(1 - B)$	α	$(1 - B)$	α
Nukers	0.850 ± 0.040	1.000	0.841 ± 0.040	1.000
	0.889 ± 0.065	1.167 ± 0.125	0.875 ± 0.067	1.145 ± 0.121
Nukers	$0.80 \pm 0.04 \pm 0.05$	1.00	$0.79 \pm 0.04 \pm 0.05$	1.00
corrected	$0.84 \pm 0.07 \pm 0.05$	1.17 ± 0.13	$0.83 \pm 0.07 \pm 0.05$	1.15 ± 0.13

might be indicative of a possible dependence of the $(1 - B)$ with the mass, but the results are not significant enough to make that claim. For comparison, von der Linden et al. (2014) and Hoekstra et al. (2015) find a slope around 0.7, which goes in the direction of inverse dependence of the mass bias with mass. Their results were obtained using the CMLE method (Kelly 2007). I note that in our particular case, the simulations show that this method presents a significant bias, of approximately 20% (see section 4.4.1). A direct evaluation of the slope using CMLE gives $\alpha = 0.70 \pm 0.06$ for our sample, but after the bias correction, this number moves up to $\alpha = 0.88 \pm 0.07$, which is less than $2\text{-}\sigma$ from unity.

I find no significant difference in the $(1 - B)$ mass bias when considering different samples, suggesting that the effect of the interlopers in the region $1 - 1.5 \times r_{200}$ is smaller than the quoted statistical error, as expected. For this reason, I restrict the following analysis to the case of the full sample ($1.5 \times r_{200}$). The results for the mass bias using this sample are shown in Fig. 4.7.

I investigate the robustness of the results when selecting only those clusters with smaller error bars in the determination of the dynamical mass. For this, I have repeated the analysis using different selections according to the number of cluster members used to determine the velocity dispersion (parameter $N_{1.5}$ in Table 4.2). Table 4.6 shows the results when restricting our sample to those clusters with $N_{1.5} > 15, 20, 30,$ and 50 . The values of the mass bias and the slope are consistent with each other in all cases. However, I note that there is a marginal trend (smaller than $1\text{-}\sigma$) towards lower values of the bias for the sub-samples with more cluster members. I can understand this trend by noting that those clusters with more members are, on average, less massive as they are mostly low-redshift systems. As there is a marginal detection of a slope $\alpha > 1$, then we would expect low-mass clusters to present a lower $(1 - B)$.

4.4.2.1 Eddington bias

The effect of the Eddington bias correction is shown in Table 4.7. Clusters are distributed in five bins, keeping the same number of objects per bin. In this case, there are not enough clusters to perform the regression with a free slope, so I restrict the analysis here

Este documento incorpora firma electrónica, y es copia auténtica de un documento electrónico archivado por la ULL según la Ley 39/2015.
 Su autenticidad puede ser contrastada en la siguiente dirección <https://sede.ull.es/validacion/>

Identificador del documento: 3248012 Código de verificación: RmbjVJW6

Firmado por: ALEJANDRO AGUADO BARAHONA
 UNIVERSIDAD DE LA LAGUNA

Fecha: 01/03/2021 09:35:30

María de las Maravillas Aguiar Aguilár
 UNIVERSIDAD DE LA LAGUNA

22/03/2021 13:39:32

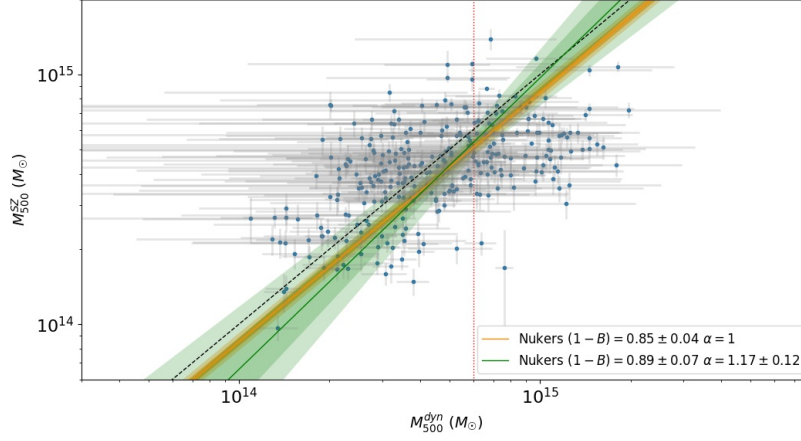


Figure 4.7: Scaling relation for the sample of 297 PSZ2 clusters ($1.5 \times r_{200}$ sample). The dashed black line shows the 1 : 1 line. The orange line represents our best fit using the Nukers method with $\alpha = 1$ (see text for details). The green line is the fit using the complete Nukers method, for a free slope. The shaded regions represent the 1- and 2- σ errors of the reconstructed parameters. The vertical red dotted line corresponds to the pivot mass of $6 \times 10^{14} M_{\odot}$.

Table 4.6: Results for the mass bias using the sample ($1.5 \times r_{200}$), when restricting the analysis to those clusters with total number of spectroscopic members N in a certain range or interval. See text for details.

	$N > 15$		$N > 20$	
	$(1 - B)$	α	$(1 - B)$	α
Nukers	0.845 ± 0.041	1.000	0.841 ± 0.043	1.000
	0.881 ± 0.067	1.154 ± 0.127	0.880 ± 0.070	1.163 ± 0.131
N_{clusters}	214		164	
	$N > 30$		$N > 50$	
	$(1 - B)$	α	$(1 - B)$	α
Nukers	0.824 ± 0.045	1.000	0.815 ± 0.051	1.000
	0.859 ± 0.080	1.143 ± 0.155	0.860 ± 0.100	1.175 ± 0.181
N_{clusters}	100		55	

Este documento incorpora firma electrónica, y es copia auténtica de un documento electrónico archivado por la ULL según la Ley 39/2015.
 Su autenticidad puede ser contrastada en la siguiente dirección <https://sede.ull.es/validacion/>

Identificador del documento: 3248012 Código de verificación: RmbjVJW6

Firmado por: ALEJANDRO AGUADO BARAHONA
 UNIVERSIDAD DE LA LAGUNA

Fecha: 01/03/2021 09:35:30

María de las Maravillas Aguiar Aguilár
 UNIVERSIDAD DE LA LAGUNA

22/03/2021 13:39:32

Table 4.7: Nukers $(1 - B)$ estimates before and after the Eddington bias correction in signal-to-noise ratio bins for the sample with aperture cut $1.5 \times r_{200}$.

SNR bin	$(1 - B)$	
	Before	After
$S/N < 4.97$	1.009 ± 0.075	0.900 ± 0.071
$4.97 \leq S/N < 5.57$	0.919 ± 0.065	0.818 ± 0.056
$5.57 \leq S/N < 6.35$	0.789 ± 0.058	0.730 ± 0.053
$6.35 \leq S/N < 8.26$	0.912 ± 0.062	0.873 ± 0.057
$S/N \geq 8.26$	0.882 ± 0.082	0.876 ± 0.079

Table 4.8: Nukers $(1 - B)$ estimates for different bins in redshift for the sample with aperture cut $1.5 \times r_{200}$.

Redshift bin	$(1 - B)$
$z < 0.107$	0.810 ± 0.059
$0.107 \leq z < 0.200$	1.013 ± 0.061
$0.200 \leq z < 0.292$	0.784 ± 0.052
$0.292 \leq z < 0.379$	0.799 ± 0.055
$z \geq 0.379$	1.038 ± 0.068

to the case of a fixed slope ($\alpha = 1$). As expected, the correction applied reduces the mass bias between 10% and less than 1%, depending on the SZ S/N of the *Planck* SZ detection. I note that the central bin ($5.57 < S/N \leq 6.35$) does not follow the trend of the others, but it is still less than $2\text{-}\sigma$ away from the mean value for the full sample. I also note that the errors shown here are only the statistical ones so when included the systematic this apparent discrepancy is even less.

4.4.2.2 Redshift dependence

Table 4.8 presents the results for the mass bias in five different redshift bins with the same number of objects. As in the previous study, there are not enough clusters in each bin to make the regression with a free varying slope, so I restrict the analysis again to the case of fixed ($\alpha = 1$) slope. I find that three of the five bins show consistent results with the mean bias for the full sample. However, there are two bins ($0.107 \leq z < 0.200$ and $z \geq 0.379$), which are inconsistent with the mean bias at the level of approximately $2.7\text{-}\sigma$. I refer to them as second and fifth bins. As noted in the previous section, when adding the systematic uncertainties, this tension is alleviated.

I have carried out several tests to explain the origin of these two outliers, but none of the analyses are conclusive. First, I have explored if this difference could be ascribed to a significantly different mean mass in the bin. In principle, the low redshift bins could span a larger range of masses due to the survey selection function (see Fig. 26 in *Planck*

Este documento incorpora firma electrónica, y es copia auténtica de un documento electrónico archivado por la ULL según la Ley 39/2015.
 Su autenticidad puede ser contrastada en la siguiente dirección <https://sede.ull.es/validacion/>

Identificador del documento: 3248012 Código de verificación: RmbjVJW6

Firmado por: ALEJANDRO AGUADO BARAHONA
 UNIVERSIDAD DE LA LAGUNA

Fecha: 01/03/2021 09:35:30

María de las Maravillas Aguiar Aguilár
 UNIVERSIDAD DE LA LAGUNA

22/03/2021 13:39:32

Table 4.9: Summary of mass bias value from the literature.

SURVEY	REFERENCE SAMPLE	N. CLUSTERS	(1-b)	reference
X-RAY				
	<i>Planck</i> PSZ1	189	$0.8^{+0.1}_{-0.2}$	<i>Planck</i> Collaboration XXIX (2014)
VELOCITY DISPERSION				
	SPT	44	0.72 ± 0.57	Ruel et al. (2014)
	ACT	21	1.10 ± 0.13	Sifón et al. (2016)
	<i>Planck</i> PSZ2	17	0.64 ± 0.11	Amodeo et al. (2018)
	<i>Planck</i> PSZ1	207	$0.83 \pm 0.07 \pm 0.02$	Ferragamo et al. (2021, submitted)
	<i>Planck</i> PSZ2	297	$0.80 \pm 0.04 \pm 0.05$	This work
WEAK LENSING				
WtG	<i>Planck</i> PSZ1	38	0.688 ± 0.072	von der Linden et al. (2014)
CCCP	<i>Planck</i> PSZ1	37	0.76 ± 0.05	Hoekstra et al. (2015)
LoCuSS	<i>Planck</i> PSZ2	44	0.95 ± 0.04	Smith et al. (2016)
CSS2	ACT	19	0.87 ± 0.50	Battaglia et al. (2016)
PSZ2LenS	<i>Planck</i> PSZ2	32	0.76 ± 0.08	Sereno et al. (2017)
CLASH	<i>Planck</i> PSZ1	21	0.73 ± 0.10	Penna-Lima et al. (2017)
HSC-SSP	<i>Planck</i> PSZ2	5	0.80 ± 0.15	Medezinski et al. (2018)
HSC-SSP	ACTPol	8	$0.74^{+0.13}_{-0.12}$	Miyatake et al. (2019)

Collaboration XXVII 2016). The median mass values that I find for those five bins are 3.6, 4.3, 7.1, 6.7 and $5.9 \times 10^{14} M_{\odot}$, respectively. These values do not show any specific trend that could explain the two outliers. This is also the case for the mean number of galaxies (90, 27, 19, 18 and 22) and the mean S/N (8.8, 7.5, 7.7, 6.1 and 5.9) in each of the five bins. I have also divided the two anomalous bins in two new sub-bins in redshift, S/N and number of galaxies. There is no appreciable difference in any sub-bin for the case of $0.107 \leq z < 0.200$. However, when I do the same for the fifth bin ($z \geq 0.379$), it seems that the outlier here might be due to the high redshift clusters. This is in agreement with the result showed before of a small dependence of the mass bin with mass.

Thus, I cannot find a simple explanation for the outlier in the second redshift bin ($0.107 \leq z < 0.200$), and if confirmed with better statistics, this could be ascribed to a real physical effect. For comparison, I note that Ferragamo et al. (2021, submitted) also find a similar outlier in the same redshift bin when using PSZ1 clusters only. Their bin is less significant than the one found here, although it goes in the same direction, the statistical effect is lower than in our case as they have less objects inside the bin.

4.5 Comparison with literature

Through this section, I compare the result of the mass bias extracted from this thesis to those in the literature. The following works use different mass proxies and methodologies. Figure 4.8 and table 4.9 summarise the surveys describe below.

As described in section 1.4.1, the *Planck* Collaboration presented the calibration of their SZ masses using X-Ray observations of nearby clusters. Their estimation of the mass bias is very close to the HE mass bias as they used 20 nearby relaxed clusters. They assumed for the mass bias the median value obtained for the mass at the pivot

Este documento incorpora firma electrónica, y es copia auténtica de un documento electrónico archivado por la ULL según la Ley 39/2015.
 Su autenticidad puede ser contrastada en la siguiente dirección <https://sede.ull.es/validacion/>

Identificador del documento: 3248012 Código de verificación: RmbjVJW6

Firmado por: ALEJANDRO AGUADO BARAHONA
 UNIVERSIDAD DE LA LAGUNA

Fecha: 01/03/2021 09:35:30

María de las Maravillas Aguiar Aguilár
 UNIVERSIDAD DE LA LAGUNA

22/03/2021 13:39:32

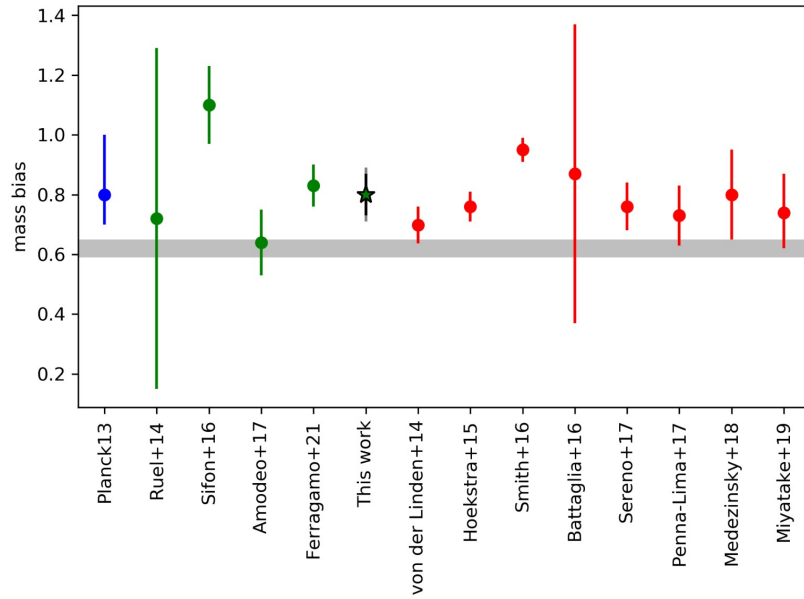


Figure 4.8: Value of the mass bias from previous studies and this work. In blue, the result from Planck Collaboration XX (2014), using a scaling relation from X-ray observations; in green, the mass bias from $M_{SZ} - M_{dyn}$ scaling relations, in red, those from weak lensing studies, respectively. The grey shaded region represents the mass bias values that reconcile the tension between CMB and SZ number counts from Planck Collaboration VI (2020). The green star represents the mass bias value found in this work ($1 - b = 0.80 \pm 0.04 \pm 0.05$). Both statistical and systematic uncertainties are plotted.

Este documento incorpora firma electrónica, y es copia auténtica de un documento electrónico archivado por la ULL según la Ley 39/2015.
 Su autenticidad puede ser contrastada en la siguiente dirección <https://sede.ull.es/validacion/>

Identificador del documento: 3248012 Código de verificación: RmbjVJW6

Firmado por: ALEJANDRO AGUADO BARAHONA
 UNIVERSIDAD DE LA LAGUNA

Fecha: 01/03/2021 09:35:30

María de las Maravillas Aguiar Aguiar
 UNIVERSIDAD DE LA LAGUNA

22/03/2021 13:39:32

point $M_{500} = 6 \times 10^{14} M_{\odot}$ (Planck Collaboration XX 2014)

$$(1 - b) = 0.8_{-0.1}^{+0.2}. \quad (4.14)$$

The result extracted from this thesis is compatible with theirs within $0.2\text{-}\sigma$.

The next four works presented here used the velocity dispersion as the mass proxy to estimate the dynamical mass and compared them to the SZ mass from different surveys and samples.

Ruel et al. (2014) estimated the mass bias from 43 SZ selected clusters from the SPT catalogues. Their sample are massive objects $2.7 \leq M_{500}^{\text{SPT}} \leq 18.0 (\times 10^{14} M_{\odot})$, clusters at $z \geq 0.3$. They found

$$\exp \left[\left\langle \ln \left(\frac{M_{200}^{\text{SPT}}}{M_{200}^{\text{dyn}}} \right) \right\rangle \right] = (1 - B) = 0.72 \pm 0.57. \quad (4.15)$$

There are some differences between their methodology and the one used here. They obtain their SZ masses using the $Y - M$ relation from Reichardt et al. (2013). This relation has a less steep slope than the *Planck* Collaboration's, which is the one used in this thesis. This results in a slight difference in the SZ mass estimate, specially for massive clusters. From the dynamical point of view, to estimate the velocity dispersion, they use the biweight method in contrast to the gapper that has been proved to be less biased in the lower limit of number of galaxies (Ferragamo et al. 2020). The last difference is the $\sigma - M$ relation, which they use the Saro et al. (2013) relation that tends to overestimate the dynamical masses (Sifón et al. 2016), when compared to the Munari et al. (2013) relation.

In Sifón et al. (2016), the authors used a sub-sample of 21 GCs from the ACT cluster sample with $S/N > 5.1$, at redshifts $0.2 \leq z \leq 1.06$, in a mass range $1.0 < M_{200}^{\text{dyn}} < 13.0 (\times 10^{14} M_{\odot})$. They found

$$\frac{\langle M_{\text{SZ}} \rangle}{\langle M_{\text{dyn}} \rangle} = \frac{(1 - b_{\text{SZ}})}{\beta_{\text{dyn}}} = 1.10 \pm 0.13, \quad (4.16)$$

with $\beta_{\text{dyn}} = \langle M_{\text{dyn}} \rangle / \langle M_{\text{true}} \rangle$. Their methodology is very similar to that of this thesis, they use the same $Y - M$ and $\sigma - M$ relations. One of the main differences is the concentration parameter used for the conversion from M_{200}^{dyn} to M_{500}^{dyn} , for which they use the one presented in Dutton & Macciò (2014). They do not perform the fit of the relation $M_{\text{SZ}} - M_{\text{dyn}}$ but estimate the mass bias as the ratio between the mean SZ and the mean dynamical mass. The tension between their result and the one presented here is $2.3\text{-}\sigma$. I note here that their value is in more than $2\text{-}\sigma$ tension with every other work.

Amodeo et al. (2018) used 17 low- z clusters ($z < 0.5$) from the PZS2 catalogue in the mass range $3.0 < M_{200}^{\text{dyn}} < 14.0 (\times 10^{14} M_{\odot})$ founding a mass bias of

$$(1 - b) = 0.64 \pm 0.11. \quad (4.17)$$

Their methodology is similar to that of the *Planck* Collaboration. They use the concentration parameter from Dutton & Macciò (2014) to convert M_{500}^{SZ} to M_{500}^{SZ} . They do

Este documento incorpora firma electrónica, y es copia auténtica de un documento electrónico archivado por la ULL según la Ley 39/2015.
 Su autenticidad puede ser contrastada en la siguiente dirección <https://sede.ull.es/validacion/>

Identificador del documento: 3248012 Código de verificación: RmbjVJW6

Firmado por: ALEJANDRO AGUADO BARAHONA
 UNIVERSIDAD DE LA LAGUNA

Fecha: 01/03/2021 09:35:30

María de las Maravillas Aguiar Aguilár
 UNIVERSIDAD DE LA LAGUNA

22/03/2021 13:39:32

not compare the masses themselves but to use the self-similar slope ($\alpha = 1/3$) on the relation $\sigma_{200}-M_{200}$ fitting it. They compare the normalisation parameter obtained to that of Evrard et al. (2008). As Evrard et al. (2008) parameter was constrained using N-Body dark matter only simulations, Amodeo et al. (2018) take into account the velocity bias. The authors also make an Eddington bias correction from a global point of view. Comparing their result to that of this thesis, I find a mild tension at $\sim 1.45\sigma$.

To finish with the works that used the velocity dispersion as the mass proxy for the dynamical masses, Ferragamo et al. (2021, submitted) used 207 GCs from the PSZ1 catalogue in the mass range $0.8 < M_{500}^{\text{dyn}} < 20 (\times 10^{14} M_{\odot})$ in the redshift interval $0.029 < z < 0.844$. They found

$$(1 - B) = \frac{(1 - b_{\text{SZ}})}{(1 - b_{\text{dyn}})} = 0.83 \pm 0.07 \pm 0.02. \quad (4.18)$$

Their methodology is the same used in this thesis but for some minor details. The threshold on the member selection is slightly different (see section 4.2). Moreover, they use 2.5 Mpc as their threshold in radii in contrast with 1 and $1.5 \times r_{200}$ used in this thesis. Their result is completely compatible with ours as well as some features of the relation explained in detail in previous sections.

Now, I compare our result with 8 works that estimated the mass bias using weak lensing (WL) masses. As noted in Chapter 1, the advantage of this type of methodologies is that this mass can be considered the true mass but it is very model dependent. I will not explain the detail about these methodologies but comment about their results compared to ours.

von der Linden et al. (2014) used 38 GCs from the Weighing the Giants (WtG) project in common with the PSZ1 and found the following value for the bias:

$$\left\langle \frac{M_{500}^{\text{SZ}}}{M_{500}^{\text{WtG}}} \right\rangle = (1 - b) = 0.698 \pm 0.062. \quad (4.19)$$

This result is in a mild tension within $\sim 1.65\sigma$ with respect to ours. They also found a dependence of the mass bias with the mass:

$$\frac{M_{500}^{\text{SZ}}}{10^{15} M_{\odot}} = (0.699^{+0.059}_{-0.060}) \left(\frac{M_{500}^{\text{WtG}}}{10^{15} M_{\odot}} \right)^{0.68^{+0.15}_{-0.11}}. \quad (4.20)$$

As discussed in section 4.4.2, their results were obtained using the CMLE method (Kelly 2007). I note that in our particular case, the simulations show that this method presents a significant bias, of approximately 20% (see Sect. 4.4.1.3). A direct evaluation of the slope using CMLE gives $\alpha = 0.70 \pm 0.06$ for our sample, but after the bias correction, this number moves up to $\alpha = 0.88 \pm 0.07$. In this case, their result is less than 1.5σ away from ours. However, the results of this thesis suggest a direct dependence on the mass, not inverse, as proposed by the authors of this work.

Hoekstra et al. (2015) used 37 WL masses from the Canadian Cluster Comparison Project (CCCP) and from the PSZ1 to obtain

Este documento incorpora firma electrónica, y es copia auténtica de un documento electrónico archivado por la ULL según la Ley 39/2015.
 Su autenticidad puede ser contrastada en la siguiente dirección <https://sede.ull.es/validacion/>

Identificador del documento: 3248012 Código de verificación: RmbjVJW6

Firmado por: ALEJANDRO AGUADO BARAHONA
 UNIVERSIDAD DE LA LAGUNA

Fecha: 01/03/2021 09:35:30

María de las Maravillas Aguiar Aguilár
 UNIVERSIDAD DE LA LAGUNA

22/03/2021 13:39:32

$$(1 - b) = 0.76 \pm 0.05, \quad (4.21)$$

compatible within $1-\sigma$ to our value. They also fitted the relation allowing a dependence on the mass obtaining

$$\frac{M_{500}^{SZ}}{10^{15} h_{70}^{-1} M_{\odot}} = (0.76 \pm 0.04) \times \left(\frac{M_{500}^{CCCP}}{10^{15} h_{70}^{-1} M_{\odot}} \right)^{0.64 \pm 0.17}. \quad (4.22)$$

The same discussion as for von der Linden et al. (2014) can be applied here, finding the same discrepancy with the result of this thesis.

In Smith et al. (2016), the authors analysed a sample of 44 GCs common to the Local Cluster Substructure Survey (LoCuSS) and the PSZ2 catalogue. They found

$$(1 - b) = 0.95 \pm 0.04. \quad (4.23)$$

The discrepancy with our result might come from the fact that they use clusters within the range $0.15 \leq z \leq 0.30$ and I show in section 4.4.2.2 that the GCs from that bin present higher value of the mass bias (see table 4.8). Moreover, they do not correct the Eddington bias, which should lower their result.

Battaglia et al. (2016) determined the mass bias from two samples consisting of 9 and 10 GCs from the Canada France Hawaii Telescope Stripe- Survey (CS82) in common with the ACT equatorial sample. They found

$$(1 - b)_{S/N > 5} = 0.87 \pm 0.50, \quad (1 - b)_{S/N < 5} = 0.82 \pm 0.75. \quad (4.24)$$

This values are compatible with ours but they are not in agreement with those of Sifón et al. (2016) that use the SZ masses from the same catalogue.

Sereno et al. (2017) used 32 clusters from the PSZ2LenS sample extracted from the Canada France Hawaii Telescope Lensing Survey (CF-HTLenS; Heymans et al. 2012). They obtained

$$\exp \left(\frac{\ln \langle M_{SZ} \rangle}{\ln \langle M_{WL} \rangle} \right) = (1 - b) = 0.76 \pm 0.08. \quad (4.25)$$

This value is compatible within $0.5-\sigma$ to our result.

Penna-Lima et al. (2017) took 21 WL masses from the Cluster Lensing And Supernova survey with Hubble (CLASH; Postman et al. 2012). Thirteen of them were included in the PSZ1 catalogue while the remaining 8 had low significance in that catalogue and were extracted directly from the *Planck* SZ maps. A Bayesian analysis lead to a mass bias of

$$(1 - b) = 0.73 \pm 0.10, \quad (4.26)$$

compatible with our value within $0.7-\sigma$.

To finish with, two more works are presented from the Hyper Suprime-Cam Subaru Strategic Program (HSC-SSP; Aihara et al. 2018). In the first one, 5 GCs in common with the PSZ2 are used by (Medezinski et al. 2018) finding a mass bias of

Este documento incorpora firma electrónica, y es copia auténtica de un documento electrónico archivado por la ULL según la Ley 39/2015.
 Su autenticidad puede ser contrastada en la siguiente dirección <https://sede.ull.es/validacion/>

Identificador del documento: 3248012 Código de verificación: RmbjVJW6

Firmado por: ALEJANDRO AGUADO BARAHONA
 UNIVERSIDAD DE LA LAGUNA

Fecha: 01/03/2021 09:35:30

María de las Maravillas Aguiar Aguilár
 UNIVERSIDAD DE LA LAGUNA

22/03/2021 13:39:32

$$\frac{\langle M_{SZ} \rangle}{\langle M_{WL} \rangle} = (1 - b) = 0.80 \pm 0.14. \quad (4.27)$$

In a second work, (Miyatake et al. 2019) used 8 GCs in common with the ACTPol sample (Hilton et al. 2018) finding

$$\frac{\langle M_{SZ} \rangle}{\langle M_{WL} \rangle} = (1 - b) = 0.74^{+0.13}_{-0.12}. \quad (4.28)$$

Both results are in good agreement with the value presented in this thesis for the mass bias.

4.6 Discussion

Section 1.5.4 showed the importance of a precise determination of the mass bias to constrain cosmological parameters using cluster counts. In particular, Ω_m and σ_8 are extremely sensitive to the value of the mass bias through the mass function. Although I do not perform a complete cosmological analysis using the result of this thesis, I am able to draw some qualitative conclusions, taking advantage of previous analyses. In a future work, a detailed cosmological study using the mass value found in this work will be carried out.

First, we note that our result of the mass bias is in agreement with that of the *Planck* Collaboration, as mentioned in Section 4.5. This result confirms the apparent tension between the constraints on the parameters Ω_m and σ_8 from the primordial CMB power spectrum analysis and those derived from cluster number counts (Planck Collaboration XXIV 2016). The reason for this tension was originally ascribed to the value of the mass bias (see Figure 4.9). Indeed, Planck Collaboration XXIV (2016) showed that the mass bias value that reconciles the primordial CMB power spectrum and the cluster counts is $(1 - b) = 0.58 \pm 0.04$, but this number is inconsistent with our mass bias determination.

There are some possible explanations that might alleviate this tension, while keeping consistency with our mass bias results. Salvati et al. (2018) took into account the new estimation of the optical depth τ from the *Planck* 2018 data release, and found $(1 - b) = 0.62 \pm 0.07$ using a joint analysis of CMB, tSZ cluster counts and tSZ power spectrum. The authors also introduced neutrino masses in the analysis, yielding to a mass bias of $(1 - b) = 0.64 \pm 0.04$. In a later work, Salvati et al. (2019) analysed the effects of a mass-redshift dependence, adopting a power-law parametrisation. They apply this parametrisation to the combination of tSZ number counts and power spectrum, finding a hint for redshift dependence that leads to an increasing value of the mass bias for higher redshift. However, they find a preferred constant value of mass bias of $(1 - b) = 0.62 \pm 0.05$. Finally, Remazeilles et al. (2019) propose to include relativistic temperature corrections in the *Planck* thermal SZ analysis, as ignoring them might lead to an overestimation of $\Delta b \simeq 0.046 (1 - b)$.

Altogether, these effects contribute to alleviate this tension, which represents an open problem in the Λ CDM model. This issue is still under investigation, and the community

Este documento incorpora firma electrónica, y es copia auténtica de un documento electrónico archivado por la ULL según la Ley 39/2015.
 Su autenticidad puede ser contrastada en la siguiente dirección <https://sede.ull.es/validacion/>

Identificador del documento: 3248012 Código de verificación: RmbjVJW6

Firmado por: ALEJANDRO AGUADO BARAHONA
 UNIVERSIDAD DE LA LAGUNA

Fecha: 01/03/2021 09:35:30

María de las Maravillas Aguiar Aguilár
 UNIVERSIDAD DE LA LAGUNA

22/03/2021 13:39:32

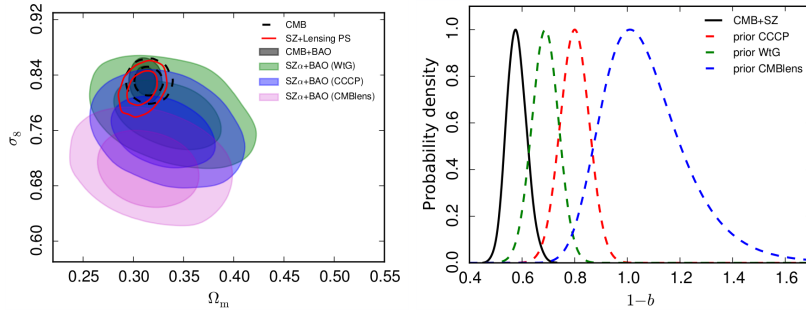


Figure 4.9: Left panel. Comparison of constraints from the CMB to those from the cluster counts in the $(\Omega_m-\sigma_8)$ -plane. The green, blue and violet contours give the cluster constraints (two-dimensional likelihood) at 68 and 95% for the WtG, CCCP, and CMB lensing mass calibrations, respectively, as listed in Table 2 in Planck Collaboration XXIV (2016). These constraints are obtained from the MMF3 catalogue with the SZ+BAO+BBN data set and α free (hence the SZ α notation). Constraints from the Planck TT,TE,EE+lowP CMB likelihood (hereafter, *Planck* primary CMB) are shown as the dashed contours enclosing 68 and 95% confidence regions (Planck Collaboration XXII 2016), while the grey shaded region also includes BAO. The red contours give results from a joint analysis of the cluster counts and the *Planck* lensing power spectrum (Planck Collaboration XV 2016), adopting the external priors on n_s and $\Omega_b h^2$ with the mass bias parameter free and α constrained by the X-ray prior (hence the SZ notation without the subscript α). Right panel. Comparison of cluster and primary CMB constraints in the base Λ CDM model, expressed in terms of the mass bias, $1-b$. The solid black curve shows the distribution of values required to reconcile the counts and primary CMB in Λ CDM; it is found as the posterior on $1-b$ from a joint analysis of the *Planck* cluster counts and primary CMB when leaving the mass bias free. Credits: Planck Collaboration XXIV (2016).

is making a great effort trying to solve this controversy.

Este documento incorpora firma electrónica, y es copia auténtica de un documento electrónico archivado por la ULL según la Ley 39/2015.
 Su autenticidad puede ser contrastada en la siguiente dirección <https://sede.ull.es/validacion/>

Identificador del documento: 3248012 Código de verificación: RmbjVJW6

Firmado por: ALEJANDRO AGUADO BARAHONA
 UNIVERSIDAD DE LA LAGUNA

Fecha: 01/03/2021 09:35:30

María de las Maravillas Aguiar Aguilár
 UNIVERSIDAD DE LA LAGUNA

22/03/2021 13:39:32

5

Conclusions

This thesis had two main goals. To perform the optical follow-up (128-MULTIPLE-16/15B) validating new galaxy cluster candidates detected by *Planck* satellite in the PSZ2 catalogue and to study the possible biases in the $M_{SZ} - M_{dyn}$ scaling relation.

The *Planck* PSZ2 optical follow-up

Chapters 2 and 3 presented the methodology and the results of the observational follow-up program (LP15) of unconfirmed SZ sources from the PSZ2 catalogue in the Northern Hemisphere ($Dec. > -15^\circ$). The observational program lasted for four complete terms (2015B-2017A) and a dedicated proposal during the term 2018A. The results of this program are the following:

- We performed a systematic follow-up of 190 targets selected from the PSZ2 catalogue with $Dec. > -15^\circ$ and with unknown counterpart in other wavelengths. For each of them, we obtained images in three different bands g' , r' and i' , using the WFC/INT or retrieve photometric information from the SDSS archive. The aim of this first step was to obtain a preliminary confirmation of an optical counterpart of the SZ source. We study the colour of likely cluster members to estimate the photometric redshift of the GCs and discriminate them between high and low redshift systems in order to perform spectroscopic observations in a more efficient manner.
- We retrieve useful spectroscopic information for 94 candidates and complement this information with SDSS spectroscopic data. The lower redshift systems ($z_{phot} < 0.35$) were observed using the DOLORS spectrograph at the TNG while the high- z objects ($z_{phot} \geq 0.35$) were observed using OSIRIS/GTC. The MOS was the technique chosen for every target, retrieving between 20-25 members, on average, in each observation. This allowed us to estimate the velocity dispersion and cluster mass.

Este documento incorpora firma electrónica, y es copia auténtica de un documento electrónico archivado por la ULL según la Ley 39/2015.
Su autenticidad puede ser contrastada en la siguiente dirección <https://sede.ull.es/validacion/>

Identificador del documento: 3248012 Código de verificación: RmbjVJW6

Firmado por: ALEJANDRO AGUADO BARAHONA
UNIVERSIDAD DE LA LAGUNA

Fecha: 01/03/2021 09:35:30

María de las Maravillas Aguiar Aguilár
UNIVERSIDAD DE LA LAGUNA

22/03/2021 13:39:32

- During the first year of observations, 106 PSZ2 sources with no known optical counterpart have been observed. A robust confirmation criterion based on velocity dispersion, when available, and richness estimations enabled us to confirm 41 candidates, for which we provided 31 spectroscopic and 10 photometric redshifts.
- During the second year of observations, 78 PSZ2 sources with no known optical counterpart have been observed. We have been able to confirm 40 new *Planck* PSZ2 sources. Among them, 18 were validated using velocity dispersion calculated from our spectroscopic redshifts and 22 using the richness estimation.
- We updated the information on 42 sources that have been validated in the original PSZ2 catalogue but lacked a redshift estimate. We provided a spectroscopic redshift for 20 of them and a photometric redshift for 20 sources. We also studied the richness and applied the same criteria as for the candidates in order to check the associations with the SZ signal. We discovered that three previously confirmed counterparts were not present in the optical range studied here.
- At the end of the whole observational program LP15, we were able to confirm 81 new cluster candidates, with a median redshift of 0.29. The mean redshift of the catalogue is 0.23. Our main contribution appears in the redshift interval $0.4 < z < 0.7$, where our confirmations correspond to 20 % of the total clusters that are confirmed in the PSZ2 in this range. The purity of the catalogue is increased from 76.7 % to 86.2 %.
- Finally, we found a clear correlation between the number of unconfirmed sources and galactic thermal dust emission. This correlation confirms that the PSZ2 catalogue contains spurious detections, as expected from the estimated purity and completeness curves published by the Planck Collaboration. Some of these false detections have been discussed here. In particular, we find that more than 50 % of the sources with a mean signal in the 857 GHz maps greater than 7 MJy/sr remain unconfirmed after this work.

$M_{SZ} - M_{dyn}$ scaling relation

Chapter 4 presented the spectroscopic results of the LP15 program. We use the confirmed candidates to build the $M_{SZ} - M_{dyn}$ scaling relation. We characterise the relation and extract information concerning the mass bias. I summarise the main results in the following list:

- We presented the spectroscopic data of the full program (including the complementing program CAT18A-12). In total, 94 PSZ2 sources were observed, 55 at the GTC and 39 at the TNG. We were able to estimate the velocity dispersion for 82 clusters. In addition, we used 47 clusters from the ITP sample and 259 clusters from the SDSS archival data to build a statistically representative sample of the PSZ2 in the Northern Hemisphere (PSZ2-North).

Este documento incorpora firma electrónica, y es copia auténtica de un documento electrónico archivado por la ULL según la Ley 39/2015.
Su autenticidad puede ser contrastada en la siguiente dirección <https://sede.ull.es/validacion/>

Identificador del documento: 3248012 Código de verificación: RmbjVJW6

Firmado por: ALEJANDRO AGUADO BARAHONA
UNIVERSIDAD DE LA LAGUNA

Fecha: 01/03/2021 09:35:30

María de las Maravillas Aguiar Aguilár
UNIVERSIDAD DE LA LAGUNA

22/03/2021 13:39:32

- We presented the velocity dispersion and dynamical mass of 362 objects confirmed as optical counterpart of a PSZ2 source, 356 from the PSZ2-North sample and nine from outside. We also discuss 26 clusters and groups that do not fulfil the matching criteria to be a counterpart of the SZ signal.
- The combination of LP15, ITP and SDSS samples yields a total sample of 297 galaxy clusters that can be used for the characterisation of the scaling relation $M_{\text{SZ}} - M_{\text{dyn}}$ for the PSZ2 catalogue. This sample represents the largest set of SZ selected clusters for which SZ and dynamical masses are available. It is, in fact, the largest sample used to determine the mass bias using dynamical mass estimates.
- Based on a set of realistic simulations which are representative of the actual noise level in our sample, we have selected the Nukers method as the least-biased regression method to extract the scaling relation.
- After correcting for the statistical bias of the regression method and the Eddington bias of the sample, we find the mass bias to be $(1 - B) = 0.80 \pm 0.04$ (stat) ± 0.05 (sys). Assuming $(1 - b_{\text{dyn}}) = 1$, our value for $(1 - b)$ is in agreement with previous studies (Ruel et al. 2014; Hoekstra et al. 2015; Battaglia et al. 2016; Sereno et al. 2017; Penna-Lima et al. 2017; Medezinski et al. 2018; Miyatake et al. 2019; Ferragamo et al. 2021, submitted), and do not solve the tension in the cosmological parameters ($\Omega_{\text{m}} - \sigma_8$ plane) between the CMB measurements and the cluster count analyses (Planck Collaboration XXIV 2016; Salvati et al. 2018; Planck Collaboration VI 2018; Remazeilles et al. 2019), which requires a value of ~ 0.6 .
- Finally, we only find marginal evidence of a possible dependence of the mass bias with mass. Our fitted slope is $\alpha = 1.17 \pm 0.13$ which is $1.3\text{-}\sigma$ away from the mass-invariant relation.

Este documento incorpora firma electrónica, y es copia auténtica de un documento electrónico archivado por la ULL según la Ley 39/2015.
Su autenticidad puede ser contrastada en la siguiente dirección <https://sede.ull.es/validacion/>

Identificador del documento: 3248012 Código de verificación: RmbjVJW6

Firmado por: ALEJANDRO AGUADO BARAHONA
UNIVERSIDAD DE LA LAGUNA

Fecha: 01/03/2021 09:35:30

María de las Maravillas Aguiar Aguilár
UNIVERSIDAD DE LA LAGUNA

22/03/2021 13:39:32

Bibliography

- Abell, G. O. 1957, AJ, 62, 2
- Abell, G. O., Corwin, Jr., H. G., & Olowin, R. P. 1989, ApJS, 70, 1
- Aghanim, N., Hurier, G., Diego, J. M., et al. 2015, A&A, 580, A138
- Aguado-Barahona, A., Barrena, R., Streblyanska, A., et al. 2019, A&A, 631, A148
- Aguado-Barahona, A., Rubiño-Martín, J. A., Ferragamo, A., et al. 2021, submitted, A&A
- Aihara, H., Arimoto, N., Armstrong, R., et al. 2018, PASJ, 70, S4
- Akritas, M. G., & Bershad, M. A. 1996, ApJ, 470, 706
- Allen, S. W., Evrard, A. E., & Mantz, A. B. 2011, ARA&A, 49, 409
- Allen, S. W., Rapetti, D. A., Schmidt, R. W., et al. 2008, MNRAS, 383, 879
- Amodeo, S., Mei, S., Stanford, S. A., et al. 2018, ApJ, 853, 36
- Barrena, R., Girardi, M., Boschin, W., & Mardirossian, F. 2012, A&A, 540, A90
- Barrena, R., Streblyanska, A., Ferragamo, A., et al. 2018, A&A, 616, A42
- Barrena, R., Ferragamo, A., Rubiño-Martín, J. A., et al. 2020, arXiv e-prints, arXiv:2004.07913
- Battaglia, N., Leauthaud, A., Miyatake, H., et al. 2016, , 2016, 013
- Beers, T. C., Flynn, K., & Gebhardt, K. 1990, AJ, 100, 32
- Bennett, C. L., Bay, M., Halpern, M., et al. 2003, ApJ, 583, 1
- Bertin, E., & Arnouts, S. 1996, A&AS, 117, 393
- Biffi, V., Borgani, S., Murante, G., et al. 2016, ApJ, 827, 112
- Birkinshaw, M. 1999, Phys. Rep., 310, 97

Este documento incorpora firma electrónica, y es copia auténtica de un documento electrónico archivado por la ULL según la Ley 39/2015.
Su autenticidad puede ser contrastada en la siguiente dirección <https://sede.ull.es/validacion/>

Identificador del documento: 3248012 Código de verificación: RmbjVJW6

Firmado por: ALEJANDRO AGUADO BARAHONA
UNIVERSIDAD DE LA LAGUNA

Fecha: 01/03/2021 09:35:30

María de las Maravillas Aguiar Aguilár
UNIVERSIDAD DE LA LAGUNA

22/03/2021 13:39:32

- Birkinshaw, M., Gull, S. F., & Northover, K. J. E. 1978a, *Nature*, 275, 40,41
- . 1978b, *MNRAS*, 185, 245
- Bleem, L. E., Stalder, B., de Haan, T., et al. 2015a, *ApJS*, 216, 27
- . 2015b, *ApJS*, 216, 27
- Bleem, L. E., Bocquet, S., Stalder, B., et al. 2020, *ApJS*, 247, 25
- Boada, S., Hughes, J. P., Menanteau, F., et al. 2019, *ApJ*, 871, 188
- Boggess, N. W., Mather, J. C., Weiss, R., et al. 1992, *ApJ*, 397, 420
- Boggs, P. T., & Rogers, J. E. 1990, in *Contemporary mathematics*, Vol. 112, Statistical analysis of measurement error models and applications: proceedings of the AMS-IMS-SIAM joint summer research conference held June 10-16, 1989, ed. P. Brown & W. A. Fuller, 186
- Bonamente, M., Joy, M. K., LaRoque, S. J., et al. 2006, *ApJ*, 647, 25
- Burenin, R. A. 2017, *Astronomy Letters*, 43, 507
- Burenin, R. A., Bikmaev, I. F., Khamitov, I. M., et al. 2018, *Astronomy Letters*, 44, 297
- Carlstrom, J. E., Holder, G. P., & Reese, E. D. 2002, *ARA&A*, 40, 643
- Carvalho, P., Rocha, G., & Hobson, M. P. 2009, *MNRAS*, 393, 681
- Carvalho, P., Rocha, G., Hobson, M. P., & Lasenby, A. 2012, *MNRAS*, 427, 1384
- Chambers, K. C., Magnier, E. A., Metcalfe, N., et al. 2016, *arXiv e-prints*, arXiv:1612.05560
- Cutri, R. M., Wright, E. L., Conrow, T., et al. 2013, *Explanatory Supplement to the AllWISE Data Release Products*, Tech. rep.
- de Haan, T., Benson, B. A., Bleem, L. E., et al. 2016, *ApJ*, 832, 95
- De Propris, R., Couch, W. J., Colless, M., et al. 2002, *MNRAS*, 329, 87
- Douspis, M. 2011, in *SF2A-2011: Proceedings of the Annual meeting of the French Society of Astronomy and Astrophysics*, ed. G. Alecian, K. Belkacem, R. Samadi, & D. Valls-Gabaud, 21–26
- Dreyer, J. L. E. 1888, *MmRAS*, 49, 1
- Duffy, A. R., Schaye, J., Kay, S. T., & Dalla Vecchia, C. 2008, *MNRAS*, 390, L64
- Dutton, A. A., & Macciò, A. V. 2014, *MNRAS*, 441, 3359

Este documento incorpora firma electrónica, y es copia auténtica de un documento electrónico archivado por la ULL según la Ley 39/2015.
Su autenticidad puede ser contrastada en la siguiente dirección <https://sede.ull.es/validacion/>

Identificador del documento: 3248012 Código de verificación: RmbjVJW6

Firmado por: ALEJANDRO AGUADO BARAHONA
UNIVERSIDAD DE LA LAGUNA

Fecha: 01/03/2021 09:35:30

María de las Maravillas Aguiar Aguilár
UNIVERSIDAD DE LA LAGUNA

22/03/2021 13:39:32

- Easton, C. 1904, *Astronomische Nachrichten*, 166, 129
- Ettori, S., Morandi, A., Tozzi, P., et al. 2009, *A&A*, 501, 61
- Evrard, A. E., Bialek, J., Busha, M., et al. 2008, *ApJ*, 672, 122
- Fasano, G., Marmo, C., Varela, J., et al. 2006, *A&A*, 445, 805
- Ferragamo, A. 2019, Optical characterization of the Planck PSZ1 galaxy cluster catalogue: building a reference sample for cosmology (PhD thesis, Universidad de La Laguna)
- Ferragamo, A., Barrena, R., Aguado-Barahona, A., Rubiño-Martín, J. A., & Streblyanska, A. 2021, submitted, *A&A*
- Ferragamo, A., Rubiño-Martín, J. A., Betancort-Rijo, J., et al. 2020, arXiv e-prints, arXiv:2006.05949
- Giacconi, R., Murray, S., Gursky, H., et al. 1972, *ApJ*, 178, 281
- Gladders, M. D., & Yee, H. K. C. 2000, *AJ*, 120, 2148
- Haehnelt, M. G., & Tegmark, M. 1996, *MNRAS*, 279, 545
- Hambly, N. C., MacGillivray, H. T., Read, M. A., et al. 2001, *MNRAS*, 326, 1279
- Hasselfield, M., Hilton, M., Marriage, T. A., et al. 2013a, , 2013, 008
- . 2013b, , 7, 008
- Herranz, D., Sanz, J. L., Hobson, M. P., et al. 2002, *MNRAS*, 336, 1057
- Herschel, W. 1785, *Philosophical Transactions of the Royal Society of London Series I*, 75, 213
- Heymans, C., Van Waerbeke, L., Miller, L., et al. 2012, *MNRAS*, 427, 146
- Hill, J. C., Sherwin, B. D., Smith, K. M., et al. 2014, arXiv e-prints, arXiv:1411.8004
- Hilton, M., Hasselfield, M., Sifón, C., et al. 2018, *ApJS*, 235, 20
- Hilton, M., Sifón, C., Naess, S., et al. 2020, arXiv e-prints, arXiv:2009.11043
- Hoekstra, H., Herbonnet, R., Muzzin, A., et al. 2015, *MNRAS*, 449, 685
- Huang, N., Bleem, L. E., Stalder, B., et al. 2020, *AJ*, 159, 110
- Hubble, E. 1929, *Proceedings of the National Academy of Science*, 15, 168
- Hubble, E. P. 1936, *Realm of the Nebulae*
- Humason, M. L., Mayall, N. U., & Sandage, A. R. 1956, *AJ*, 61, 97

Este documento incorpora firma electrónica, y es copia auténtica de un documento electrónico archivado por la ULL según la Ley 39/2015.
Su autenticidad puede ser contrastada en la siguiente dirección <https://sede.ull.es/validacion/>

Identificador del documento: 3248012 Código de verificación: RmbjVJW6

Firmado por: ALEJANDRO AGUADO BARAHONA
UNIVERSIDAD DE LA LAGUNA

Fecha: 01/03/2021 09:35:30

María de las Maravillas Aguiar Aguilár
UNIVERSIDAD DE LA LAGUNA

22/03/2021 13:39:32

- Jansen, F., Lumb, D., Altieri, B., et al. 2001, A&A, 365, L1
- Kelly, B. C. 2007, ApJ, 665, 1489
- Kennicutt, Jr., R. C. 1992, ApJS, 79, 255
- Khatri, R. 2016, A&A, 592, A48
- Kim, S., Rey, S.-C., Jerjen, H., et al. 2014, ApJS, 215, 22
- Kozmanyán, A., Bourdin, H., Mazzotta, P., Rasia, E., & Sereno, M. 2019, A&A, 621, A34
- Lamarre, J. M., Puget, J. L., Bouchet, F., et al. 2003, , 47, 1017
- LaRoque, S. J., Bonamente, M., Carlstrom, J. E., et al. 2006, ApJ, 652, 917
- Le Brun, A. M. C., McCarthy, I. G., Schaye, J., & Ponman, T. J. 2014, MNRAS, 441, 1270
- Liddle, A. R., & Lyth, D. H. 2000, Cosmological Inflation and Large-Scale Structure
- Lopes, P. A. A. 2007, MNRAS, 380, 1608
- Lynds, R., & Petrosian, V. 1989, ApJ, 336, 1
- Mamon, G. A., Biviano, A., & Murante, G. 2010, A&A, 520, A30
- Mandolesi, N., Bersanelli, M., Burigana, C., & Villa, F. 2000, Astrophysical Letters and Communications, 37, 151
- Mantz, A., Allen, S. W., Ebeling, H., Rapetti, D., & Drlica-Wagner, A. 2010, MNRAS, 406, 1773
- Mantz, A. B., von der Linden, A., Allen, S. W., et al. 2015, MNRAS, 446, 2205
- Marriage, T. A., Acquaviva, V., Ade, P. A. R., et al. 2011, ApJ, 737, 61
- Mazure, A., Katgert, P., den Hartog, R., et al. 1995, Astrophysics, 38, 367
- Medezinski, E., Battaglia, N., Umetsu, K., et al. 2018, PASJ, 70, S28
- Melin, J. B., Bartlett, J. G., & Delabrouille, J. 2006, A&A, 459, 341
- Messier, C. 1781, Catalogue des Nébuleuses et des Amas d'Étoiles (Catalog of Nebulae and Star Clusters), Connaissance des Temps ou des Mouvements Célestes
- Miyatake, H., Battaglia, N., Hilton, M., et al. 2019, ApJ, 875, 63
- Monet, D. G., Levine, S. E., Canzian, B., et al. 2003, AJ, 125, 984

Este documento incorpora firma electrónica, y es copia auténtica de un documento electrónico archivado por la ULL según la Ley 39/2015.
Su autenticidad puede ser contrastada en la siguiente dirección <https://sede.ull.es/validacion/>

Identificador del documento: 3248012 Código de verificación: RmbjVJW6

Firmado por: ALEJANDRO AGUADO BARAHONA
UNIVERSIDAD DE LA LAGUNA

Fecha: 01/03/2021 09:35:30

María de las Maravillas Aguiar Aguilár
UNIVERSIDAD DE LA LAGUNA

22/03/2021 13:39:32

- Munari, E., Biviano, A., Borgani, S., Murante, G., & Fabjan, D. 2013, MNRAS, 430, 2638
- Navarro, J. F., Frenk, C. S., & White, S. D. M. 1997, ApJ, 490, 493
- Ogrean, G. A., van Weeren, R. J., Jones, C., et al. 2015, ApJ, 812, 153
- Old, L., Skibba, R. A., Pearce, F. R., et al. 2014, MNRAS, 441, 1513
- Padmanabhan, T. 1993, Structure Formation in the Universe
- Pen, U.-L. 1997, , 2, 309
- Penna-Lima, M., Bartlett, J. G., Rozo, E., et al. 2017, A&A, 604, A89
- Perrott, Y. C., Olamaie, M., Rumsey, C., et al. 2015, A&A, 580, A95
- Piffaretti, R., Arnaud, M., Pratt, G. W., Pointecouteau, E., & Melin, J.-B. 2011, A&A, 534, A109
- Pike, S. R., Kay, S. T., Newton, R. D. A., Thomas, P. A., & Jenkins, A. 2014, MNRAS, 445, 1774
- Planck Collaboration I. 2020, A&A, 641, A1
- Planck Collaboration int. I. 2012, A&A, 543, A102
- Planck Collaboration int. LII. 2017, A&A, 607, A122
- Planck Collaboration int. XIV. 2014, A&A, 564, A45
- Planck Collaboration int. XXVI. 2015, A&A, 582, A29
- Planck Collaboration int. XXXVI. 2016, A&A, 586, A139
- Planck Collaboration IV. 2020, A&A, 641, A4
- Planck Collaboration IX. 2016, A&A, 594, A9
- Planck Collaboration VI. 2018, arXiv e-prints, arXiv:1807.06209
- . 2020, A&A, 641, A6
- Planck Collaboration VIII. 2011, A&A, 536, A8
- Planck Collaboration X. 2016, A&A, 594, A10
- Planck Collaboration XI. 2014, A&A, 571, A11
- Planck Collaboration XII. 2014, A&A, 571, A12
- Planck Collaboration XIV. 2014, A&A, 571, A14

Este documento incorpora firma electrónica, y es copia auténtica de un documento electrónico archivado por la ULL según la Ley 39/2015.
Su autenticidad puede ser contrastada en la siguiente dirección <https://sede.ull.es/validacion/>

Identificador del documento: 3248012 Código de verificación: RmbjVJW6

Firmado por: ALEJANDRO AGUADO BARAHONA
UNIVERSIDAD DE LA LAGUNA

Fecha: 01/03/2021 09:35:30

María de las Maravillas Aguiar Aguilár
UNIVERSIDAD DE LA LAGUNA

22/03/2021 13:39:32

- Planck Collaboration XV. 2011, A&A, 536, A15
— . 2016, A&A, 594, A15
- Planck Collaboration XX. 2014, A&A, 571, A20
- Planck Collaboration XXII. 2016, A&A, 594, A22
- Planck Collaboration XXIV. 2016, A&A, 594, A24
- Planck Collaboration XXIX. 2014, A&A, 571, A29
- Planck Collaboration XXV. 2016, A&A, 594, A25
- Planck Collaboration XXVII. 2016, A&A, 594, A27
- Planck Collaboration XXXII. 2015, A&A, 581, A14
- Planelles, S., Borgani, S., Fabjan, D., et al. 2014, MNRAS, 438, 195
- Postman, M., Coe, D., Benítez, N., et al. 2012, ApJS, 199, 25
- Pratt, G. W., Arnaud, M., Biviano, A., et al. 2019, Space Sci. Rev., 215, 25
- Predehl, P., Andritschke, R., Böhringer, H., et al. 2010, in Society of Photo-Optical Instrumentation Engineers (SPIE) Conference Series, Vol. 7732, Proc. SPIE, 77320U
- Reichardt, C. L., Stalder, B., Bleem, L. E., et al. 2013, ApJ, 763, 127
- Remazeilles, M., Bolliet, B., Rotti, A., & Chluba, J. 2019, MNRAS, 483, 3459
- Reynolds, J. H. 1923, MNRAS, 83, 147
- Rines, K. J., Geller, M. J., Diaferio, A., & Hwang, H. S. 2016, ApJ, 819, 63
- Rozo, E., Rykoff, E. S., Becker, M., Reddick, R. M., & Wechsler, R. H. 2015, MNRAS, 453, 38
- Rubiño-Martín, J. A., & Sunyaev, R. A. 2003, MNRAS, 344, 1155
- Ruel, J., Bazin, G., Bayliss, M., et al. 2014, ApJ, 792, 45
- Rykoff, E. S., Rozo, E., Busha, M. T., et al. 2014a, ApJ, 785, 104
— . 2014b, ApJ, 785, 104
- Sachs, R. K., & Wolfe, A. M. 1967, ApJ, 147, 73
- Salvati, L., Douspis, M., & Aghanim, N. 2018, A&A, 614, A13
- Salvati, L., Douspis, M., Ritz, A., Aghanim, N., & Babul, A. 2019, A&A, 626, A27

Este documento incorpora firma electrónica, y es copia auténtica de un documento electrónico archivado por la ULL según la Ley 39/2015.
Su autenticidad puede ser contrastada en la siguiente dirección <https://sede.ull.es/validacion/>

Identificador del documento: 3248012 Código de verificación: RmbjvJW6

Firmado por: ALEJANDRO AGUADO BARAHONA
UNIVERSIDAD DE LA LAGUNA

Fecha: 01/03/2021 09:35:30

María de las Maravillas Aguiar Aguilár
UNIVERSIDAD DE LA LAGUNA

22/03/2021 13:39:32

- Sarazin, C. L. 1988, X-ray emission from clusters of galaxies
- Saro, A., Mohr, J. J., Bazin, G., & Dolag, K. 2013, ApJ, 772, 47
- Sasaki, S. 1996, PASJ, 48, L119
- Schellenberger, G., & Reiprich, T. H. 2017, MNRAS, 471, 1370
- Sereno, M., Covone, G., Izzo, L., et al. 2017, MNRAS, 472, 1946
- Sifón, C., Battaglia, N., Hasselfield, M., et al. 2016, MNRAS, 461, 248
- Skrutskie, M. F., Cutri, R. M., Stiening, R., et al. 2006, AJ, 131, 1163
- Smith, G. P., Mazzotta, P., Okabe, N., et al. 2016, MNRAS, 456, L74
- Soucaill, G., Mellier, Y., Fort, B., Mathez, G., & Cailloux, M. 1987, The Messenger, 50, 5
- Staniszewski, Z., Ade, P. A. R., Aird, K. A., et al. 2009, ApJ, 701, 32
- Streblyanska, A., Aguado-Barahona, A., Ferragamo, A., et al. 2019, A&A, 628, A13
- Streblyanska, A., Barrena, R., Rubiño-Martín, J. A., et al. 2018, A&A, 617, A71
- Sunyaev, R. A., & Zeldovich, Y. B. 1970, Ap&SS, 7, 3
- . 1972, Comments on Astrophysics and Space Physics, 4, 173
- The Planck Collaboration. 2006, arXiv e-prints, astro
- Tinker, J., Kravtsov, A. V., Klypin, A., et al. 2008, ApJ, 688, 709
- Tonry, J., & Davis, M. 1979, AJ, 84, 1511
- Tremaine, S., Gebhardt, K., Bender, R., et al. 2002, ApJ, 574, 740
- Truong, N., Rasia, E., Mazzotta, P., et al. 2018, MNRAS, 474, 4089
- Tyson, J. A., Valdes, F., & Wenk, R. A. 1990, ApJ, 349, L1
- van der Burg, R. F. J., Aussel, H., Pratt, G. W., et al. 2016, A&A, 587, A23
- Varela, J., D'Onofrio, M., Marmo, C., et al. 2009, A&A, 497, 667
- Voges, W., Aschenbach, B., Boller, T., et al. 1999, VizieR Online Data Catalog, 9010
- . 2000, VizieR Online Data Catalog, 9029
- Voit, G. M. 2005, Reviews of Modern Physics, 77, 207
- von der Linden, A., Mantz, A., Allen, S. W., et al. 2014, MNRAS, 443, 1973

Este documento incorpora firma electrónica, y es copia auténtica de un documento electrónico archivado por la ULL según la Ley 39/2015.
Su autenticidad puede ser contrastada en la siguiente dirección <https://sede.ull.es/validacion/>

Identificador del documento: 3248012 Código de verificación: RmbjvJW6

Firmado por: ALEJANDRO AGUADO BARAHONA
UNIVERSIDAD DE LA LAGUNA

Fecha: 01/03/2021 09:35:30

María de las Maravillas Aguiar Aguilár
UNIVERSIDAD DE LA LAGUNA

22/03/2021 13:39:32

- Wainer, H., & Thissen, D. 1976, Psychometrika, 41, 9
- Weisskopf, M. C., Brinkman, B., Canizares, C., et al. 2002, PASP, 114, 1
- Wen, Z. L., & Han, J. L. 2018, MNRAS, 481, 4158
- Wen, Z. L., Han, J. L., & Liu, F. S. 2012, ApJS, 199, 34
- Wojtak, R., Old, L., Mamon, G. A., et al. 2018, MNRAS, 481, 324
- Wolf, M. 1901, Astronomische Nachrichten, 155, 127
- . 1903a, Publikationen des Astrophysikalischen Instituts Koenigstuhl-Heidelberg, 2, 57
- . 1903b, Publikationen des Astrophysikalischen Instituts Koenigstuhl-Heidelberg, 2, 89
- . 1906, Astronomische Nachrichten, 170, 211
- Wright, E. L., Eisenhardt, P. R. M., Mainzer, A. K., et al. 2010, AJ, 140, 1868
- York, D. G., Adelman, J., Anderson, Jr., J. E., et al. 2000, AJ, 120, 1579
- Zaznobin, I. A., Burenin, R. A., Bikmaev, I. F., et al. 2019, Astronomy Letters, 45, 49
- Zohren, H., Schrabback, T., & van der Burg, R. F. J. 2019, MNRAS
- Zubeldia, Í., & Challinor, A. 2019, MNRAS, 489, 401
- Zwicky, F. 1933, Helvetica Physica Acta, 6, 110
- . 1937, ApJ, 86, 217
- . 1938, PASP, 50, 215

Este documento incorpora firma electrónica, y es copia auténtica de un documento electrónico archivado por la ULL según la Ley 39/2015.
Su autenticidad puede ser contrastada en la siguiente dirección <https://sede.ull.es/validacion/>

Identificador del documento: 3248012 Código de verificación: RmbjVJW6

Firmado por: ALEJANDRO AGUADO BARAHONA
UNIVERSIDAD DE LA LAGUNA

Fecha: 01/03/2021 09:35:30

María de las Maravillas Aguiar Aguilár
UNIVERSIDAD DE LA LAGUNA

22/03/2021 13:39:32

Agradecimientos

Estos últimos 5 años ahora puedo decir que han sido los mejores de mi vida, aunque haya habido obstáculos y dificultades, por fin lo conseguí, y no puedo cerrar este trabajo sin agradecer a quienes han recorrido a mi lado este largo camino durante todo este tiempo.

Este trabajo de tesis no podría haber sido realizado sin la inestimable ayuda y dedicación de mis dos directores, José Alberto y Rafa. Habéis sido unos guías excepcionales, os estaré siempre agradecido.

Mis padres, ¿qué decir de ellos? Su constante apoyo, su cariño, su confianza, gracias por todo, mi carrera científica no habría sido la misma sin vosotros. ¡¡Mucho ánimo!! Sé que superaréis todo lo que se os ponga por delante.

Andrea, has sido la compañera perfecta. Sin tu confianza y ánimo durante este último año quizá no hubiera acabado la tesis. Gracias por estar ahí siempre que te he necesitado. Te quiero.

Ferra, aun con todos nuestros más y nuestros menos, has sido como un hermano mayor para mí. Me has allanado el camino y te estaré siempre agradecido por toda la ayuda que me has dado.

Gracias a John por ofrecerse a realizar la corrección lingüística de la tesis, ha mejorado considerablemente.

A todos mis compañeros y compañeras del IAC, no voy a nombraros porque seguro que se me olvida alguien y estaría feo, sabéis perfectamente quiénes sois. Muchas gracias por esas comidas, cervezas, tardes y noches de juegos y rol, borracheras... Mi estancia en la isla no habría sido la misma sin vosotros.

También quiero mostrar mi agradecimiento a mi gran familia Aguado-Barahona, en especial a mis abuelos, los que están y los que no. A mis tíos, tías, primos y primas que siempre habéis estado ahí cuando os he necesitado.

Este documento incorpora firma electrónica, y es copia auténtica de un documento electrónico archivado por la ULL según la Ley 39/2015.
Su autenticidad puede ser contrastada en la siguiente dirección <https://sede.ull.es/validacion/>

Identificador del documento: 3248012 Código de verificación: RmbjVJW6

Firmado por: ALEJANDRO AGUADO BARAHONA
UNIVERSIDAD DE LA LAGUNA

Fecha: 01/03/2021 09:35:30

María de las Maravillas Aguiar Aguilár
UNIVERSIDAD DE LA LAGUNA

22/03/2021 13:39:32